



University of Trieste

DEPARTMENT OF ENGINEERING AND ARCHITECTURE
Master's degree in Civil Engineering, Environmental curriculum

MASTER'S DEGREE THESIS

**MOSE - induced circulation patterns
in a simplified model of the Venice Lagoon**

Candidate :
GIOVANNI FARINA
IN1100271

Thesis supervisors :
Vincenzo Armenio, Paul Linden

Academic year 2019-2020

Alla Mamma

Contents

Abstract	ix
Acknowledgements	x
1 Introduction	1
The Venice Lagoon	1
The MOSE system	1
Relevant scales	2
Nondimensional numbers	7
The project	9
The model design	9
Model geometrical features	11
Implementation of tide	13
Flow calibration	13
Further reference data	14
2 Conceptual models	19
Simplifying the problem	19
Preliminary properties	20
Perfect mixing	22
Perfect mechanism	24
Reversed mechanism	25
Hybrid model	27
General model	29
Models and combinations	29
Modelling combinations	29
Modelling water exchanges	30
The efficiency logic	33
A possible physical model	35
Experimental observations	35
Conceiving the model	36
3 Experiments	39
Experiments overview	39
Closing inlets effect	41
Data processing	41

Used software: Digiflow and Matlab	41
Dye calibration	42
Height change correction	43
An example of experiment data processing	44
Matlab functions	45
Errors	46
Volume concentration as mass proportion	46
Initial distribution	46
Second reservoir exchange	46
Circulation in sea part	47
Leaking	47
Additional asymptotic concentration	48
Backlighting	49
Bubbles	51
Change of amplitude over time and estimated ratios	51
Results and comparisons	54
Single experiment example	54
Experimental data and conceptual models	60
Combinations flow patterns	62
Standard deviation patterns	68
Mean concentration and standard deviation	76
50 th and 95 th percentiles	82
Effect of ratio variation	87
Visual comparisons	89
Repeated experiments	92
Discussion on flushing or ventilation efficiency	96
Appendix: photo gallery	97
4 Numerical simulations	99
OpenFOAM	99
CINECA	100
Computational methods	100
FVM method	100
Volume of Fluid method and interFoam	103
Turbulence LES modeling	104
Cases mesh	106
Simulations setup issues and features implementation	108
Diffusion equation	108
Diffusion in air numerical error	109
Opening patterns implementation	112
Results	115
One third exchange ratio series	115
One half exchange ratio series	120
One third exchange ratio series	123
Different exchange ratios comparison	126

CONTENTS

vii

Models and experiments comparison	131
Half lagoon concentration	134
Flow features	134
Bibliography and sitography	141
Conclusions	143
Brief summary of the studied problem	143
Main results	144
Further developments	145
Final words	145
Appendix: summary in Italian (Sintesi in Italiano)	147

Abstract

The project aims to gain a basic understanding of the hydrodynamic behaviour induced by MOSE opening-closing patterns in the Lagoon of Venice.

Specifically, the lagoon and a portion of the sea are simplified in two shallow rectangular-shaped bodies of water connected through three inlets. Thanks to MOSE, the lagoon mobile barrier system, the gates at the inlets are thought to be opened and closed at half-tide switching times in *combinations*, creating a replacement circulation or *ventilation mechanism*. The main focus is not to define quantitatively the behaviour of the lagoon complex dynamics, but to abstract the essential features in a more general view, prioritising the study of the ventilation efficiency in relation to combinations.

There are around a dozen of combinations to be compared, these are performed in three different series which correspond to three different *exchange ratios* (ratio between exchanged volume in half tidal period and mean lagoon volume). The three exchange ratios take indirectly into account the variation of the mean level of the lagoon in climate change scenarios. The ventilation efficiency is studied by setting a uniform initial concentration of a passive tracer and considering its decay over time. The distribution of concentration values is examined and the decay rate of its characteristics, such as mean values and 95th percentile, provides a measure of efficiency.

The experiments, conducted at the G.K. Batchelor Laboratory (DAMTP, University of Cambridge) under the supervision of Paul Linden, have shown an improvement in the ventilation efficiency by using different combinations. However, trends were not totally clear and experimental errors caused a significant overlap between combinations. This inconvenience led to deeper theoretical reflections and brought to life the *Conceptual Models* chapter, where many fundamental properties of the exchange have been investigated, helping interpreting experimental results and, in general, the phenomena at play. The theoretical work led also to the definition of *reliability coefficients*, a useful tool to assess experimental data validity.

Moreover, CFD simulations reproduce the physical experimental conditions in a homogeneous numerical environment and shed more light on quantitative differences. The simulations have been computed with the OpenFOAM suite and generally confirm conclusions drawn from experimental data and theoretical models.

Acknowledgements

I wish to express my gratitude to my supervisor Paul Linden for welcoming me and taking me under his umbrella during my exchange period in Cambridge. I would like to thank him for the fruitful academic discussions, for providing me the basic idea of the thesis, and especially for the encouragement to persist in this research project, even when results looked inconclusive and proceeding was very difficult. I am also deeply indebted to Vincenzo Armenio, who encouraged me to apply to the Erasmus exchange before, and welcomed me in the lab group at the University of Trieste later; he believed in me and made my exchange in DAMTP possible.

Many gratitudes go to all people who helped me in DAMTP: David Page-Croft who made the lagoon structure and assisted me in several technical issues, especially for the leaking problem; the director of the G.K. Batchelor Lab, Stuart Dalziel, who helped me setting up the experiments, Jamie Partridge, for configuring the pump electronic switch, and David Parker, for his help in processing data.

My thanks also go to those who supported me in setting up the OpenFOAM simulations: Paola Alberigo who prolonged my CINECA account many times and added essential core hours to my credit; Mark Olesen and Charles L. from the *cfD-online* community; Santiago López Castaño, Giovanni Petris, and Sai Manohar Ramachandran from the lab, but especially Sara Marković, who dedicated a lot of her time in troubleshooting my OpenFOAM technical issues with calm and patience.

Desidero infine ringraziare, in italiano, la mia famiglia: mio padre Gavino e i miei fratelli Manuela e Mauro per essermi rimasti vicini e avermi dato supporto, da sempre ma anche in questi ultimi anni da studente fuoricorso cronico; e soprattutto la Mamma, Loredana, alla quale la tesi è dedicata, che mi ha sempre sostenuto e incoraggiato ad applicarmi, anche per il mio Erasmus, dandomi amore incondizionato e facendomi sentire bene in tutti i cinque anni e mezzo di questa magistrale allungata.

Chapter 1

Introduction

The Venice Lagoon

The lagoon of Venice is one of the most studied lagoons and the english word *lagoon* initially referred to it. Situated in the northwest of the Adriatic sea (45° 24' N 12°17' E), with a covered area of 500 km and a length of 10 km it is the largest mediterranean lagoon and owes its renown mainly to the city of Venice, built in the middle of it. It communicates with the Adriatic sea through three inlets: Lido, Malamocco and Chioggia, large from 500 to 1000 m, through which deep main channels, 15 m for Lido and Malamocco, 7 m for Chioggia, enter in it. The other characterising features of the lagoon are the intertidal flats, fed by the channels, the shoals, the salt marshes and the inlets of some rivers. Geographically the lagoon is surrounded by the Venetian plain and it is close to the Alps mountain chain. The two main winds are the Sirocco, a warm wind originated in the Arabian or Sahara deserts from south-east, and the Bora, a strong and cold katabatic wind from the continent in the north-east direction.

The amount of study on the lagoon is also owed to the threat of flooding that affects in an increasingly measure the city of Venice. This is caused by exceptionally high tides, which, originated in conjunction with the Sirocco wind, raise the level of the waters in the lagoon up to a more than a meter above the average level of the basin. This issue has been becoming more and more important with the global sea level rise and the necessity of preserving the artistical and historical heritage of the city makes this one of the most fascinating challenge of climate change.

The MOSE system

The MOSE (MOdulo Sperimentale Elettromeccanico, *Experimental Electromechanical Module*) is a system of three mobile barriers operating at the inlets for the flood protection of the Venice city centre. Its name refers to the mythological figure of Moses, who, according to the biblical narration, would have divided the waters of the Red Sea in ancient times. The idea of building a sea defence system for the lagoon started in 1966, when Venice, Chioggia and other important centres were

flooded by a tide of 194 cm. Since then the government had been looking for a solution to this problem for years; several projects had been proposed and, despite numerous controversies in environmental issues and funds management, alternative proposals to MOSE were discarded in 2006, when a round table of experts nominated by authorities analysed and evaluated them.

The system is formed by rows of mobile gates at the three inlets, 78 in total: at the Lido inlet there are two rows of 21 and 20 elements, connected by an artificial island; a row of 19 gates covers the Malamocco inlet and another of 18 elements the Chioggia one. Each gate consists in a metal box-type structure; this is connected to a concrete housing allocation through hinges thanks to which the upper-structure can be raised and lowered. The elements are 20 m wide with a varying length from 18.5 to 29 m and a thickness from 3.6 to 5 m .

The structures are kept full of water during periods of normal tide and are inflated with compressed air when the forecasted sea level passes the level of safeguarding. This is fixed at +100 cm with respect to the zero level of Punta Salute (on the Grand Canal in Venice), which is around 28 cm higher than the mean sea level as a consequence of global sea level rise and subsidence (Umgiesser, Maticchio 2006).

It is notable that the system is capable of functioning in many different combinations: all the inlets can be closed simultaneously, but they can also be closed selectively or, exploiting the fact that the elements are independent, partially.

Relevant scales

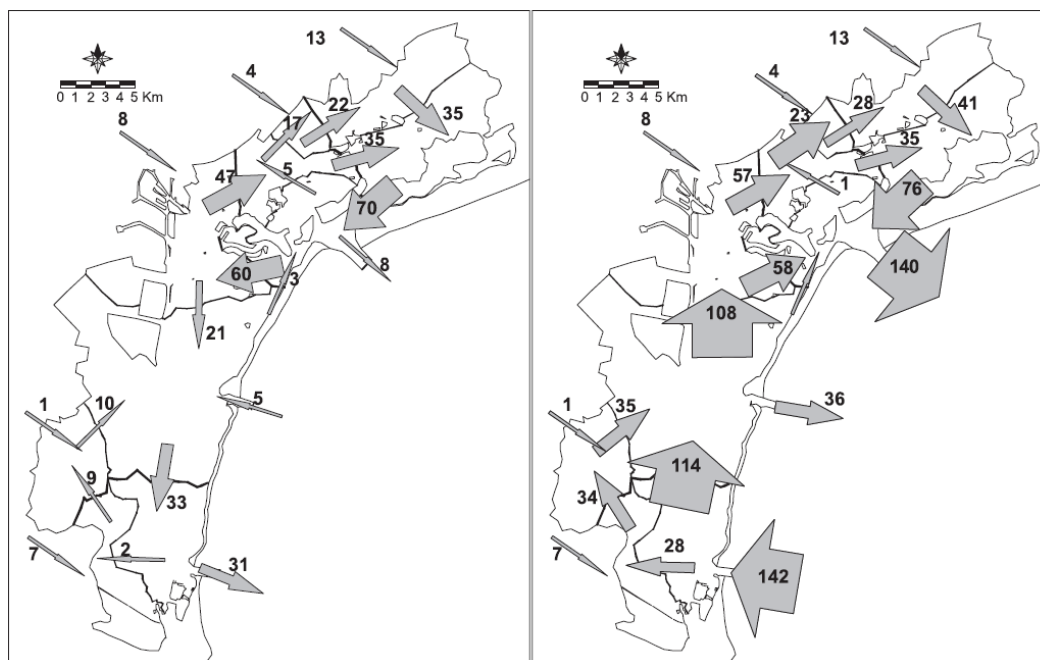
The scope of this section is to analyse the characteristic lengthscales of the various physical quantities in order to distinguish the major phenomena of the system.

BATHYMETRY

The lagoon presents an overall surface of 500 km², a 50 km vertical north-south length and a mean horizontal width of 15 km; approximately 415 km² are subjected to tidal excursion, while the remaining areas are diked to create fish farms with water exchanges limited and regulated artificially. «Only 5 % of the lagoon area has a depth greater than 5 m and 75 % is shallower than 2 m. The mean depth is 1.5 m, but there are areas deeper than 30 m» (SHYFEM archive, ISMAR-CNR). The three inlets Lido, Malamocco and Chioggia, from north to south, are respectively 14, 20 and 10 m deep and 900, 400 and 500 m wide (after the MOSE installation) (Mancero-Mosquera et al. 2010). Around 15% of the lagoon is cyclically flooded and dried by the tidal action (Umgiesser et al. 2004).

VOLUME AND WATER EXCHANGE

The mean water volume of the lagoon is around $632 \cdot 10^6$ m³ and the exchange of salt water through the inlet in each tidal cycle is about a third of the total volume of the lagoon (Gačić et al. 2004). The periodical fluxes have an amplitude of approximately $1 \div 2 \cdot 10^4$ m³ s⁻¹ (Ghezzi et al. 2010). In particular maximum values of 10,000 m³ s⁻¹ are reached for Malamocco and «all three inlets together may show flow rates as high as 24,000 m³ s⁻¹» (Bellafiore, Umgiesser, Cucco 2008). As a comparison the

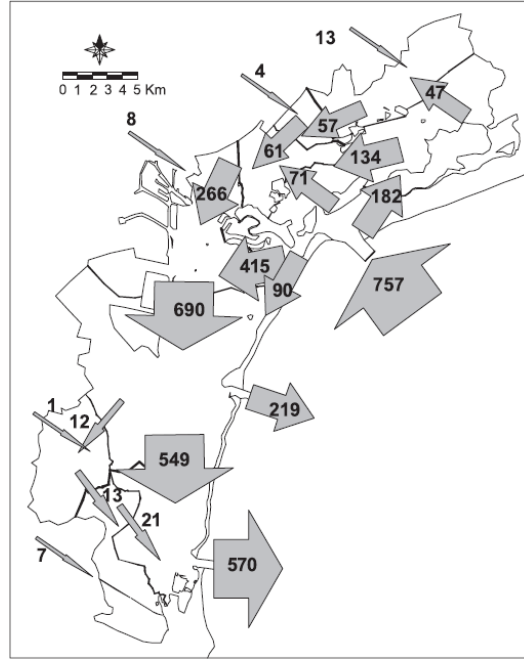


Residual fluxes in $\text{m}^3 \text{s}^{-1}$ between zones of the lagoon in a simplified model, normal conditions and Sirocco scenario (Solidoro et al. 2004)

Po river, with its close estuary, has an average discharge in the Adriatic of $1,500 \text{ m}^3 \text{ s}^{-1}$; therefore the circulation induced in the northern Adriatic can be neglected (Gačić et al. 2002). The residual fluxes, integrated over the tidal period, depend strongly on the wind action: at Lido and Chioggia there are values from $\sim 10 \text{ m}^3 \text{ s}^{-1}$ to $\sim 140 \text{ m}^3 \text{ s}^{-1}$ in the Sirocco scenario and of $550 \div 750 \text{ m}^3 \text{ s}^{-1}$ in the Bora scenario, with small residual fluxes in the central Malamocco inlet (Solidoro et al. 2004); it is notable that the Malamocco inlet, whilst having the maximum exchange amplitude, has a small residual flux. The rivers discharge in the lagoon is around $35.5 \text{ m}^3 \text{ s}^{-1}$, as an annual average value (Zuliani et al. 2001). The individual rivers amount are from south to north 7, 1, 8, 4, $13 \text{ m}^3 \text{ s}^{-1}$ (Solidoro et al. 2004) and they affect mainly the northern basin of the lagoon.

RESIDENCE TIME

There are many ways of defining the residence time; following the definition as «the time required for each element of the domain to replace most of the mass of a conservative tracer, originally released, with new water» a simulation discussed in the article *Modeling the Venice Lagoon residence time* (Cucco, Umgiesser 2006) drew a distribution of the residence time in different idealised scenarios. The results for only tide forcing give values of $25 \div 60$ days (spring tide distribution 43.1 ± 12.3 , neap tide 45.5 ± 12.1), adding the effect of the Sirocco wind give from 1 (at Chioggia inlet) to 40 days (in the closed northern part) (overall distribution 15.6 ± 14.3). In the Bora scenario the values are from less than 1 (at Lido) to 14 days in the southern



Residual fluxes in $\text{m}^3 \text{s}^{-1}$ between zones of the lagoon in a simplified model, Bora scenario (Solidoro et al. 2004)

part (4.3 ± 2.6 overall distribution and 6.5 ± 2.6 in the southern basin). The results of the article point out how the Bora-forcing gives the best ventilation mechanism in the lagoon.

TIDE

The tide varies between ± 100 cm during spring tides and about ± 50 cm in the period of neap tides (SHYFEM archive, ISMAR-CNR). The lagoon is also interested by two main seiches of the Adriatic sea with 11 h and 22 h periods, for more information also on the tidal components see the article *Modeling the water exchanges between the Venice Lagoon and the Adriatic Sea* (Bellafiore, Umgiesser, Cucco 2008).

VELOCITIES

Stratification can occur only in the external parts of the basin, where the tidal energy, transmitted through the inlets, is low. Inside the inlets the water velocities are relatively high (over 1 m s^{-1}) and «the vertical shear creates enough turbulence to mix the water column. Consequently, water exchanges between the lagoon and the sea are essentially barotropic» (Umgiesser et al. 2004, Gačić et al. 2002).

In particular it is possible to set as characteristic values for the variability over the lagoon $\Delta\zeta = 0.2 \text{ m}$, $\Delta S = 10 \text{ PSU}$ and $\Delta T = 4^\circ\text{C}$, $H = 1 \text{ m}$ for the average water depth, and operate a dimensional analysis to evaluate the saline and thermal gradients contribution to pressure and velocity field. Starting from the equation for the pressure in the z -component (depth direction)

$$p = p_0 + \rho g(\zeta - z)$$

It is possible to differentiate it with respect to the x -direction

$$\frac{1}{\rho} \frac{\partial p}{\partial x} = g \frac{\partial \zeta}{\partial x} + \frac{g}{\rho} \frac{\partial \rho}{\partial x} \frac{H}{2}$$

And with $\alpha = 2 \cdot 10^{-4} \text{ K}^{-1}$ typical thermal and $\beta = 8 \cdot 10^{-4} \text{ psu}^{-1}$ saline coefficients of expansion the ratios between barotropic and baroclinic gradients are:

$$\frac{2\Delta\zeta}{H\beta\Delta S} \approx 50$$

$$\frac{2\Delta\zeta}{H\alpha\Delta T} \approx 500$$

Therefore barotropic gradients are much larger than the baroclinic ones which can be neglected (Umgiesser et al. 2004).

WIND

The two main winds are Bora and Sirocco respectively from E-NE and SE, characteristic lengthscales for the Bora are approximately $10\text{-}15 \text{ m s}^{-1}$, while for the Sirocco 5 m s^{-1} . The wind drag coefficient can be assumed in $c_D = 2.5 \cdot 10^{-3}$ (Bellafore, Umgiesser, Cucco 2008).

TEMPERATURE

The water temperature of the lagoon varies roughly from a minimum of $3 \text{ }^\circ\text{C}$ in winter to a maximum of $30 \text{ }^\circ\text{C}$ in summer (Umgiesser et al. 2004). There exists a significant temperature gradient between the lagoon and the watershed of about $1 \text{ }^\circ\text{C}$ (from $14.5 \text{ }^\circ\text{C}$ as a mean value at the lagoon to $13.5 \text{ }^\circ\text{C}$ at the watershed) (Spiro and Guerzoni 2006).

PRECIPITATIONS

There is a «SW-SE gradient of decreasing precipitations from about 1000 mm/yr to less than 700 , about 250 mm/yr less rainfall in the lagoon than in the watershed. Precipitations have two peaks one in spring one in autumn (october) with precipitations of more than 100 mm/di » (The Ecological Implications of Climate Change on the lagoon of Venice, UNESCO Venice Office and ISMAR-CNR, 2011).

SALINITY

«The lagoon is eu-polyhaline with salinities ranging from 18 to 30 PSU in the innermost belt and over 30 PSU in the middle ranges» (Ghezzi et al. 2010). At the inlets the salinity is around 35 PSU , a value to be compared with the average salinity of the Adriatic sea, $38\text{-}39 \text{ PSU}$. Other sources give minimum values of around 22 PSU up to values of around 34 PSU (Umgiesser et al. 2004).

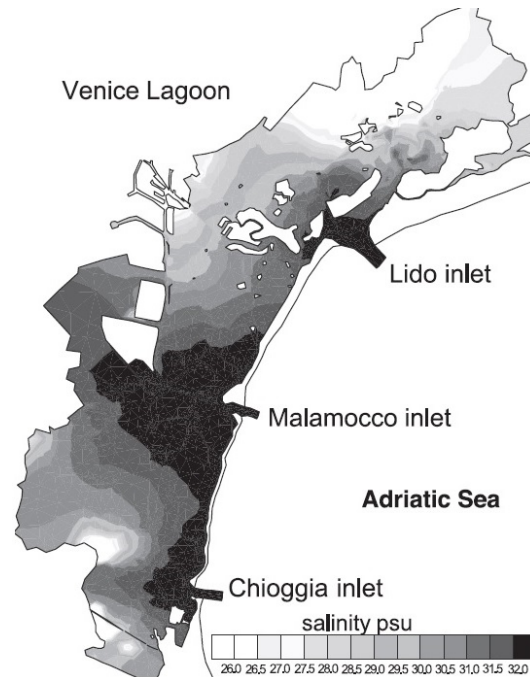
CLIMATE CHANGE EFFECTS

An A2 global scenario of high population growth and slow economic and technological development results in a sea level rise of 51 cm , decreasing wind speed (-5%), rising air temperature (from $+3.0 \text{ }^\circ\text{C}$ to $4.7 \text{ }^\circ\text{C}$ and $+3.5 \text{ }^\circ\text{C}$ in average), rising average sea temperature ($+3 \text{ }^\circ\text{C}$), salinity ($+1.3 \text{ PSU}$) and residence time, since «sea level rise leads to a major volume increase than the water exchange increment» by

year 2100 (The Ecological Implications of Climate Change on the lagoon of Venice, UNESCO Venice Office and ISMAR-CNR, 2011).

However, this is surely an underestimation: according to 2013 IPCC (Intergovernmental Panel on Climate Change) Fifth Report (the sixth is about to be published in 2022) in the scenario of a rapid cut of man-made carbon emissions (RCP2.6 scenario) the sea level rise amounts to 26-55 cm, while a more likely scenario of very high emissions, the estimate is about 52-98 cm. The current trend seems to confirm this worst-case scenario (Grinsted, Christensen, Hesselbjerg 2021) also because phenomena previously underestimated are creating a positive feedback in Greenland ice melting (Irvali, Galaasen et al. , 2019).

It is also worth noticing that the MOSE system is currently designed to sustain a sea level rise of about 60 cm; therefore, it will probably need to be upgraded or replaced by the end of the century.



Distribution of salinity in normalised conditions (Solidoro et al. 2004)

Nondimensional numbers

The Atwood number A

$$A = \frac{\rho_1 - \rho_2}{\rho_1 + \rho_2}$$

is a dimensionless density ratio between a heavier fluid with density ρ_1 and lighter fluid of density ρ_2 . Relevant especially for the study of hydrodynamic instabilities. In the case of the lagoon the density is roughly 1.025 kg dm^{-3} and the density of the sea $1.0275 \text{ kg dm}^{-3}$ giving an approximate Atwood number in the order of 10^{-3} but with significant changes over the lagoon itself.

The Froude number represents the ratio between inertial and gravitational forces, it describes the type of flow in shallow waters as gravity or inertia-dominated and recurs often in the governing equations

$$\text{Fr} = \frac{u_0}{\sqrt{g_0 l_0}}$$

where u_0 is a characteristic horizontal velocity, g_0 the field acceleration and l_0 the characteristic vertical lengthscale; with $u_0 = 0.5 \text{ m s}^{-1}$, $g \approx 10 \text{ m s}^{-2}$ and $l_0 = 1 \text{ m}$ $\implies \text{Fr} \approx 0.16$.

The Reynolds number represents the relative contribution of inertial forces in comparison with viscous forces:

$$\text{Re} = \frac{u_0 L}{\nu}$$

At the inlets a characteristic length scales is the level of the water and

$$\text{Re} \approx \frac{1 \text{ m s}^{-1} 10 \text{ m}}{10^{-6} \text{ m}^2 \text{ s}^{-1}} = 10^7$$

While in the intertidal flats we could assume a horizontal variability over tens or hundreds of meters and a velocity in the order of 10^{-2} m s^{-1} obtaining $\text{Re} \approx 10^{5\div 6}$, turbulent regime.

The Weber number represents the contribution of kinematic energy in comparison with surface tension energy. It is important that this parameter be not too low in the physical modelisation.

$$\text{We} = \frac{\rho v^2 l}{\sigma} \approx \frac{1000 \text{ kg m}^{-3} 0.01 \text{ m}^2 \text{ s}^{-2} 10 \text{ m}}{7 \cdot 10^{-2} \text{ N m}^{-1}} \approx 10^3$$

The Rossby number describes the relative importance of inertia with respect to terrestrial rotation effects:

$$\text{Ro} = \frac{U}{L f} \approx \frac{0.5 \text{ m s}^{-1}}{1000 \text{ m} 2 \cdot 7 \cdot 10^{-5} \text{ rad s}^{-1} \cdot 0.7} \approx 5$$

where f is the Coriolis frequency $2\Omega \sin \varphi$ with $\Omega = 7.2921 \times 10^{-5} \text{ rad/s}$, calculated as $2\pi/T$ on the terrestrial day period, and φ the latitude.

The Ekman number estimates the ratio of viscous to Coriolis forces

$$\text{Ek} = \frac{\nu}{f L^2} \approx \frac{10^{-6} \text{ m}^2 \text{ s}^{-1}}{2 \cdot 7 \cdot 10^{-5} \text{ rad s}^{-1} \cdot 0.7 \cdot 1 \text{ m}^2} \approx 10^{-2}$$

In particular the turbulent Ekman number evaluates the importance of turbulence with respect to geophysical rotational effects

$$\text{E} = \frac{u_*}{f L} \approx \frac{10^{-2} \text{ m s}^{-1}}{10^{-4} \text{ rad s}^{-1} 1 \text{ m}} = 10^2$$

with $u_* \approx 0.1 U$.

The Richardson number express the relative importance of buoyancy effects with respect to inertia:

$$\text{Ri} = \frac{\text{potential energy}}{\text{kinetic energy}} = \frac{g H \Delta \rho}{\rho_0 U^2} \approx 0$$

Stratification effects may be neglected because of the intertidal exchange volume which affects the lagoon (Umgiesser et al. 2004). However it is possible that a certain amount of stratification occurs in summertime in the external flats.

The project

The particular situation of the lagoon of Venice inspired the project for which these observations have been made. The idea is to study experimentally the behaviour of a simplified physical model of the lagoon: a shallow body of water with three inlets which can be opened and closed in combination. The main forcing is the tide and it is simulated by a proper piping system; the wind could be simulated by a small slope of the tank, but this has not been implemented. The simplified dynamics of this system could help in getting a better understanding of the relation between the tidal period and the circulation characteristics inside the lagoon with respect to the different combinations.

Theoretically this approach would produce a model not representative of the real system, referable to any body of water forced by tide and wind for which it is possible to modulate the fluxes at three different inlets. As far as it concerns the lagoon itself numerical modelling is the only way forward, as pointed out in the article *A finite element model for the Venice Lagoon. Development, set up, calibration and validation* (Umgiesser et al. 2004).

The main opportunity which setting a physical model gives is the possibility of accurately correlating the characteristic timescale of the model with the tidal period in different configurations. The general circulation inside the tank is observed through dye tracer.

The model design

The main criterion for the modelisation is the conservation of the exchange ratios between tidal forcing and reservoir volume, a phenomenon which characterises the lagoon circulation. To this purpose it is necessary to estimate the velocities induced by the flow rates corresponding to this ratio, accordingly to a reasonable tidal period and height modulating. Thanks to the estimated range of velocities it will be possible to evaluate the various nondimensional numbers which are important for the analysis: the Reynolds number and the Froude number; checking that the other numbers correspond to asymptotic situations both in the actual system and in the physical model.

SIMPLIFIED MODEL

The model consists in a tank of $204.5 \times 120 \times 20 \text{ cm}^3$ with the lagoon modeled in a $24 \times 120 \times 5 \text{ cm}^3$ upper part divided by the remaining deeper and wider one, which represents the relevant Adriatic Sea exchange volume. Although the tank has a rectangular shape, it is possible to estimate a horizontal scale of roughly 1 : 500,000, while the vertical scale ranges from 1 : 300 to 1 : 20 and it is not uniform due to the complex morphology of the lagoon. A pipe located at the bottom of the tank simulates the tide forcing with a sinusoidal (or piecewise linear) signal.

The first step of the design process is to ensure that the exchange volume ratio in the tidal period is the same as in the lagoon-sea system, that is approximately a third of the total average volume. The volume contained in the shallow part of the

tank is $100 \times 20 \times 5 = 10,000 \text{ cm}^3$ with this initial water depth; therefore the volume to be exchanged during the tidal cycle is approximately $3,300 \text{ cm}^3$. The total flow rate can be expressed as

$$Q = \frac{2}{3} C_c B (h - h_0) \sqrt{2g(h - h_0)}$$

This is a relation from free-flow weir theory and it is the simple result of integrating infinitesimal flows assuming falling particles at velocity $\sqrt{2gh}$ and neglecting pressure and continuity contributions; it brings to an overestimation of flow-rate and velocity. Such velocity can be obtained equivalently applying the Bernoulli theorem, rigorously valid for incompressible, inviscid and irrotational flow at stationary state, between a particle at the exchange interface and one at the top surface. C_c is the contraction coefficient, which refers to the contracted vein that forms after a weir and it is not very relevant in the present case; B is the width and g the gravitational field constant. Taking $B_{\text{eff}} \approx 0.8 B$ for the same phenomenon, with $B = 3b$ (where $b = 5 \text{ cm}$ is the single inlet width), and $h = h_0 + A_0 \sin \omega t$ the water level over the tidal period T such that $\omega = \frac{2\pi}{T}$, it is possible to formulate the condition as:

$$\int_0^{T/2} Q(h(t)) dt = V_{ex}$$

Therefore:

$$\begin{aligned} \int_0^{T/2} \frac{2}{3} C_c B_{\text{eff}} (h - h_0) \sqrt{2g(h - h_0)} dt &= \frac{2}{3} C_c B_{\text{eff}} \sqrt{2g} \int_0^{T/2} (A_0 \sin \omega t)^{3/2} dt \\ &= \frac{2}{3} C_c B_{\text{eff}} \sqrt{2g} \int_0^{T/2} (A_0 \sin \omega t)^{3/2} dt = \frac{2}{3} C_c B_{\text{eff}} \sqrt{2g} \frac{4\sqrt{2} A_0^{3/2} T \Gamma(\frac{5}{4})^2}{3\pi^{3/2}} \end{aligned}$$

And then:

$$T = \frac{\frac{16}{9} \pi^{3/2} V_{ex}}{C_c \sqrt{g} B_{\text{eff}} A_0^{3/2} \Gamma(\frac{5}{4})^2}$$

Where B_{eff} is uncertain because of the lateral contraction, so it is possible to estimate the angular frequency:

$$\omega = 0.251 \text{ rad s}^{-1}$$

then flow-rate and velocity,

$$\begin{aligned} Q &= \frac{2}{3} C_c B_{\text{eff}} \sqrt{2g} (A_0 \sin \omega t)^{3/2} \\ v_{\text{inlet}} &= \frac{2}{3} C_c \sqrt{2g} \frac{(A_0 \sin \omega t)^{3/2}}{h_0 + A_0 \sin \omega t} \end{aligned}$$

Thanks to these relatively rough and simple relations it is possible to give as an input the geometry of the tank and get an estimation of the numbers previously analysed for the lagoon system. The number $\Gamma(\frac{5}{4})^2$ is approximately 0.82.

INPUT VALUES		RESULTING QUANTITIES	
B	18 cm	T	150 s
A_0	1.666 cm	ω	0.042 rad/s
h_0	5 cm	Q_{max}	0.114 l/s
h_0/A_0	3	v_{max}	1.0 cm/s

	MODEL	LAGOON
Re	476	10^7
Fr	0.136	0.10
We	0.07	1000
Ro	1945	5
Ek	4	0.01
E	194	100

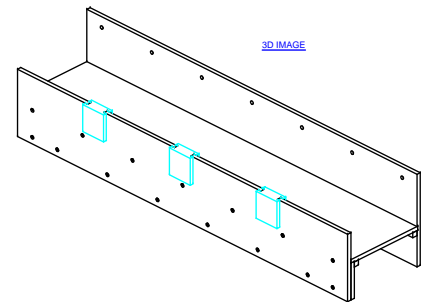
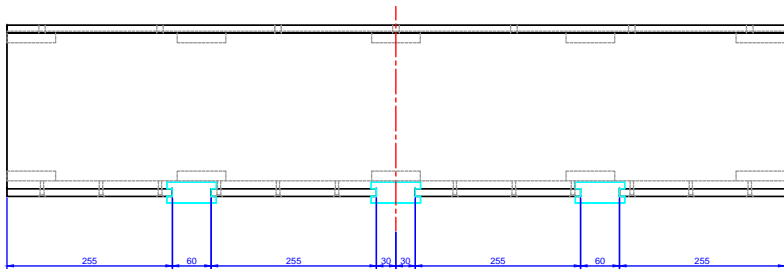
$$We = \frac{\rho v_{max}^2 h_0}{\sigma} \approx \frac{10^3 \text{ kg m}^{-3} \cdot 1^2 \cdot 10^{-4} \text{ m}^2 \text{ s}^{-2} \cdot 5 \cdot 10^{-2} \text{ m}}{7 \cdot 10^{-2} \text{ N m}^{-1}} = 0.07$$

It is remarkable that while the period depends both on geometry and wave amplitude, v_{max} does not depend on horizontal scales, but primarily on wave amplitude and secondarily on height. The Froude number depends linearly on the h_0/A_0 ratio. On the other hand the Reynolds number depends more than linearly on amplitude and very weakly on mean depth. As for the Reynolds number the 476 of the model can be acceptable if the roughness of the lagoon is considered, this approximation is in the same spirit of the geometry modelization: the purpose is to create a simple and practical model to study ventilation mechanisms. Note that the numbers are estimated at the inlets both in model and lagoon system.

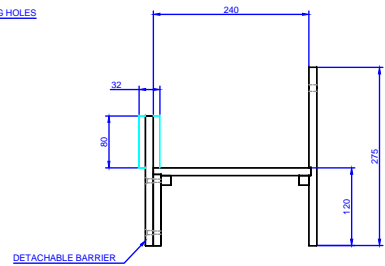
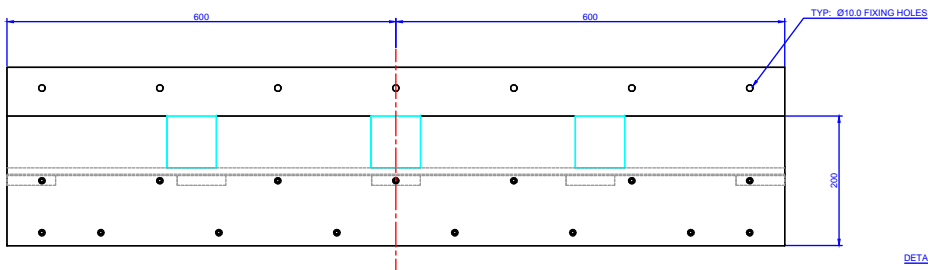
To implement the "lagoon" basin an acrylic structure has been built. The tide is simulated by the combination of a continuous drain and an inflow made from a submersible pump: the pump is located in another reservoir, it switches on and off periodically and the inflow is diffused into multiple holes made in lateral pipe. The flow calibration has been made through monitoring the water level on a ruler (sensitivity: 1 mm).

Model geometrical features

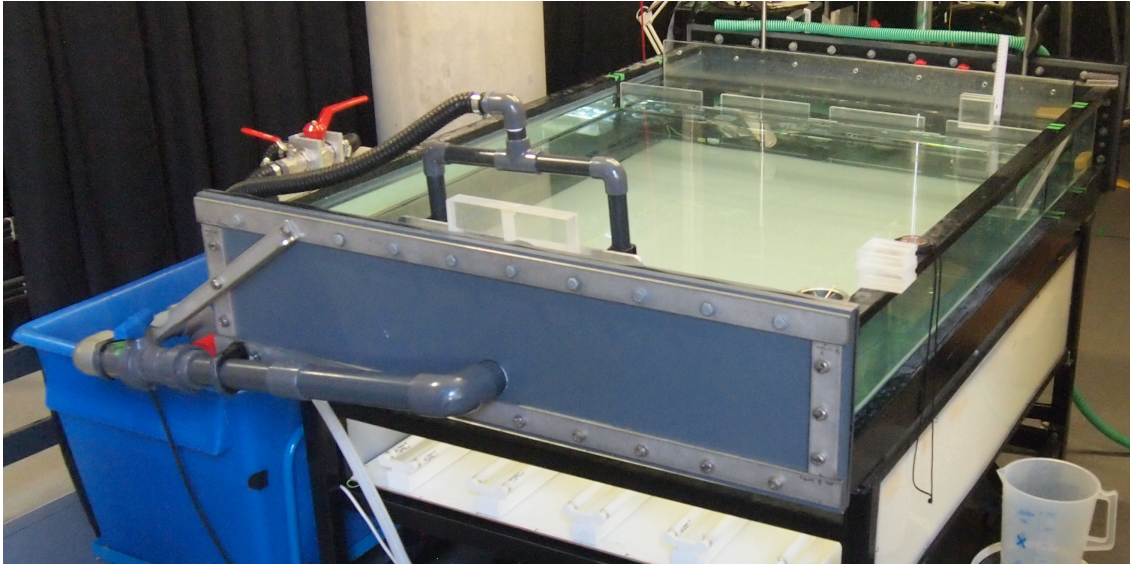
"sea" part	length	180,5 cm
	Mean height	17 cm ³
	width	120 cm
	Vol sea	368220 cm ³
"lagoon" part	length	24 cm
	Mean height	5 cm
	width	120 cm
	Vol lag	14400 cm ³
	lag/sea	3,91 %



MAT: 12mm CAST ACRYLIC SHEET
ALL JOINTS TO BE GLUED
ACRYLIC FOR THE GATES



SCALE: 1:4@A2	UNIVERSITY OF CAMBRIDGE		
MAT: GREY PVC	FLUID DYNAMICS LABORATORY		
QTY: 1 OFF	DEPARTMENT OF APPLIED MATHS		
DIM: in MM	TITLE		
TOL: ±0.1 UNLESS STATED	VENICE LAGOON ASSEMBLY		
DRN: D.PAGE-CROFT	DATE: 28/02/17	Dwg No:	



Experimental setup

Implementation of tide

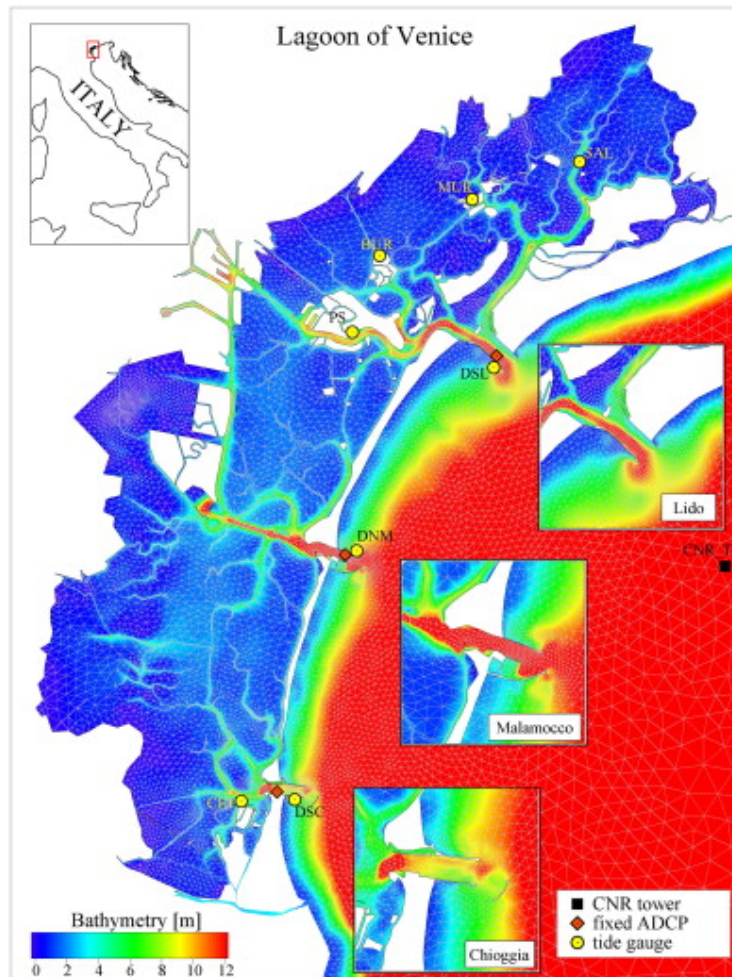
For practical reasons the tide is simulated by a constant flow switching sign periodically (as said, there is a continuous drain with the set flowrate and a pump with double flowrate switching on and off every half period time). The resulting profile for the tide is piecewise linear instead of being sinusoidal; this is another approximation and it is especially valid for multiple cycles.

As a consequence of this there are some disturbances in the flow at each flow switch.

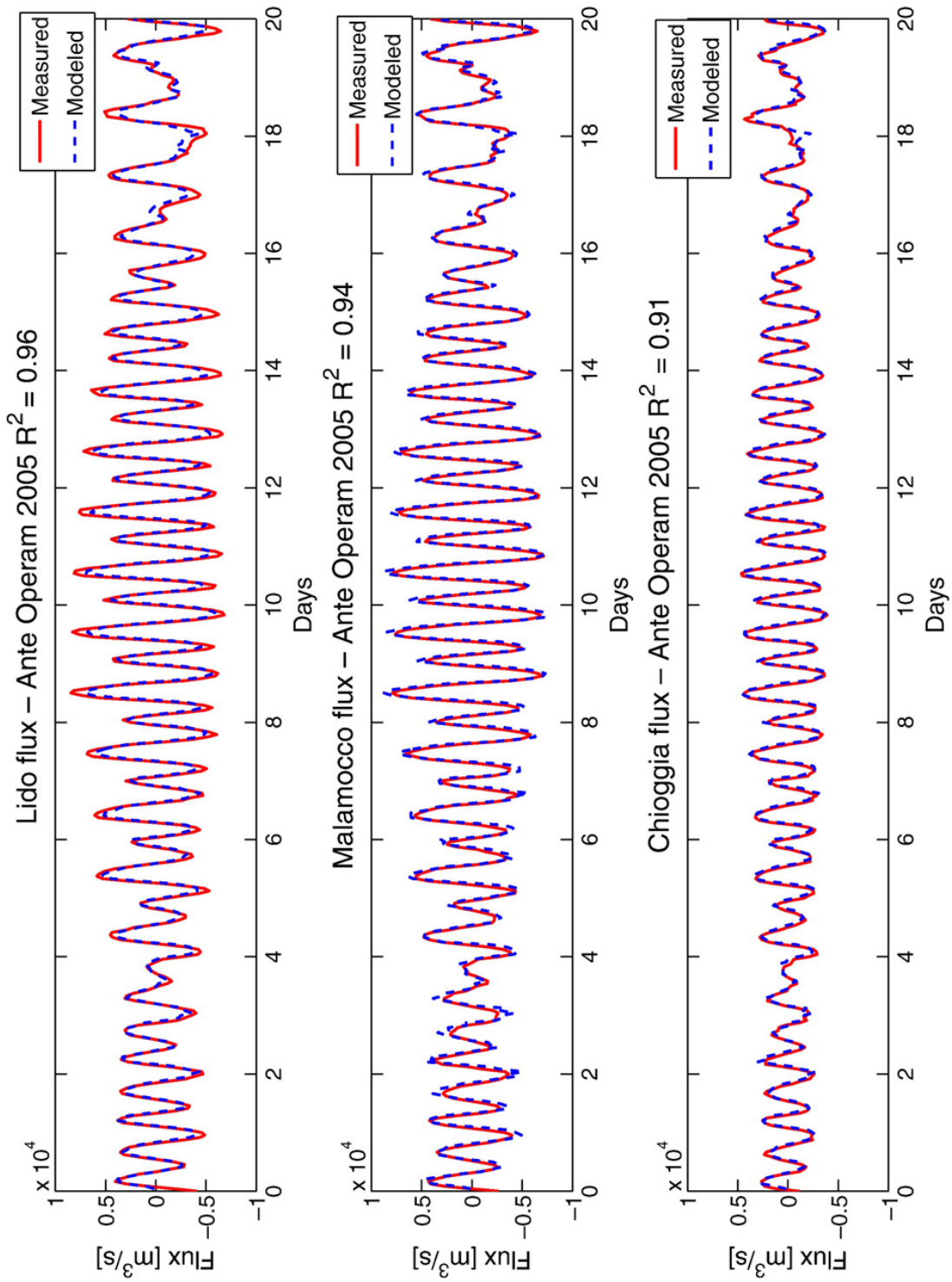
Flow calibration

As flowmeters usually measure small flows, the pump flow and the drain one have been calibrated adjusting the corresponding valves with reference to water level. This method is not accurate; however, it is coherent with the other approximations made in experimental setup.

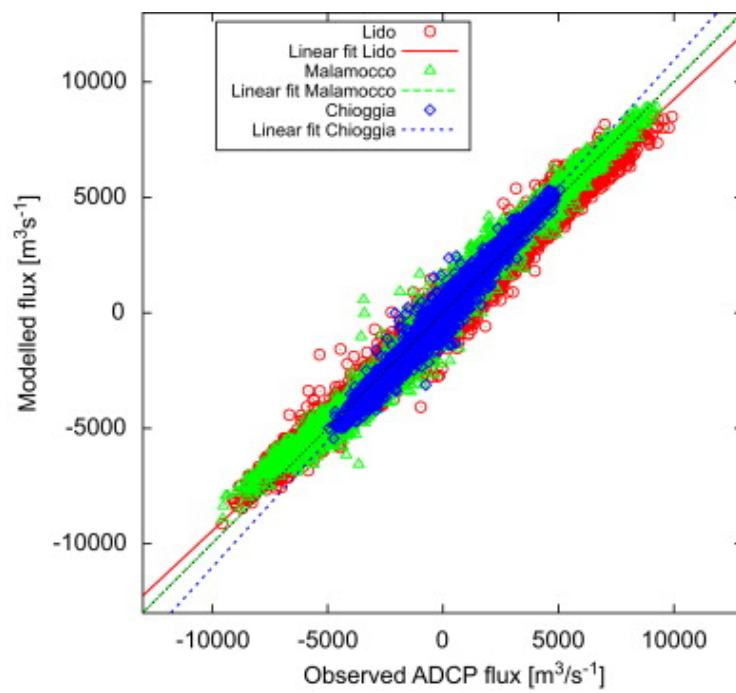
Further reference data



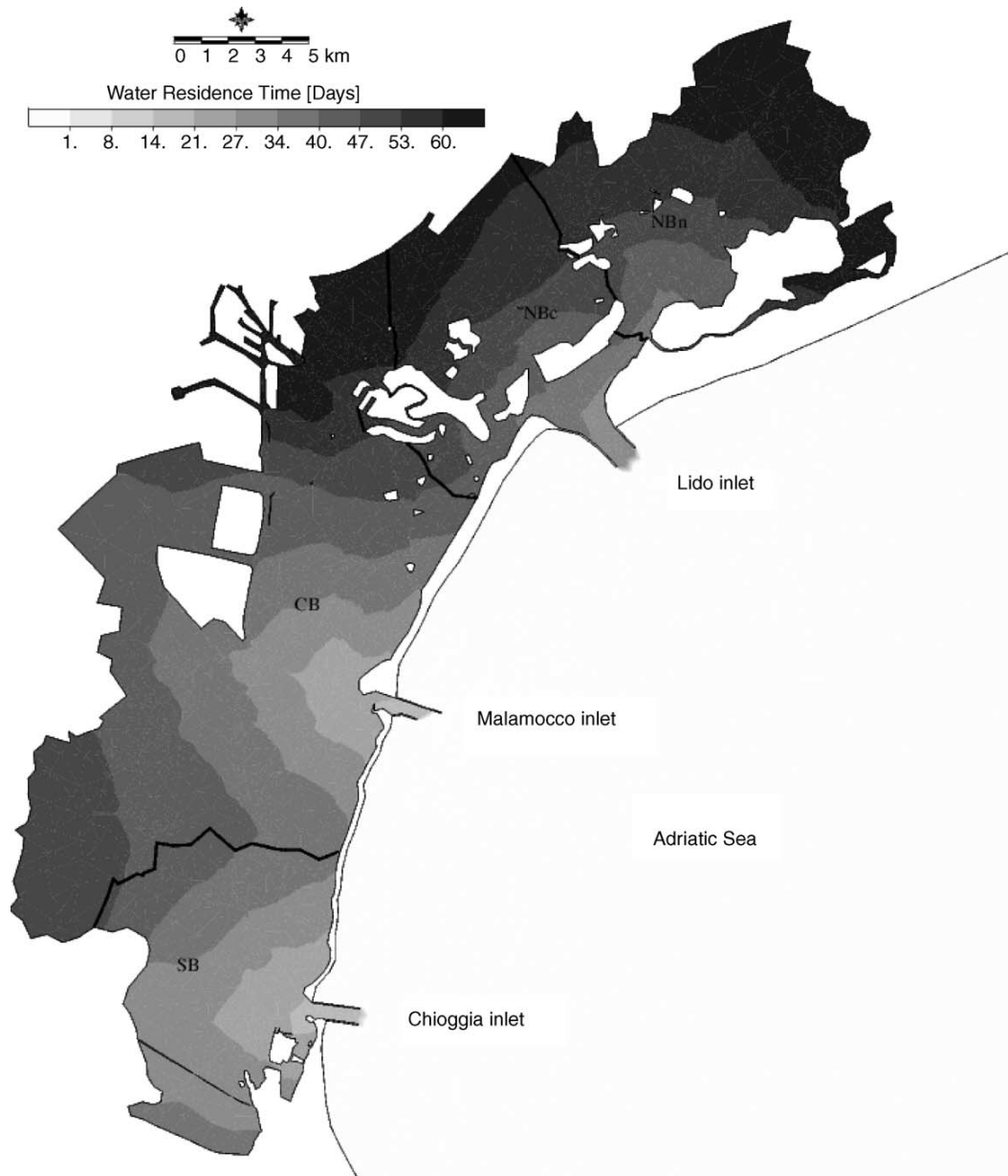
Bathymetry of the lagoon with indication of the ADCP stations (Ferrarin et al. 2009)



Comparison of modeled values and dataset in a specific range (Ghezzi et al. 2010)



Comparison of modeled values and dataset for fluxes at the different inlets (Ferrarin et al. 2009)



Residence time modeled distribution for only tidal forcing (Cucco, Umgiesser 2006)

Bibliography

A finite element model for the Venice Lagoon. Development, set up, calibration and validation (Georg Umgiesser, Donata Melaku Canu, Andrea Cucco, Cosimo Solidoro; Journal of Marine Systems, Volume 51, Issues 1–4, 2004, Pages 123-145)

Shyfer (Shallow Water Finite elements Model) website: <https://sites.google.com/site/shyfer/home>

Modeling the Venice Lagoon residence time (A Cucco, G Umgiesser; Ecological modelling 193 (1-2), 2006, pages 34-51)

Simulating the mobile barrier (MOSE) operation in the Venice Lagoon, Italy: global sea level rise and its implication for navigation (Georg Umgiesser, Bruno Matticchio; Ocean Dynamics volume 56, 2006, pages 320–332)

The effect of wind on the residual current velocities in the inlets of Venice lagoon (I. Mancero-Mosquera, M. Gačić, A. Mazzoldi; Continental Shelf Research, Volume 30, Issue 8, 2010, Pages 915-923)

Temporal variations of water flow between the Venetian lagoon and the open sea (Miroslav Gačić, Isaac Mancero Mosquera, Vedrana Kovačević, Andrea Mazzoldi, Vanessa Cardin, Franco Arena, Giorgio Gelsi; Journal of Marine Systems, Volume 51, Issues 1–4, 2004, Pages 33-47)

Changes in Venice Lagoon dynamics due to construction of mobile barriers, Michol Ghezzi, Stefano Guerzoni, Andrea Cucco, Georg Umgiesser; Coastal Engineering, Volume 57, Issue 7, 2010, Pages 694-708)

Modeling the water exchanges between the Venice Lagoon and the Adriatic Sea (Bellafiore, D., Umgiesser, G. Cucco, A. ; Ocean Dynamics 58, 2008, pages 397–413)

A partition of the Venice Lagoon based on physical properties and analysis of general circulation (C. Solidoro, D. Melaku Canu, A. Cucco, G. Umgiesser, Journal of Marine Systems, Volume 51, Issues 1–4, 2004, Pages 147-160)

Measuring water exchange between the Venetian Lagoon and the open sea (M. Gačić V. Kovačević A. Mazzoldi J. Paduan F. Arena I. Mancero Mosquera G. Gelsi G. Arcari, First published: 03 June 2011)

Freshwater discharge from the drainage basin to the Venice Lagoon (Italy) (Aleardo Zuliani, Luca Zaggia, Flaviano Collavini, Roberto Zonta; Environment International, Volume 31, Issue 7, 2005, Pages 929-938)

The Ecological Implications of Climate Change on the Lagoon of Venice (UNESCO Venice Office and ISMAR-CNR, 2011; D.Tagliapietra et al.)

A low climate threshold for south Greenland Ice Sheet demise during the Late Pleistocene (Irvali, Nil; Galaasen, Eirik V.; Ninnemann, Ulysses S.; Rosenthal, Yair; Born, Andreas; Kleiven, Helga (Kikki) F. (2019-12-18); Proceedings of the National Academy of Sciences. 117 (1): 190–195)

The transient sensitivity of sea level rise (Grinsted, Aslak; Christensen, Jens Hesselbjerg (2021-02-02). Ocean Science. 17 (1): 181–186)

Chapter 2

Conceptual models

In this chapter different schematisations of the problem are studied in increasing order of complexity. The features and the issues addressed give a deeper understanding of the phenomena at play and help to interpret experimental data.

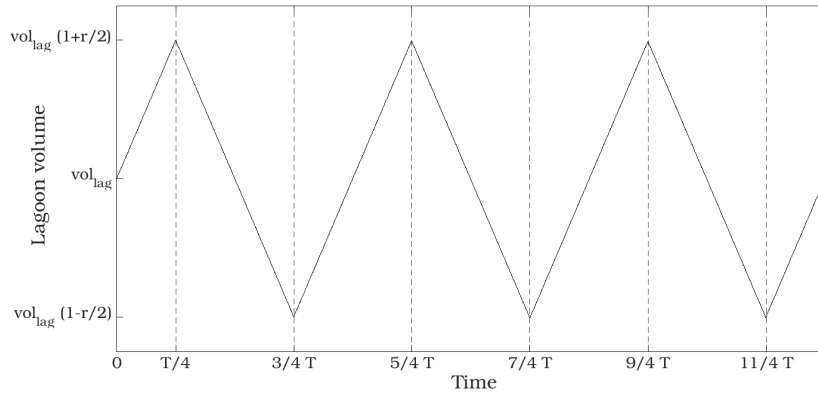
Simplifying the problem

The tidal exchange between the lagoon and the sea could be seen simply as a periodic volume exchange between two water bodies. Every half period $T/2$ a certain portion of the mean lagoon volume $r \text{ vol}_{lag}$ is either added to (inflow phase) or removed from (outflow phase) the lagoon body. The *exchange ratio* r is the ratio between this volume and the mean lagoon volume (vol_{lag}). If a certain tracer or pollutant is added and uniformly spread in the lagoon it is possible to model the concentration decay by making strong but simple assumptions:

- *Perfect mixing*: added water mixes perfectly with lagoon water and concentration is uniform after each step (or even instantly);
- *Perfect mechanism*: concentration does not spread into added water and is selectively removed in outflow phase;
- *Reversed mechanism*: concentration does not spread into added water and added water is selectively removed in outflow phase;

The 'sea' body (with volume $\text{vol}_{sea} = R \text{ vol}_{lag}$) can be temporarily set as infinite ($R = +\infty$) and the assumption of perfect mixing is made for a finite body ($R < +\infty$). The initial conditions are uniform concentration c_0 or 1 (as the problem is found to be self-similar to the case c/c_0) and mean lagoon volume. The inflow phase is chosen as the first one and lasts until $t = T/4$, when the volume reaches the value $\text{vol}_{lag} (1 + r/2)$; then the outflow phase until $t = T/4 + T/2 = 3/4 T$, $V = \text{vol}_{lag} (1 - r/2)$, the inflow phase again until $t = (3/4 + 1/2) T = 5/4 T$, $V = \text{vol}_{lag} (1 + r/2)$, and so on, as a periodical tidal exchange.

The *Reversed Mechanism* accounts for the backflow during outflow phase of newly added water during inflow phase. It is worth noting that the same phenomenon



Lagoon volume over time

happens during inflow phase: incoming water from the 'sea' body could be the same flushed lagoon water in precedent outflow phase. However, as the volume ratio R between the two bodies is significantly high and a circulation flow mixes the sea body in experiments, this second phenomenon is considered negligible and it is not modeled. In fact, the assumption of perfect mixing in the sea body is kept in all models.

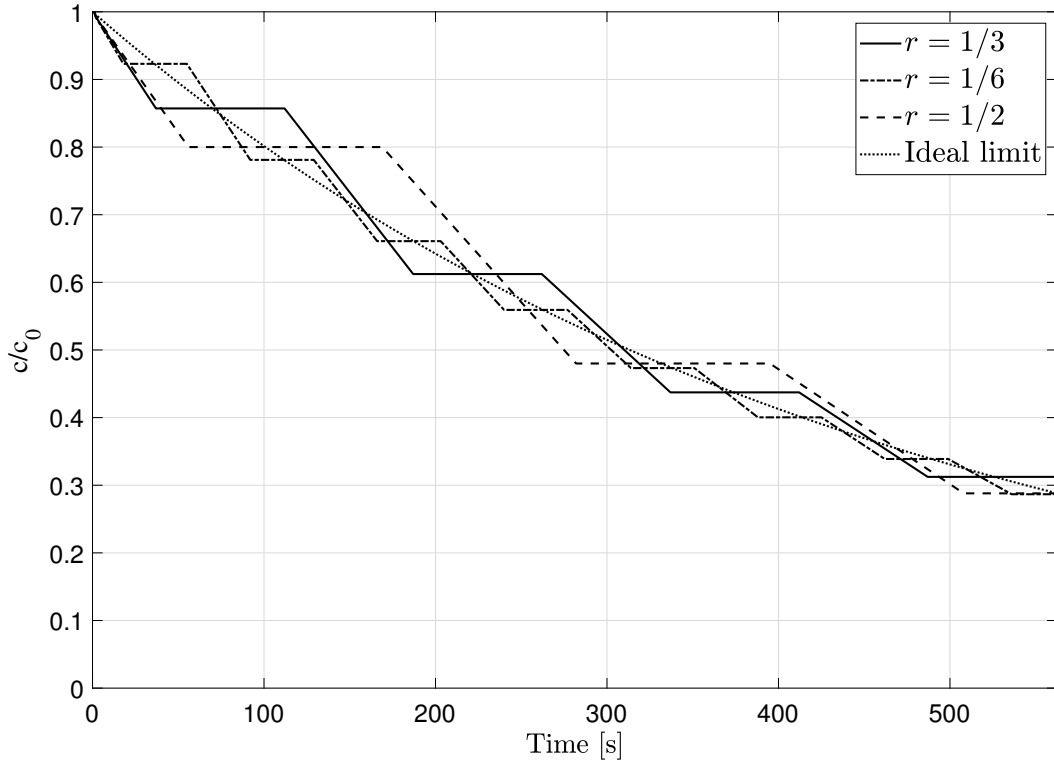
At this stage it does not matter how the volume exchange happens (as long as the periodicity is respected) because the assumptions determine alone the concentration, step by step. However, a simple piecewise linear interpolation can be used to visualise better the behaviour of concentration and volume over time.

Preliminary properties

The main variables of the set problem are the time period T , the exchange ratio r , the initial concentration c_0 , the 'lagoon' volume vol_{lag} and the 'sea' volume vol_{sea} . However, they are not independent: the 'sea' volume can be made dependent on the 'lagoon' volume or assumed infinite and then fixed; even the 'lagoon' volume is not relevant as concentration is defined as a ratio and therefore different volumes with the same exchange ratio show the same concentration decay. For the same reason cases with different initial concentration have the same c/c_0 decay, or, in other words, all problems are self-similar to the c/c_0 case. Therefore, the problem can be seen in terms of c/c_0 , r , T and R in case of finite 'sea' body.

What is more, different cases with the same r/T ratio show a similar behaviour. As r/T represents the exchange rate it can be conjectured that the concentration decay over time depends only on this ratio: different cases with r/T fixed exchange the same amount of volume over a fixed time τ (with respect to corresponding 'lagoon' volume).

If two situations $r_1, T_1, vol_{lag,1}$ and $r_2, T_2, vol_{lag,2}$ are such that $\frac{r_1}{T_1} = \frac{r_2}{T_2}$ after a time $\tau = n_1 T_1/2 = n_2 T_2/2$ ($n_1, n_2 \in \mathbb{N}$) the total exchanged volumes are $n_1 r_1 vol_{lag,1}$



Different ratios comparison over time according to the perfect mixing model ($r/T = 1/450\text{s}^{-1}$ fixed)

and $n_2 r_2 vol_{lag,2}$. Dividing them by their corresponding mean lagoon volume:

$$n_1 r_1 = \frac{\tau}{T_1/2} r_1 = 2\tau \frac{r_1}{T_1} = 2\tau \frac{r_2}{T_2} = \frac{\tau}{T_2/2} r_2 = n_2 r_2$$

As the result holds for any multiple of n_1 and n_2 the two cases are equivalent, and as $T \rightarrow 0$ (and also $r \rightarrow 0$ so that $r/T = 2k$ is constant) the process of exchanging water between the two bodies becomes continuous. Three simple analytic expressions for the three assumptions are derived in the next paragraphs and all three provide the result that dilution depends only on exchanged volume rate and not r or T singularly. Nevertheless, because these hypothesis could be found more difficulty to be valid in reality as periods become shorter and shorter (and ratios smaller and smaller), other parameters and geometry could also play some role.

A simple point to keep in mind is that mean concentration after each inflow phase depends only on the concentration of the introduced 'sea' water and on the concentration resulting from preceding outflow phase. In terms of mean concentration, models differ in the behaviour during outflow phase .

Perfect mixing

The model requires a complete mixing of the lagoon (at each time for a continuous representation): the concentration is always uniform and, as water flows into the lagoon, linearly decays, while in the outflow phase is constant. Concentration c is given as quantity of tracer over volume, and thanks to this modelization it is possible to calculate it step by step. After each inflow phase concentration is given as a weighted average between lagoon concentration of previous outflow phase and entrained water concentration during inflow phase:

$$c = \frac{c_{outflow} vol_{lag,outflow} + c_{sea} vol_{exchange}}{vol_{lag,inflow}} = \frac{c_{out} vol_{lag} (1 - r/2) + c_{sea} r vol_{lag}}{vol_{lag}(1 + r/2)}$$

And then:

$$c = \frac{c_{out} (1 - r/2) + c_{sea} r}{(1 + r/2)}$$

Time	c/c_0	Time	c/c_0	Time	c/c_0	Time	c/c_0
0	1	$1/4 T$	$\frac{1}{1+r/2}$	$3/4 T$	$\frac{1}{1+r/2}$	$5/4 T$	$\frac{(1-r/2)}{(1+r/2)^2}$
$7/4 T$	$\frac{(1-r/2)}{(1+r/2)^2}$	$9/4 T$	$\frac{(1-r/2)^2}{(1+r/2)^3}$	$11/4 T$	$\frac{(1-r/2)^2}{(1+r/2)^3}$	$13/4 T$	$\frac{(1-r/2)^3}{(1+r/2)^4}$

Starting from $t = T/4$ (when $c = 1/(1 + r/2)$) it follows that the concentration after each step i (inflow or outflow phase) is given by:

$$\begin{cases} c_i = c_{i-2} \frac{1-r/2}{1+r/2} \\ c_{i+1} = c_i \end{cases} \quad (2.1)$$

In particular for end of inflow phase values:

$$c(n) = c_0 \frac{(1 - r/2)^{n-1}}{(1 + r/2)^n}$$

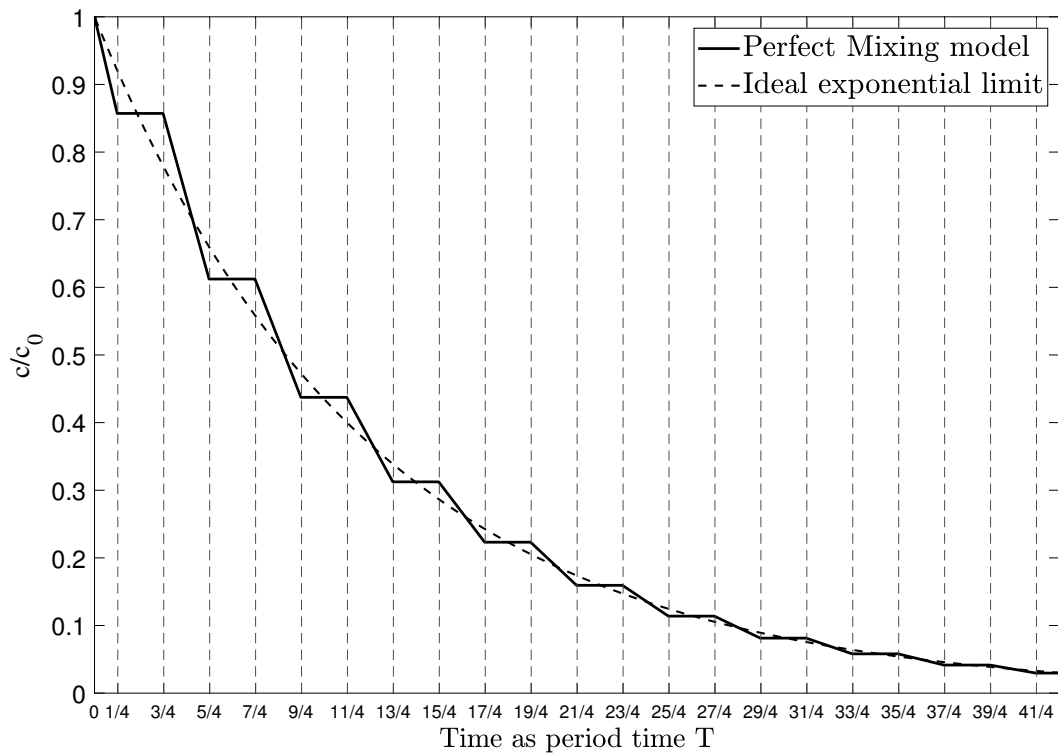
Assuming $c_{sea} = 0$ at any time (infinte 'sea' body), $n \in \mathbb{N}^+$ is the number of the inflow phases and for $n = 0$ $c = c_0$.

The index n is correlated to the times corresponding to end of inflow phases; therefore, taking only those values, $n = t/T + 3/4$. Extending this relation to all times brings to a lower interpolation curve:

$$c(t) = c_0 \frac{(1 - r/2)^{\frac{t}{T} - \frac{1}{4}}}{(1 + r/2)^{\frac{t}{T} + \frac{3}{4}}}$$

Fixing $r/T = 2k \rightarrow r = 2kT$

$$\frac{(1 - r/2)^{\frac{t}{T} - \frac{1}{4}}}{(1 + r/2)^{\frac{t}{T} + \frac{3}{4}}} = \frac{(1 - kT)^{\frac{t}{T} - \frac{1}{4}}}{(1 + kT)^{\frac{t}{T} + \frac{3}{4}}}$$



Concentration over time according to the model ($r = \frac{1}{3}$)

and taking the limit for $T \rightarrow 0$:

$$\begin{aligned} \lim_{T \rightarrow 0} \frac{(1 - kT)^{\frac{t}{T} - \frac{1}{4}}}{(1 + kT)^{\frac{t}{T} + \frac{3}{4}}} &= \lim_{\frac{1}{T} \rightarrow +\infty} \frac{(1 - kT)^{\frac{t}{T} - \frac{1}{4}}}{(1 + kT)^{\frac{t}{T} + \frac{3}{4}}} = \lim_{n \rightarrow +\infty} \frac{(1 - \frac{k}{n})^{nt - \frac{1}{4}}}{(1 + \frac{k}{n})^{nt + \frac{3}{4}}} \\ &= \lim_{n \rightarrow +\infty} \left(\frac{1 - \frac{k}{n}}{1 + \frac{k}{n}} \right)^{nt} \frac{1}{(1 - \frac{k}{n})^{\frac{1}{4}} (1 + \frac{k}{n})^{\frac{3}{4}}} = \frac{\left(\lim_{n \rightarrow +\infty} (1 + \frac{-k}{n})^n \right)^t}{\left(\lim_{n \rightarrow +\infty} (1 + \frac{k}{n})^n \right)^t} \cdot 1 \\ &= \frac{e^{-kt}}{e^{+kt}} = e^{-2kt} = e^{-\frac{r}{T} t} \end{aligned}$$

Having used the limit

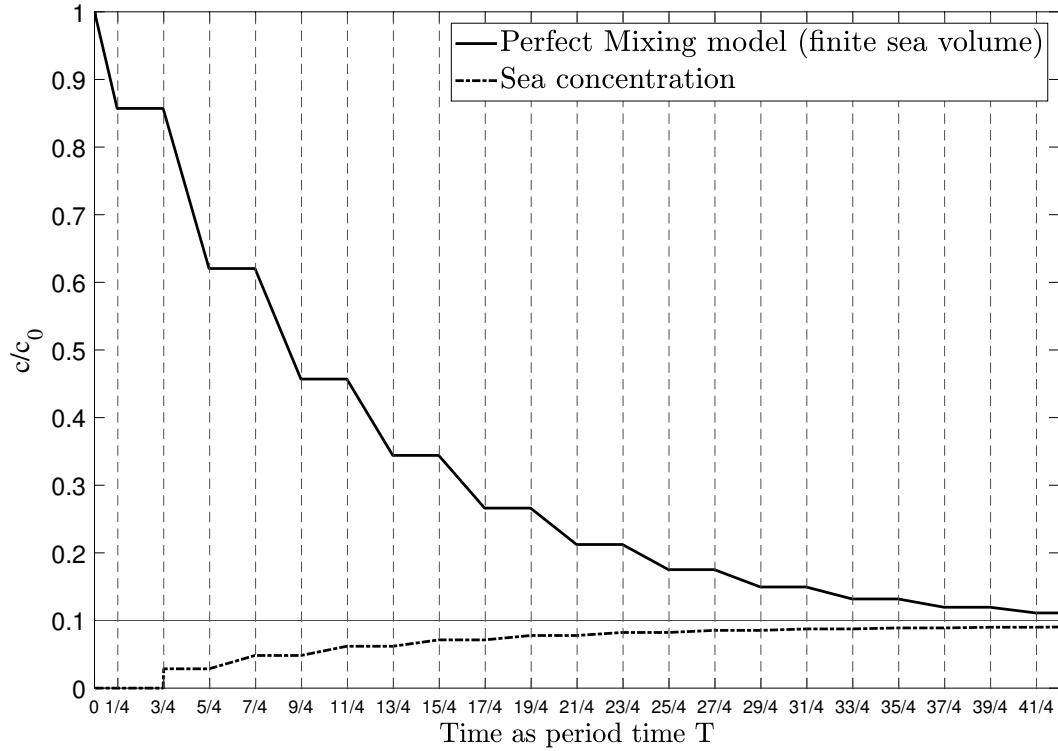
$$e^x = \lim_{n \rightarrow +\infty} \left(1 + \frac{x}{n} \right)^n$$

Therefore, the concentration decay in the perfect mixing model is purely exponential, with the exponent given by the exchange rate r/T .

$$c(t)/c_0 = e^{-\frac{r}{T} t}$$

Corresponding to the law:

$$\frac{dc}{dt} = -\frac{r}{T} c$$



Concentration over time according to the model ($r = \frac{1}{3}$, $R = 10$)

In the case of finite 'sea' body of volume $R vol_{lag}$ the concentration decay can be estimated by:

$$c(t)/c_0 = e^{-\frac{r}{T} t} + 1/R(1 - e^{-\frac{r}{T} t})$$

But this is not exact and a further model could be developed for addressing the case.

Perfect mechanism

In this model there is no mixing between newly added water from the 'sea' body and the lagoon water; concentration is not uniform and the outflow water comes from the fraction with the highest concentration. The model is thought as the most efficient flushing system possible in the limits of the exchange. The concentration decay is treated in terms of mean concentration over the 'lagoon' body and the assumption of infinite 'sea' body is made.

After the first inflow phase the mean concentration is always $c/c_0 \frac{1}{1+r/2}$ in any case, then during the outflow phase only the fraction with the initial concentration is flushed, resulting in a remaining mean concentration of:

$$c/c_0 \frac{1-r}{1-r/2}$$

after the subsequent inflow phase the same volume $vol_{lag}(1-r)$ with original concentration c/c_0 is now a fraction of high tide volume $vol_{lag}(1+r/2)$. Then, after the second outflow, the remaining fraction with the original concentration is $1-2r$. This proceeding brings to:

Time	c/c_0	Time	c/c_0	Time	c/c_0	Time	c/c_0
0	1	$1/4T$	$\frac{1}{1+r/2}$	$3/4T$	$\frac{1-r}{1-r/2}$	$5/4T$	$\frac{1-r}{1+r/2}$
$7/4T$	$\frac{1-2r}{1-r/2}$	$9/4T$	$\frac{1-2r}{1+r/2}$	$11/4T$	$\frac{1-3r}{1-r/2}$	$13/4T$	$\frac{1-4r}{1+r/2}$

In this case of infinite 'sea' body the concentration reaches zero when $1-nr < 0$ with n being some natural number.

In the same way as for the perfect mixing model the mean concentration values are taken after each inflow phase and then extended to all times leading to an upper interpolation curve:

$$\frac{1-nr}{1+r/2} = \frac{1 - (\frac{t}{T} - \frac{1}{4})r}{1+r/2} = \bar{c}(t)$$

The ratio $r/T = 2k$ is fixed and the limit for $T \rightarrow 0$ is taken:

$$\lim_{T \rightarrow 0} \frac{1 - (\frac{t}{T} - \frac{1}{4})r}{1+r/2} = \lim_{T \rightarrow 0} \frac{1 - (\frac{t}{T} - \frac{1}{4})2kT}{1+kT} = \lim_{T \rightarrow 0} \frac{1 - 2kT + \frac{kT}{2}}{1+kT} = 1 - 2kT$$

Therefore the analytical expression for this 'Perfect Mechanism' model is:

$$\bar{c}(t)/c_0 = 1 - \frac{r}{T}t$$

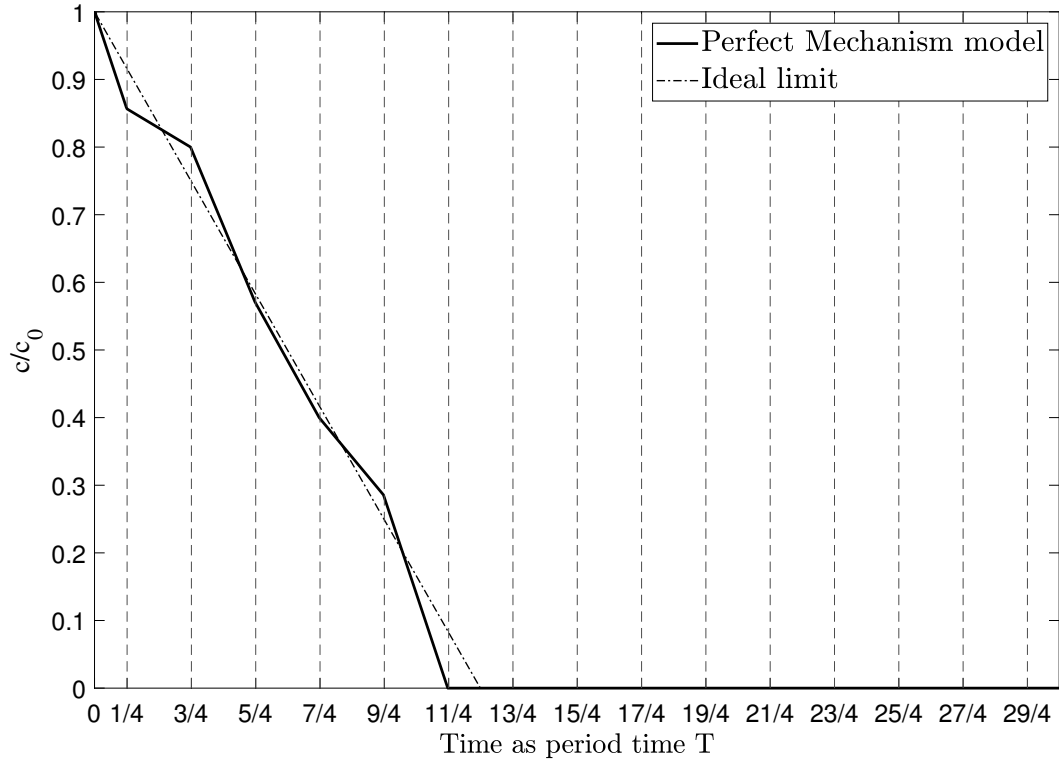
Corresponding to the law:

$$\frac{d\bar{c}(t)/c_0}{dt} = -\frac{r}{T}$$

Reversed mechanism

The model is thought as the most conservative behaviour with practically no concentration decay: newly added water does not mix with present lagoon water and is promptly flushed away in subsequent outflow phase. This model represents well also what happens when 'sea' body concentration reaches values close to the ones of 'lagoon' body concentration.

As in any case the first (half)inflow phase cause a decay from $c/c_0 = 1$ to $c/c_0 = \frac{1}{1+r/2}$, during the first outflow phase the introduced 'sea' volume $r/2 vol_{lag}$ and the 'lagoon' volume $r/2 vol_{lag}$ are removed, $c/c_0 = \frac{1-r/2}{1-r/2} = 1$, then the second (full)inflow phase leads to the minimum value of $c/c_0 = \frac{1-r/2}{1+r/2}$ and this value holds for every inflow phase, alternating with the outflow phase value $c/c_0 = 0$ periodically.



Perfect mechanism model and its ideal analytical limit ($r = \frac{1}{3}$)

Time	c/c_0	Time	c/c_0	Time	c/c_0	Time	c/c_0
0	1	$1/4T$	$\frac{1}{1+r/2}$	$3/4T$	1	$5/4T$	$\frac{1-r/2}{1+r/2}$
$7/4T$	1	$9/4T$	$\frac{1-r/2}{1+r/2}$	$11/4T$	1	$13/4T$	$\frac{1-r/2}{1+r/2}$

Proceeding in the same way as previous models, end of inflow values are extended to the continuous temporal domain, the flushing rate $\frac{r}{T} = 2k$ is fixed and the limit for $T \rightarrow 0$ is taken:

$$c(n) = \frac{1-r/2}{1+r/2} \rightarrow c(t) = \frac{1-r/2}{1+r/2} = \frac{1-kT}{1+kT}$$

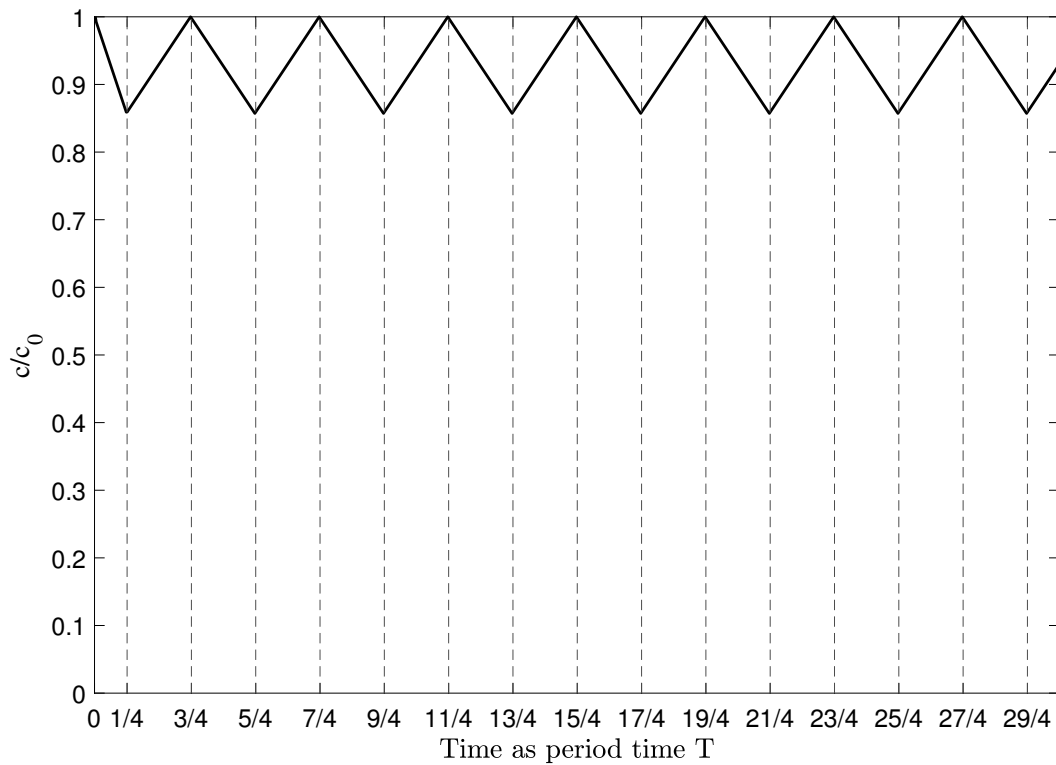
$$\lim_{T \rightarrow 0} \frac{1-kT}{1+kT} = 1$$

Therefore the analytical expression for the model is simply:

$$\bar{c}(t)/c_0 = 1$$

Corresponding to the law:

$$\frac{d\bar{c}(t)/c_0}{dt} = 0$$



Reversed mechanism model

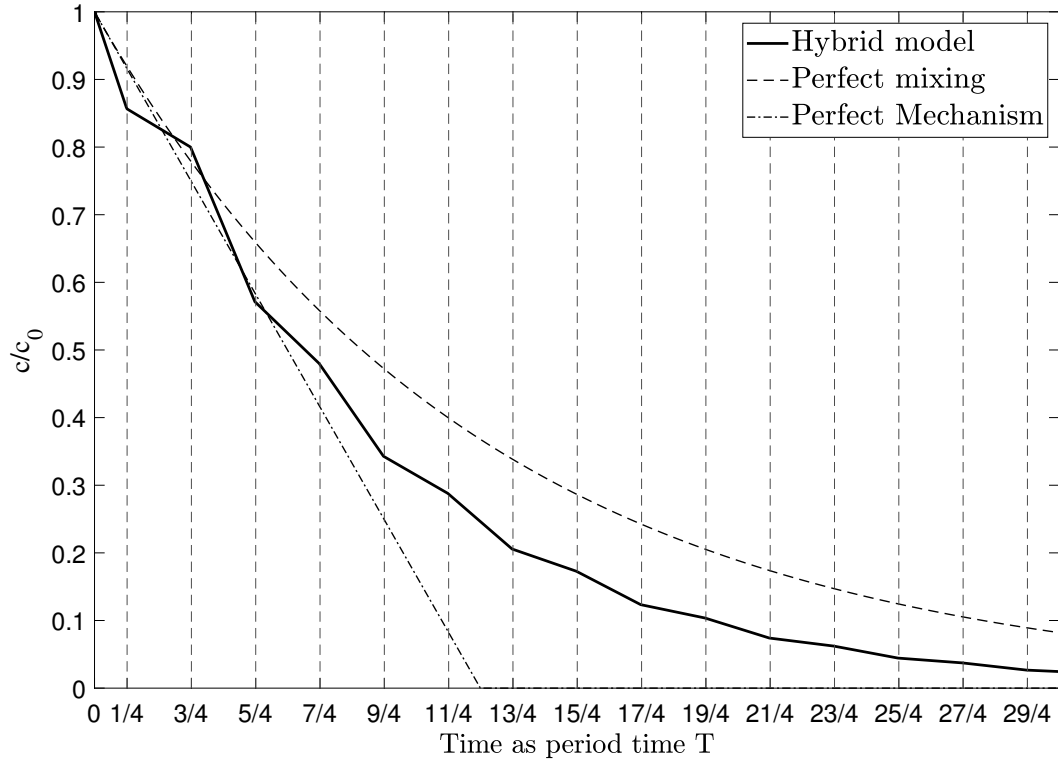
Hybrid model

In this model the combined effect of mechanism and mixing is studied in the most simple way: during the inflow phase the 'sea' water is imagined to be introduced in one half of the 'lagoon' body, there is no mixing between the two parts of the lagoon; during the outflow phase the water is removed from the half with original (and higher) concentration, then, before the subsequent inflow phase, an instantaneous mixing equalises the concentration to the mean value.

It is worth to notice that, despite the quite arbitrary assumption of dividing the lagoon in two equal halves, thanks to the mixing at each period other dividing ratios are equivalent (as long as $r \leq 1/2$). For the sake of simplicity the assumption that $r \leq 1/2$ is made.

After the first (half) inflow phase ($t = T/4$) one half has the same original concentration (and same volume $\frac{1}{2} vol_{lag}$), while the other one is diluted from c/c_0 to $c/c_0 \frac{1 - \frac{1}{2}}{\frac{1}{2} + \frac{r}{2}} = c/c_0 \frac{1}{1+r}$ (volume $\frac{1}{2} + \frac{r}{2}$). The mean concentration is $c/c_0 \frac{1}{1+r/2}$ as in any case. After the outflow phase the concentration in the part with initial concentration is the same but its volume is decreased to $(\frac{1}{2} - r) vol_{lag}$. The mean concentration at $t = 3/4 T$ is then $c/c_0 \frac{1-r}{1-r/2}$.

Fixing the concentration c^* after each mixing and before inflow phase, two step-multipliers can be identified for end of inflow and end of outflow mean concentration:



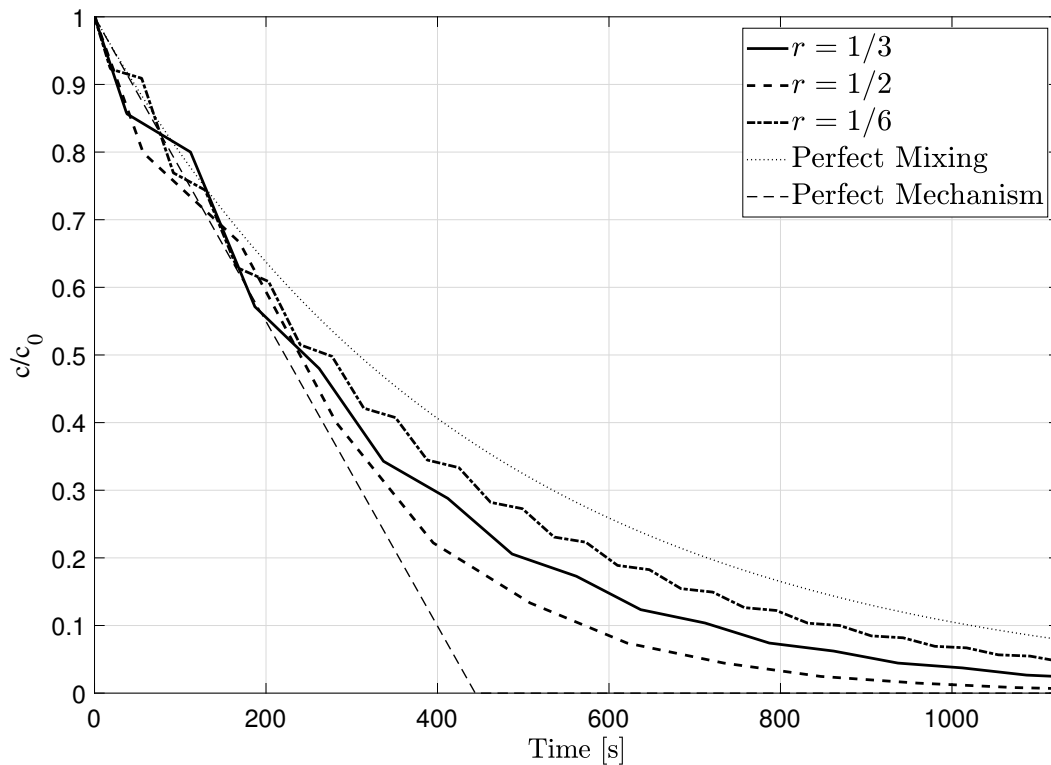
Comparison between hybrid, ideal mixing and mechanism models ($r = \frac{1}{3}$)

<i>Inflow phase</i>	C	END VOLUME	RESULTING C	MEAN C
high concentration part	c^*	$\frac{1}{2}(1 - \frac{r}{2})$	c^*	$c^* \frac{1-r/2}{1+r/2}$
low concentration part	c^*	$\frac{1}{2}(1 - \frac{r}{2}) + r$	$c^* \frac{1-r/2}{1+3/2r}$	
<i>Outflow phase</i>	C	END VOLUME	RESULTING C	MEAN C
high concentration part	c^*	$\frac{1-5/2r}{2}$	c^*	$c^* \frac{1-3/2r}{1-r/2}$
low concentration part	$c^* \frac{1-r/2}{1+3/2r}$	$\frac{1+3/2r}{2}$	$c^* \frac{1-r/2}{1+3/2r}$	

Because the end of inflow mean concentration value is the same as the one of the 'Perfect mixing' case, fixing $\frac{r}{T}$ and taking the limit for $T \rightarrow 0$ brings to the same analytical expression.

This result is not unexpected as complete mixing occurs after each period. However, there is a significant discrepancy between this model and the 'Perfect mixing' one which depends on the ratio r and, therefore, the hybrid decay does not depend on the flush rate r/T alone.

Unluckily, the model is not sufficiently realistic: in experiments the opposite trend is valid because of localisation of entrained water at inlets in lower exchange ratios. In addition to topological features, the "mixing frequency" should be equal for all ratios in order for a proper comparison. However, calibrated adjustments in the subsequent *General Model* do show the validity of the experimental trend.



Comparison between different ratios ($r/T = 1/450 \text{ s}^{-1}$ fixed) - hybrid model

General model

Models and combinations

In the defined conceptual models no hypothesis is made about geometry and actual flow. However, physical models show all three behaviours and inlets configuration in space and time can affect the proportion of each effect outlined in models. If all inlets are open the mixing is enhanced (*all open* combination in experiments), while if only one is open and the lateral position is chosen (*two close* combination in experiments) mixing is diminished and the tendency to exchange the same volume of water (as in the 'Reversed mechanism' model) is present.

Modelling combinations

A basic model has been conceived to account for combination effects in the concentration decay: the lagoon is divided into three parts or sections of equal volume $vol_{lag}/3$ and initial concentration c_0 . Each part is characterized by:

- *position* : position 1 and 3 for lateral parts and 2 for middle one
- *inlet type*: opening combination for infow and outflow phase
- *Composition*: present concentration values at different volumes

Each lagoon section has its own "composition" (different sub-volumes) of different concentration "phases" (different values of concentration resulting from exchange dynamics). The composition is represented in two vectors: a vector for concentration values and a vector for corresponding volumes. The sum of volume components matches the section volume, and the average of concentration values weighted with volume components is the average concentration of the lagoon section.

The opening combinations (inlet *types*) can be classified in:

- *pure inlet*: open during inflow phase, closed during outflow phase, conveniently identified by the vector [1 0]
- *pure outlet*: closed during inflow phase, open during outflow phase, identified by [0 1]
- *active inlet*: open in both phases, identified by [1 1]
- *neutral inlet*: closed in both phases, identified by [0 0]

The symbol convention for the inlets is intuitive: values are booleans identifying open (1) or closed (0) state, the value position represents inflow (first value) and outflow (second value) phases. In the same way combinations are represented by two vectors, one for each phase, where the component order resembles the position of the lagoon parts. For example, a composition of a lateral pure inlet, a lateral pure outlet, and a neutral (closed) inlet in the centre corresponds to:

$$\begin{bmatrix} 1 & 0 & 0 \\ 0 & 0 & 1 \end{bmatrix}$$

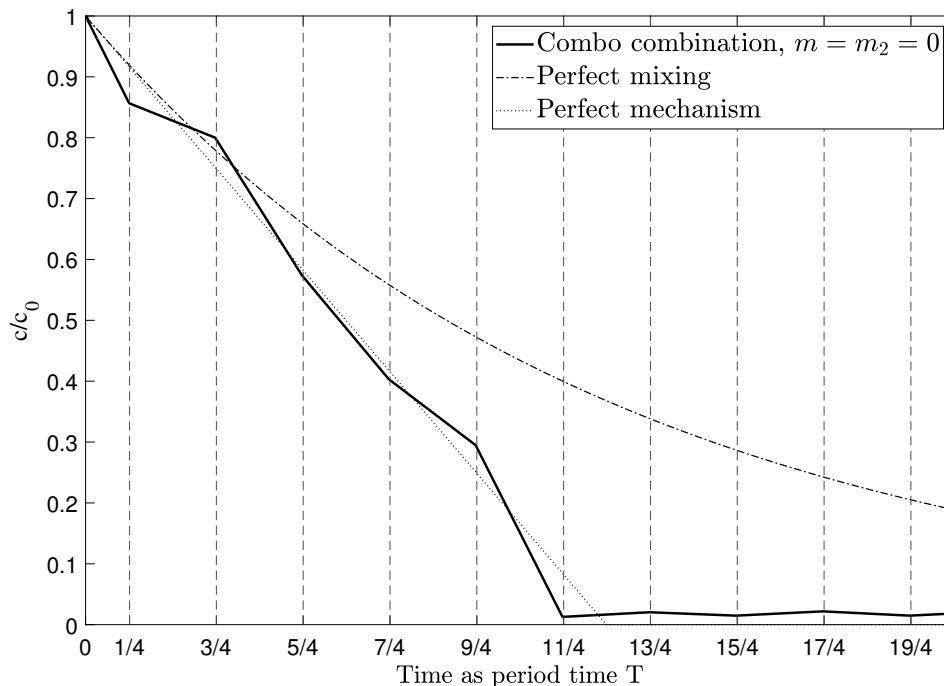
Due to the symmetry setting inlets can be also classified in "lateral" and "central"/"middle" as their position alters the exchange dynamics.

Modelling water exchanges

The tidal exchange involves the inlets open in the corresponding phase (pure inlets in inflow phase, pure outlets in outflow phase, active inlet in both) and the sea body: a volume $r vol_{lag}$ of "sea" water is added to inlets open in inflow phase, then the volume of the three bodies is equalised, the same amount of volume exit from outlets and the lagoon volume is equalised a second time.

The exchange between the three bodies is modeled in three subphases:

- Nonzero net volume (or equalisation) exchanges: volume exchange from open inlets to the rest of the lagoon (after inflow phase) and from the rest of the lagoon to outlets (after outflowphase). The result is volume equalization over the three lagoon bodies.
- Zero net volume (or intermixing) exchanges: volume exchange between neighbouring parts, bodies exchange the same amount of volume with each other but with concentration dependant on their own composition

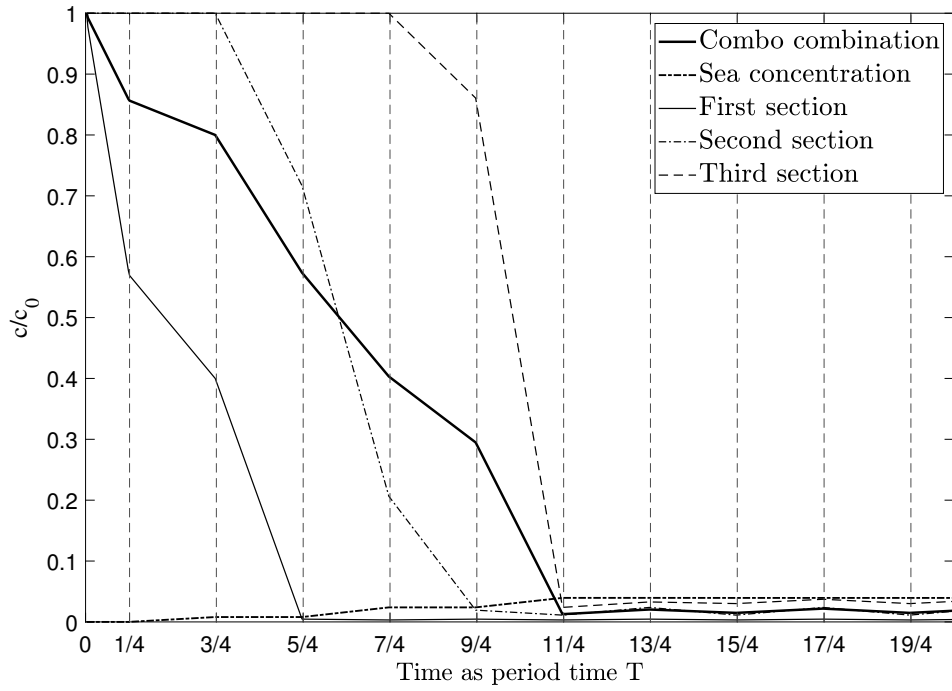


Combo combination reproducing the *Perfect Mechanism* model with $m = m_2 = 0$

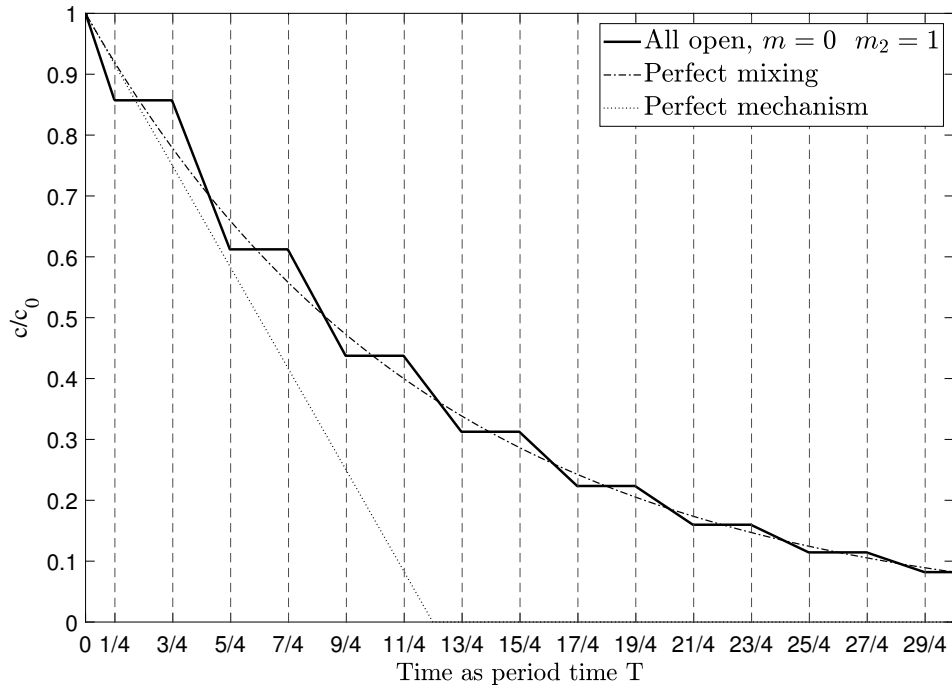
- Internal mixing (or intramixing): a new concentration phase is created as a mean of present concentrations (the overall mean concentration the lagoon section is the same)

The main purpose of the model is to match all previous ideal models with a common general rule. To this purpose exchanges follow an *efficiency logic*: inlets are intended to pass the concentration phase with most concentration ("unclean" water) to outlets and retain the concentration phase with least concentration ("clean" water); the same logic applies for the exchange with the sea basin in the outflow phase. In order to reproduce both the least efficient situation (*reversed mechanism* model) and the most efficient one (*perfect mechanism* model), while representing all intermediate scenarios, an *efficiency coefficient* $m \in [0, 1]$ is defined. Its function is simply to determine the entity of pro-efficiency exchanges and against-efficiency ones: for example, given a generic exchange of volume vol_{ex} , a portion $(1 - m) vol_{ex}$ of the phase with least or most concentration is passed in the view of performing efficiently, while a complementary portion $m vol_{ex}$ is passed against efficiency logic. Therefore, the extreme $m = 1$ matches the reversed mechanism and $m = 0$ the perfect mechanism.

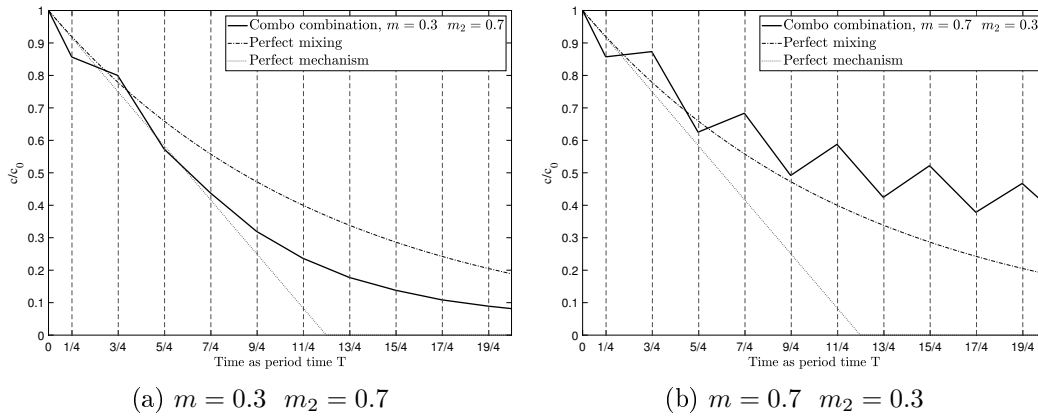
To match the *perfect mixing* model another coefficient $m_2 \in [0, 1]$ accounts for grading the internal mixing in each section: a new concentration phase with the average concentration of the lagoon section, and whose volume is a fraction m_2 of the section volume ($m_2 vol_{lag}/3$), is created. A $m_2 = 1$ scenario matches the perfect mixing case, while a $m_2 = 0$ matches with perfect and reversed mechanism models.



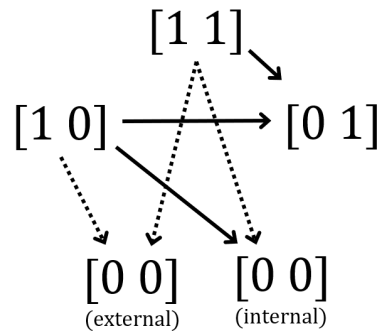
Single sections concentrations in *combo* combination model with $m = m_2 = 0$



All open combination reproducing the *Perfect mixing* model with any m and $m_2 = 1$



Combo combination with different coefficients



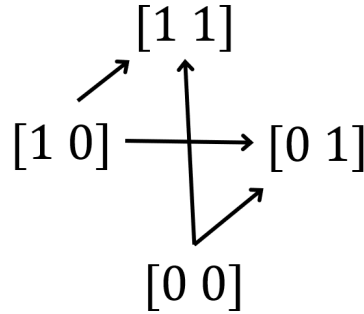
Efficiency logic for inflow phase, equalisation exchanges, most efficient situation presented ($m = 0$). Full line for unclean exchange and dotted line for clean exchange

The efficiency logic

Whether the phase with most concentration or the one with the least concentration is passed is determined by the *efficiency logic*: according to inlets types the logic is to make them flush the most concentration in the $m = 0$ scenario; for example, simple inlets give most concentrated phases to simple outlets while retaining least concentrated ones. The following schemes show the efficiency logic for *nonzero net exchanges* in inflow and outflow phases.

The efficiency logic for *zero net volume exchanges* is very similar to the one for equalisation flows but is more dependant on the topology of the lagoon, i.e. the combination itself with its inlet types in their specific positions. In general simple inlets (type $[1 \ 0]$) and neutral inlets (type $[0 \ 0]$) exchange "unclean" water for "clean" water in the $m = 0$ scenario while simple outlets (type $[0 \ 1]$) exchange clean water for unclean water ($m = 0$); active inlets (type $[1 \ 1]$) tend to act as simple outlets. If a central inlet exchanges water with a lateral inlet of the same type the exchanges can be different according to the third inlet type. The following table covers undetermined cases.

According to the efficiency logic, the volume entity for zero net volume exchanges



Efficiency logic for outflow phase, equalisation exchanges, most efficient situation presented ($m = 0$). Full line for unclean exchange

$$\begin{array}{ll}
 [0\ 0] \xrightarrow{\text{dotted}} [0\ 0] \xrightarrow{\text{dotted}} [1\ 1] & [0\ 1] \xrightarrow{\text{dotted}} [0\ 1] \xrightarrow{\text{dotted}} [1\ 0] \\
 [1\ 0] \xrightarrow{\text{dotted}} [1\ 0] \xrightarrow{\text{dotted}} [0\ 1] & [0\ 1] \xrightarrow{\text{dotted}} [0\ 1] \xrightarrow{\text{dotted}} [1\ 1] \\
 [1\ 0] \xrightarrow{\text{dotted}} [1\ 0] \xrightarrow{\text{dotted}} [1\ 1] & [1\ 1] \xrightarrow{\text{dotted}} [1\ 1] \xrightarrow{\text{dotted}} [0\ 0] \\
 [1\ 1] \xrightarrow{\text{dotted}} [1\ 1] \xrightarrow{\text{dotted}} [0\ 1] & [1\ 1] \xrightarrow{\text{dotted}} [1\ 1] \xrightarrow{\text{dotted}} [1\ 0]
 \end{array}$$

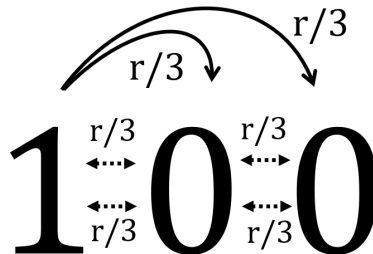
Efficiency logic for intermixing zero-net volume exchanges, most efficient situation presented ($m = 0$). Full line for unclean exchange and dotted line for clean exchange

depends on the combination itself and it represents the volume necessary for moving a volume $r\ vol_{lag}$ of 'unclean' water to outlets in one phase, just as it happens in the *Perfect mechanism* model. For example, in the *combo* combination

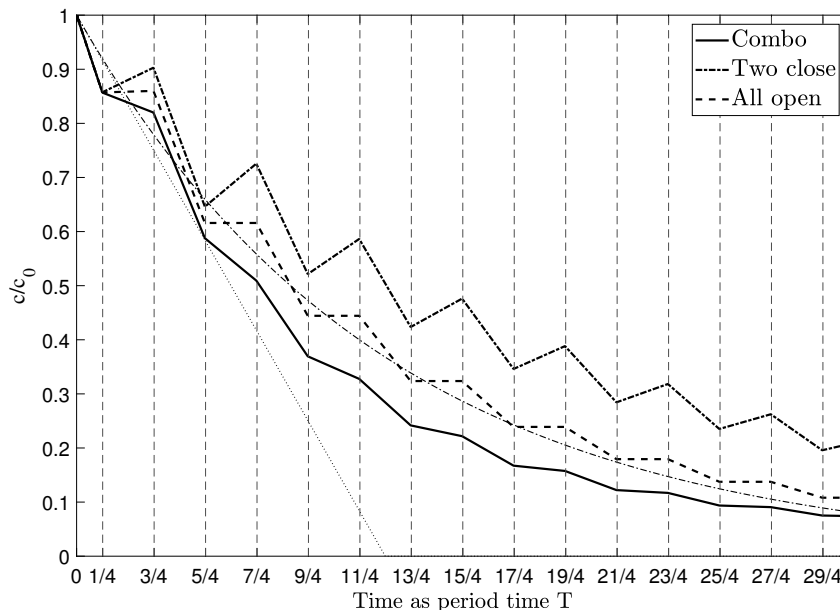
$$\begin{bmatrix} 1 & 0 & 0 \\ 0 & 0 & 1 \end{bmatrix}$$

two zero-net volume exchanges (in addition to equalisation flows) are required to transfer a total amount of $r\ vol_{lag}$ from the simple inlet to the simple outlet. Therefore, the exchange volume for intermixing is $2\ r/3\ vol_{lag} = 2\ ex.vol_{eq}$.

In order to compare different combinations, two coefficients have been defined for the zero net volume exchanges, one for each phase: the coefficients are multipliers



Equalisation (full line) and intermixing (dotted line) flows during inflow phase in *combo* combination



Combo, All open and Two close combinations with $m = 0.45$ and $m_2 = 0.8$

of the exchanged volume

$$\frac{r \text{ vol}_{lag}}{\text{number of inlets/outlets}}$$

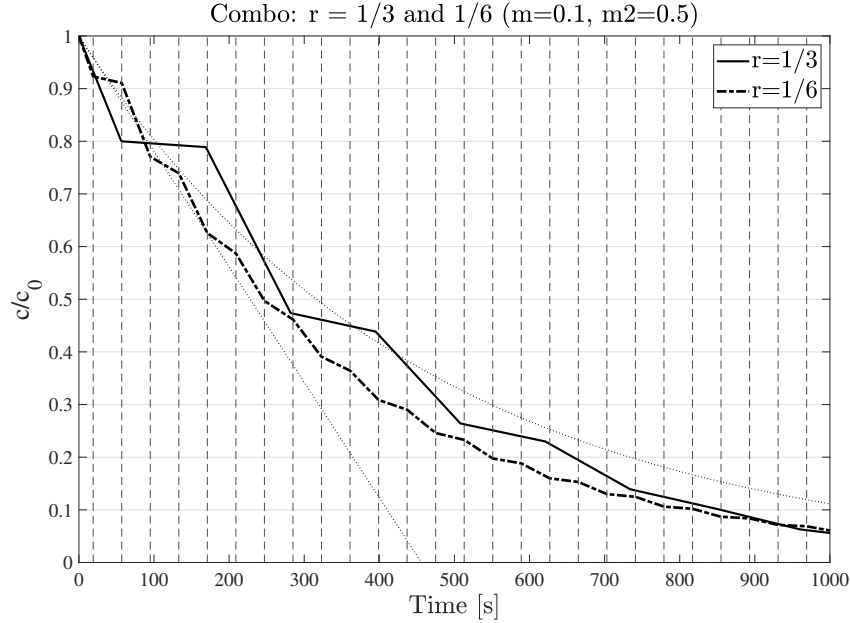
and are assumed to be 1 for inflow phase and 0.5 for outflow phase.

A possible physical model

It is important to notice that, while the efficiency logic addresses the necessity of representing previous models, part of the physical interpretation is lost in its assumptions. A new model which accounts for physical behaviour could be adapted from the one based on the efficiency logic.

Experimental observations

In the effort of connecting the combination general model to the physical phenomena at play in the sea-lagoon basins exchange, it is necessary to point out some observations from physical experiments. Experiments show a jet-like behaviour from inlets for inflow phase and a plug flow towards outlets, with residual inertial effects, for outflow phase. When the jet reaches the opposite wall it divides in two opposite flows along the wall; these two flows tend to turn inward because of velocity gradient across the jet. The rectangular shape of the basin enhances wall effects at the sides, here the flow tends to stop and mixing occurs poorly. The flow of the jet continues during the outflow phase, it adds to the quite uniform plug flow and forms a pattern which is unique to the opening combination.



Varying exchange ratio in the model confirms that lower ratios have better mechanism in artificial combinations.

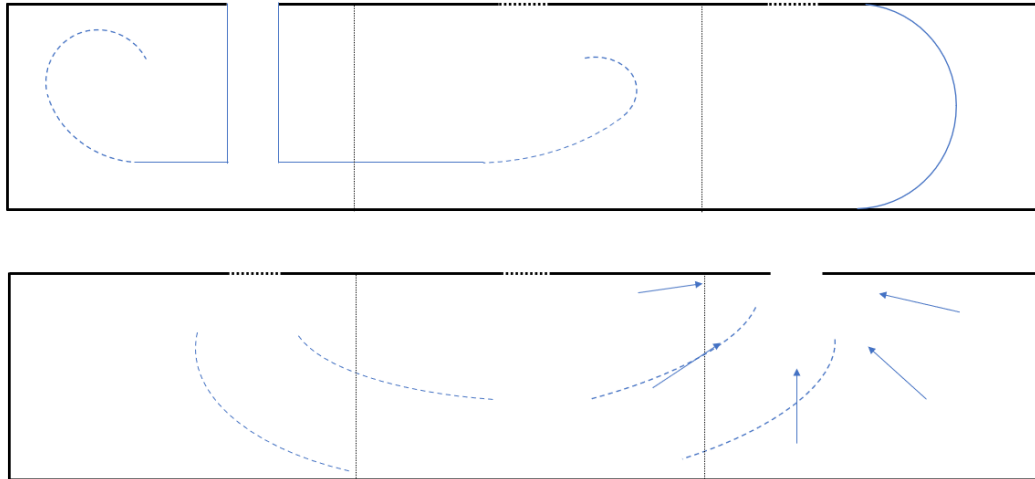
This process forms a natural mechanism internal to the lagoon basin which is influenced by the opening combination; however, it does not adhere to previous ideal models: in *combo* combination the inertia of the jet causes relatively "clean" water to exit instead of closer "unclean" water; in *all open* combination the three jets form rotational cells which push more concentrated water to the openings and at their centres.

Conceiving the model

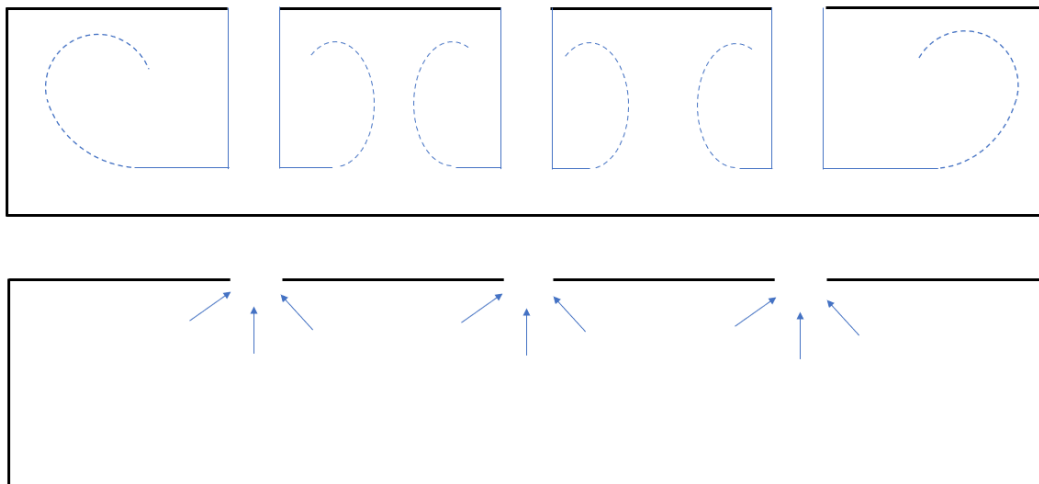
Comparing the main physical features at play with the ones of the model based on efficiency, a new modelisation could be conceived through a specification of efficiency coefficient m and mixing efficiency m_2 : the coefficients now depend on opening combinations, types of inlets exchanging water, their position, and tidal phase. To each combination is assigned a total of 21 coefficients which characterise the opening combination itself from a physical point of view:

- 2 possible equalisation exchanges for each possible inlet (3 possible inlets)
- 2 flow phases
- 3 more coefficients for modulating outflow from the 3 possible outlets
- 3 coefficients as m_2 mixing coefficients specified for each section, in 2 phases

However, some of them are not active as not all section act as inlets or outlets;



Conceptual schematisation of main physical behaviour over the lagoon basin during inflow and outflow phase in *combo* combination



Conceptual schematisation of main physical behaviour over the lagoon basin during inflow and outflow phase in *all open* combination

mixing in the outflow phase can be neglected and some hypothesis can be made based on experimental observations.

For the sake of simplicity, the example of the *combo* combination is taken: intuitively, during inflow phase, at least half of the clean water (as the jet divides in two) is kept in the first section, while the other half is distributed between the other two sections; most mixing occurs in the swirls and therefore the first two sections, while the third section remains less mixed. In the outflow phase, the flow is more uniform and there is less mixing; inertial effects of the inflow jet cause more newly entered sea water to continue its motion close to the outlet.

Nevertheless, the model is still not physical coherent as coefficients act on extreme concentration phases: this is acceptable in first phases, but does not hold in mid-time behaviour, as mean sections concentration are more likely to be exchanged. On top of this modelling issue, which could potentially bring to an overcomplication of the model, the idea of calibrating coefficients with experiments or simulation is quite a challenge.

Chapter 3

Experiments

In this chapter experiments methodology, errors and results are discussed in detail.

Experiments overview

Three series of experiments have been conducted. Each series corresponds to a particular *exchange ratio* between the sea basin and the lagoon one.

Q_{pump} cm ³ /s	Period s	cycles	Ex. vol. cm ³	Tot ex. vol cm ³	Amplitude cm	Ex. ratio	Q_{lagoon} cm ³ /s
545,3	75	30	20450	144000	0,833	0,166	64
545,3	150	15	40900	144000	1,666	0,33	64
545,3	225	10	61350	144000	2,5	0,5	64

The quantity fixed to compare different exchange ratios is the total exchanged volume: in the three different cases the same amount of water is exchanged at the same time but in a different number of cycles, therefore longer cycles correspond to higher amplitude. This condition results in having the same $r/T = 1/450 \text{ s}^{-1}$. The one third ratio scenario is close to the one occurring in the lagoon of Venice.

Initially inlets are closed and some food colouring is spread through the lagoon set at its mean height (5 cm), then experiments begin at inflow phase, just before a high tide, as it could happen in a high tide risk scenario; the exact timing is at the second half of an inflow phase, when sea and lagoon level are the same. Thus the inflow lasts for a quarter of total period T, then the outflow for T/2, the inflow phase for T/2 and so on.

A camera records experiments from above at 1 frame per second. Combinations are implemented by manually switching gates at the right timing.

There are three exchange ratios (0.5, 0.333 and 0.166) and 0.333 ratio has two series, as old0.333 series is more affected by errors. Some experiments have addressed the influence of a large object inside the lagoon, as the city of Venice could be.

These are the main combinations, \updownarrow stays for open in both inflow and outflow phases, – stays for closed, \downarrow for opening in inflow phase and \uparrow for opening in outflow phase:

Allopen	↑	↑	↑	
Oneopen	-	↑	-	
Twoopen	↑	-	↑	
Twoopen lateral	↑	↑	-	
Twoclose	↑	-	-	
Combo	↓	-	-	in
	-	-	↑	out
Badcombo	↓	-	-	in
	-	↑	-	out
Goodcombo	↓	-	↓	in
	-	↑	↑	out
Easycombo	↓	↓	-	in
	-	↑	↑	out
Bigcombo	-	↓	-	in
	↑	-	↑	out
Bigcombo inverted	↓	-	↓	in
	-	↑	-	out
Supercombo	↓	-	-	in
	-	↑	-	out
	-	-	↓	in
	-	↑	-	out
Supercombo inverted	-	↓	-	in
	↑	-	-	out
	-	↓	-	in
	-	-	↑	out

In addition to these 13 combinations, two combinations called *strangecombo* and *strangebigcombo* (one sixth ratio series 0.166) have been implemented in order to investigate the effect of shifting the phase of opening combination with respect to the one of tidal forcing: initially, while the inflow phase lasts until $t = T/4$, the opening configuration is left unchanged until $t = T/2$, when changes to the one it normally should have in the outflow phase. This configuration is then kept both for the second part of the outflow phase and for the first part of inflow phase (which starts at $t = 3/4T$), and then the cycle repeats itself. The resulting flow pattern is quite irregular, thus the appellative "strange".

Closing inlets effect

The flow calibration has been made with open gates but combinations often have only one gate open. The flowrate at inlets and therefore the tide behaviour in the lagoon is different as the inlet total area is just one third of the "all open" case. However, as the flow diminishes, the height gradient increases, and so velocity, readjusting the flow so that water level is even throughout the tank. As this readjustment happens on a much smaller timescale than the one of the tide, the resulting differences induced by closing inlets can be neglected. This also been verified experimentally with a very reduced width: no height differences could be detected with the ruler and thus are well within approximation errors.

The issue addressed in this section is whether closing selectively some inlets (thus reducing flow rate section) causes an important difference in amplitude and phase between the sea basin and the lagoon basin water levels. As combinations need to be compared in the same conditions, underestimating this phenomenon could lead to a systematic error.

Following a simplified approach, water levels of sea and lagoon basins are considered uniform over their respective domains. The velocity at inlets is considered to be some fraction $C_c\sqrt{2g\Delta h}$ (free fall velocity with a correction coefficient C_c) in such a way that the flow rate from the sea to the lagoon is simply:

$$\begin{aligned} Q_{lag} &= \frac{dV_{lag}(t)}{dt} = Area \cdot velocity = n_{inlets} b_{inlet} h_{lag}(t) C_c \sqrt{2g \Delta h(t)} \\ &= n_{inlets} b_{inlet} \frac{V_{lag}(t)}{A_{lag}} C_c \sqrt{2g \left(h_0 + \frac{Q_{sea} t}{A_{sea} + A_{lag}} - \frac{V_{lag}(t)}{A_{lag}} \right)} \end{aligned}$$

where n_{inlets} is the number of inlets, b_{inlet} the inlet width, $h_{lag} = V_{lag}/A_{lag}$ the dimensions of the lagoon basin and Q_{sea} is the fixed flow rate at the opposite side of the lagoon.

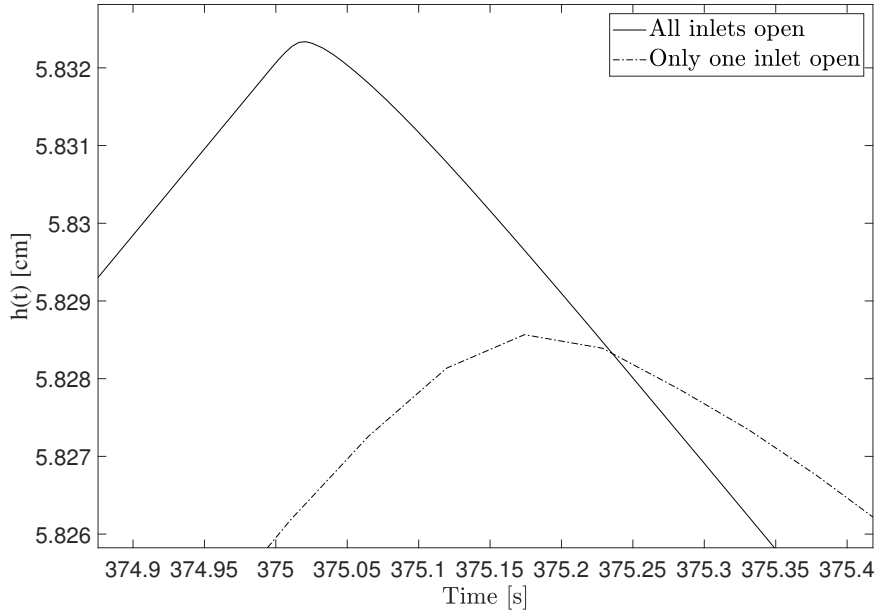
As Q_{sea} switches sign periodically, the equation is in a non-trivial form of non-linear ordinary differential equation. The equation is solved numerically: first considering all inlets open and then only one. Even with a coefficient $C_c = 0.6$ the difference in amplitude is about 0.4 mm, well below the experimental error. In fact, as the ruler sensitivity is 1 mm, no error has been experimentally detected.

The delay of the peak height is about 0.2 s; it is worth noticing that these numbers reflect the model features and not the ones of lagoons in general, where such phenomena are very far by being negligible.

Data processing

Used software: Digiflow and Matlab (to be rephrased)

DIGIFLOW is an image processing tool for fluid mechanics. It provides many features which are specific to fluid flows experimental data acquisition. Coupled with a macro



Comparison between lagoon water level over time in two different scenarios: all three inlets are open, only one inlet is open ($C_c = 0.6$)

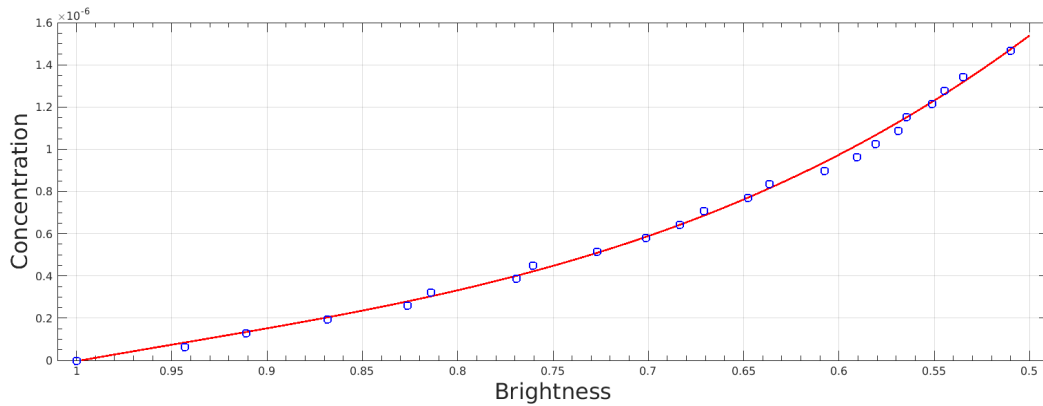
language, it allows to implement user-defined routines to manipulate frames. Videos are intuitively treated as image streams and a graphical user interface makes *DigiFlow* use quick and easy. The manual provides guidance over many issues which arise typically in fluid flows data processing, as the dye calibration addressed afterwards.

MATLAB (matrix laboratory) is a facilitated numerical environment with an intuitive high-level programming language. It comes with many built-in functions and toolboxes for several uses in applied sciences, engineering and economics. Written in *C/C++ language*, it is a commercial software developed by MathWorks and a license is necessary for its use.

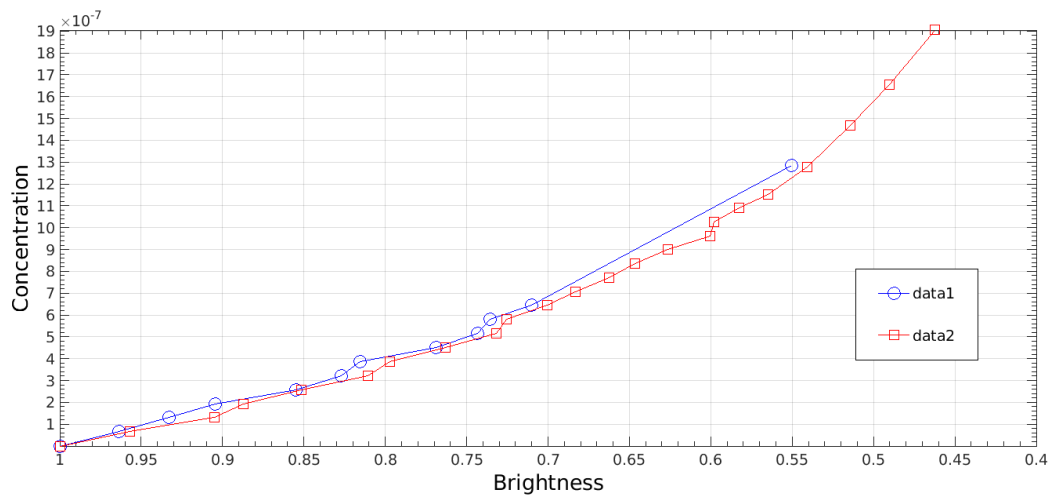
Matrices are the main computation unit in Matlab and are treated in an intuitive way; plotting data, implementing algorithms and even creating user interfaces is made easy with Matlab. It can also interface with other programming languages.

Dye calibration

Experimental data consist in photographic frames taken through a camera: brightness has been correlated to dye concentration thanks to a preliminary dye calibration. This is made through a quite simple process: a known quantity of concentration is dispersed and mixed in the lagoon set at mean height (5 cm), mean brightness is then correlated, and then another quantity is added and mixed in the lagoon, giving another sample of the concentration-brightness relation. Because of worries about the influence of environmental lighting the process was repeated and no significant



Concentration against brightness relation



Comparison between the two data collections series, *data2* is not influenced by environmental lighting

difference was found.

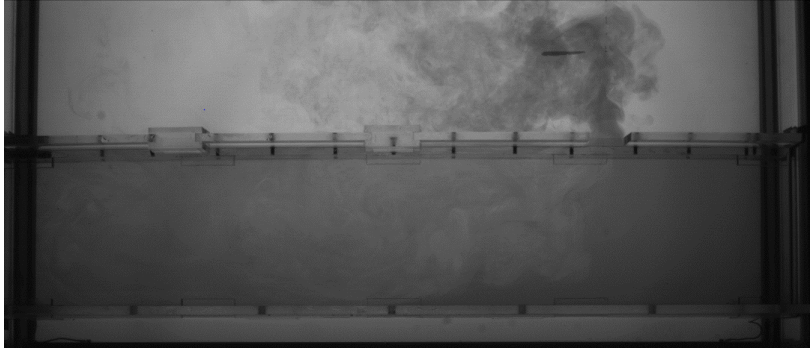
The most appropriate fitting was cubic:

$$c(b) = -8,6433 \cdot 10^{-6} b^3 + 2,4568 \cdot 10^{-5} b^2 - 2,4812 \cdot 10^{-5} b + 8,8835 \cdot 10^{-6}$$

the relation is then inverted and used to convert brightness pixel information in integrated concentration. Change in lagoon height does not seem to affect the relation.

Height change correction

Dye calibration is strictly valid at mean lagoon height of 5 cm; thus, every half-period $T/2$. For higher water levels, as in the second half of inflow phases or the first part of outflow phases, concentration appears to be higher than the actual value; conversely for lower water levels in the lagoon basin, as in the second half of



Raw image

outflow phases or the first half of inflow phases, concentration appears to be lower than the actual value.

Without going into the details, the law of attenuation for monochrome light passing in the z direction through the dye is:

$$\frac{di}{dz} = -\alpha c i$$

where i is the light intensity, c the concentration of dye, and α depends on the colour of the dye. Assuming the rays to be parallel to the z -direction, the intensity of light at the camera is:

$$i_C = i_0 \exp(-\alpha \int c dz) = i_0 \exp(-\alpha \bar{c} H)$$

where \bar{c} is the mean concentration along the ray connecting observation point and camera, and $H(t)$ is the water level. Knowing concentration values at mean height \bar{H} from the calibration phase, an apparent value of concentration $c_{\bar{H}}$ is given; then, equaling light intensity for mean height and for different height:

$$c_{\bar{H}} \bar{H} = c^* H(t) \quad \rightarrow \quad c^* = \frac{\bar{H}}{H(t)} c_{\bar{H}}$$

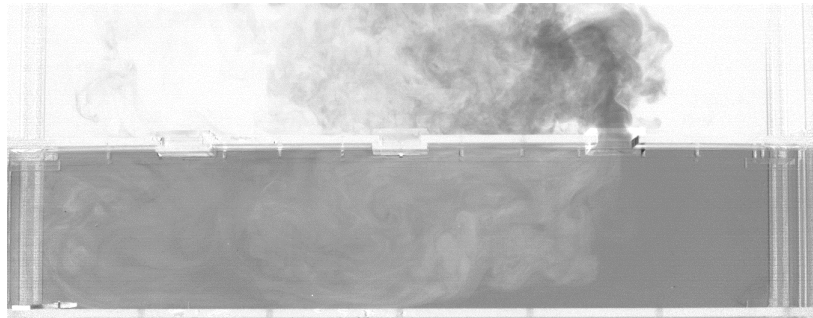
where $c_{\bar{H}}$ is the apparent concentration as calibrated for \bar{H} and c^* is the actual concentration.

An example of experiment data processing

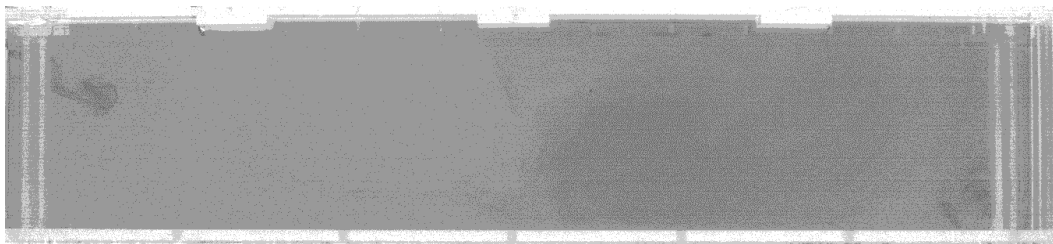
The followed example is the *combo* experiment from the 0.333 ratio series.

Firstly we consider the .dfm digiflow file with all frames captured by the camera at 1 fps (so the frame index is also the time passed in seconds) and we apply the correction with the background image. The correction is simply a division of image brightness values with the background image ones, pixel by pixel.

From the experiments record we know that experiment was performed on 17th august, frame for defining the region is 378, the experiment starts at 379 and finishes at 2939 with 3600 total frames.



Corrected image



Background image

Then thanks to the correlation between brightness and dye concentration (found in the calibration experiments) the frames are converted in concentration data. The concentration data are then processed obtaining:

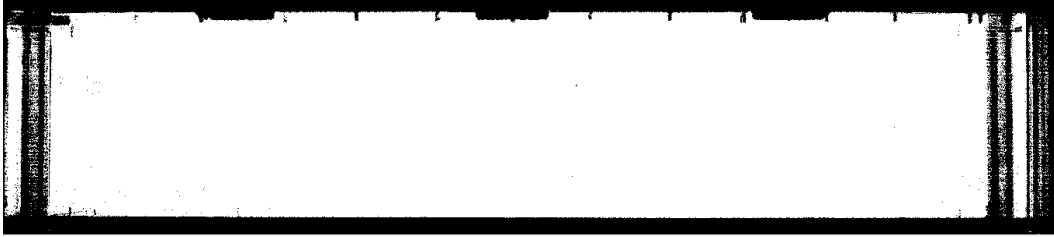
- Mean concentration over the lagoon (over the significant region) over time
- Frequency histogram over time
- Standard deviation (and then normalized standard deviation) of the concentration distribution over the lagoon over time

This is one example (from easycombo experiment same series) of how the region is defined: once the initial dye has been mixed before the experiment and is approximately uniform, the region over which computations are made is defined as the 80 % of the lagoon image for which the concentration is closest to the most frequent value of concentration;

Then over this region the concentration distribution data are processed

Matlab functions

Data in Digiflow format have been read and converted in Matlab. Then average, histogram and percentiles have been calculated for each experiment. Matlab is also used for most of the graphs and visualisations.



Region matrix in Matlab

Errors

Experiments are intrinsically affected by errors, as it is not practically possible to set ideal conditions in reality. However, it is possible to assess their nature and influence, gaining a precious perspective and interpret data consequently. In this section error sources are studied and an estimation on their relative importance is given.

Volume concentration as mass proportion

Food colouring concentration is given as mass proportion but then is treated as volume concentration: concentration estimation is not made by measuring mass but looking at water level in a graduated cylinder, with the further issue of the meniscus formation (this can be easily verified through the brightness-concentration relation). However, food colouring density is very close to water density and luckily the error is not important. Moreover, looking at normalised concentration $c(t)/c_0$ (where c_0 is the initial concentration) avoids completely its relevance.

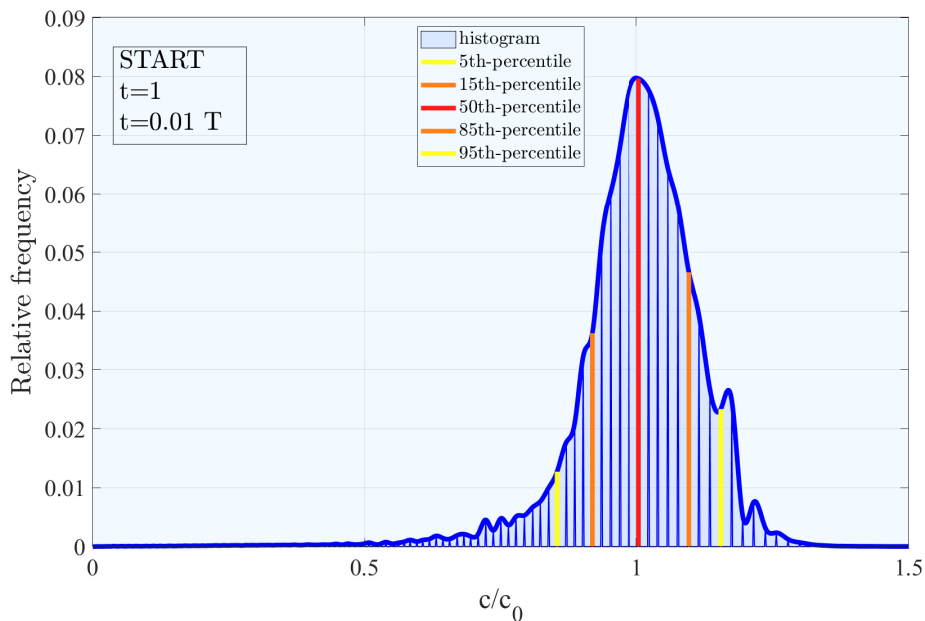
Initial distribution

This is the concentration frequency distribution at time 378, so just before the experiment, when ideally it should be a spike at $1.29 \cdot 10^{-6}$ (or 1 in the case of normalised concentration). As the dye is well mixed over the lagoon the influence of some local variability is probably negligible and not predictable.

Second reservoir exchange

In experiments the implementation of a periodical flow made an exchange reservoir necessary. This introduces a non-linear boundary condition for concentration, a decay term located opposite to lagoon inlets.

This decay happens far from inlets and, creating a small concentration gradient, propagates to the lagoon. Intuitively it is relevant only at later times, when concentration tends to plateau to a homogeneous distribution. The asymptotic concentration can be estimated from 5th percentiles; this value varies from 3 to $5 \cdot 10^{-8}$ approximately (or 0.025-0.04 in normalised terms). This variation can be partly explained by the influence of dilution in the second reservoir, which seems to happen



Histogram at beginning (normalised concentration), experiment *supercombo*, *1/6 series*

more in the 0.5 series. The second reservoir volume has not been fixed in different tide calibrations; however, the resulting effect is minimal affects only the very last stage of experiments.

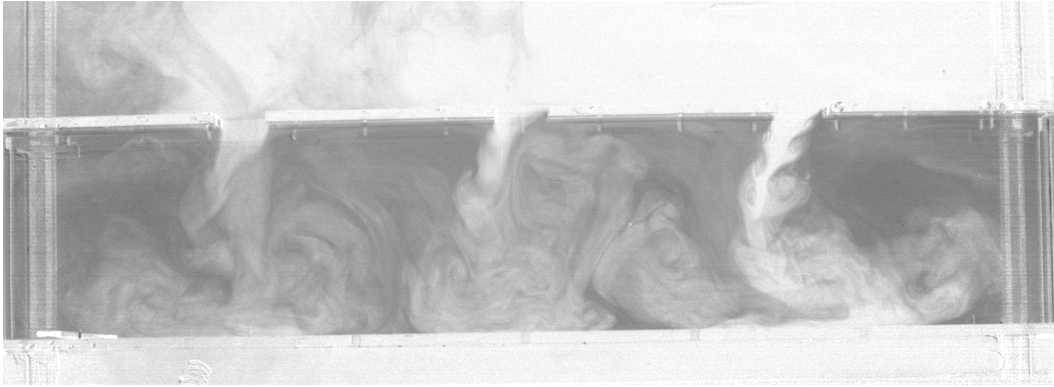
Circulation in sea part

A rotatory circulation outside the lagoon structure forms affecting entrance and exit exchange angles. An angle between the structure and the sea basin enhances this phenomenon which affects greatly several experiments from the *old0.33* series. The dye tends to accumulate on one side of the sea basin and the angle of the jets modify the combination pattern. In addition to these phenomena, an enhanced ventilation can result in enhanced exchange ratio, in a way that is not beneficial to concentration decay.

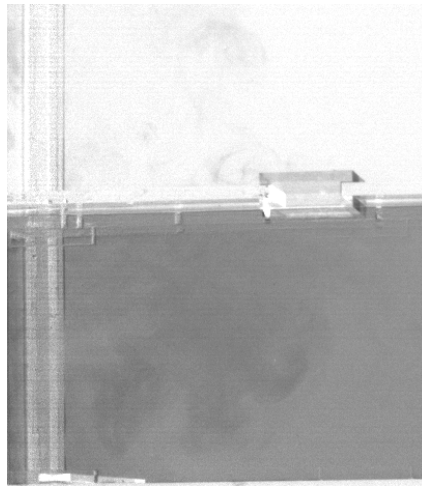
Leaking

Especially in first experiments, an inadequate sealing of lagoon structures sides causes some dye leaking in between lagoon structure and tank. Leaked dye can diffuse in a shadow below lagoon structure and then mask concentration decay. As water levels are equalised the leaking stops and the effect fade thanks to leaked dye dilution.

The issue is still present in other series, especially the *0.5* series, and it will be partly correlated to the r_1 coefficient defined later in the *Errors* section. The error



combo from old0.33; inclination generates an additional circulation which affects concentration decay



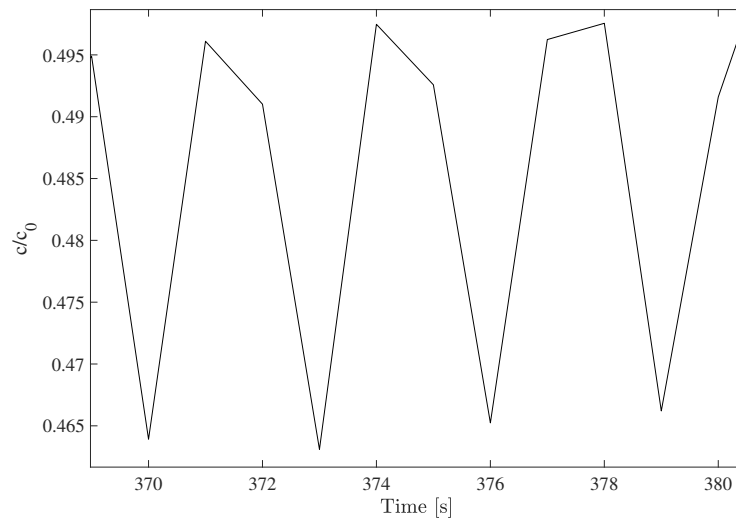
combo from old0.33; leaking dye in the sea basin and below lagoon structure (as a shadow) before experiment start

can be quite significant, as concentration is maximum at the beginning and even small flows can affect it, rapidly changing initial concentration and shifting down the concentration decay curve.

Leaking has been avoided as much as possible but it may still explain a great part of errors which unfortunately affect experiments.

Additional asymptotic concentration

As in the leaking phenomenon, dye can accumulate below lagoon structure over time and thus create the effect of additional concentration. The error is in the order of $4 - 8 \cdot 10^{-8}$ and varies slightly from one experiment to another. The error influence is limited to later times.

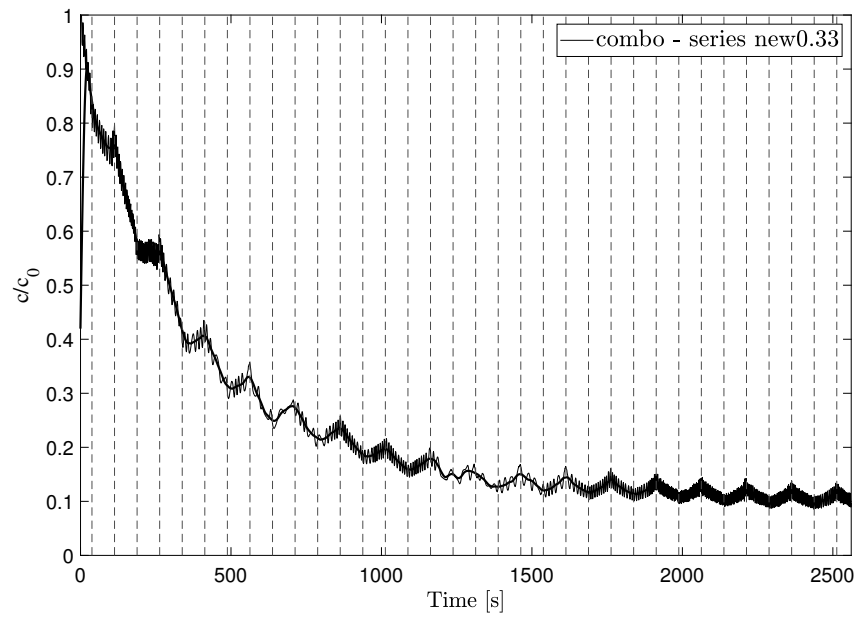


Concentration fluctuation of about $4 \cdot 10^{-8}$ (or $0.03 c_0$) over a period of 3 s

Backlighting

Data have a systematic fluctuation of about $4 \cdot 10^{-8}$ (or $0.03 c_0$) over a period of 3 s. This fluctuation is most probably caused by the backlighting conditions and has no influence on average.

For better readability, some graphs show smoothed data, treated with a mobile average.



Example of data fitting by filtering high signal frequencies

Bubbles

Cavitation is a natural unavoidable process and different factors play a role in it: rapid decreases of depression, temperature and air saturation in water. All three elements are present in experimental conditions; water below the lagoon structure has a delayed response to tidal forcing and during outflow phase is in depression. This effect alone is rather small and a high saturation of the water, replaced and freshly introduced before each experiment, could trigger the process, together with a small temperature increase due to lighting lamps. The phenomenon, even if forced very weakly, sums up over time (about forty minutes) and produces a uniform layer of small bubbles, entrapped below the lagoon structure.

The process results in an additional false concentration in the order of 10^{-8} , bringing little influence to overall experimental errors.

Change of amplitude over time and estimated ratios

From the *Conceptual Models* chapter a simple property of average concentration over time is known: the average concentration after each inflow phase is independent of particular combination and must be in any case

$$c_2 = \frac{c_1 (1 - r/2) + c_{sea} r/2}{1 + r/2} \approx c_1 \frac{1 - r/2}{1 + r/2}$$

where c_1 is the concentration at the end of each outflow phase and c_{sea} is the concentration present in the sea basin.

Given the experimental data, it is possible to invert this simple relation in order to determine the *exchange ratio* r and estimate the error made on the tide forcing simulation and how reliable are data in general.

$$r^* = 2 \frac{c_1 - c_2}{c_1 + c_2 - c_{sea}} \approx 2 \frac{c_1 - c_2}{c_1 + c_2}$$

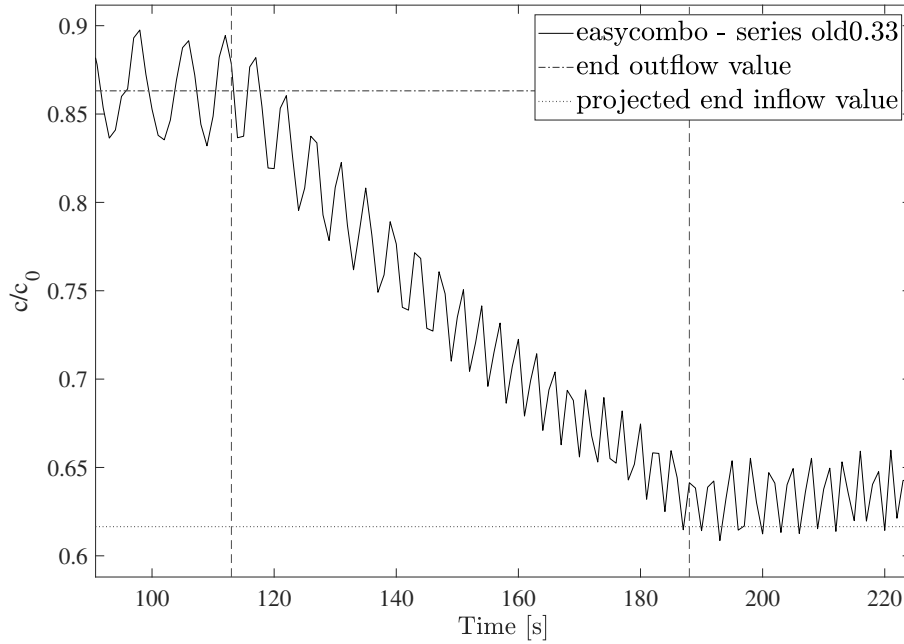
where c_1 is the concentration at the end of the outflow phase and c_2 the concentration at the end of the inflow phase.

c_{sea} is not known in the experiments and could be estimated in

$$c_{sea} = (1 - c_1) \frac{1 - r/2}{R} \approx \frac{1 - c_1}{R}$$

where R is the volume ratio between the sea basin and the lagoon basin ($R \approx 25$) and the hypothesis of perfect mixing in the sea basin is made. The contribution of the estimated c_{sea} is very small and can be neglected. Nevertheless, higher values of sea concentration could be present locally and affecting the concentration decay in the lagoon.

In the figure example, taking the two experimental values results in an exchange ratio $r^* = 0.303$ instead of 0.333 . However, the procedure is not meant to be precise and other errors play a role in creating this discrepancy.



Projected value at the end of inflow and experimental data (neglecting c_{sea})

The estimated ratio is a tool to assess reliability of single experiments: in each graph two exchange ratios, r_1 for the initial half inflow phase, and r_2 as an average of subsequent inflow cycles, are given. A higher ratio at the beginning (high r_1) could lead to an overestimation of the decay, while a higher ratio at later cycles (high r_2) seems to have the opposite effect. The two ratios act as *reliability coefficients* and depict well the inadequacy of some initial experiment in the *old0.33* series due to leaking.

The coefficients should not be seen as a source of information of the actual ratio, as different errors play a role in determining the decay and a small difference in ratio may not denote any error. For example, the correction for the height variation in the brightness-concentration relation has a major influence on values at switching phase times. Estimated ratios vary and the ratios for the taken example (*easycombo* from series *old0.33*) are:

$$r'_1 = 0.336; \quad r'_2 = 0.303; \quad r'_3 = 0.303; \quad r'_4 = 0.326 \quad r'_5 = 0.289; \quad r'_6 = 0.236;$$

Backlight variation, leaking, height correction, accumulation of dye close to inlets and circulation, definition of the averaging region, shadow of moving gates at switching times: many factors could affect the estimated ratios. Nevertheless, as *reliability coefficients* they are in perfect accordance with the graphs, especially the mean concentration decay, giving precious information about the distance between experimental and ideal conditions.

old0.33	r_1	r_2	new0.33	r_1	r_2
all open	0.34	0.29	allopen	0.31	0.26
badcombo	0.22	0.32	badcombo	0.47	0.30
combo	0.70	0.42	combo	0.45	0.28
easycombo	0.34	0.27	easycombo	0.30	0.27
oneopen	0.71	0.57	oneopen	0.34	0.26
goodcombo	0.28	0.23	supercombo	0.31	0.31
twoclose	0.92	0.40	supercombainverted	0.32	0.27
twoopen	0.44	0.53	twoopen	0.45	0.29
twoopen lateral	0.37	0.30	twoopen lateral	0.42	0.29
0.166			twoopen2	0.30	0.24
allopen	0.22	0.12	twoopen3	0.34	0.24
allopenagain	0.18	0.15	twoopen mystery	0.28	0.25
allopen withskip	0.16	0.12	0.5		
bigcombainverted	0.14	0.15	allopen	0.64	0.39
badcombo	0.12	0.15	badcombo	0.04	0.49
combo	0.22	0.15	combo	-0.01	0.40
combo25	0.19	0.17			
strangecombo	0.12	0.15	bigcombo	0.50	0.42
strangebigcombo	0.11	0.15	bigcombo actual	1.06	0.59
bigcombochange	0.19	0.15	easycombo	0.40	0.36
easycombo	0.21	0.13	goodcombo	0.68	0.38
goodcombo	0.10	0.15	oneopen	0.48	0.41
oneopen	0.21	0.15	supercombo	0.03	0.42
supercombo	0.20	0.15	supercombainverted	0.46	0.32
supercombainverted	0.19	0.16			
twoopen	0.16	0.26	twoopen lateral	0.27	0.45
twoopen lateral	0.17	0.23	twoclose	0.16	0.44
twoclose	0.22	0.16	cuttwoclose	0.18	0.39
twoclose withmylittleskip	0.15	0.17			
combohalfc0	0.09	0.16			

Results and comparisons

There are about 55 experiment runs; for each, average, histogram, standard deviation and percentiles have been calculated. The resulting graphs have been compared, accounting as far as possible for experimental errors. Unluckily, even if some conclusions can be drawn from comparisons, they are not always confirmed by data and validity ranges could be smaller than experimental uncertainties.

First it is shown an example of data graphs to get familiar to the main features of experiments; then it is discussed how experimental data compare with the conceptual models drawn in the second chapter. This analysis is completed by some examples of combination flow patterns. Having outlined the most important factors in determining data variation, all experiments are thus compared to each other thanks to four standardised coefficients:

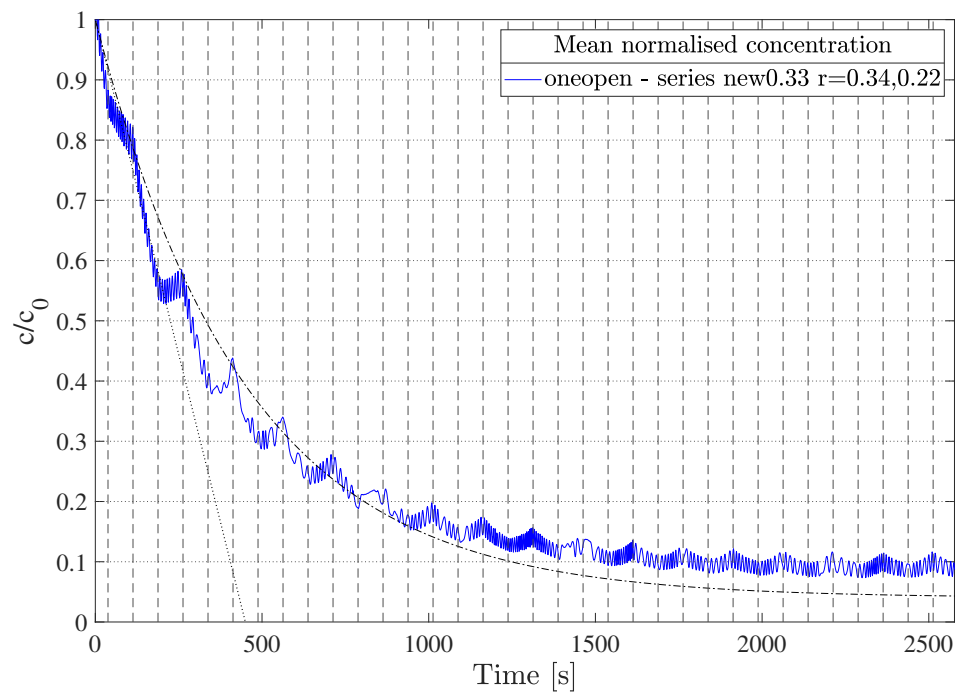
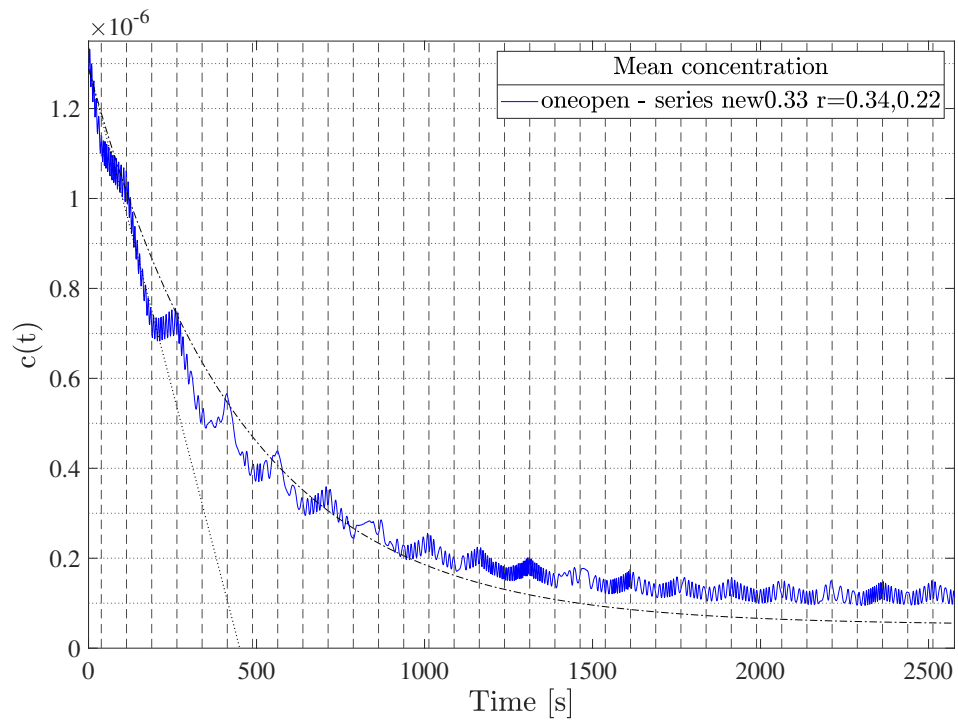
- Average mean normalised concentration \bar{c}_{956} in first 956 s
- Average normalised standard deviation $\bar{\sigma}_{N,956}$ in first 956 s
- Average 50th percentile 50^{th}_{956} of normalised concentration frequency distribution (in first 956 s)
- Average 95th percentile 95^{th}_{956} of normalised concentration frequency distribution (in first 956 s)

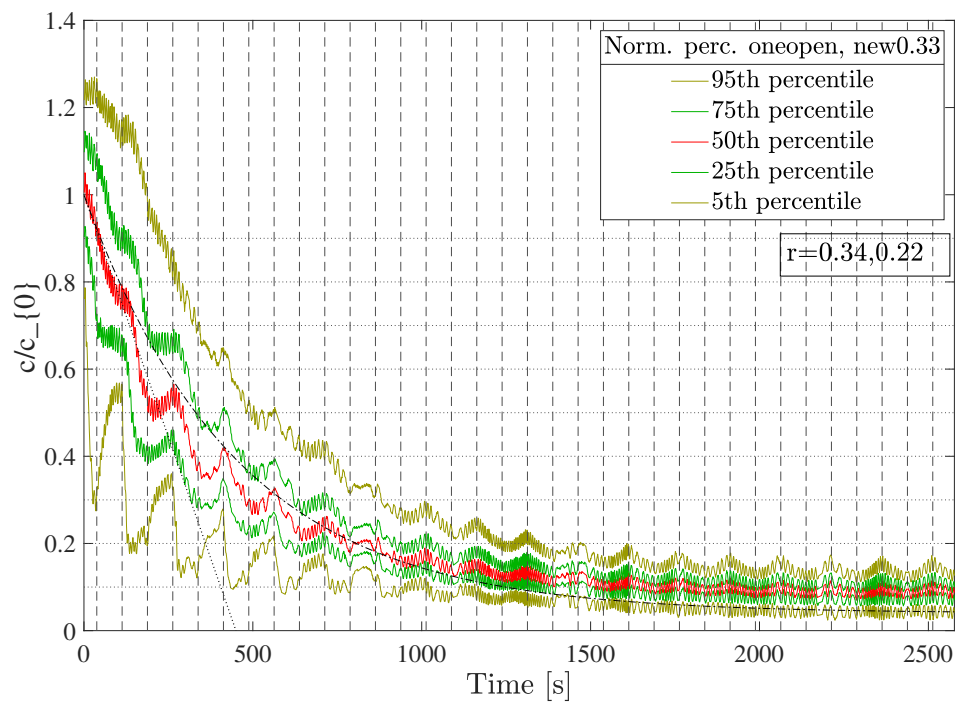
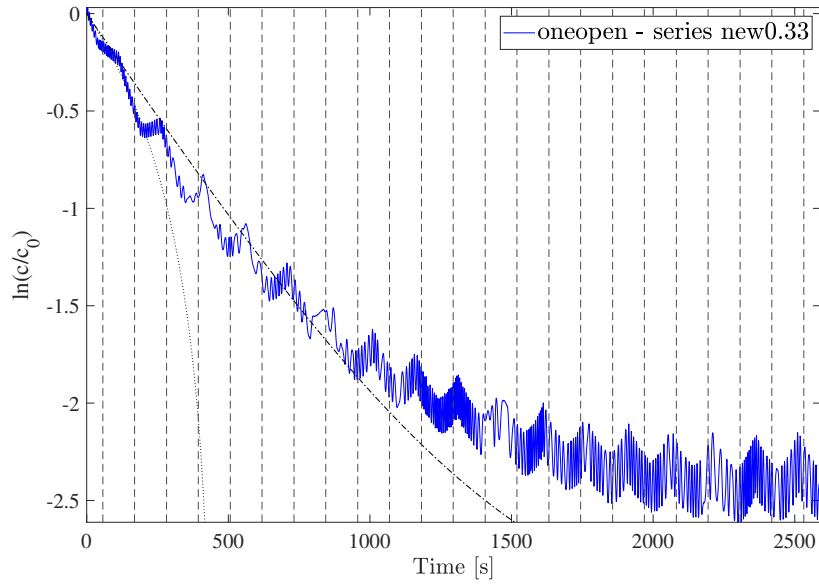
The time interval of 956 s has been chosen as sufficiently short to represent combinations features range of variation (as all experiments tend to the same asymptotic state) and sufficiently long to reduce the influence of the first half period, when most errors tend to impact data (leaking, change of ratio, circulation, backflow from the sea). The period is also sufficiently short to avoid all later time errors (second reservoir exchange, additional concentration under the lagoon structure, bubbles) and sufficiently long to address for the different timing of different periods (corresponding to different exchange ratios). $956.25\text{s} = T_{0.5}/4 + 8 T_{0.5}/2 = T_{0.166}/4 + 25 T_{0.166}/2 = T_{0.33}/4 + 12.5 T_{0.33}/2$.

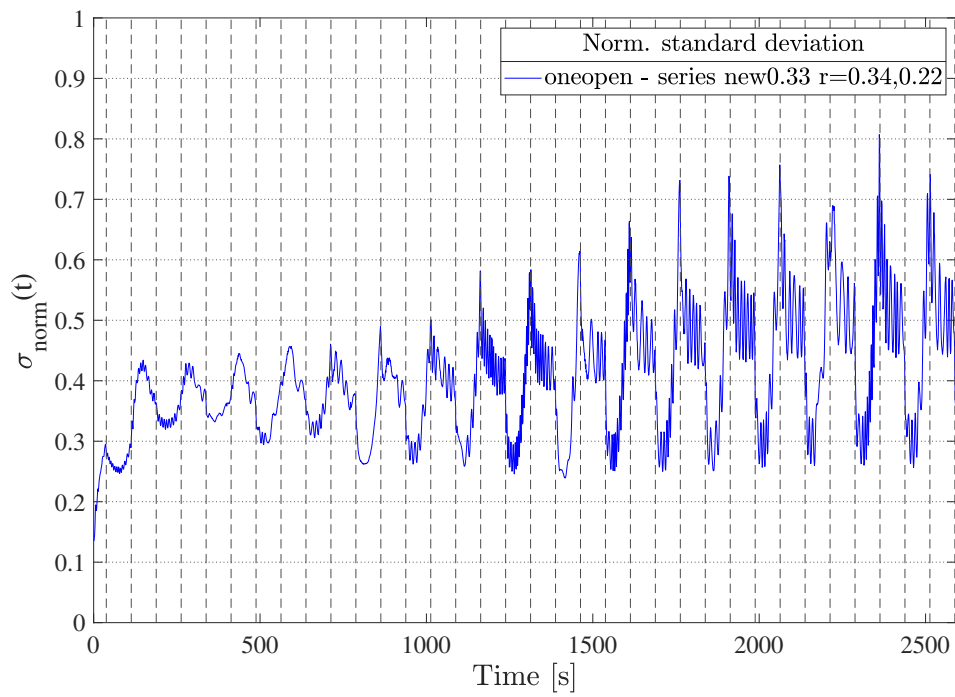
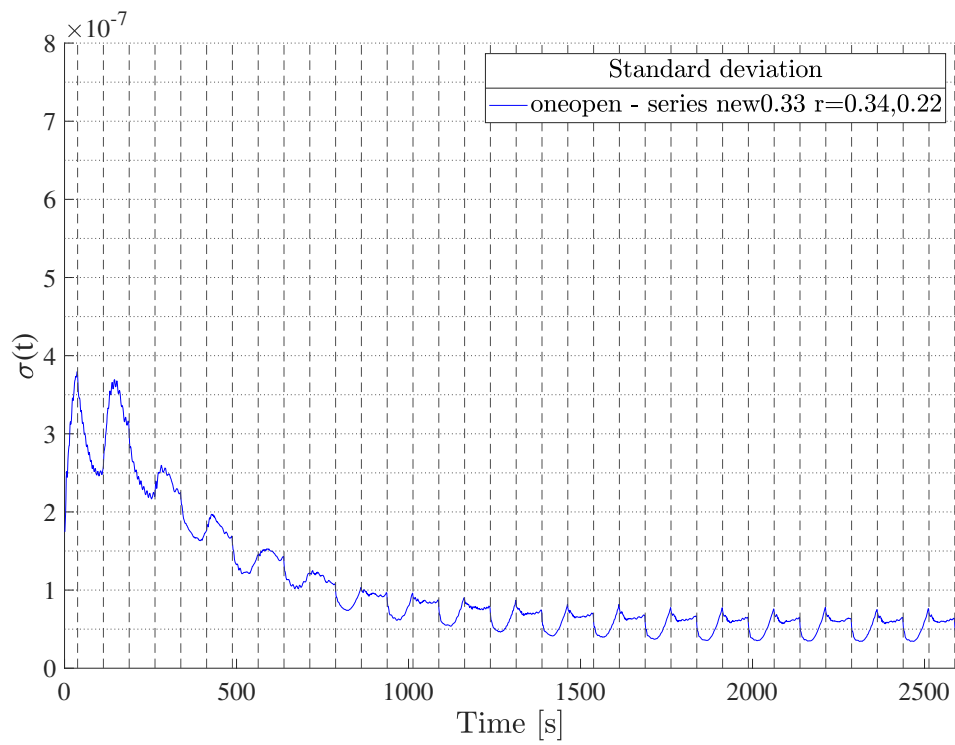
A closer look to combinations legend at the beginning of this chapter is recommended.

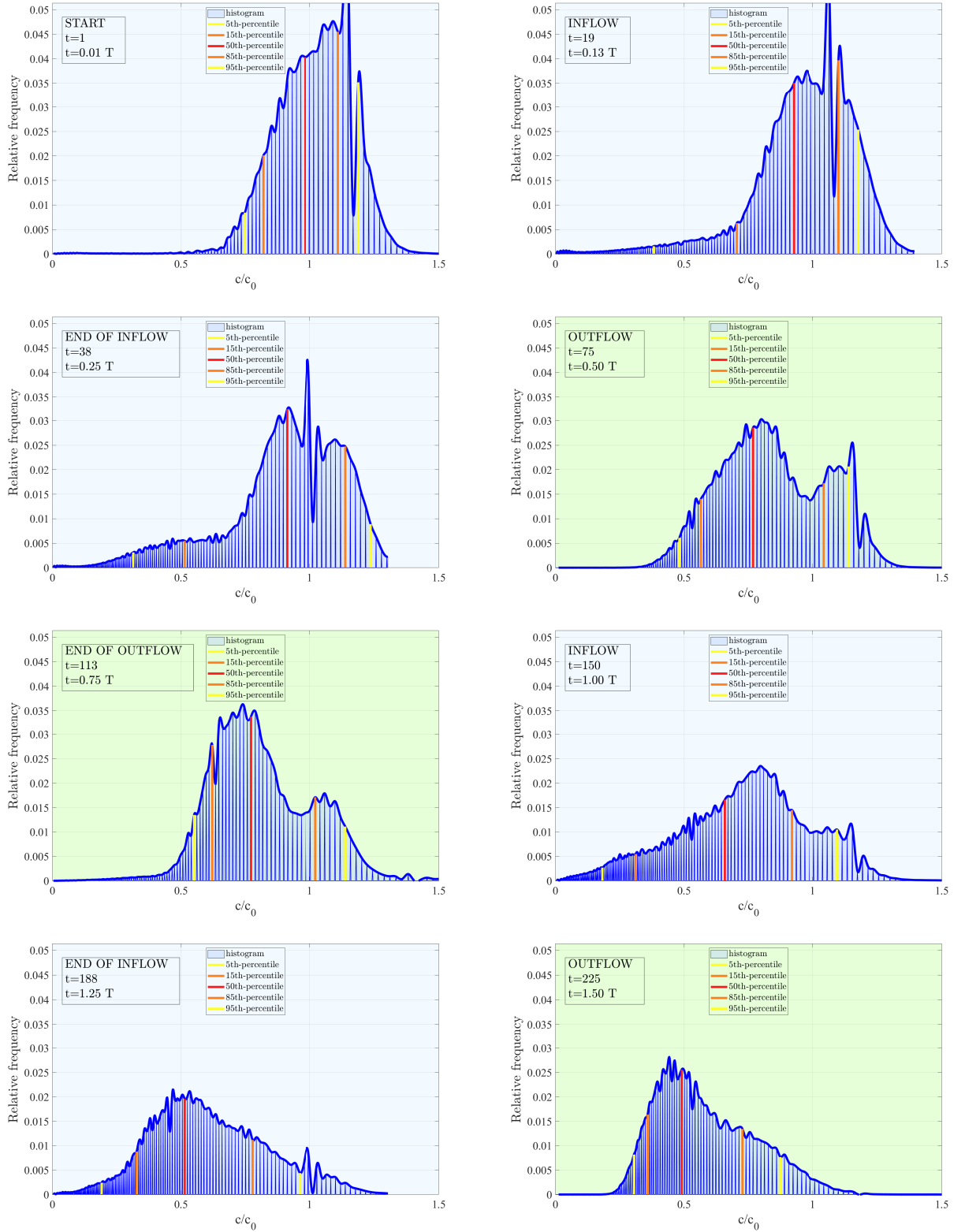
Single experiment example

The chosen example is the *oneopen* combination (only the central inlet open in both inflow and outflow phases) from the series *new0.33*. The given graphs show also the estimated ratio from the procedure described in the *Errors* section of this chapter (the so called *reliability coefficients*). As a solid theoretical reference, ideal decays of perfect mixing and perfect mechanism models are given in each graph (exponential line-dotted curve and linear dotted curve).

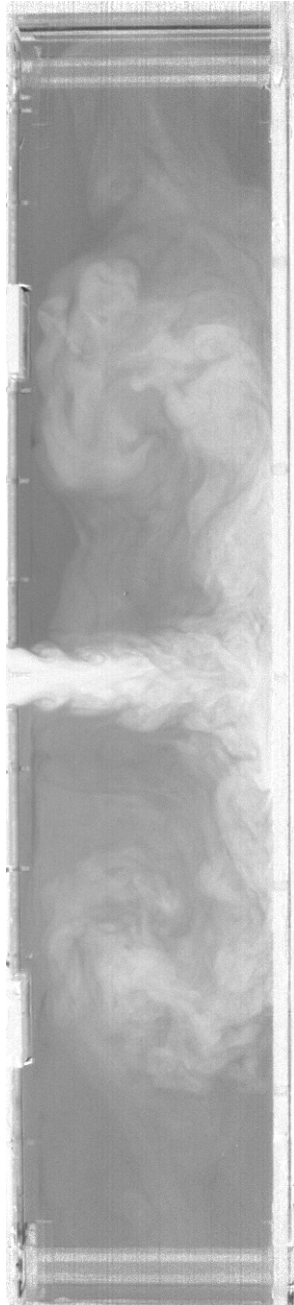




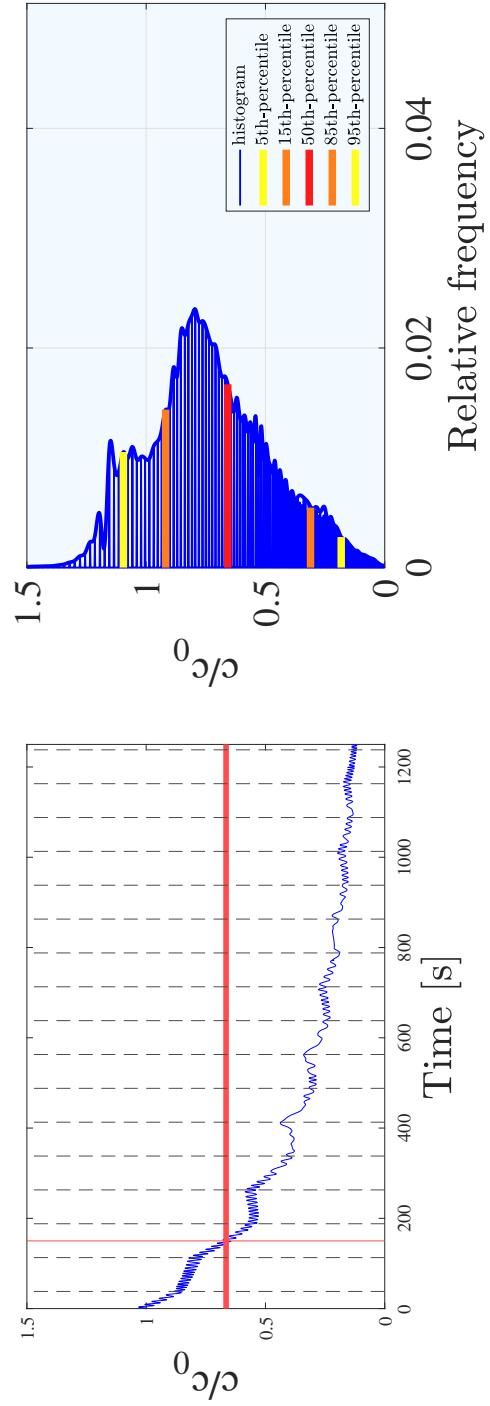




Frequency distribution over time in the first cycles, *oneopen* combination, series *new0.33*. Inflow phases increases lower concentration values frequency while outflow phases compact and smooth the curve to central values.



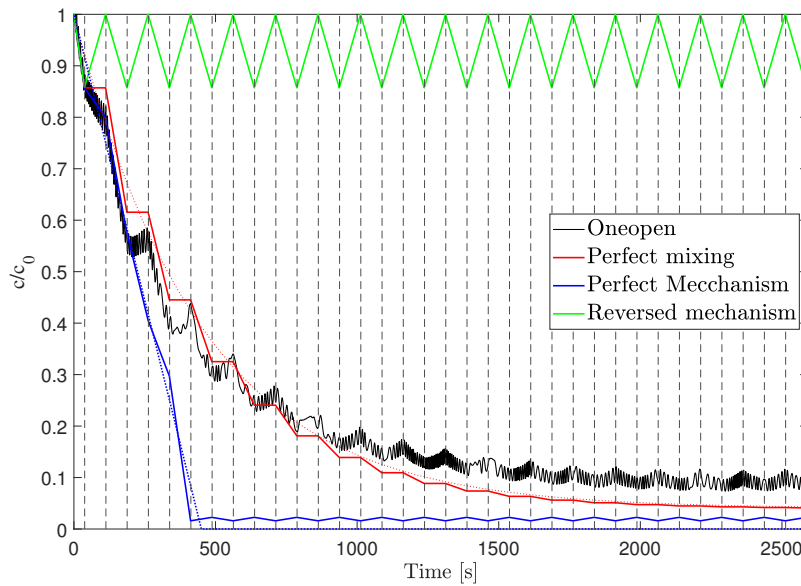
INFLOW $t=150$ (1.00 T)



Example of mean concentration and frequency distribution relative to actual photographic frame, *oneopen* combination, *new0.33* series

Experimental data and conceptual models

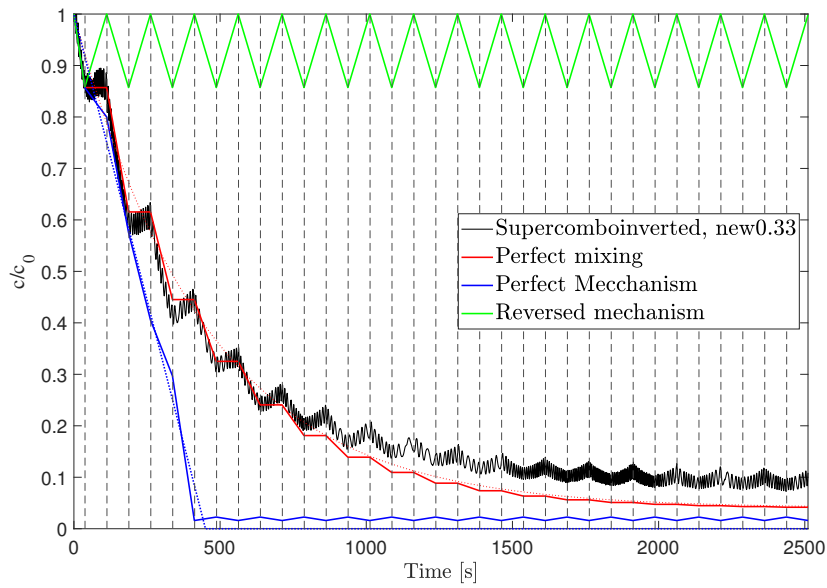
Coming back to theoretical results of the *Conceptual models* chapter, most combinations have an initial decay below the perfect mixing one, with negative slope for the outflow phase. This confirms the hypothesis of the formation of a "natural mechanism", as conjectured in the chapter. However, the flow forms a defined pattern and soon flushes away concentration on selected regions: over time the remaining regions keep part of their initial concentration and the decay is similar to the one of the *Reversed mechanism* model. The pattern is characteristic of the combination and results in different concentration decays.



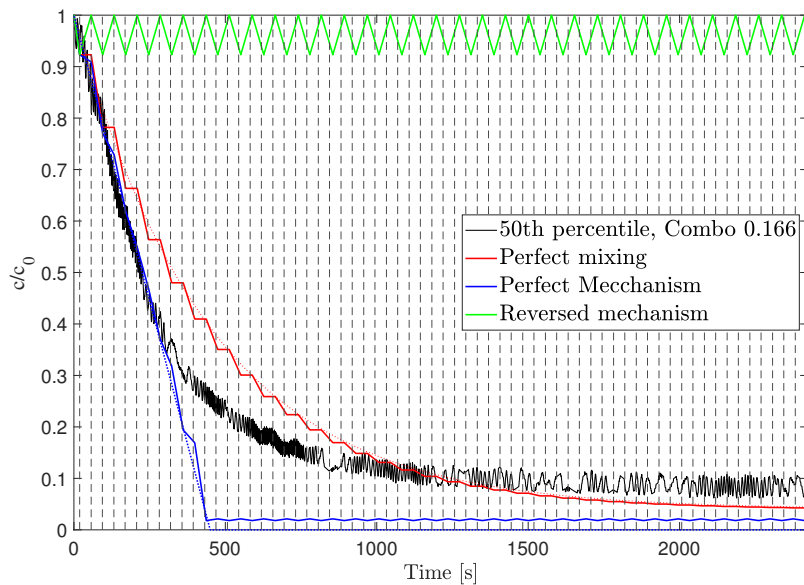
Ideal models and actual experimental data comparison, *oneopen* series *new0.33*. Mean concentration decay follows the perfect mechanism decay during first outflow, then the pattern becomes counter-efficient

Models define a frame of reference for experimental data, confirming their validity and pointing out what needs to be further investigated. In this section some important cases outline the similarity between some combinations and ideal models:

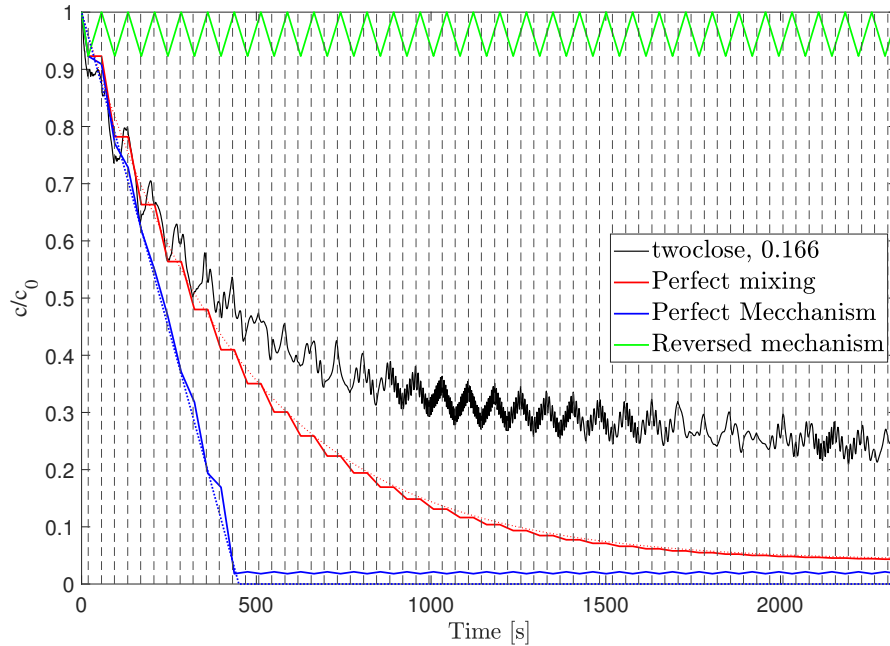
- *Allopen* (*o o o*) was expected to be the combination which resembled the most the *Perfect mixing* model; nonetheless, other combinations seem to have a better mixing (i.e. *supercomboinverted*, *twoopen*)
- *Combo* (*o c c (in)*, *c c o (out)*) and in general "artificial" or "forced" combinations (the ones in which inflow phase opening differs from outflow phase one) reproduce well the *Perfect mechanism* model in terms of bulk concentration (median values)



Ideal models and actual experimental data comparison, *supercomboinverted* series *new0.33*. Mean concentration decay follows the perfect mixing decay during first cycles



Ideal models and actual experimental data comparison, *combo* series *0.166*. Median concentration decay follows the perfect mechnisim decay during many cycles, then the pattern becomes counter-efficient



Ideal models and actual experimental data comparison, *twoclose* series *0.166*. Mean concentration decay shows a *reversed mechanism* behaviour

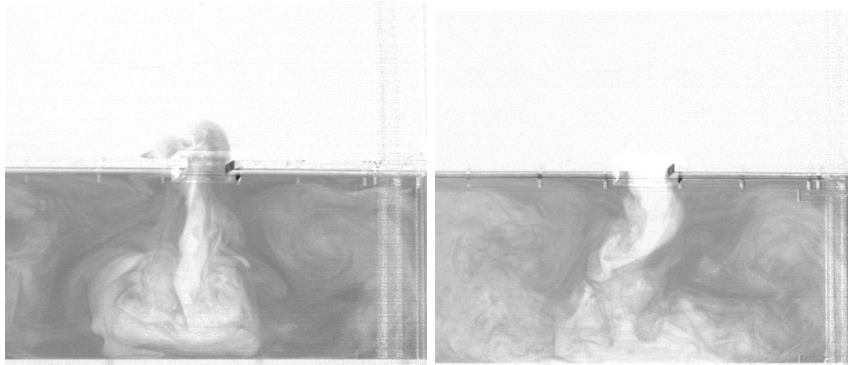
- *Twoclose* (*o c c*), having only one fixed inlet open, resembles the most the *Reversed Mechanism* model, with most of entrained water coming back to the sea basin during outflow phase

More generally, the combination which results in the perfect mixing decay is the one minimising concentration dispersion and thus the standard deviation σ . The perfect mechanism can be seen at best in median concentration, looking at bulk values of concentration; the *Reversed Mechanism* main feature is a very slow decay in maximum concentration values (95th percentile).

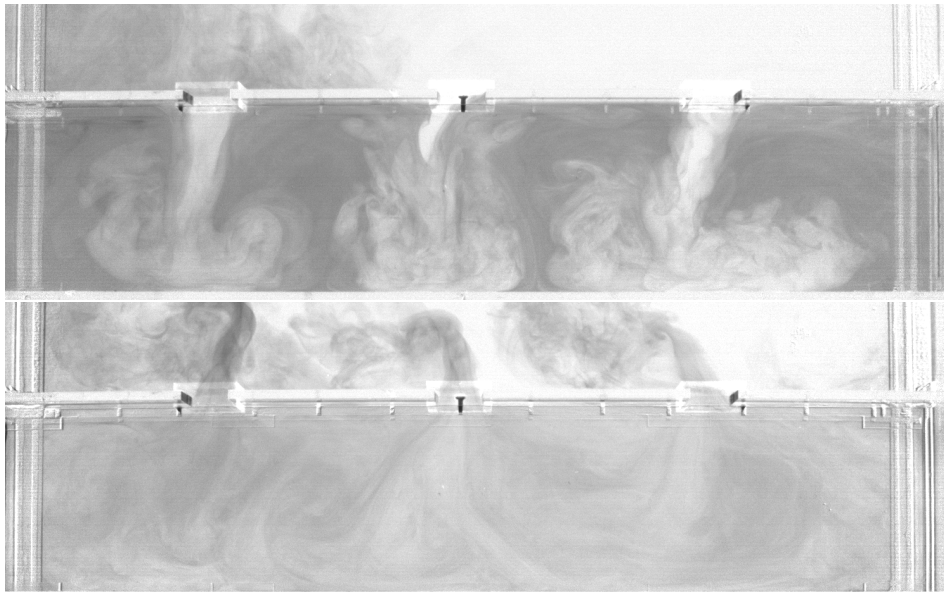
Combinations flow patterns

Flow patterns are characteristic of combinations and influence the concentration decay inside the lagoon, both in terms of median concentration (50th percentile), and in terms of maximum concentration (95th percentile). They are what conceptual models miss the most: as pointed in the previous section, even unforced "natural" combinations (the ones with fixed openings in both inflow and outflow phase) have their own mechanisms resulting from the interaction of jets with physical boundaries. In particular, after the jet impact the end boundary of the lagoon structure, two swirls form on its sides, mixing certain areas and avoiding others.

In forced or "artificial" combinations (the ones in which opening combination changes in inflow and outflow phase), jet energy is concentrated in one single inlet and meant



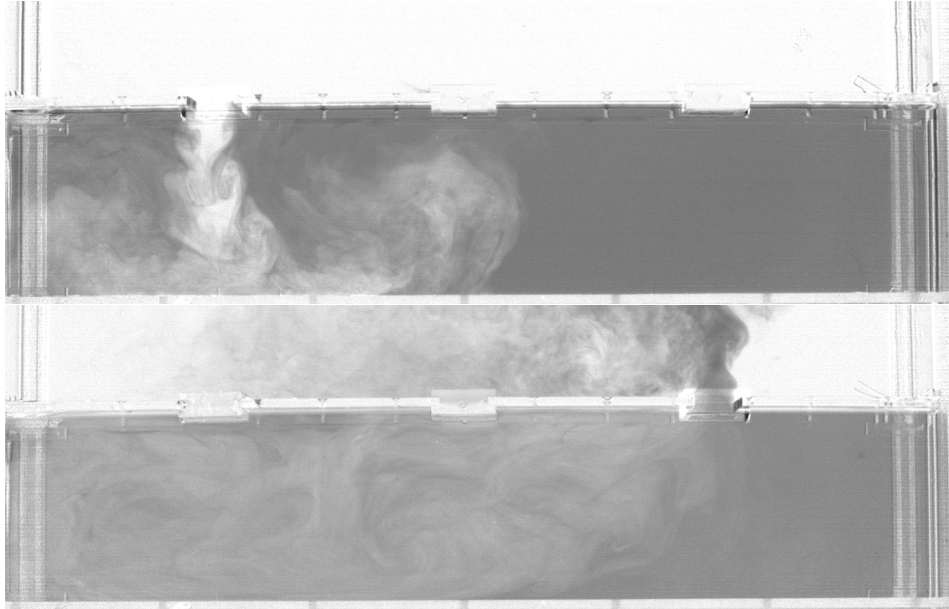
Inflow jets for $r = 1/6$ and $r = 1/2$, *allopen*



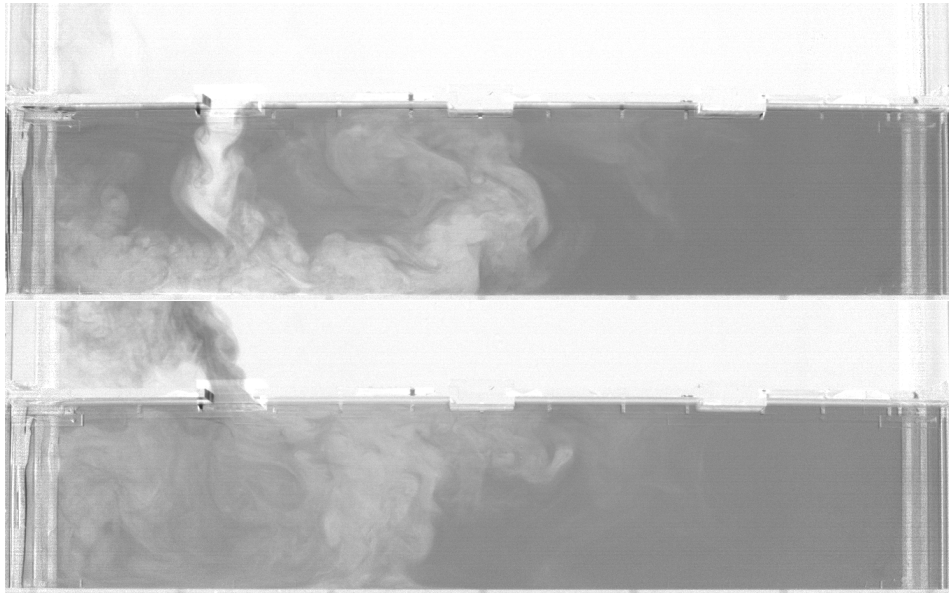
Flow pattern for inflow and outflow phase, *allopen*

to act on broader regions in its proximity, leaving other areas stationary for subsequent outflow. However, outflow phase plug flow is rather weak and mobilises left areas with difficulty: *supercombo* combination (*o c c (in)*, *c o c (out)*, *c c o (in)*, *c o c (out)*) is meant to address this issue by shifting entraining jet inlet.

Period duration is an important time scale for flow patterns: even if the quantity r/T is fixed (and then the flowrate), longer periods allow jets to proceed further and involve more areas in their entrainment. This change may increase the decay rate when it involves areas which would have been otherwise left stationary, but it may also decrease the decay rate if jets form full rotational cells bringing in the proximity of outlets the newly entered water from the inflow phase.



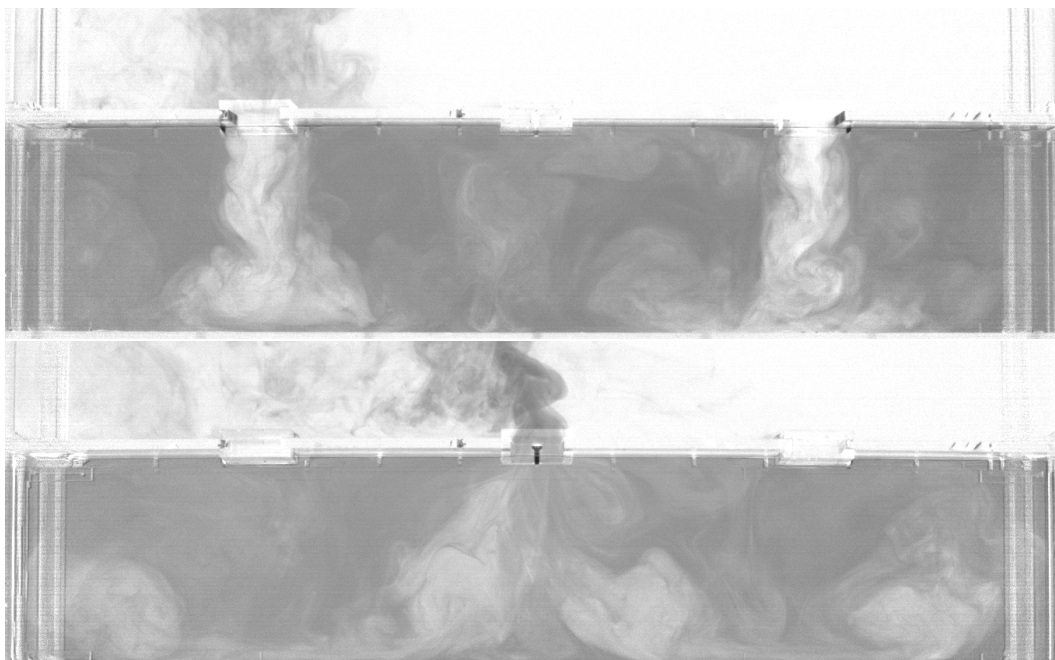
Flow pattern for inflow and outflow phase, *combo*



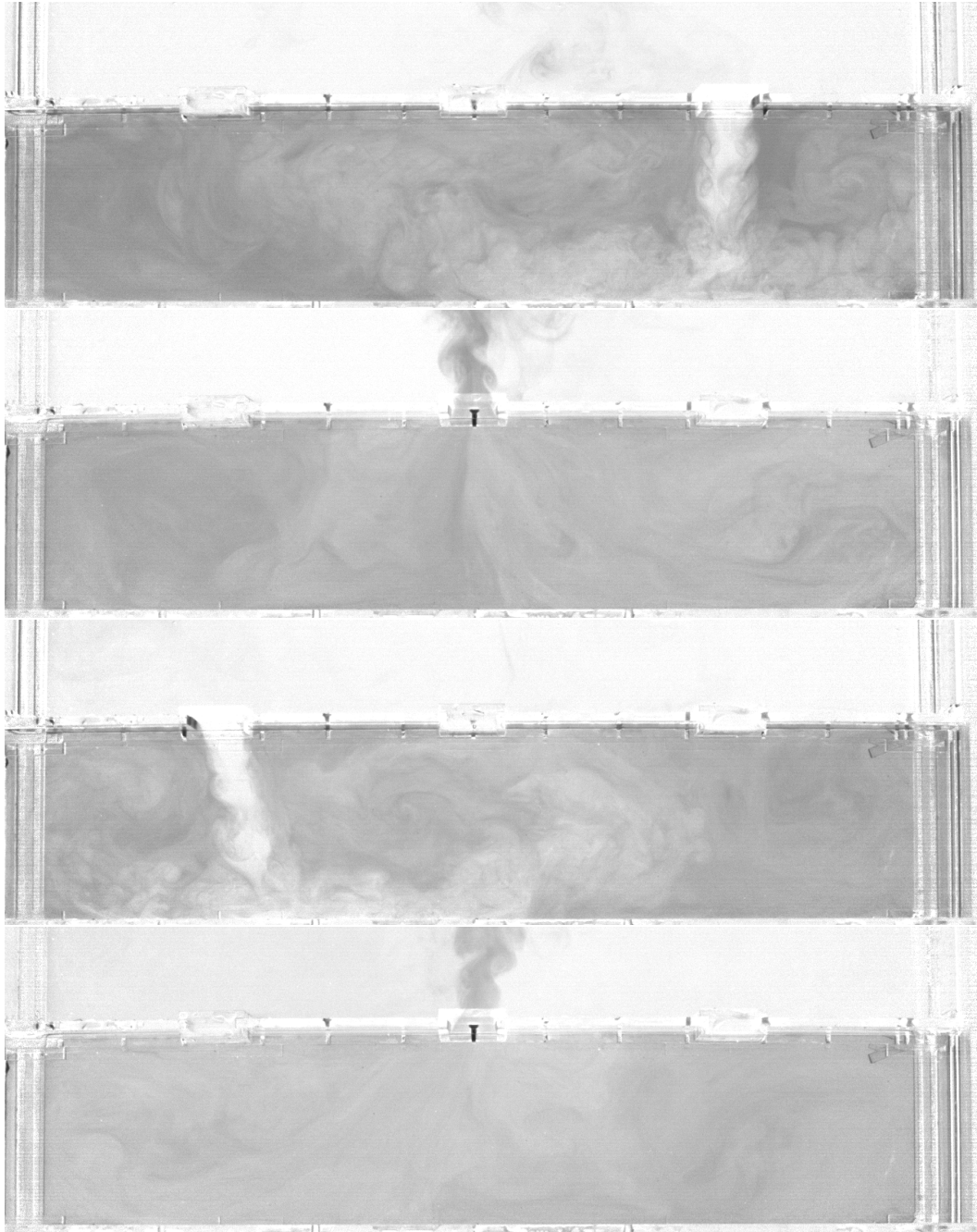
Flow pattern for inflow and outflow phase, *twoclose*



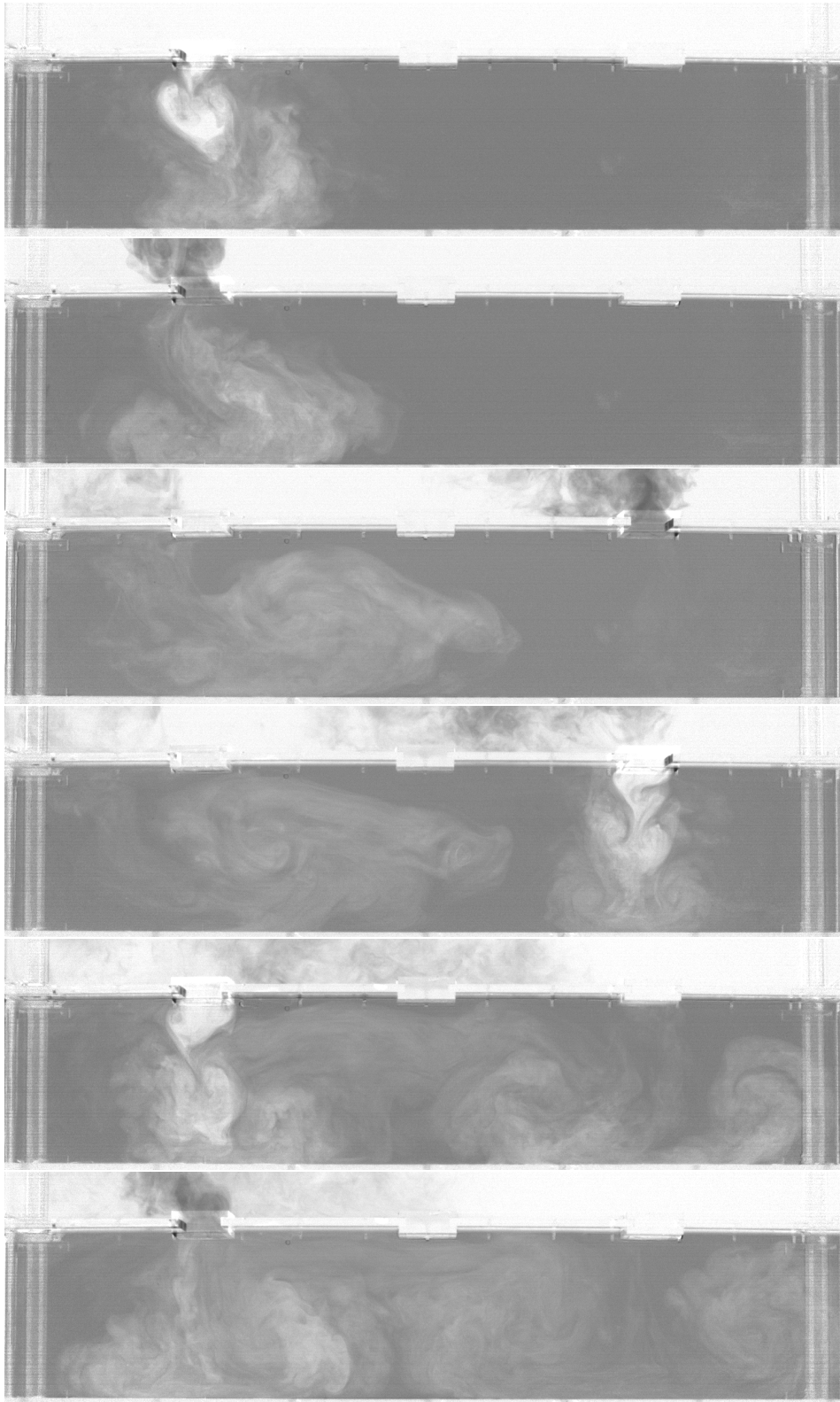
Flow pattern for inflow and outflow phase, *twoopen*



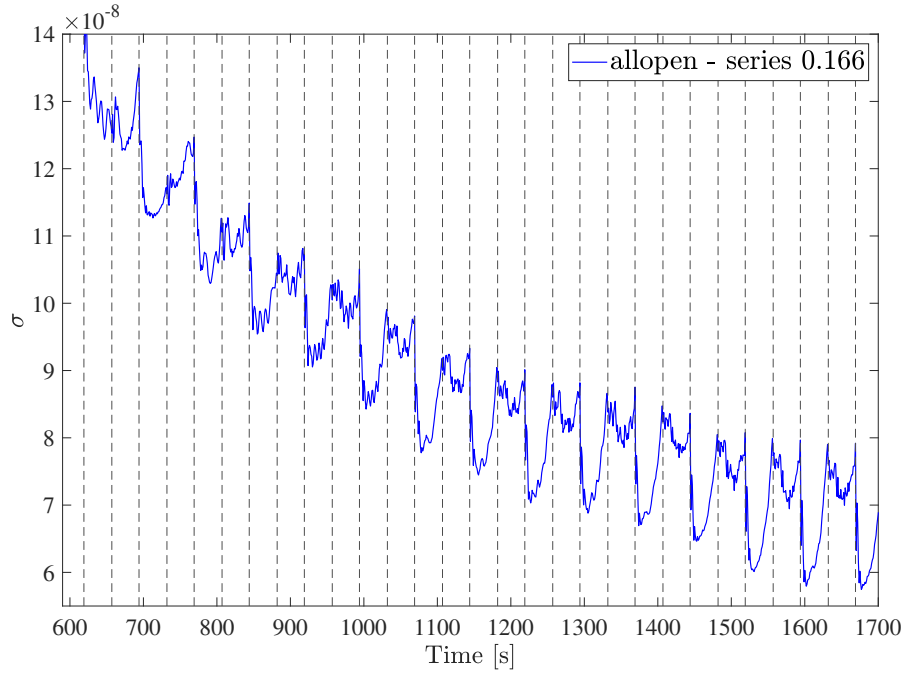
Flow pattern for inflow and outflow phase, *bigcomboinverted*



Flow pattern for inflow and outflow phases, *supercombo*



Flow pattern for *strangecombo*: first frame refers to initial inflow phase, second and third to outflow phase, fourth and fifth to inflow phase and sixth again to outflow phase



Progressive pattern formation in $\sigma(t)$ over time, *allopen* from 0.166

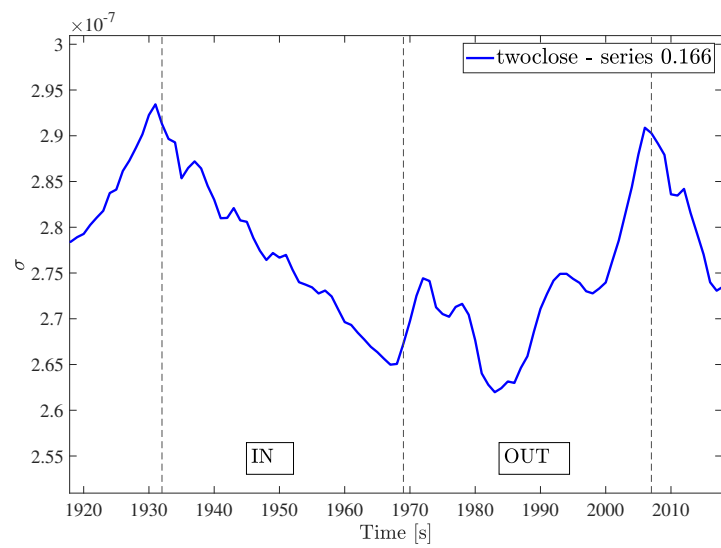
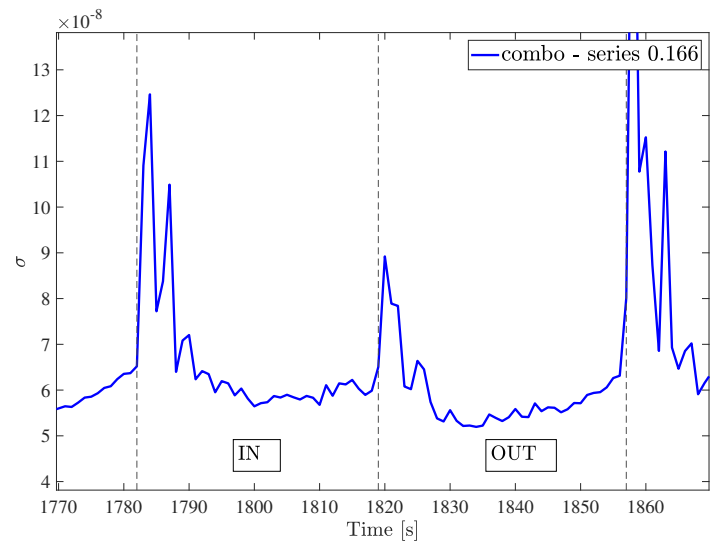
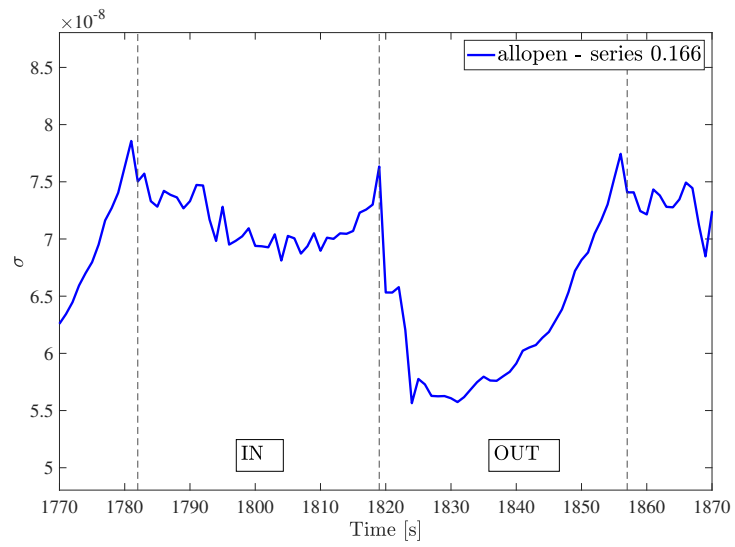
Standard deviation patterns

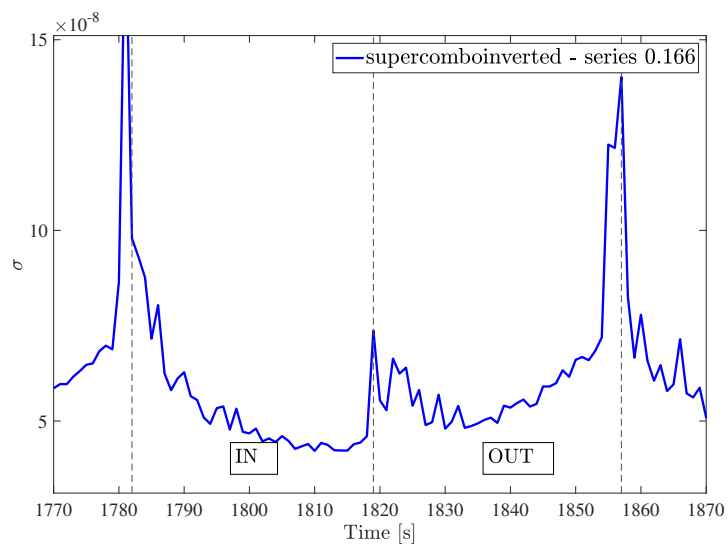
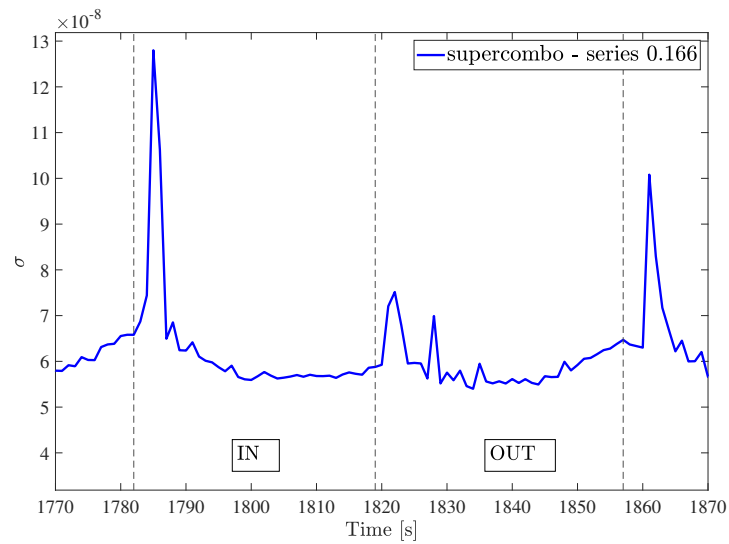
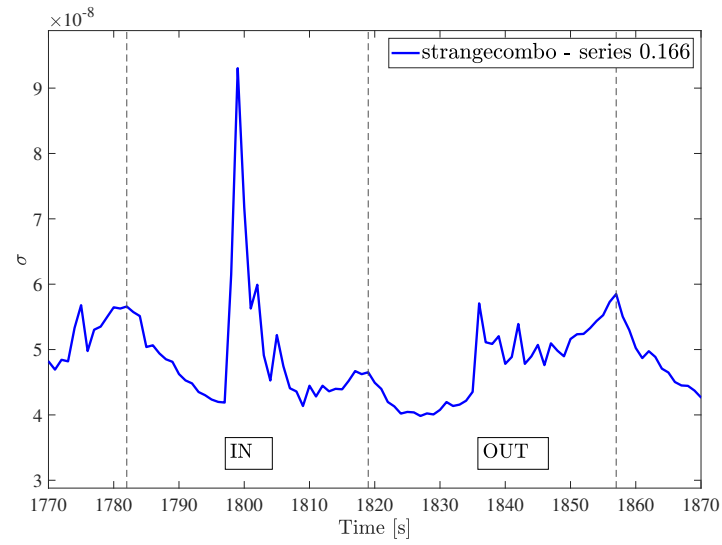
In standard deviation $\sigma(t)$ graph the formation over time of certain pattern has been observed. It is worth noticing that the same regularity does not appear in the normalised standard deviation graph, which means that height variation plays an important role in regularising the pattern. Yet, each combination has its own characteristic pattern, which resembles a periodical signal.

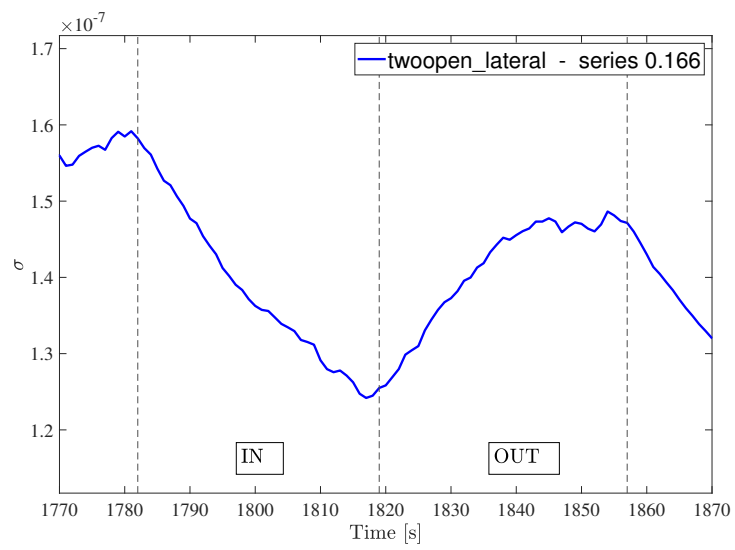
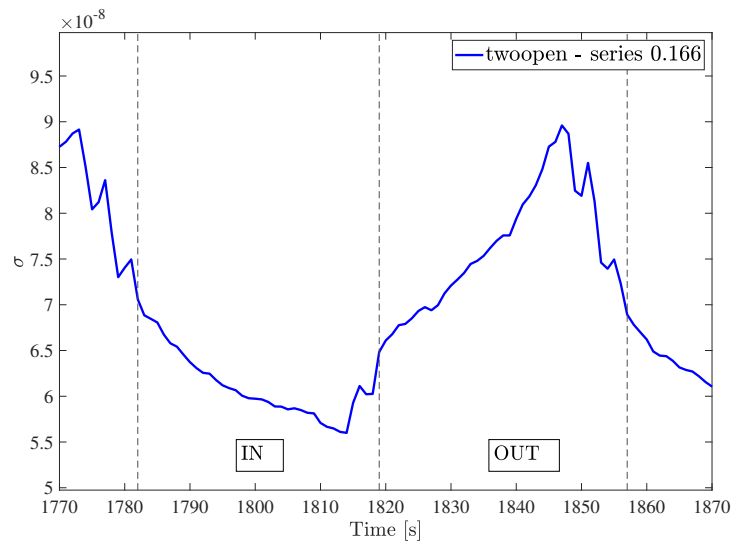
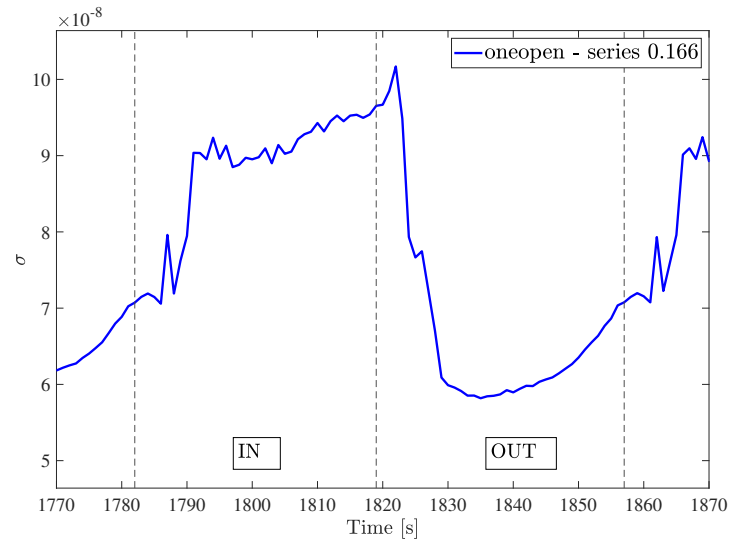
Some spikes could be sharpened by moving gates at opening configuration switching times.

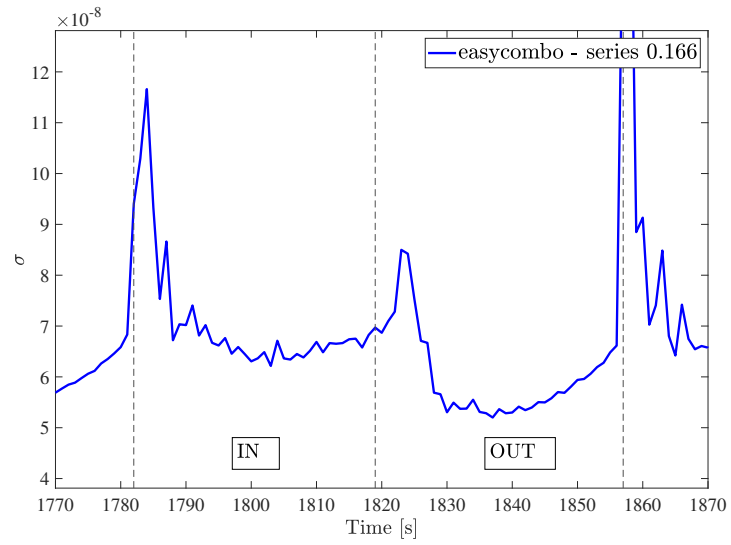
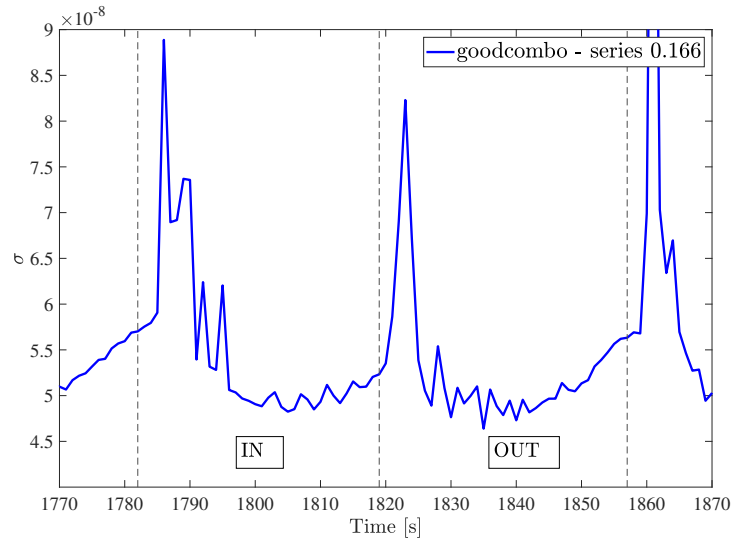
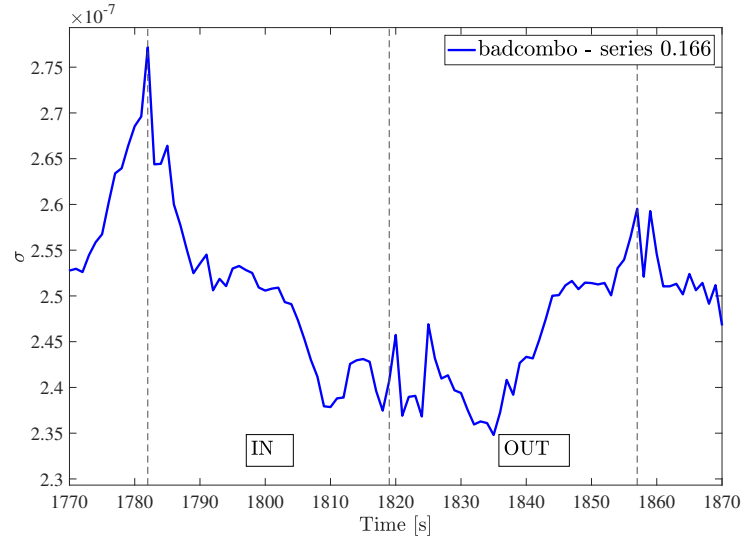
However, it is not clear how the standard deviation increases over the outflow phase: it could be a sign of good flushing mechanism or indication of dark pixels which affect variability at low water levels. For example, in *twoclose* σ decreases over inflow phases and increases over outflow phase, while in *oneopen* the opposite seem to happen.

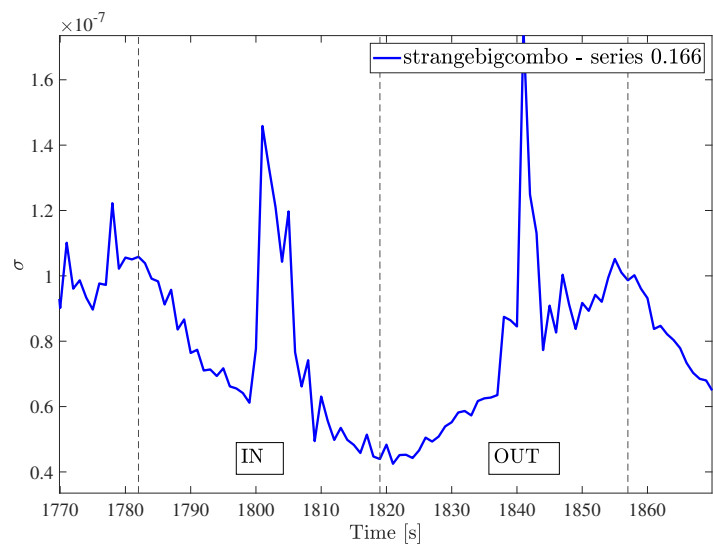
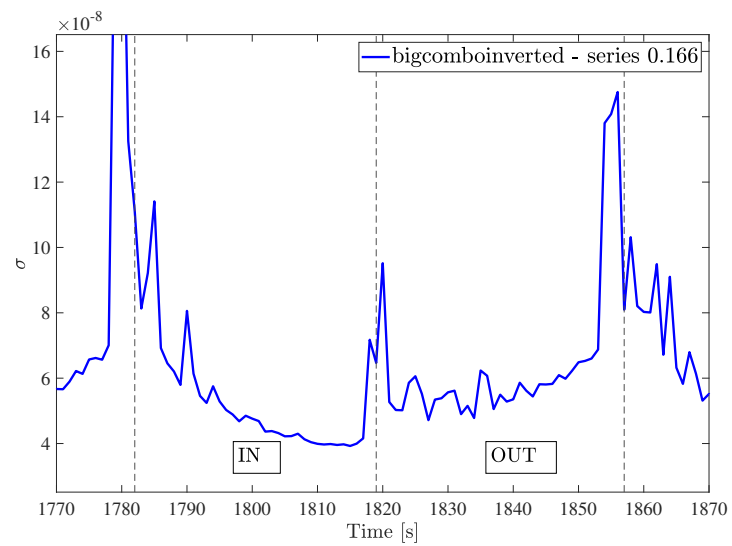
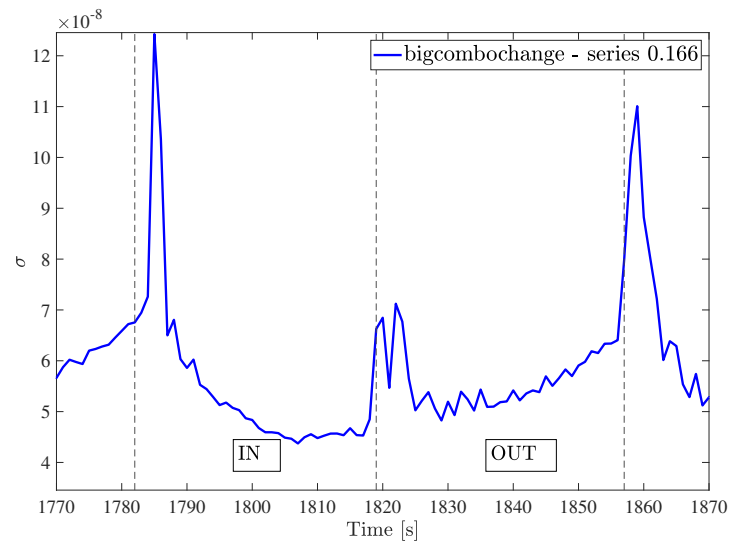
In general, it is not clear how the flow influences the σ pattern and more thinking is necessary. Later time errors could also play a role in it.

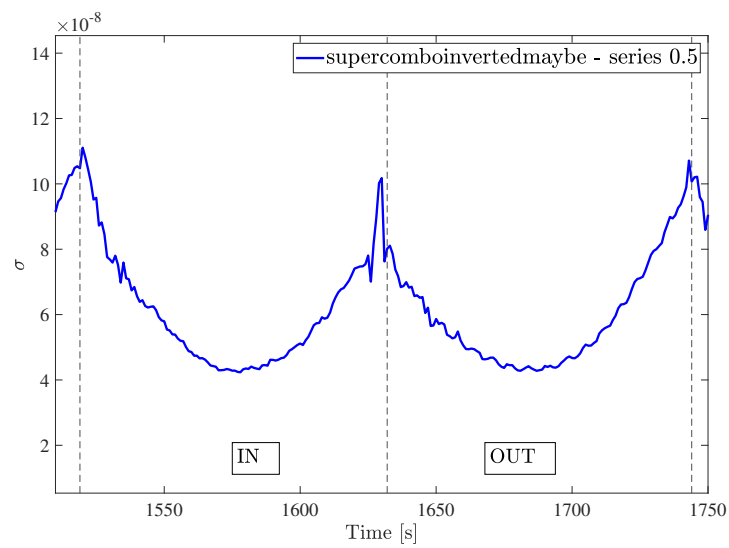
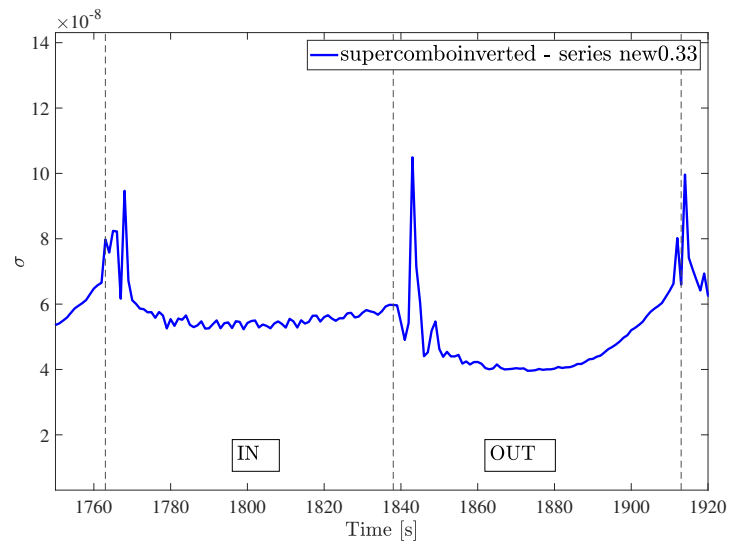
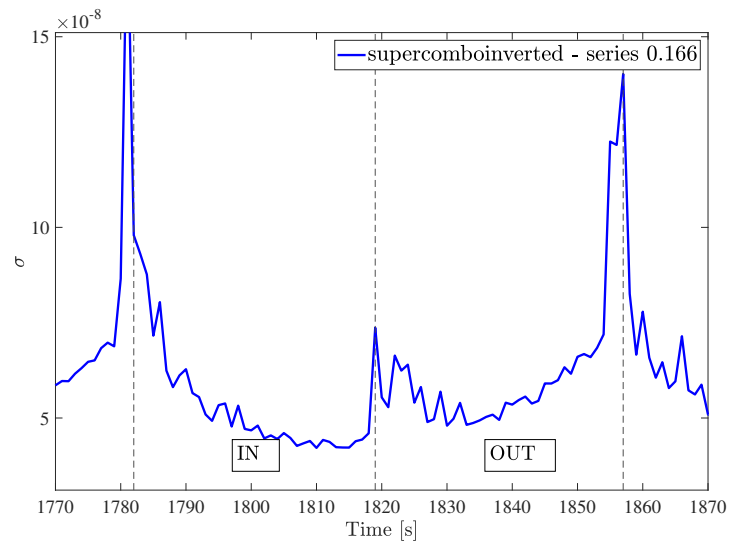


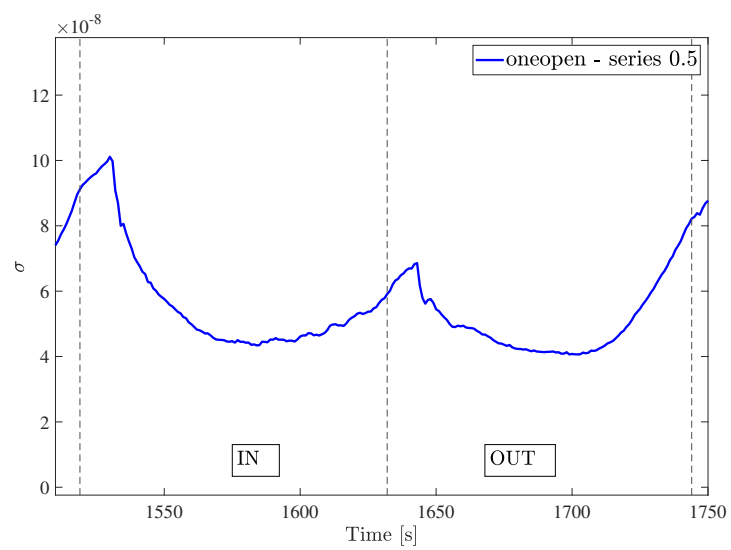
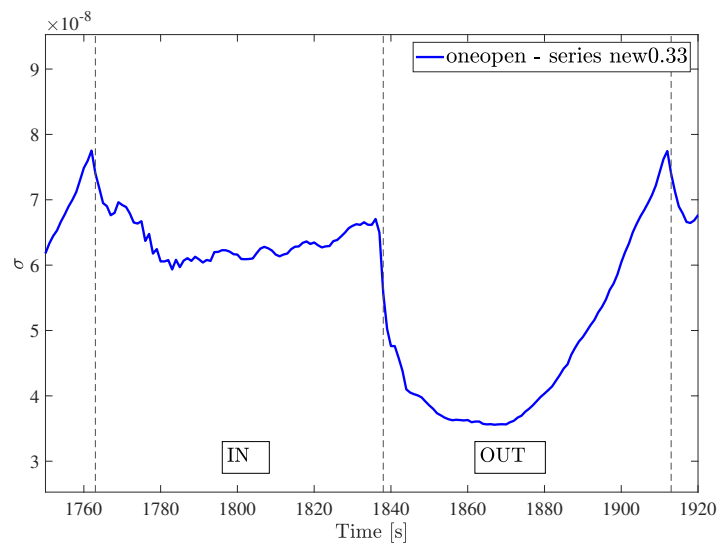
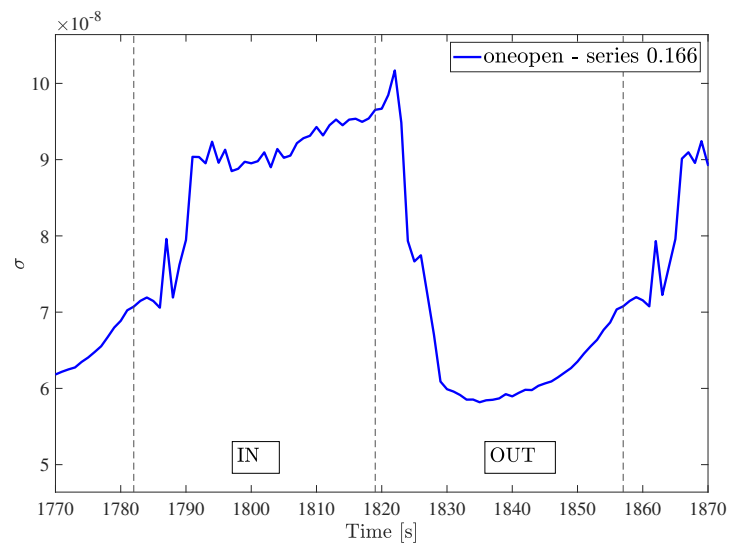












Mean concentration and standard deviation

Mean concentration decay is intuitively associated to combination efficiency. However, the decay of mean concentration could be paired with a high value of normalised standard deviation, suggesting that high concentration values could be kept during the decay. Data are given for each combination, together with the so-called *reliability coefficients* r_1 and r_2 (roughly estimated exchange ratio in first cycle and first subsequent cycles). Experiments which seem to be affected by a significant error are in italics. Data are given for each series sorted by average mean concentration, than an overall order is given, both for \bar{c}_{956} and $\bar{\sigma}_{N,956}$.

In the one third ratio series *twoopen* (*o c o*), *oneopen* (*c o c*), *combo* (*(o c c (in), c c o (out))*) and *supercomboinverted* (*c o c (in), o c c (out), c o c (in), c c o (out)*) show a steeper decay than the natural configuration *allopen*. *Twoopen* and *supercombo* show also a significant reduction in normalised standard deviation. The closeness between *oneopen*, *twoopen*, *allopen* and *supercombo* suggests a comparable flushing efficiency of symmetric combinations, as symmetry allows flow patterns to cover most of the lagoon area.

	<i>series 0.33</i>	r_1	r_2	\bar{c}	σ_N
new0.33	twoopen	0.45	0.26	0.39	0.32
new0.33	oneopen	0.34	0.22	0.41	0.36
new0.33	combo	0.45	0.26	0.41	0.54
new0.33	supercomboinverted	0.32	0.24	0.43	0.39
old0.33	all open	0.34	0.29	0.43	0.37
new0.33	supercombo	0.31	0.26	0.43	0.29
new0.33	twoopen mystery	0.28	0.24	0.44	0.33
<i>new0.33</i>	<i>badcombo</i>	<i>0.47</i>	<i>0.28</i>	<i>0.44</i>	<i>0.62</i>
<i>old0.33</i>	<i>oneopen</i>	<i>0.71</i>	<i>0.51</i>	<i>0.45</i>	<i>0.38</i>
new0.33	twoopen2	0.30	0.23	0.45	0.29
new0.33	allopen	0.31	0.23	0.45	0.41
<i>old0.33</i>	<i>combo</i>	<i>0.70</i>	<i>0.39</i>	<i>0.46</i>	<i>0.46</i>
new0.33	twoopen lateral	0.42	0.26	0.46	0.52
old0.33	goodcombo	0.28	0.23	0.47	0.32
<i>old0.33</i>	<i>twoopen</i>	<i>0.44</i>	<i>0.46</i>	<i>0.47</i>	<i>0.34</i>
new0.33	twoopen3	0.34	0.23	0.47	0.24
old0.33	easycombo	0.34	0.25	0.48	0.40
old0.33	twoopen lateral	0.37	0.30	0.48	0.50
new0.33	easycombo	0.30	0.26	0.48	0.42
<i>old0.33</i>	<i>twoclose</i>	<i>0.92</i>	<i>0.37</i>	<i>0.51</i>	<i>0.53</i>
old0.33	badcombo	0.22	0.32	0.60	0.58

In general results are coherent with the conceptual models, especially if the phenomenon of natural mechanism is accounted (as seen in the flow patterns section). The minimum σ_N of *twoopen3* is due to a high ambient concentration: *twoopen2*

has been operated right after *twoopen* and *twoopen3* right after *twoopen2*, without replacing water tank.

Considering repeated experiments, the error on \bar{c}_{956} is related to the coefficient r_1 (looking at *allopen*, *twoopen* and *badcombo*). This leads to the conclusion that *twoopen* and *combo* could have a slower decay. Thus, *supercombo* might be the fastest decay, considering both \bar{c}_{956} and $\bar{\sigma}_{N,956}$.

As expected, *twoclose* and *badcombo* show the slowest decay, with high values both in mean concentration and standard deviation. *Twoopen lateral* has also comparable values due to the lack of mobilisation of water on the lagoon side of fixed closed gate. Surprisingly also *easycombo* show high values in \bar{c}_{956} and $\bar{\sigma}_{N,956}$, meaning that closing the central inlet (as in *combo* combination) might be beneficial to concentration decay: this result does not seem to hold for $\bar{\sigma}_{N,956}$ in *0.166* series and it is not very reliable in *0.5* series.

The relative smaller value of $\bar{\sigma}_{N,956}$ for *supercombo* in comparison to the one of *supercomboinverted* might suggest that "injecting" low concentration water on the sides and "collecting" high concentration centrally is more beneficially to mixing than the opposite. However, the same comparison in the *0.166* series points to the opposite result. This could mean that either data are not reliable or that the forementioned advantage depends on the sea-lagoon exchange ratio, which could be the case. Unluckily, in the *0.5* series *supercombo* is quite problematic as it is not clear how it is affected by errors.

<i>series 0.166</i>	r_1	r_2	\bar{c}	σ_N
combo	0.22	0.15	0.38	0.59
bigcomboinverted	0.14	0.15	0.38	0.34
combo25	0.19	0.16	0.40	0.56
strangecombo	0.12	0.14	0.40	0.27
bigcombochange	0.19	0.13	0.40	0.40
oneopen	0.21	0.15	0.41	0.45
supercomboinverted	0.19	0.15	0.42	0.30
goodcombo	0.10	0.15	0.43	0.34
strangebigcombo	0.11	0.14	0.43	0.35
supercombo	0.20	0.15	0.43	0.43
twoopen lateral	0.17	0.22	0.43	0.58
easycombo	0.21	0.12	0.43	0.42
allopen	0.22	0.12	0.43	0.38
twoopen	0.16	0.24	0.44	0.32
allopen withskip	0.16	0.11	0.45	0.38
allopenagain	0.18	0.14	0.45	0.41
twoclosewithmylittleskip	0.15	0.17	0.51	0.63
badcombo	0.12	0.16	0.51	0.67
twoclose	0.22	0.17	0.51	0.65

The one sixth ratio series shows a marked improvement in average concentration decay in "artificial" combinations (the ones in which opening in the two phases differ). *Combo* and *bigcombo* (and their variants) show the steepest decay. *Strangecombo* is an alternative version of *combo* in which the opening are switched in the middle of inflow and outflow phase, creating an irregular pattern which seems to increase mixing (lowest value of $\bar{\sigma}_{N,956}$). The efficiency of "strange" combinations could be related to the higher frequency of overall external forcing (every $T/4$ either tide or opening configuration shifts).

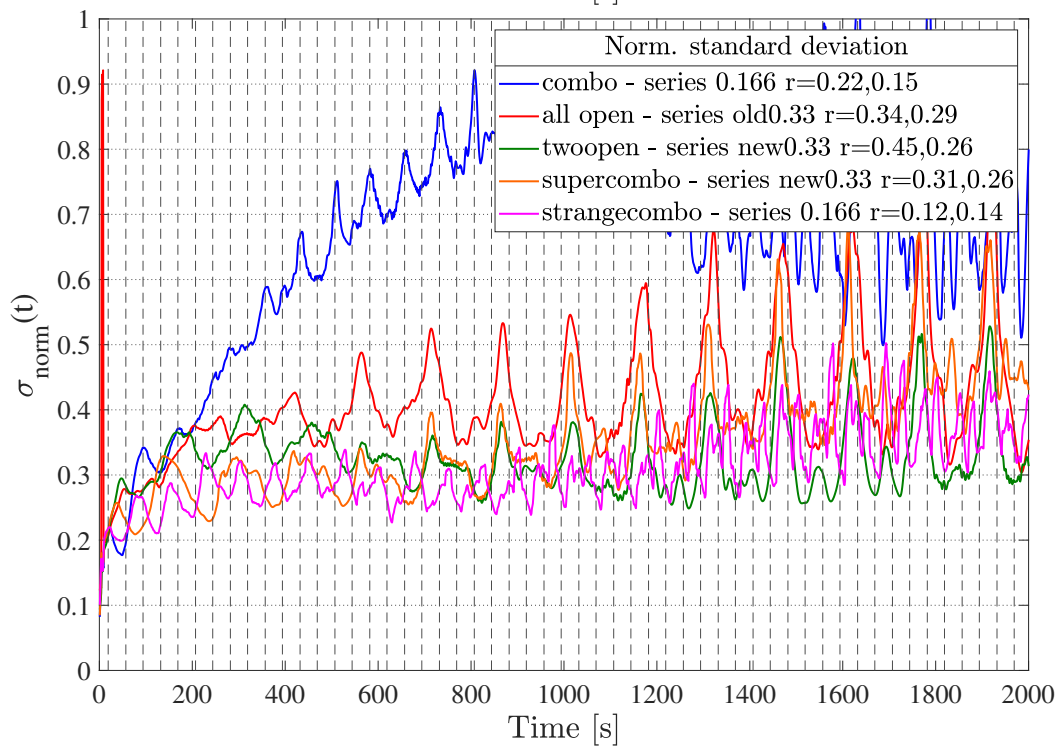
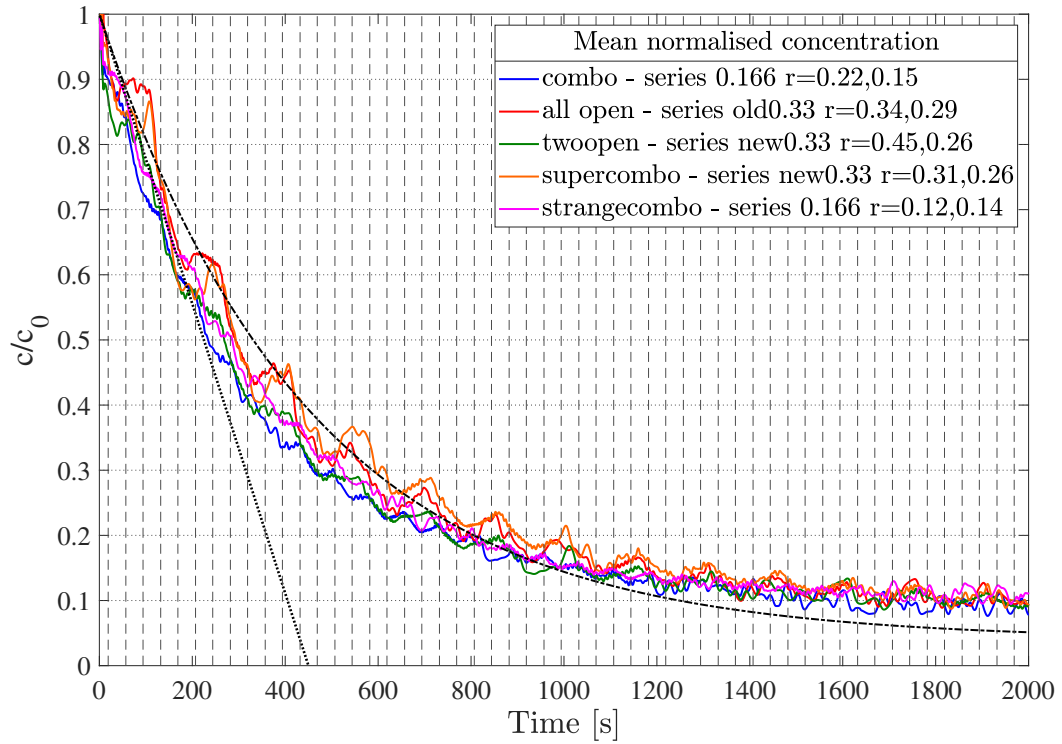
The advantage of *bigcomboinverted* (*o c o (in)*, *c o c (out)*) over *bigcombo* (*c o c (in)*, *o c o (out)*) is coherent with the conjecture that "injecting" from the sides and collecting centrally is better than the opposite, but in contrast with the *supercombo-supercomboinverted* comparison in the same series. This could mean that either data are not reliable, or that injecting on one side at time is different than injecting on the two sides together: weaker jets on the sides over a short period do not reach the central part of the lagoon, keeping high concentration water in the proximity of the central outlet.

<i>series 0.5</i>	r_1	r_2	\bar{c}	σ_N
allopen	0.64	0.34	0.39	0.35
<i>bigcombo actual</i>	<i>1.06</i>	<i>0.61</i>	<i>0.39</i>	<i>0.49</i>
goodcombo	0.68	0.37	0.41	0.34
bigcombo	0.50	0.40	0.43	0.41
supercomboinverted	0.46	0.31	0.45	0.37
oneopen	0.48	0.36	0.46	0.37
easycombo	0.40	0.36	0.48	0.47
<i>supercombo</i>	<i>0.03</i>	<i>0.35</i>	<i>0.49</i>	<i>0.28</i>
<i>combo</i>	<i>-0.01</i>	<i>0.40</i>	<i>0.52</i>	<i>0.48</i>
twoopen lateral	0.27	0.43	0.53	0.44
twoclose	0.16	0.47	0.60	0.40
badcombo	0.04	0.49	0.69	0.44

Overall the *0.5* series is more affected than other series to errors in initial phase, as represented by the r_1 coefficient. This could be caused by an increased leaking due to higher water level difference in setting initial conditions: lagoon basin needs to be isolated and mixed uniformly, then gates are opened when the water level in the sea basin is the same in the lagoon basin in inflow phase. The relatively low values of \bar{c}_{956} and $\bar{\sigma}_{N,956}$ with respect to *allopen* are suspicious, as in other series the two combinations are relatively similar and the r_1 coefficient is high in the *allopen* experiment. This shift could be present also in *goodcombo*. The comparison between *bigcombo* and *oneopen* is more appropriate and could indicate an advantage of "artificial" combinations also in this series. *Supercombo*, as in the other series, has a very low value of $\bar{\sigma}_{N,956}$.

<i>All series</i>		r_1	r_2	\bar{c}	σ_N
0.166	combo	0.22	0.15	0.38	0.59
0.166	bigcomboinverted	0.14	0.15	0.38	0.34
new0.33	twoopen	0.45	0.26	0.39	0.32
0.5	allopen	0.64	0.34	0.39	0.35
0.5	<i>bigcombo actual</i>	<i>1.06</i>	<i>0.61</i>	<i>0.39</i>	<i>0.49</i>
0.166	combo25	0.19	0.16	0.40	0.56
0.166	strangecombo	0.12	0.14	0.40	0.27
0.166	bigcombochange	0.19	0.13	0.40	0.40
0.5	goodcombo	0.68	0.37	0.41	0.34
new0.33	oneopen	0.34	0.22	0.41	0.36
0.166	oneopen	0.21	0.15	0.41	0.45
new0.33	combo	0.45	0.26	0.41	0.54
0.166	supercomboinverted	0.19	0.15	0.42	0.30
0.166	goodcombo	0.10	0.15	0.43	0.34
new0.33	supercomboinverted	0.32	0.24	0.43	0.39
0.166	strangebigcombo	0.11	0.14	0.43	0.35
0.166	supercombo	0.20	0.15	0.43	0.43
old0.33	all open	0.34	0.29	0.43	0.37
0.166	twoopen lateral	0.17	0.22	0.43	0.58
new0.33	supercombo	0.31	0.26	0.43	0.29
0.5	bigcombo	0.50	0.40	0.43	0.41
0.166	easycombo	0.21	0.12	0.43	0.42
0.166	allopen	0.22	0.12	0.43	0.38
0.166	twoopen	0.16	0.24	0.44	0.32
new0.33	twoopen mystery	0.28	0.24	0.44	0.33
new0.33	twoopen2	0.30	0.23	0.45	0.29
new0.33	allopen	0.31	0.23	0.45	0.41
0.5	supercomboinverted	0.46	0.31	0.45	0.37
0.166	allopen withskip	0.16	0.11	0.45	0.38
0.166	allopenagain	0.18	0.14	0.45	0.41
new0.33	twoopen lateral	0.42	0.26	0.46	0.52
0.5	oneopen	0.48	0.36	0.46	0.37
old0.33	goodcombo	0.28	0.23	0.47	0.32
new0.33	twoopen3	0.34	0.23	0.47	0.24
old0.33	easycombo	0.34	0.25	0.48	0.40
old0.33	twoopen lateral	0.37	0.30	0.48	0.50
0.5	easycombo	0.40	0.36	0.48	0.47
new0.33	easycombo	0.30	0.26	0.48	0.42
0.5	supercombo	0.03	0.35	0.49	0.28
0.166	twoclose withmylittleskip	0.15	0.17	0.51	0.63
0.166	badcombo	0.12	0.16	0.51	0.67
0.166	twoclose	0.22	0.17	0.51	0.65
old0.33	<i>twoclose</i>	<i>0.92</i>	<i>0.37</i>	<i>0.51</i>	<i>0.53</i>
0.5	<i>combo</i>	<i>-0.01</i>	<i>0.40</i>	<i>0.52</i>	<i>0.48</i>
0.5	twoopen lateral	0.27	0.43	0.53	0.44
old0.33	badcombo	0.22	0.32	0.60	0.58
0.5	twoclose	0.16	0.47	0.60	0.40
0.5	badcombo	0.04	0.49	0.69	0.44

<i>All series</i>		r1	r2	\bar{x}	$\bar{\sigma}_N$
new0.33	twoopen3	0.34	0.23	0.47	0.24
0.166	strangecombo	0.12	0.14	0.40	0.27
0.5	supercombo	0.03	0.35	0.49	0.28
new0.33	twoopen2	0.30	0.23	0.45	0.29
new0.33	supercombo	0.31	0.26	0.43	0.29
0.166	supercomboinverted	0.19	0.15	0.42	0.30
old0.33	goodcombo	0.28	0.23	0.47	0.32
0.166	twoopen	0.16	0.24	0.44	0.32
new0.33	twoopen	0.45	0.26	0.39	0.32
new0.33	twoopen mystery	0.28	0.24	0.44	0.33
0.5	goodcombo	0.68	0.37	0.41	0.34
0.166	goodcombo	0.10	0.15	0.43	0.34
0.166	bigcomboinverted	0.14	0.15	0.38	0.34
0.166	strangebigcombo	0.11	0.14	0.43	0.35
0.5	allopen	0.64	0.34	0.39	0.35
new0.33	oneopen	0.34	0.22	0.41	0.36
0.5	oneopen	0.48	0.36	0.46	0.37
0.5	supercomboinverted	0.46	0.31	0.45	0.37
old0.33	all open	0.34	0.29	0.43	0.37
0.166	allopen	0.22	0.12	0.43	0.38
0.166	allopen withskip	0.16	0.11	0.45	0.38
new0.33	supercomboinverted	0.32	0.24	0.43	0.39
0.5	twoclose	0.16	0.47	0.60	0.40
old0.33	easycombo	0.34	0.25	0.48	0.40
0.166	bigcombochange	0.19	0.13	0.40	0.40
0.166	allopenagain	0.18	0.14	0.45	0.41
0.5	bigcombo	0.50	0.40	0.43	0.41
new0.33	allopen	0.31	0.23	0.45	0.41
new0.33	easycombo	0.30	0.26	0.48	0.42
0.166	easycombo	0.21	0.12	0.43	0.42
0.166	supercombo	0.20	0.15	0.43	0.43
0.5	twoopen lateral	0.27	0.43	0.53	0.44
0.5	badcombo	0.04	0.49	0.69	0.44
0.166	oneopen	0.21	0.15	0.41	0.45
0.5	easycombo	0.40	0.36	0.48	0.47
0.5	combo	-0.01	0.40	0.52	0.48
0.5	<i>bigcombo actual</i>	<i>1.06</i>	<i>0.61</i>	<i>0.39</i>	<i>0.49</i>
old0.33	twoopen lateral	0.37	0.30	0.48	0.50
new0.33	twoopen lateral	0.42	0.26	0.46	0.52
<i>old0.33</i>	<i>twoclose</i>	<i>0.92</i>	<i>0.37</i>	<i>0.51</i>	<i>0.53</i>
new0.33	combo	0.45	0.26	0.41	0.54
0.166	combo25	0.19	0.16	0.40	0.56
old0.33	badcombo	0.22	0.32	0.60	0.58
0.166	twoopen lateral	0.17	0.22	0.43	0.58
0.166	combo	0.22	0.15	0.38	0.59
0.166	twoclose withmylittleskip	0.15	0.17	0.51	0.63
0.166	twoclose	0.22	0.17	0.51	0.65
0.166	badcombo	0.12	0.16	0.51	0.67



Comparison between some relevant combinations

50th and 95th percentiles

The comparison between average values of 50th and 95th percentiles of normalised concentration frequency distribution is quite analogous to the one between average mean concentration and standard deviation: the median value represent the bulk decay in the lagoon basin. while the 95th percentile the maximum concentration left in more stagnant areas of the lagoon basin. The first value can be seen as the short-term efficiency and the second one as the long-term efficiency. However. as discussed later. the definition of *efficiency* is subjective and both decays could be valuable according to different requirements.

Even if high values of r_1 suggest a leaking-enhanced decay for fastest decaying experiments, "artificial" combinations are the best way to reduce concentration in a short amount of time (median concentration). *Badcombo*, in particular, provides the fastest decay considering the half of the lagoon in which is active (*c c o* for inflow phase and *c o c* for outflow phase). *Supercombo* and *twoopen* minimise the maximum concentration, in accordance with their values of σ_N

<i>series 0.33</i>		r_1	r_2	50 th	95 th
<i>new0.33</i>	<i>badcombo</i>	0.47	0.28	0.36	0.88
new0.33	combo	0.45	0.26	0.37	0.80
new0.33	twoopen	0.45	0.26	0.39	0.58
new0.33	oneopen	0.34	0.22	0.40	0.64
new0.33	supercomboinverted	0.32	0.24	0.41	0.68
<i>old0.33</i>	<i>combo</i>	0.70	0.39	0.41	0.83
old0.33	all open	0.34	0.29	0.41	0.71
<i>new0.33</i>	<i>twoopen lateral</i>	0.42	0.26	0.42	0.87
old0.33	twoopen lateral	0.37	0.30	0.44	0.85
new0.33	supercombo	0.31	0.26	0.44	0.61
<i>old0.33</i>	<i>oneopen</i>	0.71	0.51	0.44	0.71
new0.33	twoopen mystery	0.28	0.24	0.44	0.64
new0.33	allopen	0.31	0.23	0.44	0.73
<i>old0.33</i>	<i>twoclose</i>	0.92	0.37	0.44	0.97
new0.33	twoopen2	0.30	0.23	0.45	0.66

The main difference between mean and median concentration decays is the faster decay of forced combinations in terms of median decay. More mixing combinations as *supercombo* while having a fast decay of 95th percentile concentration, appear to be slower than other combinations in terms of median concentration.

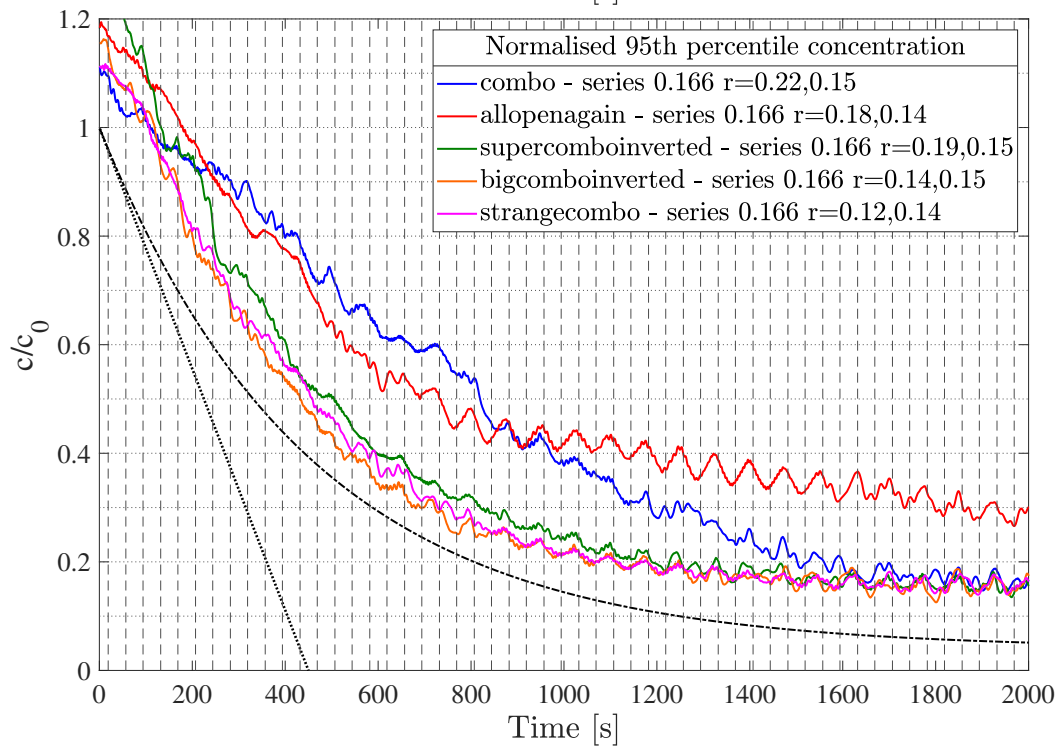
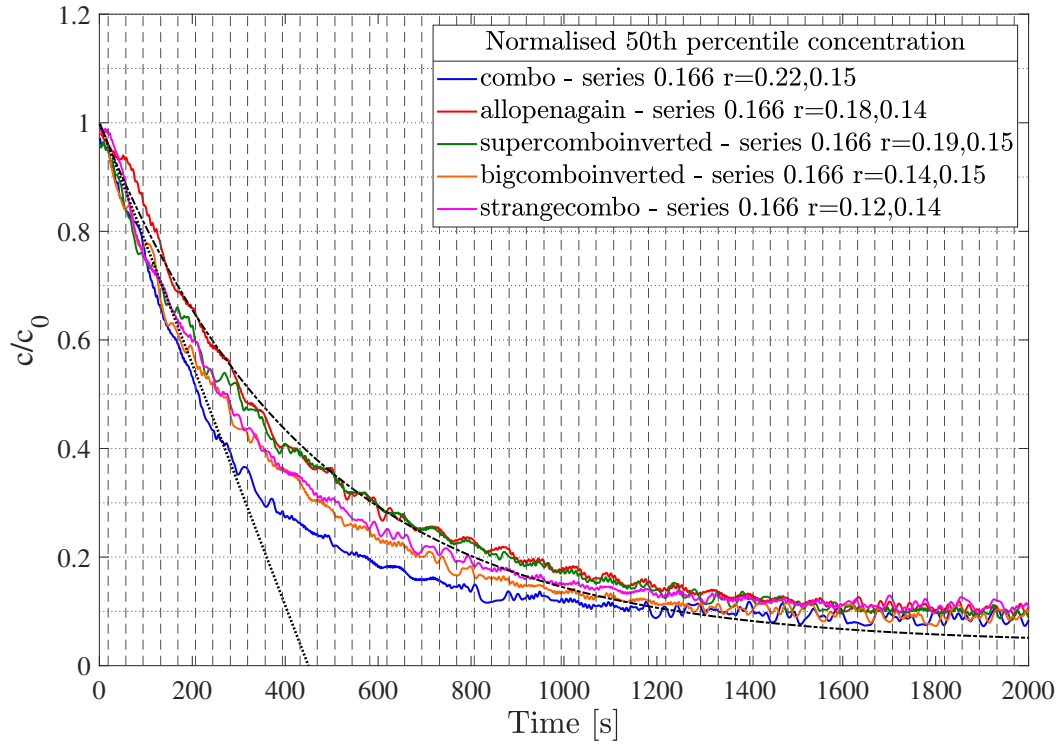
<i>series 0.166</i>	r_1	r_2	50 th	95 th
combo	0.22	0.15	0.34	0.75
combo25	0.19	0.16	0.36	0.77
twoopen lateral	0.17	0.22	0.37	0.85
bigcomboinverted	0.14	0.15	0.39	0.55
bigcombochange	0.19	0.13	0.39	0.65
supercombo	0.20	0.15	0.40	0.72
oneopen	0.21	0.15	0.40	0.67
badcombo	0.12	0.16	0.40	1.07
strangecombo	0.12	0.14	0.41	0.57
easycombo	0.21	0.12	0.42	0.73
strangebigcombo	0.11	0.14	0.42	0.63
goodcombo	0.10	0.15	0.43	0.63
supercomboinverted	0.19	0.15	0.43	0.62
twoclose	0.22	0.17	0.43	1.06
allopen	0.22	0.12	0.43	0.68
twoopen	0.16	0.24	0.44	0.62
twoclose withmylittleskip	0.15	0.17	0.44	0.98
allopen withskip	0.16	0.11	0.44	0.72
allopenagain	0.18	0.14	0.45	0.73

According to the 95th percentile sorting *bigcomboinverted* (*o c o (in)*, *c o c (out)*) has the fastest decay in terms of maximum concentration. *Allopen* and *goodcombo* from *0.5*, and *twoopen* from *new0.33* are not very reliable because of high r_1 coefficient, but they are probably quite efficient as well. *Strangecombo* from *0.166*, *supercombo* and *supercomboinverted* from *new0.33* are in the highest part of the sorting and with no clear presence of errors in them. Therefore, it seems that a well-designed forcing can provide better mixing and faster maximum concentration decay than the *allopen* natural configuration.

<i>series 0.5</i>	r_1	r_2	50 th	95 th
<i>bigcombo actual</i>	<i>1.06</i>	<i>0.61</i>	<i>0.36</i>	<i>0.70</i>
allopen	0.64	0.34	0.40	0.58
bigcombo	0.50	0.40	0.41	0.71
goodcombo	0.68	0.37	0.41	0.62
supercomboinvertedmaybe	0.46	0.31	0.43	0.72
easycombo	0.40	0.36	0.43	0.85
oneopen	0.48	0.36	0.44	0.76
<i>combo</i>	<i>-0.01</i>	<i>0.40</i>	<i>0.47</i>	<i>0.87</i>
supercombo	0.03	0.35	0.50	0.66
twoopen lateral	0.27	0.43	0.50	0.88
twoclose	0.16	0.47	0.60	0.96
badcombo	0.04	0.49	0.66	1.12

<i>All series</i>		r_1	r_2	50^{th}	95^{th}
0.166	combo	0.22	0.15	0.34	0.75
0.5	<i>bigcombo actual</i>	1.06	0.61	0.36	0.70
new0.33	<i>badcombo</i>	0.47	0.28	0.36	0.88
0.166	combo25	0.19	0.16	0.36	0.77
new0.33	combo	0.45	0.26	0.37	0.80
0.166	twoopen lateral	0.17	0.22	0.37	0.85
0.166	bigcomboinverted	0.14	0.15	0.39	0.55
0.166	bigcombochange	0.19	0.13	0.39	0.65
new0.33	twoopen	0.45	0.26	0.39	0.58
0.5	allopen	0.64	0.34	0.40	0.58
0.166	supercombo	0.20	0.15	0.40	0.72
new0.33	oneopen	0.34	0.22	0.40	0.64
0.166	oneopen	0.21	0.15	0.40	0.67
0.166	badcombo	0.12	0.16	0.40	1.07
0.166	strangecombo	0.12	0.14	0.41	0.57
0.5	bigcombo	0.50	0.40	0.41	0.71
0.5	goodcombo	0.68	0.37	0.41	0.62
new0.33	supercomboinverted	0.32	0.24	0.41	0.68
old0.33	all open	0.34	0.29	0.41	0.71
0.166	easycombo	0.21	0.12	0.42	0.73
new0.33	twoopen lateral	0.42	0.26	0.42	0.87
0.166	strangebigcombo	0.11	0.14	0.42	0.63
0.166	goodcombo	0.10	0.15	0.43	0.63
0.166	supercomboinverted	0.19	0.15	0.43	0.62
0.166	twoclose	0.22	0.17	0.43	1.06
0.5	supercomboinverted	0.46	0.31	0.43	0.72
0.166	allopen	0.22	0.12	0.43	0.68
0.5	easycombo	0.40	0.36	0.43	0.85
old0.33	twoopen lateral	0.37	0.30	0.44	0.85
new0.33	supercombo	0.31	0.26	0.44	0.61
0.5	oneopen	0.48	0.36	0.44	0.76
0.166	twoopen	0.16	0.24	0.44	0.62
new0.33	twoopen mystery	0.28	0.24	0.44	0.64
0.166	twoclose withmylittleskip	0.15	0.17	0.44	0.98
0.166	allopen withskip	0.16	0.11	0.44	0.72
new0.33	allopen	0.31	0.23	0.44	0.73
old0.33	twoclose	0.92	0.37	0.44	0.97
new0.33	twoopen2	0.30	0.23	0.45	0.66
0.166	allopenagain	0.18	0.14	0.45	0.73
old0.33	badcombo	0.22	0.32	0.46	1.15
old0.33	easycombo	0.34	0.25	0.46	0.78
new0.33	easycombo	0.30	0.26	0.46	0.85
0.5	<i>combo</i>	-0.01	0.40	0.47	0.87
old0.33	goodcombo	0.28	0.23	0.47	0.64
new0.33	twoopen3	0.34	0.23	0.48	0.64
0.5	supercombo	0.03	0.35	0.50	0.66
0.5	twoopen lateral	0.27	0.43	0.50	0.88
0.5	twoclose	0.16	0.47	0.60	0.96
0.5	badcombo	0.04	0.49	0.66	1.12

<i>All series</i>		r_1	r_2	50^{th}	95^{th}
0.166	bigcomboinverted	0.14	0.15	0.39	0.55
0.166	strangecombo	0.12	0.14	0.41	0.57
0.5	allopen	0.64	0.34	0.40	0.58
new0.33	twoopen	0.45	0.26	0.39	0.58
new0.33	supercombo	0.31	0.26	0.44	0.61
0.166	supercomboinverted	0.19	0.15	0.43	0.62
0.5	goodcombo	0.68	0.37	0.41	0.62
0.166	twoopen	0.16	0.24	0.44	0.62
0.166	goodcombo	0.10	0.15	0.43	0.63
0.166	strangebigcombo	0.11	0.14	0.42	0.63
new0.33	twoopen3	0.34	0.23	0.48	0.64
new0.33	twoopen mystery	0.28	0.24	0.44	0.64
new0.33	oneopen	0.34	0.22	0.40	0.64
old0.33	goodcombo	0.28	0.23	0.47	0.64
0.166	bigcombochange	0.19	0.13	0.39	0.65
new0.33	twoopen2	0.30	0.23	0.45	0.66
0.5	<i>supercombo</i>	<i>0.03</i>	<i>0.35</i>	<i>0.50</i>	<i>0.66</i>
0.166	oneopen	0.21	0.15	0.40	0.67
0.166	allopen	0.22	0.12	0.43	0.68
new0.33	supercomboinverted	0.32	0.24	0.41	0.68
0.5	bigcombo actual	1.06	0.61	0.36	0.70
old0.33	all open	0.34	0.29	0.41	0.71
0.5	bigcombo	0.50	0.40	0.41	0.71
0.5	supercomboinverted	0.46	0.31	0.43	0.72
0.166	supercombo	0.20	0.15	0.40	0.72
0.166	allopen withskip	0.16	0.11	0.44	0.72
new0.33	allopen	0.31	0.23	0.44	0.73
0.166	allopenagain	0.18	0.14	0.45	0.73
0.166	easycombo	0.21	0.12	0.42	0.73
0.166	combo	0.22	0.15	0.34	0.75
0.5	oneopen	0.48	0.36	0.44	0.76
0.166	combo25	0.19	0.16	0.36	0.77
old0.33	easycombo	0.34	0.25	0.46	0.78
new0.33	combo	0.45	0.26	0.37	0.80
old0.33	twoopen lateral	0.37	0.30	0.44	0.85
new0.33	easycombo	0.30	0.26	0.46	0.85
0.166	twoopen lateral	0.17	0.22	0.37	0.85
0.5	easycombo	0.40	0.36	0.43	0.85
new0.33	twoopen lateral	0.42	0.26	0.42	0.87
0.5	combo	-0.01	0.40	0.47	0.87
new0.33	badcombo	0.47	0.28	0.36	0.88
0.5	twoopen lateral	0.27	0.43	0.50	0.88
0.5	twoclose	0.16	0.47	0.60	0.96
old0.33	twoclose	0.92	0.37	0.44	0.97
0.166	twoclose withmylittleskip	0.15	0.17	0.44	0.98
0.166	twoclose	0.22	0.17	0.43	1.06
0.166	badcombo	0.12	0.16	0.40	1.07
0.5	badcombo	0.04	0.49	0.66	1.12
old0.33	badcombo	0.22	0.32	0.46	1.15



Comparison between some relevant combinations

Effect of ratio variation

Varying exchange ratio has surely effects on the concentration decay. This influence is not linear and can not be described entirely in the simplified terms of *Conceptual models*, according to which higher ratios favoured induced mechanisms. Even if the data are not always reliable, higher ratios seem to favour "natural" combinations instead, and lower ratios "artificial" ones. A possible explanation could lay in the different type of mechanism, one forced externally (and thus more forced in the case of shorter periods) and the other occurring naturally inside the lagoon and which could be inhibited by shifting phase frequently.

\bar{c}	0.166	0.33	0.5
allopen	0.59	0.6	0.55
combo	0.53	0.56	0.71
twoclose	0.64	0.66	0.75
supercombo	0.58	0.59	0.67
twoopen	0.6	0.54	
oneopen	0.56	0.56	0.62
bigcombo	0.55		0.55
easycombo	0.59	0.63	0.62
goodcombo	0.59	0.62	0.56
badcombo	0.64	0.57	0.84
twoopen lateral	0.56	0.6	0.69
supercomboinverted	0.58	0.59	0.62

σ_N	0.166	0.33	0.5
allopen	0.35	0.34	0.33
combo	0.44	0.39	0.35
twoclose	0.48	0.42	0.30
supercombo	0.38	0.28	0.25
twoopen	0.29	0.33	
oneopen	0.39	0.35	0.37
bigcombo	0.33		0.35
easycombo	0.35	0.38	0.35
goodcombo	0.31	0.28	0.35
badcombo	0.48	0.48	0.32
twoopen lateral	0.44	0.41	0.34
supercomboinverted	0.30	0.34	0.33

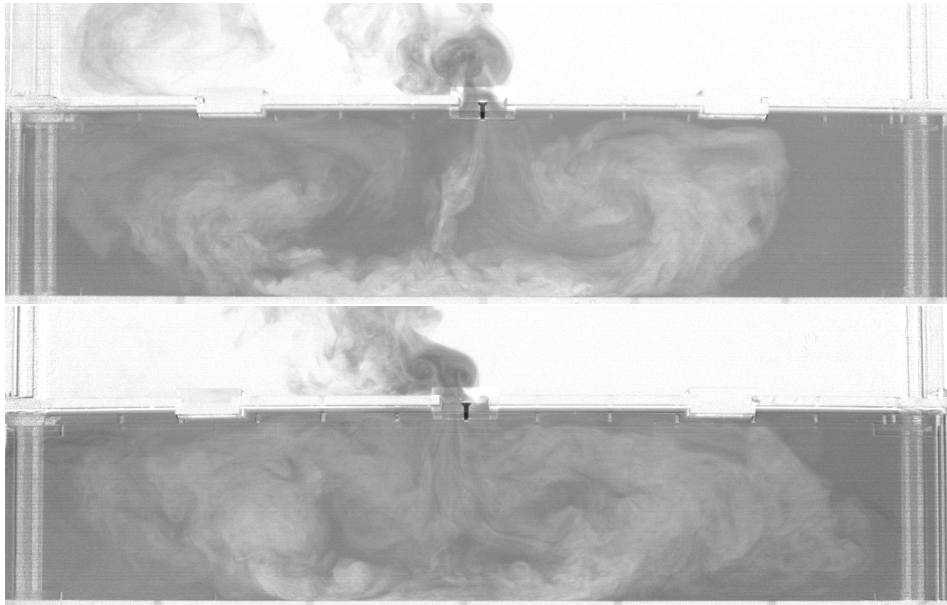
In the *Flow patterns* section it was suggested that longer periods could allow for deeper penetration of jets and this could result in a rotational cell, bringing newly added low concentration water close to outlets. Another possibility, as in *combo* combination, is that the elongated jet could reach more easily the other side of the lagoon, reaching otherwise stationary water.

50 th percentile	0.166	0.33	0.5
allopen	0.60	0.60	0.55
combo	0.51	0.54	<i>0.69</i>
twoclose	0.59	<i>0.61</i>	<i>0.77</i>
supercombo	0.56	0.60	<i>0.69</i>
twoopen	0.61	0.55	
oneopen	0.56	0.55	0.59
bigcombo	0.56		0.57
easycombo	0.58	0.61	0.60
goodcombo	0.60	0.63	0.57
badcombo	0.57	0.51	<i>0.86</i>
twoopen lateral	0.53	0.57	0.69
supercomboinverted	0.59	0.59	0.61

95 th percentile	0.166	0.33	0.5
allopen	0.93	0.96	0.80
combo	0.91	0.95	<i>1.06</i>
twoclose	1.07	<i>1.08</i>	<i>1.06</i>
supercombo	0.92	0.82	<i>0.87</i>
twoopen	0.84	0.81	
oneopen	0.85	0.88	1.01
bigcombo	0.82		0.92
easycombo	0.92	0.99	0.97
goodcombo	0.84	0.85	0.86
badcombo	1.11	1.26	<i>1.18</i>
twoopen lateral	0.98	0.99	1.03
supercomboinverted	0.85	0.90	0.95

In general, increasing the period T :

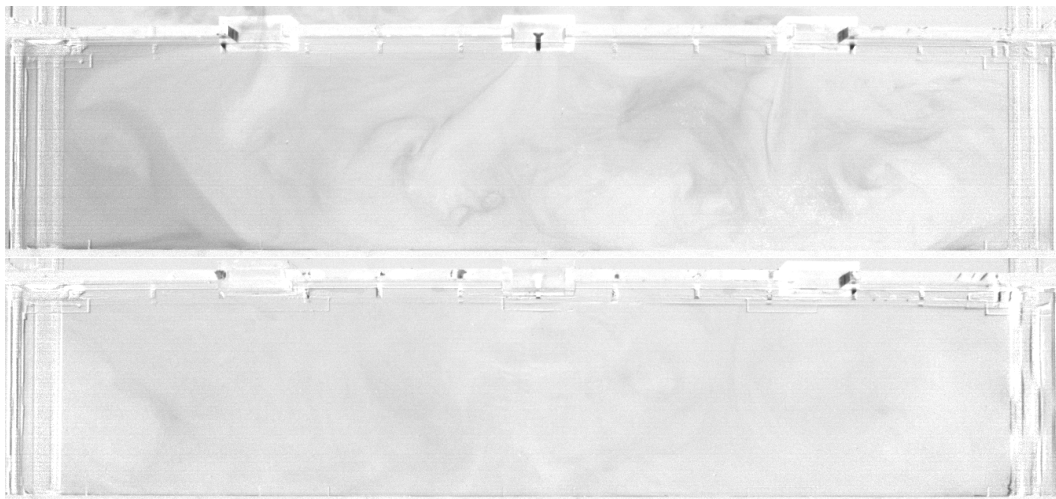
- Natural mechanisms could be helped as bigger swirls push stationary water to outlets (i.e. *allopen*); or could be penalised as rotational cells create an enclosed circulation inside the lagoon (*oneopen*);
- Forced mechanisms could be hindered as low concentration water is pushed too close to the outlets (i.e. *combo*);
- Reversed mechanism combinations have the same pattern and are not much affected (i.e. *twoclose*);
- Mixing-designed combinations could also not be much affected for the same reason (i.e. *supercombo*);



Comparison between *oneopen* pattern in one sixth (half rotational cell) and one half ratio (full rotational cell)

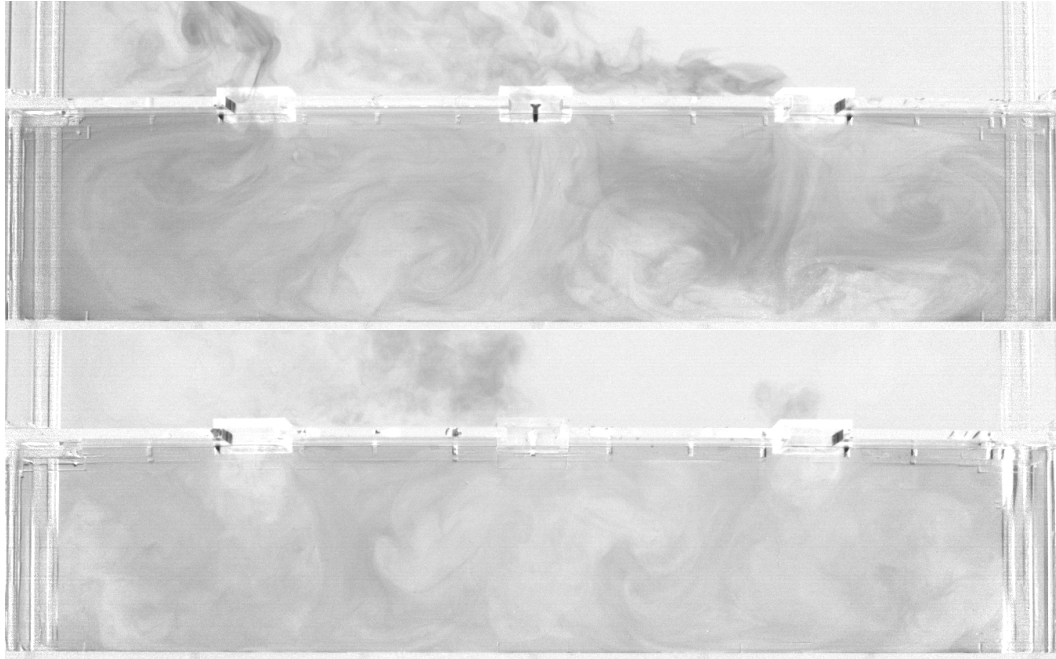
Visual comparisons

It could be not straightforward to realise how relevant is the difference between specific combinations. In this section some camera frames at time 956 are given to get an idea of how numbers relate visually to experiments.



Allopen and *bigcomboinverted* from 0.166 at $t = 956$

It is interesting to notice how the *narrow gap* experiment, a *twoclose* combination with a restrained inlet, compare with the *twoclose* experiment: the stronger jet seem to allow for more mixing and overall the *narrowgap* has a faster decay. However, for its peculiarity, this experiment has not been included in the general comparison.



Allopen and bigcomboinverted from 0.166 at $t = 509$



Combo, supercomboinverted, strangecombo, twoclose and narrowgap from 0.166 at $t = 956$

Repeated experiments

In this section some comparisons between different experiment runs of the same combination are given. This is relevant to assess general error in experiments and predictability of r_1 and r_2 coefficients.

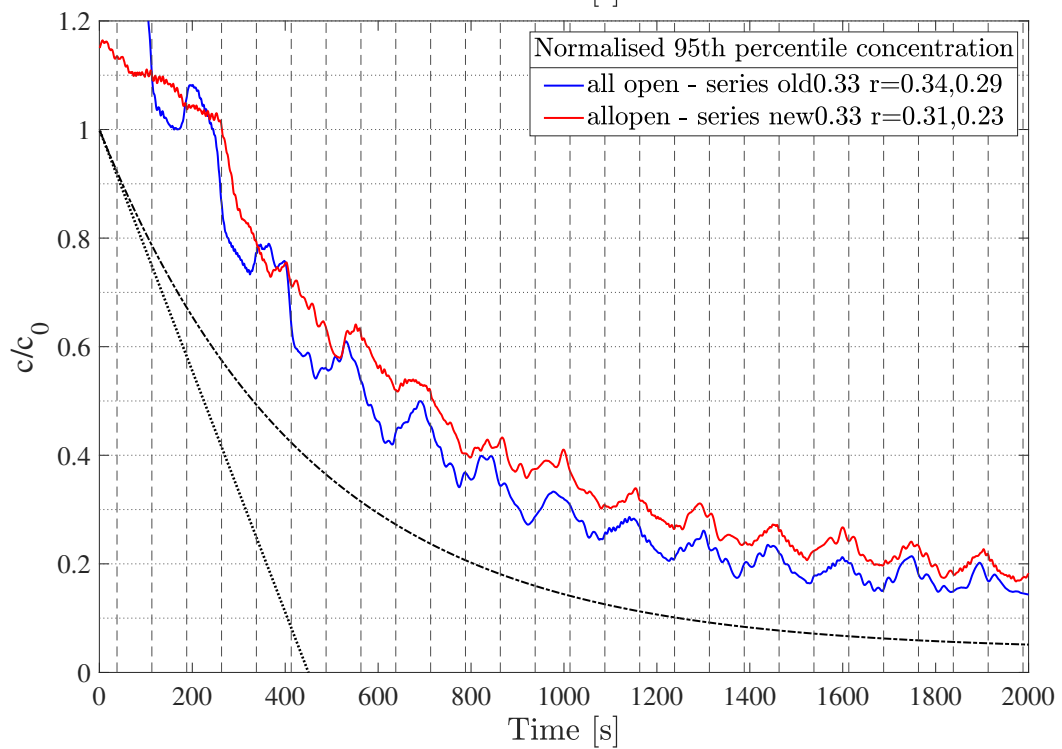
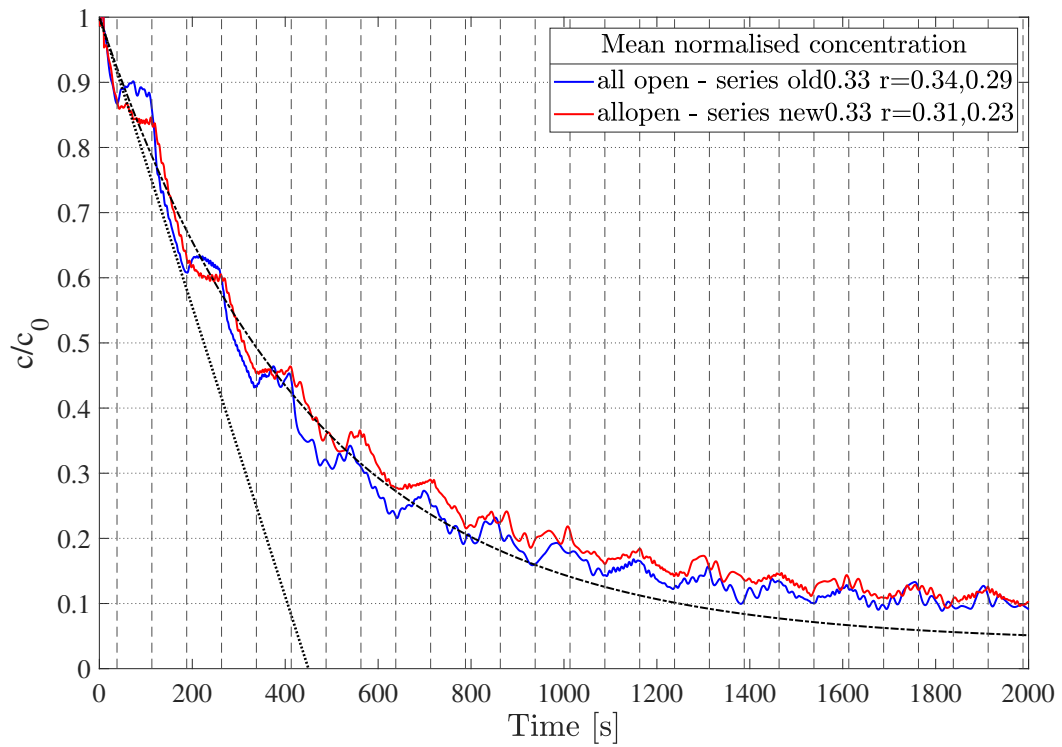
The first example is *allopen* from *old0.33* and *new0.33*:

Twoopen has been repeated in *new0.33* without replacing the water in the tank, therefore a residual concentration is present and affects concentration decays.

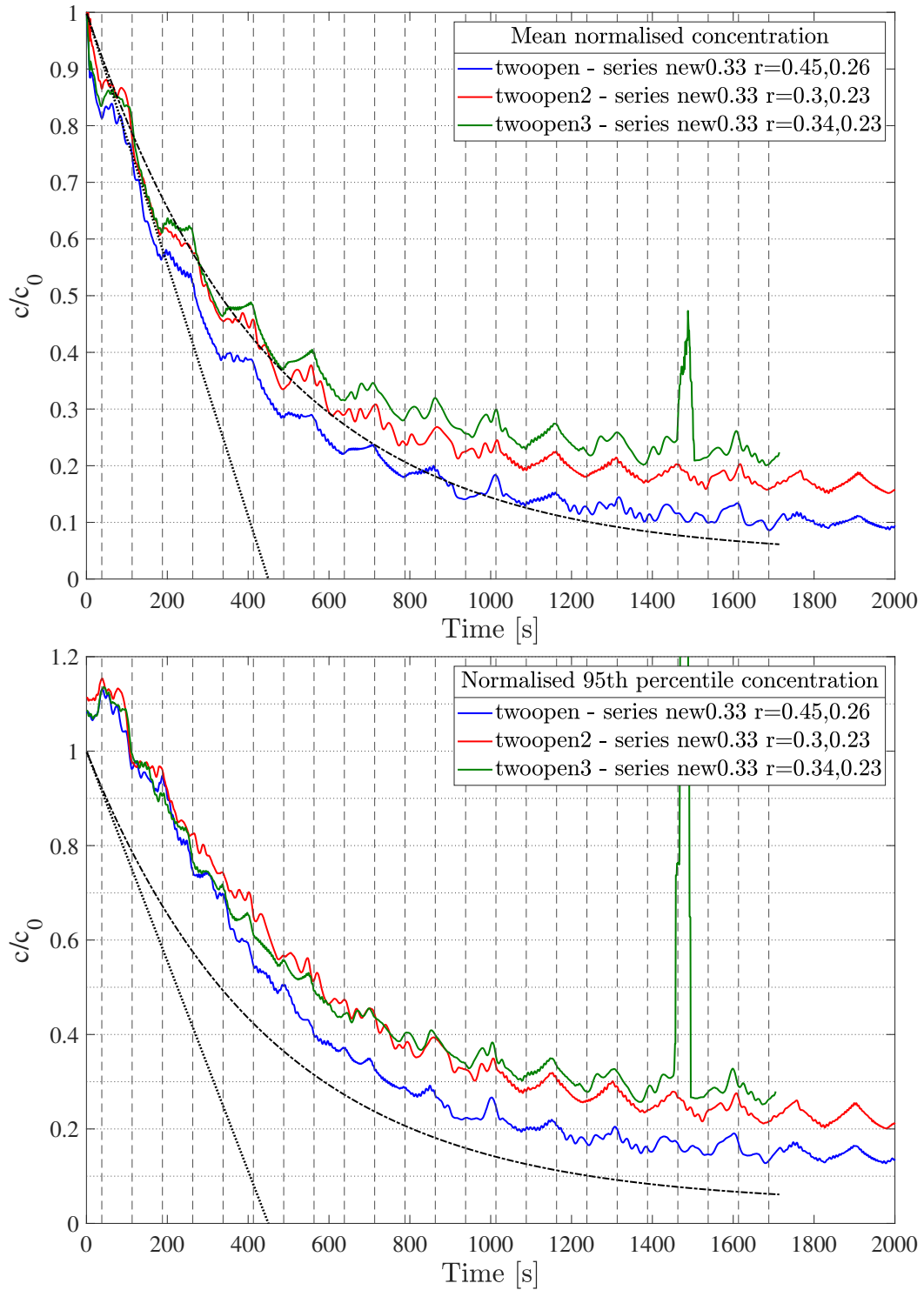
A good example of the validity of *reliability* coefficients r_1 and r_2 is the *bigcombo* comparison in *0.5* series.

<i>956-averaged</i>	r_1	r_2	\bar{c}	σ_N	50^{th}	95^{th}
bigcombo	0.50	0.40	0.43	0.41	0.41	0.71
bigcombo actual	1.06	0.61	0.39	0.49	0.36	0.70

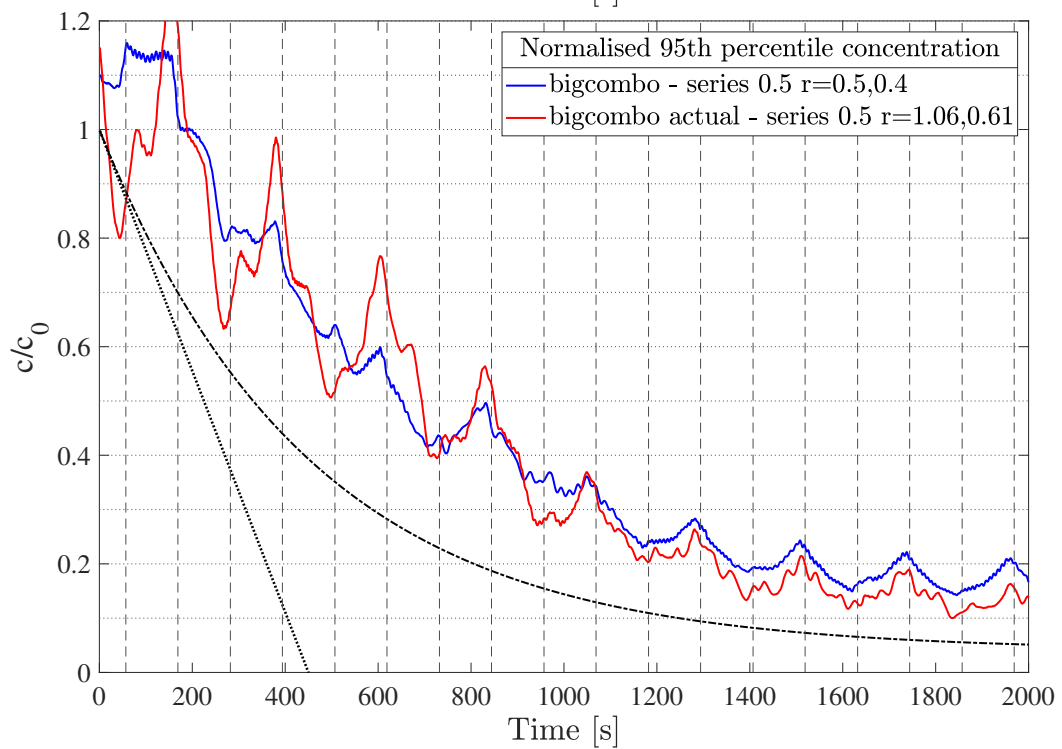
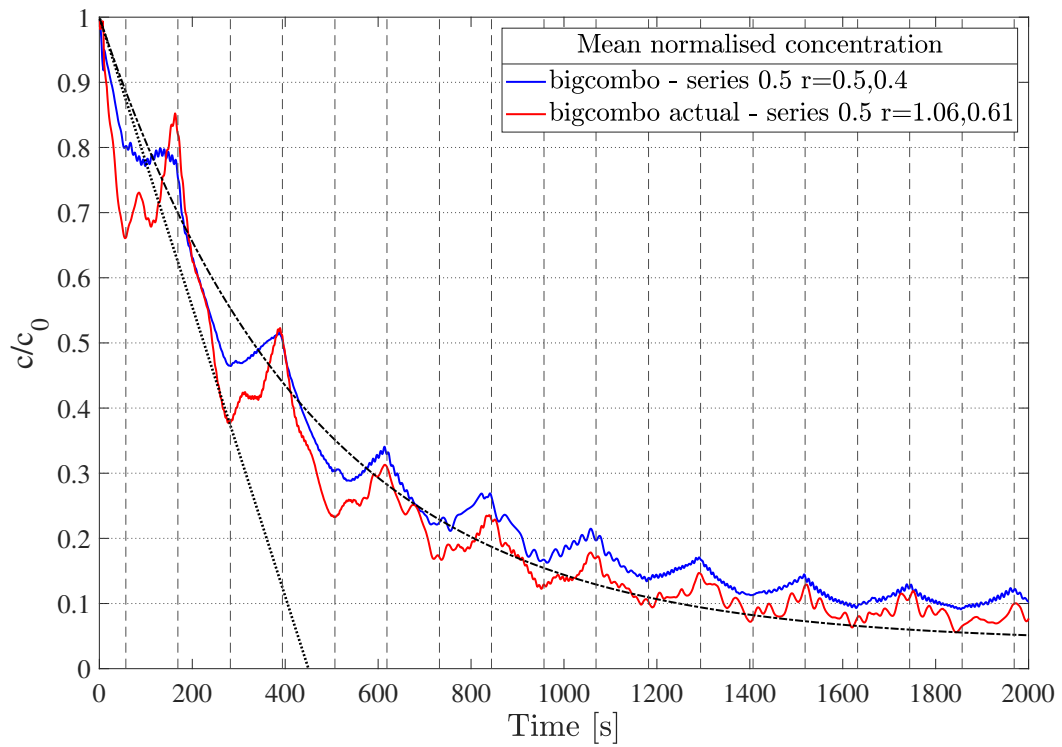
More generally comparisons can be drawn also looking at table coefficients for \bar{c} , σ_N , 50^{th} percentile and 95^{th} percentile averaged over the first 956 s. *Reliability* coefficients seem to address a great part of same combination experiments error.



Normalised mean and 95th percentile concentration of *twoopen* combinations with $r = 1/3$.



Normalised mean and 95th percentile concentration of *twoopen* combinations run consecutively without replacing tank water.



Normalised mean and 95th percentile concentration of *bigcombo* combinations with $r = 1/2$.

Discussion on flushing or ventilation efficiency

In order to characterize the mixing efficiency of the system a three parameters exponential interpolation was chosen previously for mean concentration over time data.

$$c_{mean}(t) = b_1 \exp b_2 t + b_3$$

This worked very well for most combinations, less well for inefficient combinations in short intervals.

Sum $b_1 + b_3$ represents initial concentration, $b_2 < 0$ is the exponential decay and b_3 the asymptotic concentration (as $t \rightarrow +\infty$). Therefore thanks to this interpolation an efficiency coefficient has been defined:

$$\alpha = -\frac{b_1 \cdot b_2}{b_3} T$$

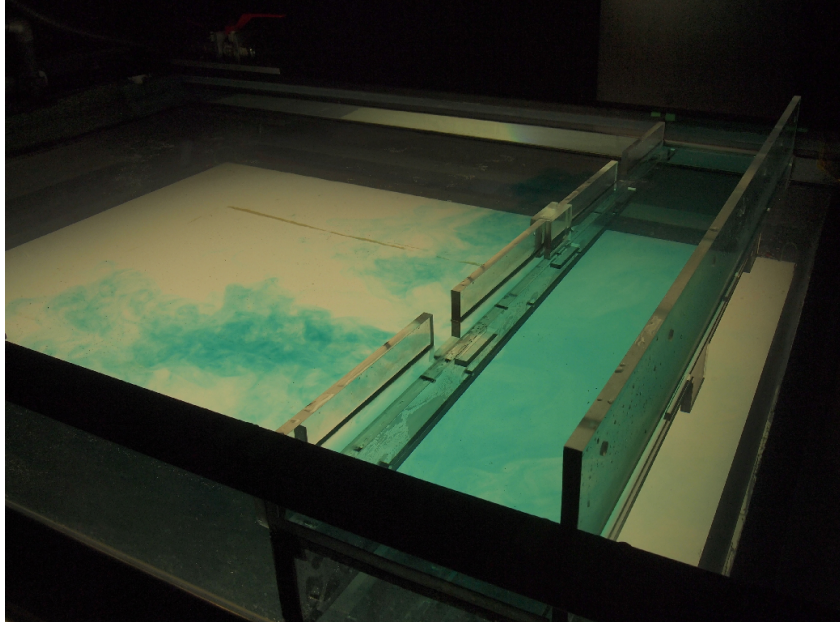
The coefficients were processed and the resulting ranking agreed for almost all cases with the one obtained by looking at later times concentration. This means that the coefficient characterises concentration decay effectively but results were not clear.

Nevertheless, the standardised coefficients which have been drawn by averaging mean concentration, standard deviation, 50th and 95th percentiles over the same time duration (first 956 s) offer a deeper look into experiments. The coefficients, even if affected by errors as experiments are, depict quite well how fast the decay is over the lagoon domain. Mean and median concentration give a quick estimation on the bulk mechanisms of decay while the high 95th percentile concentration and the standard deviation address the concentration variability over the lagoon.

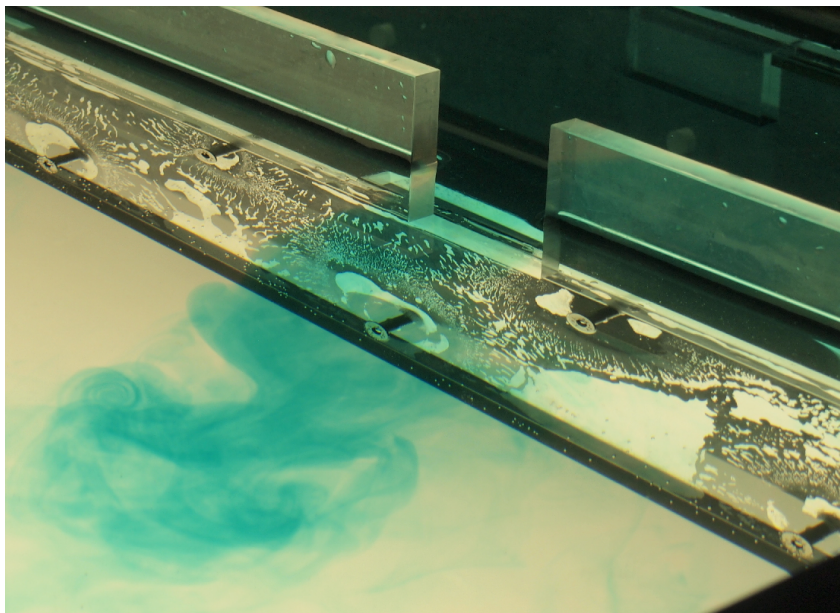
If the main concern is a quick decay, combinations which focus on median values decay mechanisms are more helpful and thus considered more efficient. On the other hand, if the main objective is to lower concentration values across all the basin, then more mixing mechanisms, with fast decay in maximum concentration and lower variability, are to be considered more efficient.

Experiments provide sufficient evidence that a well-designed combination can be more effective in reducing concentration than the natural configuration with all inlets open. For example, some combinations provide better overall mixing, others, as more potent jets are created by selectively opening specific inlets, can be useful in targeting a specific region.

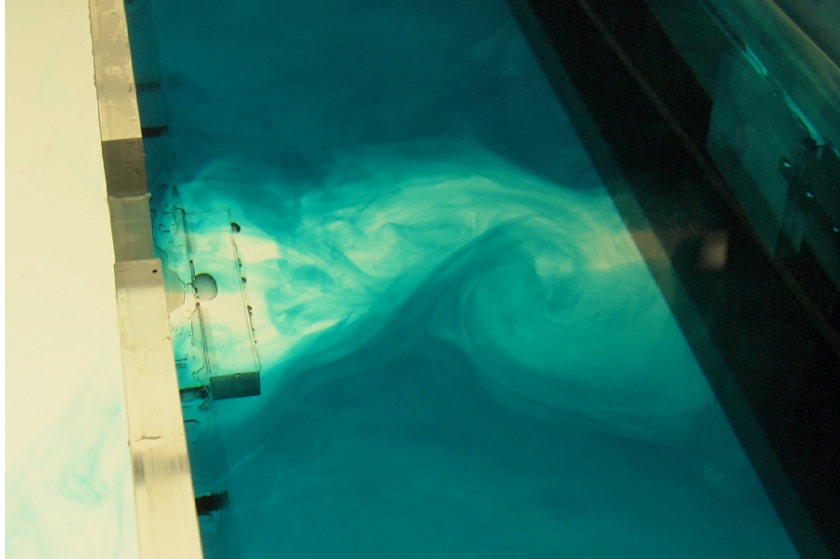
Appendix: photo gallery



Angled view of experiment run



Flow in the sea basin from lagoon outlet



Entraining jet



Flow rate valve system and reservoir

Chapter 4

Numerical simulations

As experimental results tend to overlap because of several errors, a homogeneous environment as the numerical one of CFD simulations is used to provide more accuracy. The chosen tool for this task is OpenFOAM.

OpenFOAM

OpenFOAM (Open Source Field Operation and Manipulation) is a C++ library designed as a toolkit to solve partial and ordinary differential equations, mostly regarding continuum mechanics problems (but especially computational fluid dynamics ones). Based on the Finite Volume Method (FVM), it provides many well-tested solvers, pre-processing and post-processing utilities, including mesh generation tools. Being licensed under the GNU General Public License (GPL) it is free, can be used in parallel on many computers (which makes it ideal for High Performance Computing networks), source code is accessible and can be modified, this is especially useful to tailor numerical methods on one's specific need. Thanks to its versatility it is wide-spread in industry, academia and research laboratories and it is under continuous development.

In comparison to commercial CFD applications it suffers from the lack of a native GUI, it is not well documented and often the user needs to read the source code and modify it, which is empowering and frustrating at the same time.

The interface in OpenFOAM is the bash terminal, and a plugin (*paraFoam*) allows for visualisation of solution data and mesh in *ParaView*. There is a characteristic directory structure with classes, executables and libraries; in particular, the *run* directory hosts *cases*, i.e. directories where all necessary information for a specific simulation is stored. OpenFOAM allocates two directories for user-defined solvers and user-defined libraries.

For the purpose of processing the simulations object of the present chapter, a standard solver, *interFoam*, has been modified to include a passive tracer diffusion and a specific correction has been implemented in it; to simulate the opening combinations three boundary conditions have been coded. Additionally, some *Python* scripts are used for post-processing data..

CINECA

CINECA (as originally named "Consorzio Interuniversitario per il Calcolo Automatico dell'Italia Nord Orientale") is a non-profit consortium, made up of 67 Italian universities, 9 national research centres, and the Ministry of Universities and Research (MIUR) and hosts the most powerful supercomputing centre for scientific research in Italy; *MARCONI-100*, for example, is a part of the *CINECA* network and represents the 11th most powerful computer system commercially available in the world, as of november 2020 *Top500* ranking. The newcoming *Galileo100* will furtherly upgrade the network in May 2021.

Given the need for large computational resources, an application was made to *CINECA* for an IS CRA type C project. The project was approved and a total of 67448 core hours on *GALILEO* nodes have been used for the simulations.

Computational methods

FVM method

In this paragraph a brief overview of the *Finite Volume Method*, one of the theoretical foundations of CFD, is provided; the aim is not to describe the method in detail, but just to give a simple idea of how a physical problem can be reduced to a large set of numerical equations.

The method consists in dividing the solution domain into a finite number of arbitrary control volumes (or cells): through appropriate approximations one or more partial differential equations are converted into an equivalent system of algebraic equations, for which the solution can be numerically sought. The discretisation takes place in two steps: discretisation of the domain (the cells of the mesh) and discretisation of the equation. The cells represent the control volumes, over which integral balance equations are applied; they cover all the computational domain and do not overlap. In each control volume a particular point, called *centroid*, is representative of the cell, and it is defined by the subsequent property:

$$\int_{V_P} (\vec{x} - \vec{x}_P) dV = 0$$

where \vec{x} is the space vector, \vec{x}_P the coordinates of the centroid, and V_P the volume of the cell. Likewise the centroid of each bounding surface, assuming the cell has polyhedral form, is $\int_{S_f} (\vec{x} - \vec{x}_P) dS = 0$

The last assumption is that any quantity ϕ can be represented as a piecewise constant profile through space, where the constant in each cell is the mean value:

$$\phi_P = \bar{\phi} = \frac{1}{V_P} \int_{V_P} \phi(x) dV$$

At this point it is possible to apply the general transport equation, the true starting point of the Finite Volume Method:

$$\int_{V_P} \frac{\partial \rho \phi}{\partial t} dV + \int_{V_P} \vec{\nabla} \cdot (\rho \vec{u} \phi) dV - \int_{V_P} \vec{\nabla} \cdot (\rho \Gamma_\phi \vec{\nabla} \phi) dV = \int_{V_P} S_\phi(\phi) dV$$

where ρ is the density of the fluid, \vec{u} the velocity, Γ is the tensor diffusion coefficient matrix and $S_\phi(\phi)$ the source term per unit volume.

Given that the second derivative in space appears in the diffusion term, the equation is of second order, and the approximate solution needs to be second order-accurate, and, as the truncation error in the Taylor expansion scales with $|(\vec{x} - \vec{x}_P)^2|$, this means that the solution must be linear in both space and time:

$$\phi(\vec{x}) = \phi_P + (\vec{x} - \vec{x}_P) \cdot (\vec{\nabla}\phi)_P \quad \phi(t + \delta t) = \phi^t + \delta t \left(\frac{\partial\phi}{\partial t}\right)^t$$

where $\phi_P = \phi(\vec{x}_P)$ and $\phi^t = \phi(t)$

Making use of the Gauss divergence theorem:

$$\int_V \vec{\nabla} \cdot \vec{a} dV = \oint_{\partial V} \vec{a} \cdot d\vec{S}$$

where $d\vec{S} = \vec{n}dS$ (positive sign for outward surface normal vector), the equation takes the form:

$$\int_{V_P} \frac{\partial\rho\phi}{\partial t} dV + \oint_{\partial V_P} d\vec{S} \cdot (\rho\vec{u}\phi) - \oint_{\partial V_P} d\vec{S} \cdot (\rho\Gamma_\phi\vec{\nabla}\phi) = \int_{V_P} S_\phi(\phi) dV$$

Using the surfaces centroid notation (midpoint rule approximation) and the assumption of polyhedral cell:

$$\oint_{\partial V_P} d\vec{S} \cdot (\rho\vec{u}\phi) = \sum_f \int_f d\vec{S} \cdot (\rho\vec{u}\phi)_f \approx \sum_f \vec{S}_f \cdot (\rho\vec{u}\phi)_f$$

And for the diffusive term:

$$\oint_{\partial V_P} d\vec{S} \cdot (\rho\Gamma_\phi\vec{\nabla}\phi) = \sum_f \int_f d\vec{S} \cdot (\rho\Gamma_\phi\vec{\nabla}\phi)_f \approx \sum_f \vec{S}_f \cdot (\rho\Gamma_\phi\vec{\nabla}\phi)_f$$

The gradient term, again thanks to the Gauss theorem, can be expressed as:

$$(\partial\phi)_P = \frac{1}{V_P} \sum_f (\vec{S}_f \phi_f)$$

And the source term, dependent of ϕ , is linearised in:

$$\int_{V_P} S_\phi(\phi) dV = S_c V_P + S_p V_P \phi_P$$

Putting altogether:

$$\int_{V_P} \frac{\partial\rho\phi}{\partial t} dV + \sum_f \vec{S}_f \cdot (\rho\vec{u}\phi)_f - \sum_f \vec{S}_f \cdot (\rho\Gamma_\phi\vec{\nabla}\phi)_f = (S_c V_P + S_p V_P \phi_P)$$

Where the convective flux is:

$$\vec{S} \cdot (\rho\vec{u}\phi) = F^C$$

and the diffusive flux is:

$$\vec{S} \cdot (\rho \Gamma_\phi \vec{\nabla} \phi) = F^D$$

The surface values which appear in the terms should be calculated through an *interpolation scheme*, of which the simplest is the linear interpolation scheme:

$$\phi_f = f_x \phi_P + (1 - f_x) \phi_N$$

where f_x is the fraction of distance between the two cells centroids P and N . Other interpolation schemes are possible and provide different convergence outcomes in terms of numerical computation.

As for the temporal discretisation the linearisation brings to:

$$\int_t^{t+\Delta t} [(\frac{\partial \rho \phi}{\partial t})_P V_P + \sum_f \vec{S}_f \cdot (\rho \vec{u} \phi)_f - \sum_f \vec{S}_f \cdot (\rho \Gamma_\phi \vec{\nabla} \phi)_f] dt = \int_t^{t+\Delta t} [(S_c V_P + S_p V_P \phi_P)] dt$$

$$(\frac{\partial \rho \phi}{\partial t})_P = \frac{\rho_P^n \phi_P^n - \rho_P^0 \phi_P^0}{\Delta t}$$

$$\int_t^{t+\Delta t} \phi(t) dt = \frac{1}{2} (\phi^0 + \phi^n) \Delta t$$

where $\phi^n = \phi(t + \Delta t)$ and $\phi^0 = \phi(t)$

$$\frac{\rho_P^n \phi_P^n - \rho_P^0 \phi_P^0}{\Delta t} V_P + \frac{1}{2} \sum_f F \phi_f^n - \frac{1}{2} (\rho \Gamma_\phi)_f \vec{S} \cdot (\vec{\nabla} \phi)_f^n + \frac{1}{2} \sum_f F \phi_f^0 - \frac{1}{2} (\rho \Gamma_\phi)_f \vec{S} \cdot (\vec{\nabla} \phi)_f^0$$

$$= S_u V_p + \frac{1}{2} S_p V_p \phi_P^n + \frac{1}{2} S_p V_p \phi_P^0$$

$$a_P \phi_P^n + \sum_N a_N \phi_N^n = R_P$$

for each control volume. As ϕ_P^n depends on the neighbouring cells values of ϕ_P^n , a system of algebraic equations is created:

$$[A][\phi] = [R]$$

This procedure represents is the Crank-Nicolson temporal discretisation method, it is an implicit method and it is unconditionally stable, but it could give unbounded solutions. Using old time-field values for the face values of ϕ and $\vec{\nabla} \phi$ brings to the *explicit discretisation*, where ϕ_P^n is expressed only in terms of old-time values:

$$\phi_P^n = \phi_P^0 + \frac{\Delta t}{\rho_P V_P} [\sum_f F \phi_f - \sum_f (\rho \Gamma_\phi)_f \vec{S} \cdot (\vec{\nabla} \phi)_f + S_u V_P + S_p V_P \phi_P^0]$$

While this second method allows a direct calculation of ϕ_P , the system becomes unstable when a particular ratio, called the Courant number, is lesser than 1:

$$Co = \frac{\vec{u} \cdot \Delta \vec{x}}{\Delta t}$$

Intuitively, this number represents the ratio between physical velocity and numerical velocity, as a discretisation constraint, and it is an important parameter for numerical stability.

Volume of Fluid method and interFoam

As the main problem of the thesis presents a moving free surface whose shape largely characterises the internal flow, it is of paramount importance to model it accurately, and the only way to do so is to model both water and air phases, which leads to a multiphase flow problem. The *Volume of Fluid* (VoF) Method, presented by C. W. "Tony" Hirt and B. D. Nichols in 1981, represents one of the most succesful and simple approaches in dealing with multiphase flow simulations. The solver used for the simulations, *interFoam*, is based on this method and then it is modified to the specific purposes of the work.

The basic idea behind the method is the introduction of an *indicator function* α , which determines wether one fluid (e.g. liquid phase, water, $\alpha = 1$) or another (e.g. gaseous phase, air, $\alpha = 0$) occupies a certain portion of space (e.g. a cell). When both phases are present, as at the interface between the two, the function assumes values between 0 and 1. In fact, the interface can be defined at the centroids of the cells where α is closest to $\frac{1}{2}$.

The indicator function α can be seen as a water fraction quantity, as far as the simulations of the present thesis are concerned, and the conservation equation can be applied to it, leading to the subsequent three equations set:

$$\begin{cases} \vec{\nabla} \cdot \vec{u} = 0 \\ \frac{\partial(\rho\vec{u})}{\partial t} + \vec{\nabla} \cdot (\rho\vec{u}\vec{u}) = -\vec{\nabla}p + \vec{\nabla} \cdot \vec{\vec{T}} + \rho\vec{f}_b \\ \frac{\partial\alpha}{\partial t} + \vec{\nabla} \cdot (\vec{u}\alpha) = 0 \end{cases}$$

in which \vec{u} is the velocity of the fluid, ρ the density, p the pressure, $\vec{\vec{T}} = 2\mu\vec{\vec{S}} - 2\mu(\vec{\nabla} \cdot \vec{u})I/3$ is the deviatoric stress tensor ($\vec{\vec{S}} = \frac{1}{2}[\vec{\nabla}\vec{u} + (\vec{\nabla}\vec{u})^T]$ the mean rate of stress tensor, and $\vec{\vec{I}} = \delta_{ij}$ the identity tensor denoted with the Kronecker delta), \vec{f}_b is a term to mean all body forces per unit mass.

In order to make sense of the same variables used to define fluid properties of two different phases density and viscosity are simply modeled as

$$\rho = \rho_1\alpha + \rho_2(1 - \alpha) \quad \mu = \mu_1\alpha + \mu_2(1 - \alpha)$$

wherein the indices denote the two phases, in this case 1 for water phase and 2 for air phase.

However, this modelisation has some issues in dealing with phase conservation, and later developments of the method rely on a particular two-fluid formulation in which the conservation of each phase is invoked:

$$\begin{cases} \frac{\partial\alpha}{\partial t} + \vec{\nabla} \cdot (\vec{u}_1\alpha) = 0 \\ \frac{\partial(1-\alpha)}{\partial t} + \vec{\nabla} \cdot (\vec{u}_2(1 - \alpha)) = 0 \end{cases}$$

With the further introduction of a weighted velocity $\vec{u} = \alpha\vec{u}_1 + (1 - \alpha)\vec{u}_2$.

Thanks to this formulation the phase conservation equation can be rearranged in:

$$\frac{\partial\alpha}{\partial t} + \vec{\nabla} \cdot (\vec{u}\alpha) + \vec{\nabla} \cdot (\vec{u}_r\alpha(1 - \alpha)) = 0$$

which now is able to capture the dynamics of the phase in time and track adequately the interface. In particular, the new term is non-zero only when a mix of the two phases is at play, as at the interface, and $\vec{u}_r = \vec{u}_1 - \vec{u}_2$ is the relative velocity between the two phases and is also called *compression velocity*. This velocity is determined from the gradient of phase fraction α and the flux in a certain cell, its computation can include other parameters to allow for a better control of the simulation behaviour at the interface.

MULES (Multidimensional Universal Limiter for Explicit Solution) is also a useful tool to smooth α values at the interface and return a behaviour closer to the one of a free surface. The correction is conservative and redistributes the phase fraction values according to a minimising logic, reducing drastically numerical oscillations around the solution. When coupled with an α -equation subcycling it provides great accuracy and stability.

Additionally, a ratio similar to the Courant number is defined, the *interface Courant number*:

$$\phi Co = \frac{1}{2} \max\left(\frac{\sum \phi}{V}\right) \Delta t$$

where the sum of $\phi = \vec{u} \cdot \vec{S}$ is the total flux and V is the volume of the cell. The meaning for the ϕCo is similar to the one of the Co number, but the focus is not on velocity in itself but on how much volume can be exchanged in a timestep. This number needs to be much smaller than 1 for the simulation to carry sensible results, even values of 0.1, which is usually considered low for the Courant number, can provide dangerously realistic but unacceptably inaccurate results.

Turbulence LES modeling

Turbulence can be described as an unsteady, aperiodic, multiscale motion of fluids in which velocity and pressure fluctuate unpredictably in space and time. This phenomenon is one of the most fascinating and studied in fluid dynamics, in mathematical terms it can be seen as a very high sensitivity of equations to initial and boundary conditions. A good measure of turbulence is the *Reynolds* number:

$$Re = \frac{\rho UL}{\mu}$$

From which it is clear that high velocities (U), low viscosity (μ) and large scales (L) favour turbulence, as common experience suggests. As already seen in the introductory chapter, the Reynolds number for the experiments is about $Re = \frac{10^3 \cdot 10^{-2} \cdot 10^{-1}}{10^{-3}} \approx 1000$, a value for a transient flow, more laminar than turbulent but with defined turbulence features, and thus, requiring a proper turbulence modelisation.

For CFD it is quite a challenge to produce an accurate depiction of this aspect of fluids motion and typically computational methods rely on modelling the smaller scales which have a more universal behaviour. Elaborated models are much less demanding in terms of computational cost, but require a lot of calibration and mathematical complexity, simple models provide more realistic results at the expense of much more

computational time. *RANS* (*Reynolds Averaged Navier-Stokes equations*) modelling can be seen as a good example of the first case: fundamental fluid quantities are described in terms of an average and a fluctuating component, the development in the equations bring to a characteristic tensor of mixed fluctuating terms which can be modelled in different ways. The outcome is usually an average image, reliable for the computation of pressure and forces in industrial applications, but sometimes not appropriate for diffusive processes. At the other end of the spectrum *DNS* (*Direct Numerical Simulations*) require no modelling whatsoever (pure Navier Stokes equations) but an extremely fine mesh and are not applicable for medium scale flows. *Large Eddy Simulations* (LES) is a simple way to solve directly turbulence at large-medium scale by filtering the small length scales, where computation is more demanding. The filtering operation can be viewed as a spatial average over an assigned length scale. In general, a *filter function* $G(\vec{x}, \vec{x}', \Delta)$ is defined as:

$$\bar{\phi}(\vec{x}, t) = \int_{-\infty}^{+\infty} \int_{-\infty}^{+\infty} \int_{-\infty}^{+\infty} G(\vec{x}, \vec{x}', \Delta) \phi(\vec{x}', t) dx'_1 dx'_2 dx'_3$$

where $\bar{\phi}(\vec{x}, t)$ is the filtered function and Δ is the cutoff width. One simple example of filter function, typically used in the Finite Volume Method, is the "top-hat" or "box" filter:

$$G(\vec{x}, \vec{x}', \Delta) = \begin{cases} 1/\Delta^3 & |\vec{x} - \vec{x}'| \leq \Delta/2 \\ 0 & |\vec{x} - \vec{x}'| > \Delta/2 \end{cases}$$

The cut-off width represents the indicative measure of the size of the eddies which are retained in the computation; its value can be arbitrary but in CFD applications there is no advantage in having a cutoff width smaller than the grid size, and usually the cubic root of the cell volume is taken.

The filtering is a linear operator and can be applied to Navier Stokes equations (NSE) in a similar way of the average operator for the RANS (Reynolds Averaged Navier Stokes) equations.

$$\begin{cases} \frac{\partial \rho}{\partial t} + \vec{\nabla} \cdot (\rho \vec{u}) = 0 \\ \frac{\partial \rho \bar{u}}{\partial t} + \vec{\nabla} \cdot (\rho \bar{u} \vec{u}) = -\frac{\partial \bar{p}}{\partial x} + \mu \vec{\nabla} \cdot (\vec{\nabla} \bar{u} - (\vec{\nabla} \cdot (\rho \bar{u} \vec{u}) - \vec{\nabla} \cdot (\rho \bar{u} \vec{u})) \\ \frac{\partial \rho \bar{v}}{\partial t} + \vec{\nabla} \cdot (\rho \bar{v} \vec{u}) = -\frac{\partial \bar{p}}{\partial y} + \mu \vec{\nabla} \cdot (\vec{\nabla} \bar{v} - (\vec{\nabla} \cdot (\rho \bar{v} \vec{u}) - \vec{\nabla} \cdot (\rho \bar{v} \vec{u})) \\ \frac{\partial \rho \bar{w}}{\partial t} + \vec{\nabla} \cdot (\rho \bar{w} \vec{u}) = -\frac{\partial \bar{p}}{\partial z} + \mu \vec{\nabla} \cdot (\vec{\nabla} \bar{w} - (\vec{\nabla} \cdot (\rho \bar{w} \vec{u}) - \vec{\nabla} \cdot (\rho \bar{w} \vec{u})) \end{cases}$$

Where the terms

$$\vec{\nabla} \cdot (\rho \bar{u}_i \vec{u} - \rho \bar{u}_i \vec{u}) = \frac{\partial \tau_{ij}}{\partial x_j}$$

represent the *sub-grid scale stresses* effects, which can be furtherly developed and then modeled in different ways. The discussion of the various models goes beyond the scope of the present work, and, as far as the simulations are concerned, they have low impact on results, because of the low Reynolds number of the flow at play.

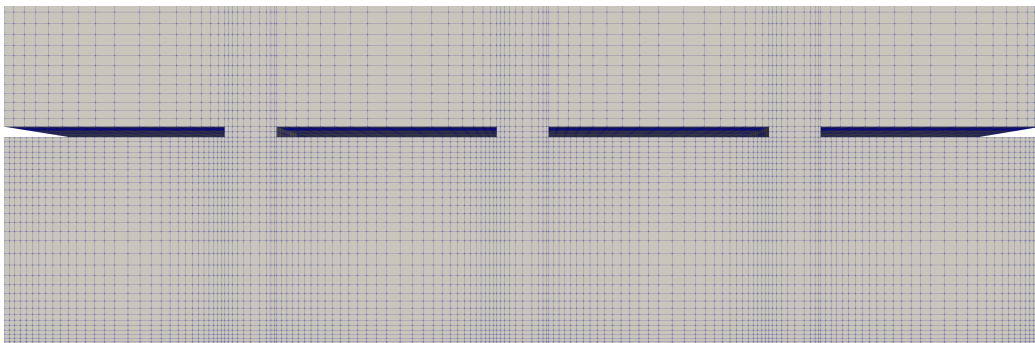
Cases mesh

In general a mesh is a collection of vertices, edges and faces which defines an object geometrically. In continuum mechanics the mesh generation is especially a domain discretization: the geometrical representation of the physical domain is divided into a finite number of discrete regions or cells. Each cell represents a control volume in which the physical laws of the phenomena at play are approximated and a numerical solution is sought.

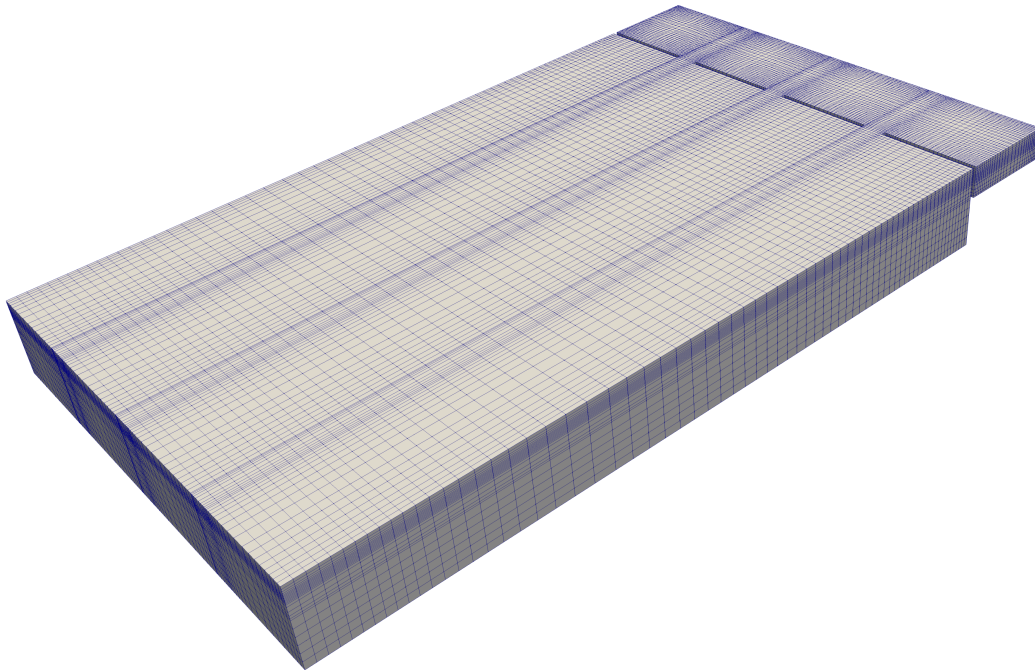
For best results, mesh resolution needs to address all the scales involved in the problem of interest. A coarse mesh could be blind to the phenomena under consideration, while a very fine mesh could cause numerical instabilities, be unnecessarily precise and excessively costly in terms of computational time and resources. Usually the mesh is refined or coarsened depending on where accuracy is needed.

As the original geometry of the experimental setup is rather simple, an orthogonal structured mesh has been implemented with the simple utility *blockMesh*. The mesh is conveniently graded towards the walls and the inlets, to capture adequately the physics involved. To account for the tidal waves an AMR (Adaptive Mesh Refinement) procedure was initially set on water and air interface, optimising refinement right at the wave interface. However, this approach would have cost the loss of the orthogonality and a resulting degradation of the mesh quality: considering the very small time step used to manage the rapid variations at the inlets, a vertical grading spread over the tidal amplitude was preferred, with the choice of relying on the solver algorithms to deal properly with the interface effects.

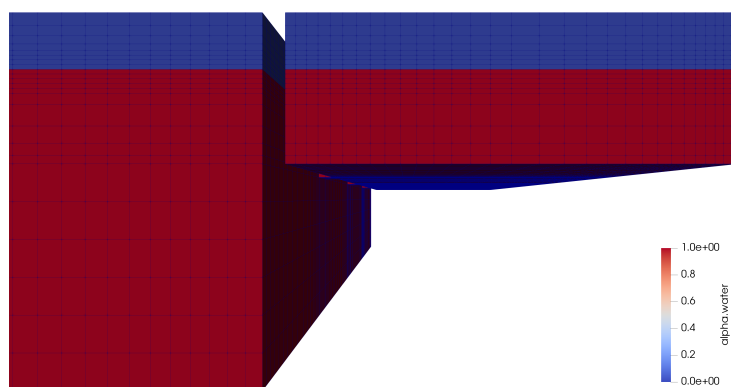
The geometry of the tank is quite simple and can be seen as a union of parallelepipeds (the sea basin, the lagoon basin and the inlets), making the perfect case for a structured orthogonal mesh. The mesh has exactly 240 thousands cells, 157920 for the sea basin and 82080 for the lagoon basin (including inlets); the second one is about ten times finer as its volume represents 5.1 % of the total one.



Top view of the mesh on lagoon area



3D view of the mesh



Mesh with alpha.water (red/1 for water and blue/0 for air)

Simulations setup issues and features implementation

Many features required for the simulations were not available in OpenFOAM. However, as OpenFOAM is conceived as a modifiable and adaptable tool these were implemented and represent original work:

- The solver *interFoam* has been modified to include the diffusion process
- To avoid diffusion of tracer in air a very important correction has been coded in the solver
- Opening patterns in time required creating new surface objects in the mesh (baffles) onto which apply a new boundary condition
- To calculate percentiles and standard deviation accounting for cell volumes and air-water phase required a script written in Python (coding by courtesy of Sara Marković)

Diffusion equation

The *interFoam* solver has been modified to include the classic diffusion equation:

$$\frac{\partial c}{\partial t} + \vec{\nabla} \cdot (\phi c) = -\vec{\nabla} \cdot (D \vec{\nabla} c)$$

where t is time, c is mass fraction concentration, D is the diffusivity and ϕ is the flow through cell faces.

The equation in C++ OpenFOAM code simply becomes:

```

solve
(
    fvm::ddt(conc)
    + fvm::div(phi, conc)
    - fvm::laplacian(D, conc)
);

```

where *conc* and *D* are defined as *volScalarField* entities, *conc* is defined with the utility *setFields* according to the initial conditions of the experiments; *D* is set to $5 \cdot 10^{-8} \frac{\text{m}^2}{\text{s}}$, halved in comparison to the estimated experimental value to account for numerical diffusion. Numerical diffusion is an artificial diffusion contribution which consists in the inevitable averaging that happens when a continuum is discretised in volume cells. Also time discretisation create diffusive terms in the equations and accurate analysis, out of the scope of the present work, can be performed.

It is worth noticing that diffusion enhances mixing and thus tends to level out opening combinations differences in simulations. It is of primary interest, therefore, not to overestimate this parameter.

Diffusion in air numerical error

As a consequence of the volume of fluid method, diffusion happens in both air and water. The diffusion in air is more present when level water rises and reduces as it lowers, because of the positive combination of concentration gradient and mass flow. This is an unwanted effect, which causes an important mass concentration decay and hinders the relevance of comparisons between simulations, experiments and models.

Solutions found in literature are:

- Weighting diffusivity with the indicator function α ($\alpha = 1$ in water, $\alpha = 0$ in air):

$$D = \alpha D_0$$

- Using a dumping factor, $\frac{1}{|\nabla\alpha|}$, for diffusion term
- Multiply concentration by the indicator function α so that concentration is removed
- Use thermodynamic equilibrium between air and water phases
- Use of compression velocity as in the VoF method

The first solution is quick and simple, but it does not address inertial effects and a steep interface variation; therefore it is only a partial solution and an additional correction is required. Several attempts for defining a dumping factor have lead to small or no success, especially in the ebb phase of the tide, since inertial effects are not taken into account. The third solution is very simple and it is the most common, but it can be applied when mass losses are negligible and does not stop mass decay (it enhances it actually).

It is of greater interest the thermodynamic approach, strictly valid for a two-phase gas-liquid system.. If phases are called β and γ , concentration and diffusivity are defined as:

$$\begin{aligned} c &= \alpha c_\beta + (1 - \alpha)c_\gamma \\ D &= \alpha D_\beta + (1 - \alpha)D_\gamma \end{aligned}$$

For continuity in the beta-phase:

$$\vec{\nabla} \cdot D_\beta \vec{\nabla} c_\beta = 0$$

and in the gamma-phase:

$$\vec{\nabla} \cdot D_\gamma \vec{\nabla} c_\gamma = 0$$

While at the interface a flow continuity condition is set:

$$\mathbf{n}_{\beta\gamma} \cdot D_\beta \vec{\nabla} c_\beta = \mathbf{n}_{\beta\gamma} \cdot D_\gamma \vec{\nabla} c_\gamma \text{ at } \mathcal{A}_{\beta\gamma},$$

The thermodynamic equilibrium condition is set through the *Henry constant*:

$$c_\beta = H c_\gamma \text{ at } \mathcal{A}_{\beta\gamma}$$

As a consequence of these equations the diffusion term $\vec{\nabla} \cdot (D\vec{\nabla}c)$ can be formulated to account for the two phases:

$$\vec{\nabla}c = \alpha\vec{\nabla}c_\beta + (1 - \alpha)\vec{\nabla}c_\gamma + (c_\beta - c_\gamma)\vec{\nabla}\alpha$$

and therefore:

$$\vec{\nabla} \cdot D\vec{\nabla}c = \alpha\vec{\nabla} \cdot D_\beta\vec{\nabla}c_\beta + (1 - \alpha)\vec{\nabla} \cdot D_\gamma\vec{\nabla}c_\gamma + (D_\beta\vec{\nabla}c_\beta - D_\gamma\vec{\nabla}c_\gamma)\vec{\nabla}\alpha + \vec{\nabla} \cdot D(c_\beta - c_\gamma)\vec{\nabla}\alpha$$

Given that $\mathbf{n}_{\beta\gamma} = -\vec{\nabla}\alpha$:

$$\vec{\nabla} \cdot D\vec{\nabla}c = \vec{\nabla} \cdot D(c_\beta - c_\gamma)\vec{\nabla}\alpha$$

The additional term $\vec{\nabla} \cdot (Dc_\gamma\vec{\nabla}\alpha)$ represents the jump condition between the two phases. At interface

$$c_\beta = Hc_\gamma \rightarrow c_\beta - c_\gamma = (1 - H)c_\gamma = \frac{(1 - H)}{\alpha H + (1 - \alpha)}c$$

being $c = \alpha c_\beta + (1 - \alpha)c_\gamma = (\alpha H + (1 - \alpha))c_\gamma$

$$\vec{\nabla} \cdot D\vec{\nabla}c = \vec{\nabla} \cdot D\frac{(1 - H)}{\alpha H + (1 - \alpha)}c\vec{\nabla}\alpha$$

However, concentration is not a gas and does not diffuse in air; setting $H = 1$ have brought to small compensations. Nevertheless the approach points out that correction should be made where concentration is (dependance on c) and at interface (dependance on $\vec{\nabla}\alpha$).

In *interFoam* the interface between the two phases (characterised by the indicator function: $\alpha = 1$ for liquid, $\alpha = 0$ for gas and $\alpha = 0.5$ at the interface) is numerically compressed making use of the *compression velocity*: a compression term $\nabla \cdot (\alpha(1 - \alpha)\vec{U}_r)$ can be added to continuity equation of α

$$\frac{\partial\alpha}{\partial t} + \vec{\nabla} \cdot (\alpha\vec{U}) + \nabla \cdot (\alpha(1 - \alpha)\vec{U}_r) = 0$$

In Henrik Rusche's thesis the compression velocity is empirically estimated to be around 1.5 times the face normal velocity. This velocity clearly acts only at the surface where the product $\alpha(1 - \alpha)$ is non-zero.

The idea of implementing a similar compression velocity in the diffusion equation is quite tempting: the velocity, not being present in the mass and momentum equation, would act as a fictional downward wind which prevents concentration to diffuse in air. In practice, transposing indicator function features to concentration is non-trivial and the correction gave unstable results: unlike the indicator function α there is no complementary phase for concentration ($1 - c$) and concentration values between 0 and 1 have very well defined physical meaning.

A last attempt for an analytical correction of concentration diffusion in air was introducing an *addition term* to compensate for the concentration loss caused by the advection term at the interface:

$$\frac{\partial c}{\partial t} = -u \frac{\partial c}{\partial z} - u \frac{c}{\Delta z}$$

The term is supposed to preserve present concentration c (given the cell scale in the vertical direction Δz) and add advected concentration to present concentration. The term would have been conveniently moduled by some term function of the indicator function α in order to act solely at the interface. However, implementations of the idea brought little or no success.

The definitive solution was found with the most simple yet new approach: identify "air" cells according to their α value ($\alpha < 0.5$) and adding their mass concentration to the cells immediately below them, thus exploiting the regularity of the mesh (structured and orthogonal).

```
forAll (conc , i)
{
  if (mesh.C()[i][0] > 1.805 && mesh.C()[i][2] > 0.16
      && alpha1[i] < 0.49 && mesh.C()[i][2] < 0.19)
    // mesh region for correction
    {
      label neighbourCount = mesh.cellCells()[i].size();
      // counting neighbouring cells

      labelList neighbours = mesh.cellCells()[i];
      // list of neighbouring cells

      if ((conc[neighbours[0]] * mesh.V()[neighbours[0]] \
          + conc[i] * mesh.V()[i]) / (mesh.V()[neighbours[0]]) < 1)
        // initial concentration c0 limit to addition
        {
          conc[neighbours[0]] = (conc[neighbours[0]] * \
              mesh.V()[neighbours[0]] + conc[i] * mesh.V()[i]) \
              / (mesh.V()[neighbours[0]]);
          // add conc below

          conc[i] = 0;
          // remove conc above
        }
    }
}
```

Opening patterns implementation

The time-varying opening and closing combinations are not easily managed in OpenFOAM. In order to implement this fundamental feature new boundaries need to be defined at inlets, together with new coded boundary conditions. The first task is relatively easy and can be solved with the *createBaffles* OpenFOAM standard utility: two new surfaces (*baffles*), one on the side of the lagoon and one on the side of the sea basin, are defined at inlets and in such a way it is possible to apply boundary conditions in place. As for the boundary condition itself a lot of work and time were necessary; ideally the baffles should act as a wall during closed state, mirroring values at each side, and as cyclic boundary condition type during open state, mapping values from one side to the other according to cell flows.

The first attempt was an ad hoc adaptation of *groovyBC* from the *swak4Foam* package, developed by Bernhard Gschaider. After a lot of trial and error, this solution was discarded for the difficulties in mapping non-uniform fields. The second solution was writing new code in the eased environment of *codedFixedValue* (a coded boundary condition), here it is the code for the velocity field on the lagoon side:

```

const fvPatch& boundaryPatch = patch();
    // get patch ID on opposite (sea) side
word oPatchName = "inlet1faceZone_sea";
    label oPatchID = this->patch().boundaryMesh().\
        findPatchID(oPatchName);
// get face cells on opposite sea side baffle

const vectorField& Cf = boundaryPatch.Cf();
// face centres field

vectorField& fieldU = *this;
// velocity field

volVectorField U = this->\
    db().lookupObject<volVectorField>("U");
const Foam::fvPatchField<Foam::Vector<double>>\
    Usea = U.boundaryField()[oPatchID];

const scalar omega = 0.0418879;
// angular frequency for T=150 s

scalar t = db().time().value();

if(cos(omega*t)/mag(cos(omega*t))>=0)
    // defines the time phase of open state
    {

        forAll(Cf, faceI)

```

```

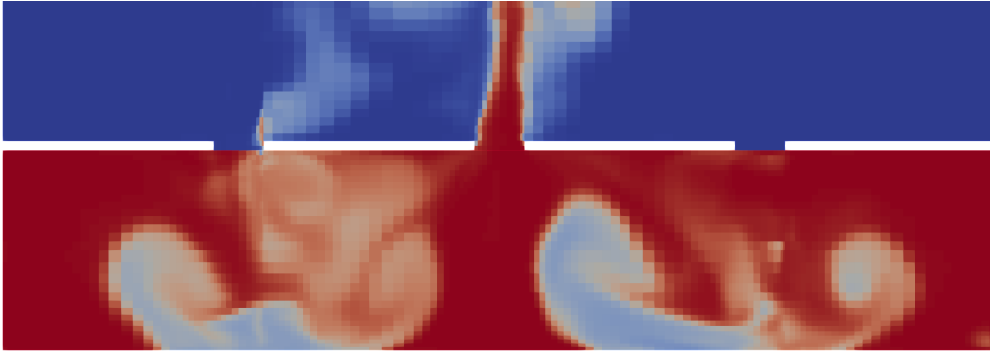
{
    label cellI = boundaryPatch.faceCells()[faceI];
    if (Usea[faceI].component(0)>0)
    {
        fieldU[faceI] = Usea[faceI];
        // if flow is coming from sea basin
        // copy that velocity
    }

    if (Usea[faceI].component(0)<0)
    {
        fieldU[faceI] = fieldU[cellI];
        // if flow is coming from lagoon basin
        // copy internal cells value
    }
}
}
else // in closed state
{
    forAll(Cf, faceI)
    {
        fieldU[faceI] = vector(0,0,0);
        // no slip condition, wall-like behaviour
    }
}
}

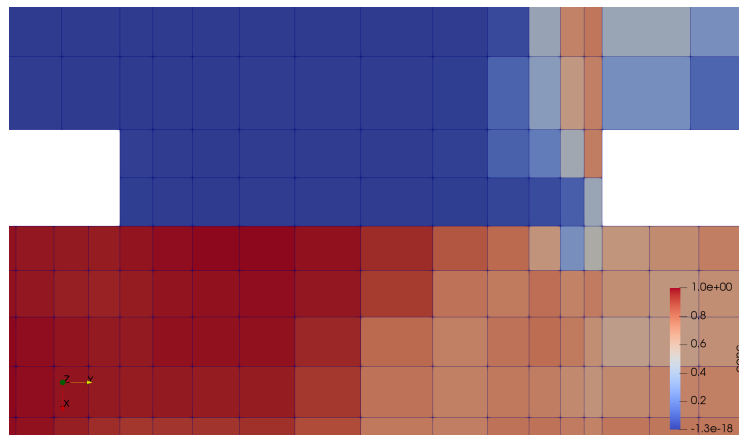
```

However, the code did not work (parallelisation would have also be troubling). Therefore, under suggestion of Charles L. (*Marpole* on cfd-online forum), a new boundary condition was coded and compiled, modifying the existing *activeBaffleVelocity*. This boundary condition combines wall and cyclic boundary conditions, and simulates an opening or closing of a baffles caused by a pressure gradient or force delta. The adaptation in the *onoffinlet* boundary condition was quite easy, but, unfortunately, standard *activeBaffleVelocity* in itself does not work correctly in OpenFOAM. The bug shows how difficult it is for OpenFOAM to manage meshwise the transition between the wall and the cyclic boundary condition.

Charles L. proposed on the forum a work-around method that resulted working in serial computation. Then the method has been adapted for parallel computation, generalising the procedure for each processor. The method consists in simply defining twice the baffles in the *boundary* file, both as cyclic type boundaries and as wall type boundaries, so that the transition can take place smoothly. It is important to do so after having initialised mesh and fields, then boundary conditions of fields need to be updated accordingly. When this procedure is conducted for parallel computation it is not viable to do it manually and some bash scripting was required in order to automatise the whole process. More details and auxiliary files can be found on the cfd-online forum discussion.



Unwanted leaking from left inlet during outflow phase (*bigcomboinverted*, one third exchange ratio, $t = 76$). It is possible to notice the absence of leaking on right inlet, even if the same boundary condition is applied.



Detailed view of the leaking inlet.

This solution did not come without further issues: an inexplicable bug occurs with part of the baffle cell faces acting as open even when supposed to be in closed state. This seems connected to mesh itself in terms of number of cells in vertical direction and possibly by whether the number of cells in horizontal direction are odd or even. Also symmetry probably plays a role and the issue could be caused by a slight lack of symmetry in cell distribution at inlets. Unfortunately, this was realised only after simulations were conducted, as the error, being small, was not detectable in inlet-averaged flow values given during computation.

Nevertheless, the error is small compared to variance of combination-induced behaviours. Additionally, the leaking is pulsating from inflow to outflow with a period much shorter than the tidal one (around 3 s compared to 150 s tidal period); therefore, the phenomenon increases the mixing component of the combination, not affecting the efficiency in terms of externally forced mechanism.

Results

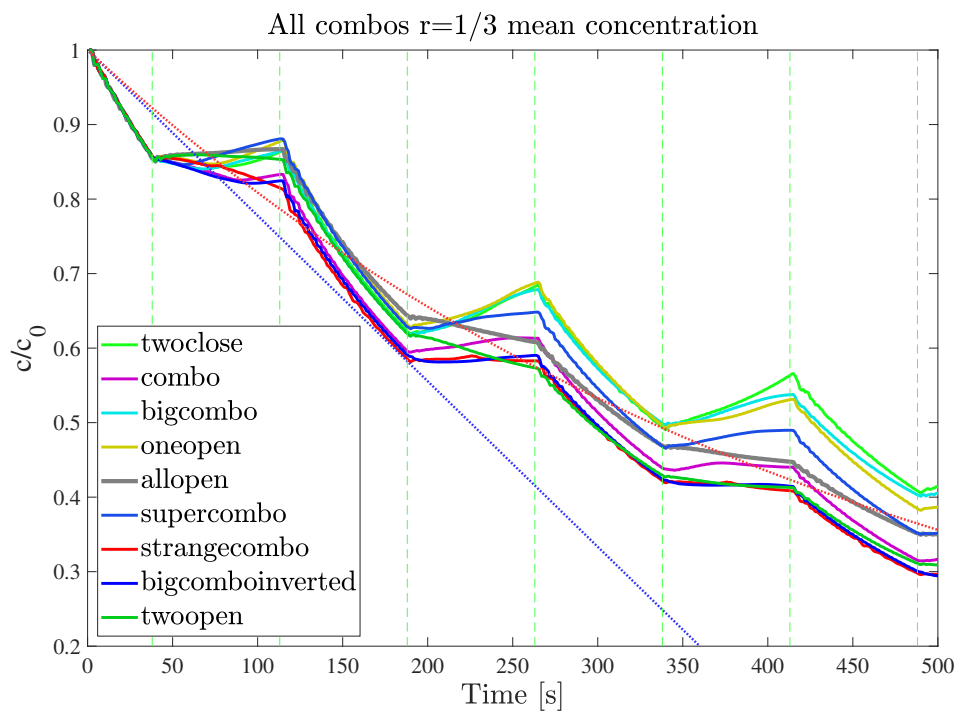
In this paragraph the results from the simulations are given in terms of average concentration, 95th percentile concentration, 50th percentile (median) concentration and normalised standard deviation. Both graphical and tabular format are used, in tables quantities are averaged over the first 500 s of the simulation, as similarly done in chapter 3.

The results tend to agree with experimental data, they are more clean and directly comparable to one another, providing a deeper insight on combinations mechanisms.

One third exchange ratio series

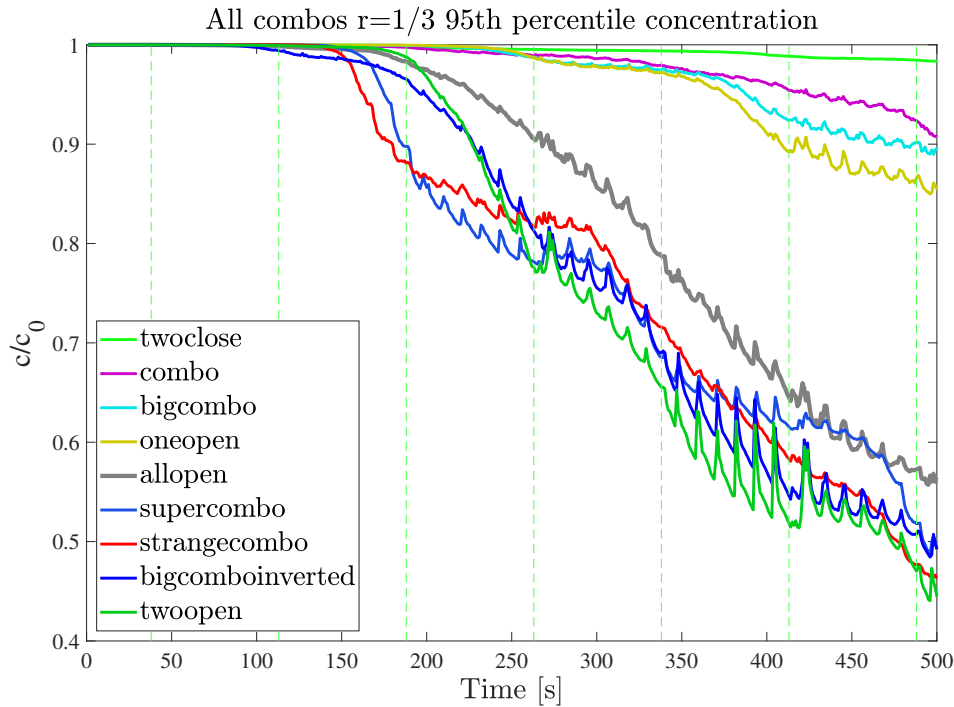
The series comprises nine combinations and it is meant to study combinations efficiency in an intermediate exchange ratio scenario.

MEAN CONCENTRATION: the decay curves in the first outflow phase (37.5 – 112.5s) show clearly which mechanisms are efficient (negative slope: outflow concentration is greater than average concentration), i.e. *bigcomboinverted*, *strangecombo*; and which are counter efficient (positive slope: outflow concentration is lower than average concentration), one of those is *allopen*, together with *oneopen* and *bigcombo*. It is very interesting to notice that in the second outflow phase (187.5 – 262.5s) *twoopen* and *allopen* are the only two with negative slope, which suggests that a longer preceding inflow phase is required for them to capture an efficient natural mechanism.



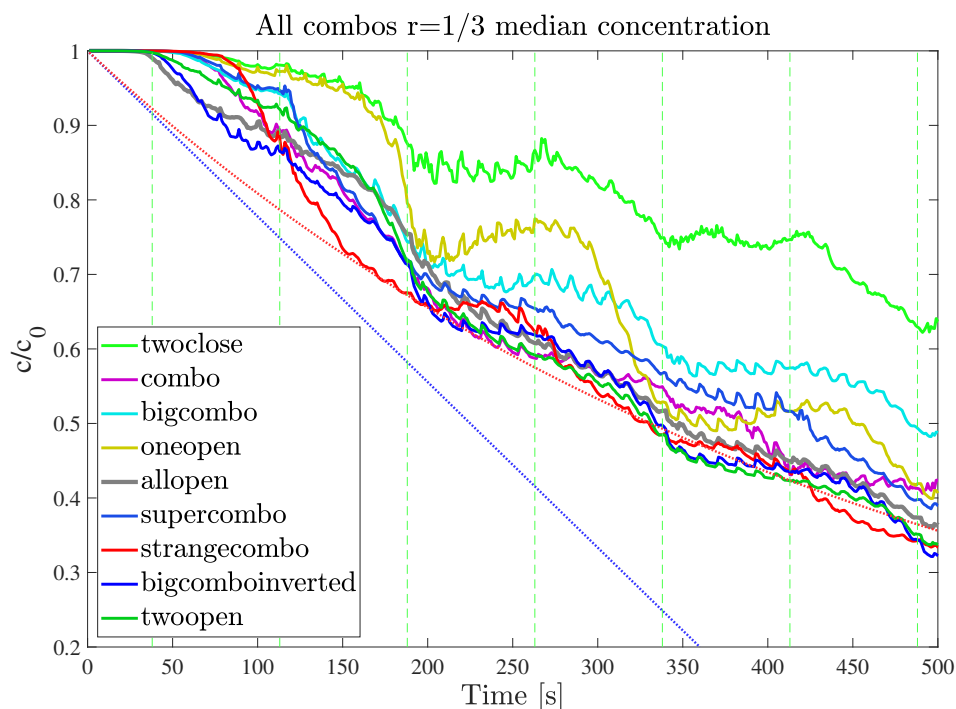
Mean Concentration	
strangecombo	0.583
bigcomboinverted	0.584
twoopen	0.594
combo	0.598
allopen	0.621
supercombo	0.630
bigcombo	0.646
oneopen	0.648
twoclose	0.651

95th PERCENTILE CONCENTRATION: in terms of maximum concentration *allopen* (in gray) acts as a watershed between least efficient combinations: *twoclose*, *combo*, *bigcombo*, *oneopen*; and most efficient ones: *twoopen*, *bigcomboinverted*, *supercombo* and *strangecombo*. The onset time for this quite linear decay is the period T , this holds true also for the one half ratio but not for the one sixth ratio; however, the slope is around $\frac{1}{600 \div 700} \text{s}^{-1}$ and significantly lower than $\frac{r}{T} = \frac{1}{450} \text{s}^{-1}$. The fast decay of *strangecombo* and *supercombo* suggests that these combinations provide the most uniform decay. *Twoopen* is also a very valid option and does not require any forced opening combination.



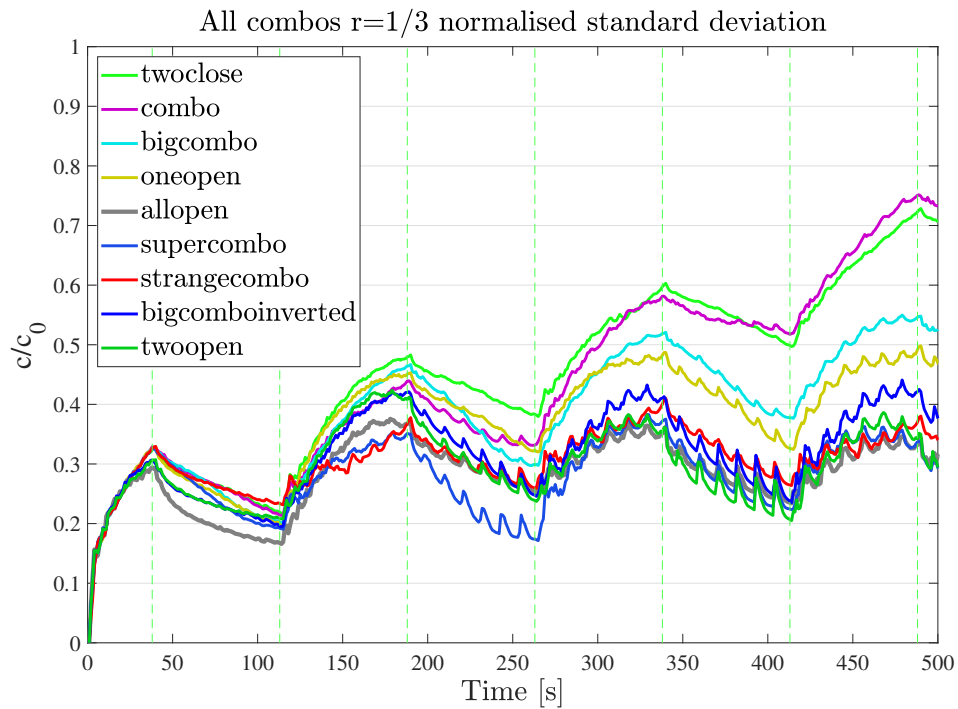
95 th percentile	
twoopen	0.794
strangecombo	0.804
bigcomboinverted	0.806
supercombo	0.808
allopen	0.857
oneopen	0.966
bigcombo	0.973
combo	0.981

50th PERCENTILE (MEDIAN) CONCENTRATION: while experiments suggested that median decay could be the most significant measure in terms of bulk decay, aligning the decay with conceptual models ones, a more homogeneous initial distribution shed some light and shows a slightly different behaviour. Combinations tend to overlap a lot and the fitting model seems to be the perfect mixing one in all combinations. *Combo* certainly has a better decay than the 95th percentile one but it is not characteristic of the *Perfect Mechanism* model. In the first outflow phase *bigcomboinverted* has the lowest value, yet *strangecombo* has a steeper descent, as a consequence of its opening phase shift. *Allopen* is also a good option, as well as *Twoopen*.



50 th percentile	
strangecombo	0.648
bigcomboinverted	0.649
twoopen	0.657
allopen	0.666
combo	0.671
supercombo	0.696
bigcombo	0.734
oneopen	0.736
twoclose	0.847

NORMALISED STANDARD DEVIATION σ_N : normalising the distribution variability of the combinations with their own average decay shows that *Allopen*, even if not very efficient, is quite uniform; *supercombo*, a combination conceived for being very uniform, is actually very uniform. Values tend to get closer at later times, while the averages are different. The distinction made in the 95th percentile decay still holds true in this case, with *twoclose*, *combo*, *bigcombo* and *oneopen* being the least efficient ones.



σ_N	
supercombo	0.281
allopen	0.283
twoopen	0.297
strangecombo	0.307
bigcomboinverted	0.318
oneopen	0.373
bigcombo	0.386
combo	0.437
twoclose	0.450

In general, it is clear that there are better combinations than *allopen*, the natural configuration. *Supercomboinverted* and *strangecombo* have the best decay overall, but also the simple *twoopen*, easy to implement, has similar performances.

Reminding the third chapter convention in defining combinations (*c* for closed state, *o* for open state; firstly the inflow phase then outflow phase and so on), it is possible to compare:

- bigcomboinverted *o c o / c o c* with bigcombo *c o c / o c o*
- supercombo *o c c / c o c / c c o / c o c* with supercomboinverted *c o c / o c c / c o c / c c o*

and conclude that lateral openings during inflow phase *o c o* provide the best decay, with a tradeoff between

- the advantage in terms of velocity given by closing one or two inlets (greater velocity greater penetration in the lagoon basin and better mixing)
- and the advantage of having more inlets open and thus affecting the largest portion of the lagoon basin (more inlets, more mixing)

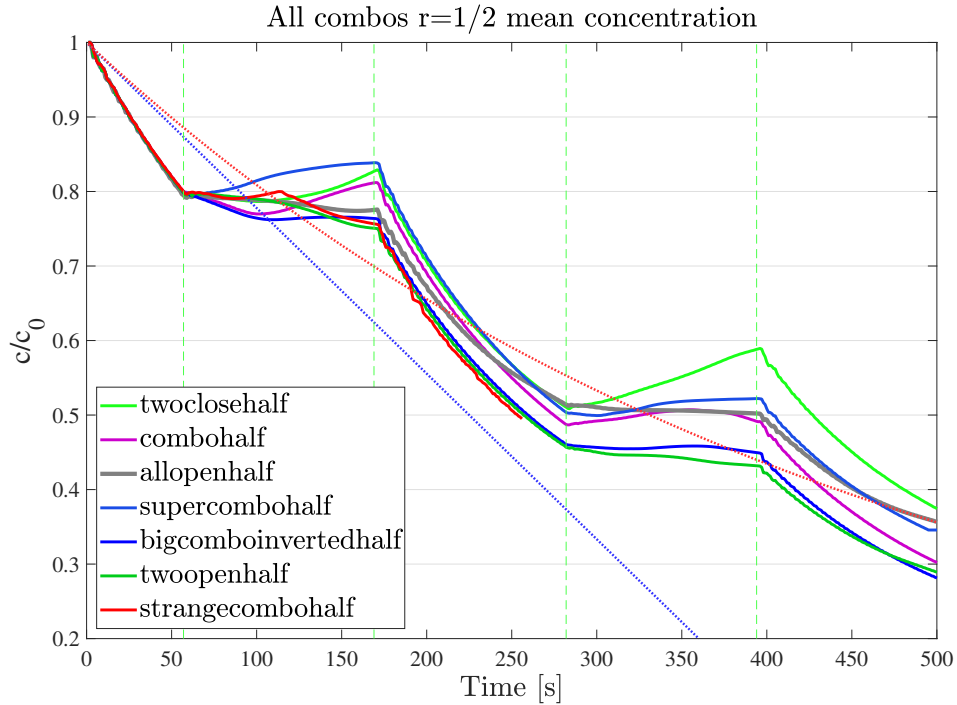
This conclusion is also supported by the fast decay of *twoopen* and by experimental data (chapter 3).

Shifting opening phase with respect to tidal phase also provides very good results.

One half exchange ratio series

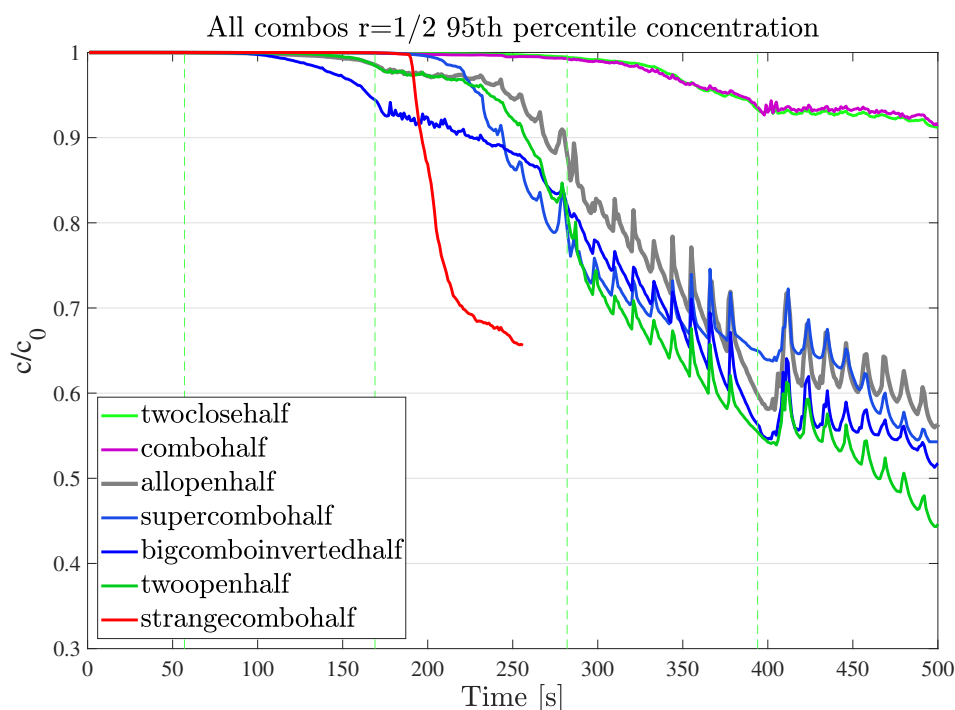
This series comprises seven combinations and it is mainly meant to be compared with the one third series and with the same series in experiments, where errors partly invalidated the results. Strangecombo has not been completed for the 500 s like other simulations and can not be shown on tables.

MEAN CONCENTRATION: *twoopen* and *bigcomboinverted* confirm also in this series their steeper decay in the first and in the second outflow phase. It is also clear that *combo* (in purple) has a good mechanism in the first half of the outflow phase (negative slope), flushing highly concentrated water, but soon, as the period is long, freshly entrained (and thus poorly concentrated) water arrives close to the open outlet and it is sucked away by the plugh flow, creating a counter-efficient mechanism.



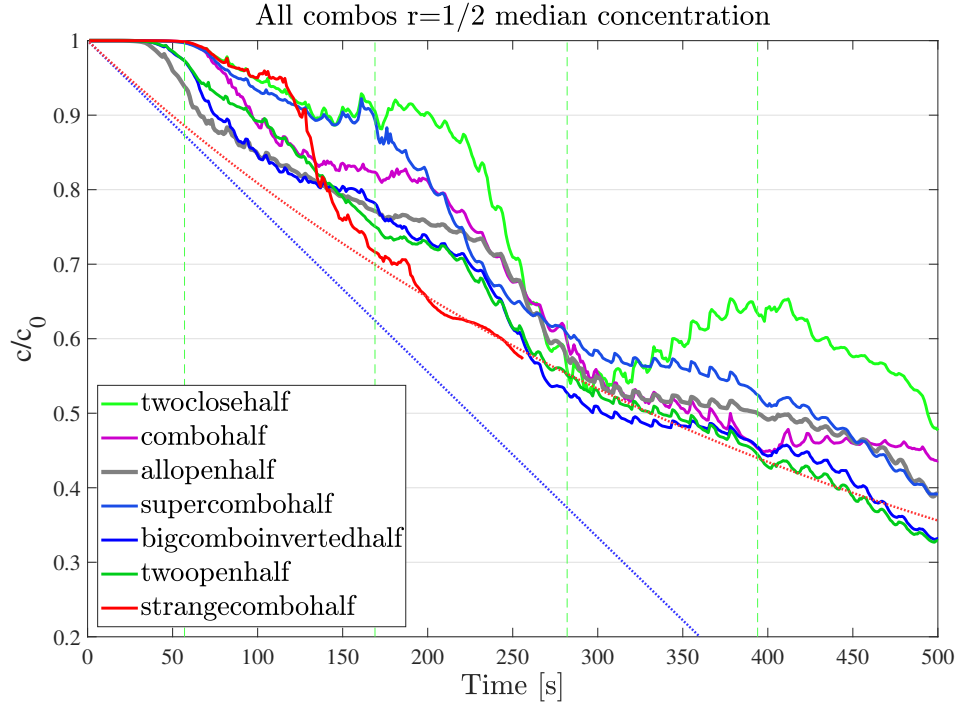
Mean Concentration	
twoopenhalf	0.580
bigcomboinvertedhalf	0.583
combohalf	0.611
allopenhalf	0.618
supercombohalf	0.633
twoclosehalf	0.645

95th PERCENTILE CONCENTRATION: what sticks out the most in the graph, the red *strangecombo* decay, is caused, unfortunately, by numerical instabilities arising at $t = 188$ s. On the other hand *bigcomboinverted*, *supercombo* and *twoopen* still have the fastest decay. Compared to the one third series graph, it is worth noticing that *bigcomboinverted* has a steeper decay than *supercombo*, this could suggest that a longer period favours a two inlet combination such as *bigcomboinverted*, which injects sea water from lateral inlets in inflow phase; while a short one favours the only-one-per-time inlet combination *supercombo*, which injects from one of the lateral inlets alternately.



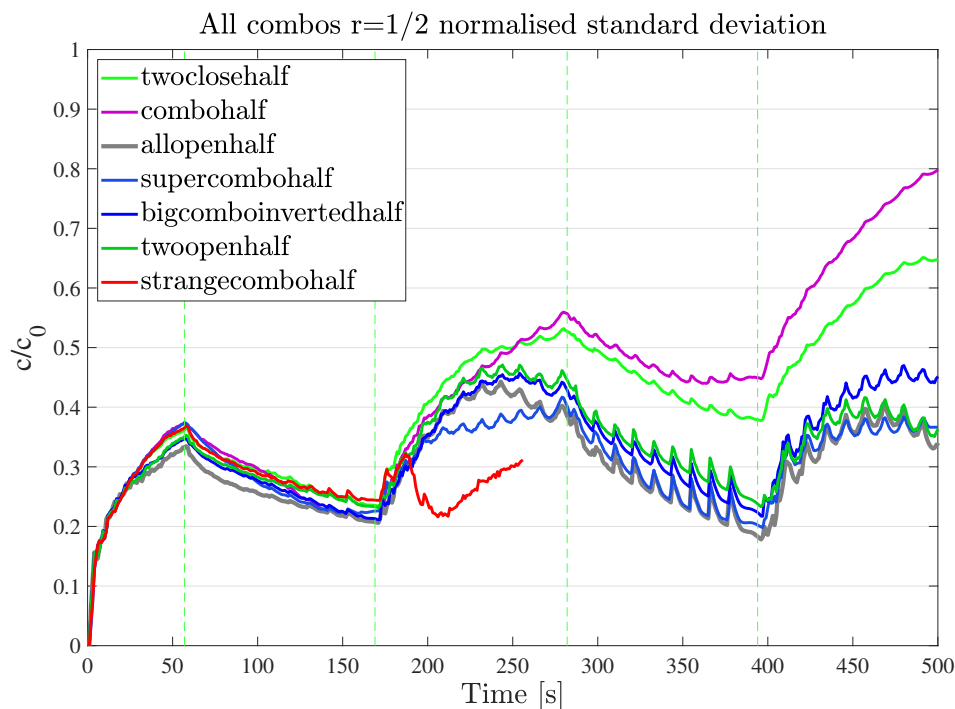
95 th Percentile	
twoopenhalf	0.808
bigcomboinvertedhalf	0.812
supercombohalf	0.835
allopenhalf	0.849
twoclosehalf	0.977
combohalf	0.978

50th PERCENTILE (MEDIAN) CONCENTRATION: the information content is similar to the one of the mean concentration graph. The instabilities affecting *strangecombo* do not seem to interfere much with median and average quantities; overall, the data available still suggest a fast decay for this combination.



50 th Percentile	
bigcomboinvertedhalf	0.649
twoopenhalf	0.651
allopenhalf	0.675
combohalf	0.691
supercombohalf	0.712
twoclosehalf	0.758

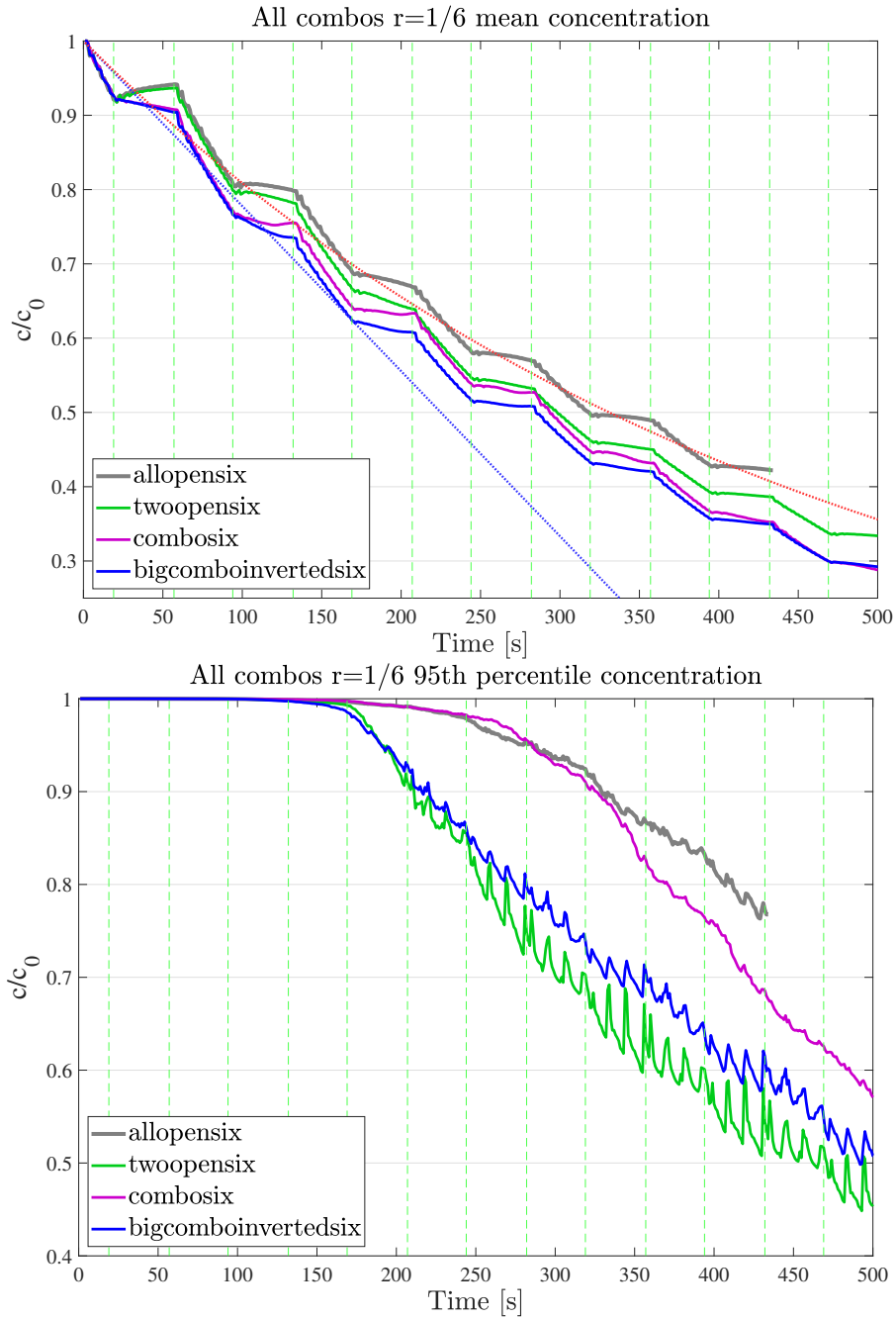
NORMALISED STANDARD DEVIATION σ_N : the graph shows similar results as the 95th percentile one, the error in *strangecombo* is also clear. As in the one third ratio series, *supercombo* and *allopen* have low values of standard deviation. Also here the spikes represent the pulsating nature of flows through inlets.

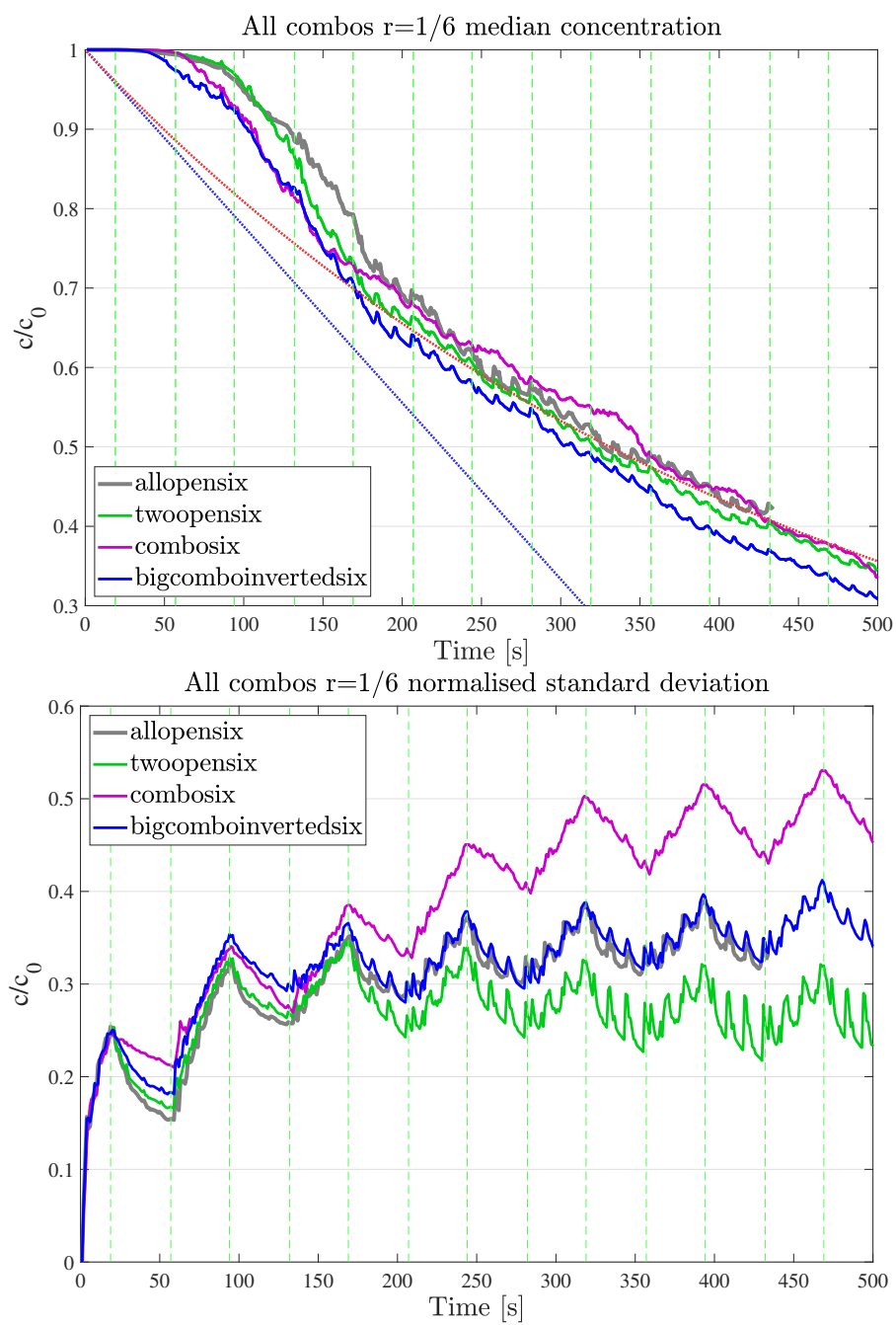


σ_N	
allopenhalf	0.299
supercombohalf	0.305
bigcomboinvertedhalf	0.329
twoopenhalf	0.331
twoclosehalf	0.411
combohalf	0.438

One sixth exchange ratio series

Given the amount of experiments in this series, only four simulations have been conducted; yet, they strongly confirm experimental data results: shorter periods (or shorter exchange ratios, as r/T is fixed), favour externally forced combinations and *combo* provides a comparable (if not steeper) decay in comparison to *allopen*. *Twoopen* still represents a very good option, especially in terms of 95th percentile and normalised standard deviation σ_N .





Different exchange ratios comparison

ALLOPEN: different ratios provide similar decays in terms of average concentration and the graph looks very similar to the one of the *Perfect Mixing* model at different ratios (chapter 2). The 95th percentile decay shows how *allopen* natural mechanism can be counter-efficient on short periods. This result is quite important and calls for the necessity of other combinations in the one sixth ratio scenario.

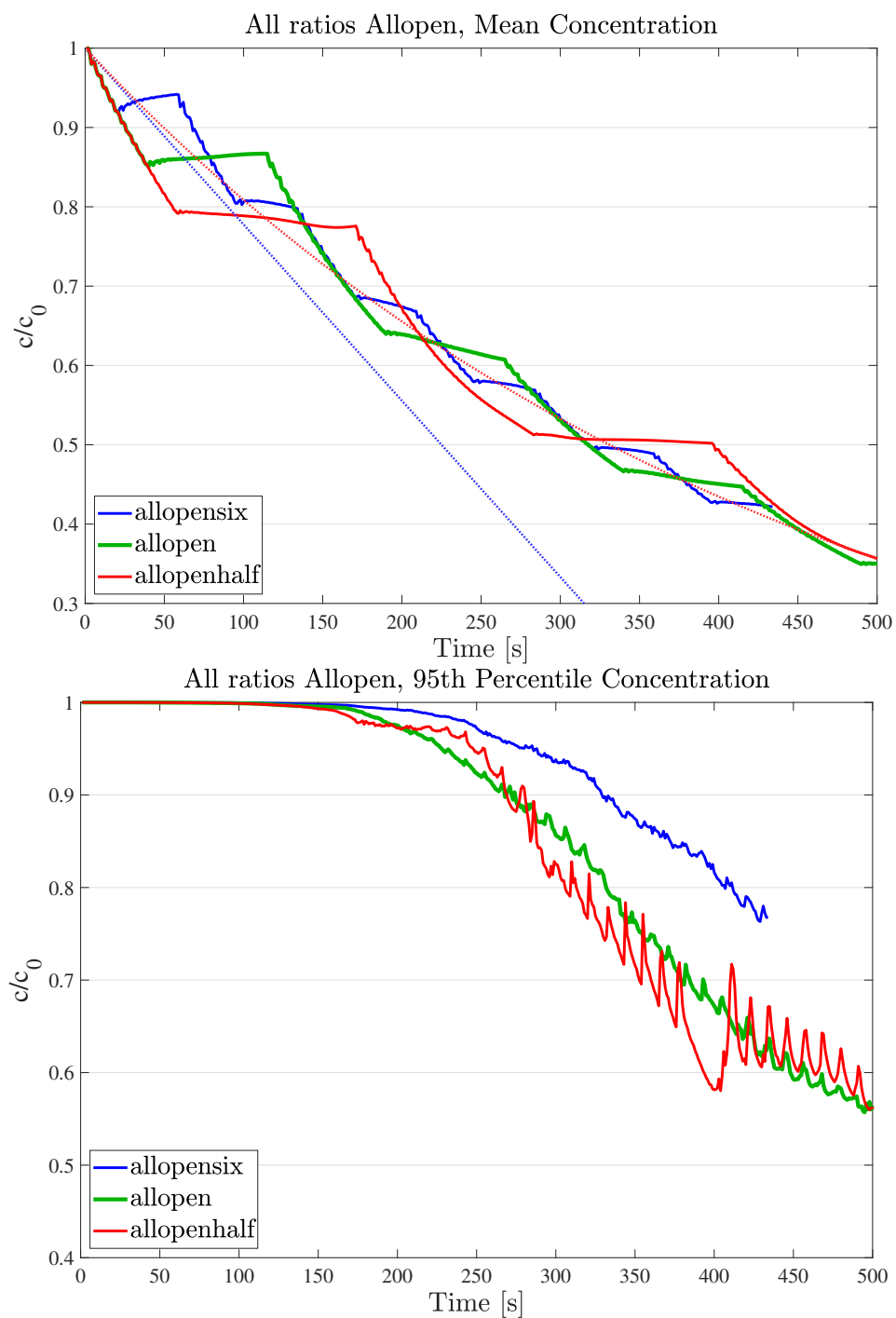
COMBO: the one sixth ratio shows a steeper decay both in average and in 95th percentile terms. This is the perfect example of the *Hybrid Model* (chapter 2): shorter periods (or lower ratios) favour externally forced "artificial" mechanisms, longer periods (or higher ratios) favour naturally mixing mechanisms, while externally forced mechanisms tend to become counter-efficient, closer to the *Reversed Mechanism* model.

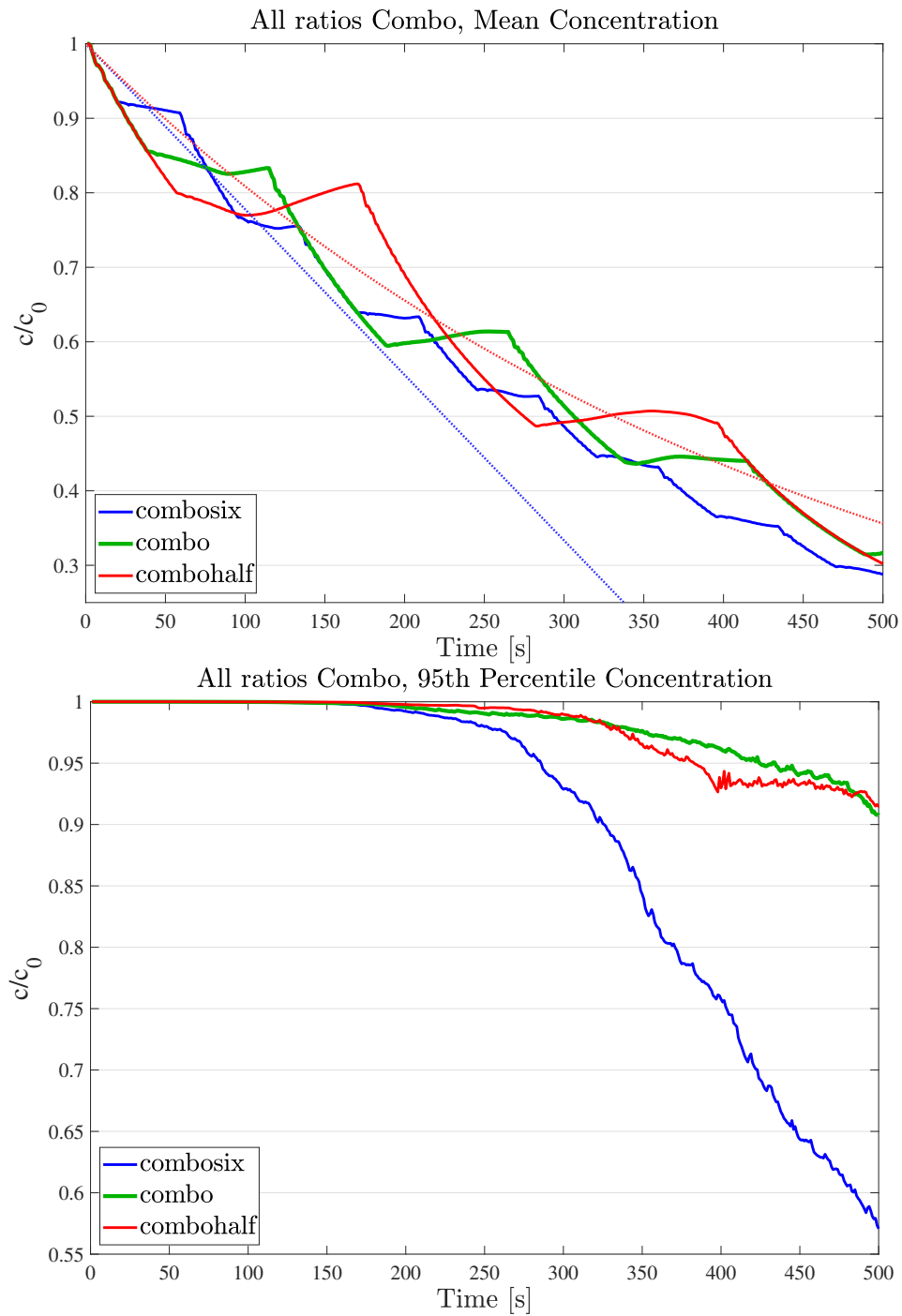
TWOOPEN: because of its natural wide mechanism *twoopen* behaviour seems to be independent of exchange ratio and period (being r/T fixed). Still, the decay seems to be slightly better at shorter periods (lower exchange ratios) as in *combo*.

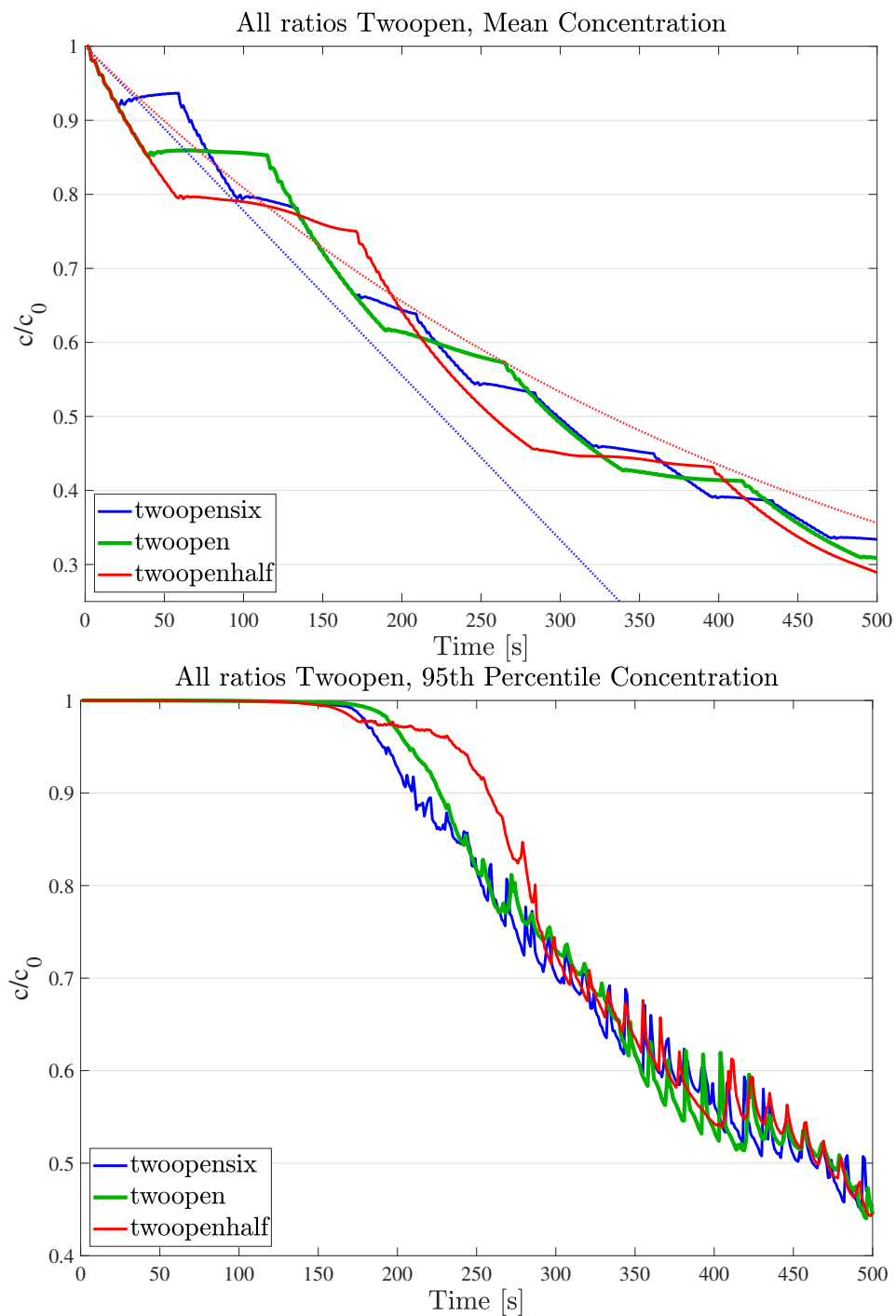
BIGCOMBOINVERTED: thanks to its wide symmetrical mixing action, *bigcomboinverted* does not seem affected by the period T or the ratio r (being r/T fixed). Considering the mean concentration decay, almost all outflow phases present a negative slope, which denotes a persistent and efficient flushing mechanism.

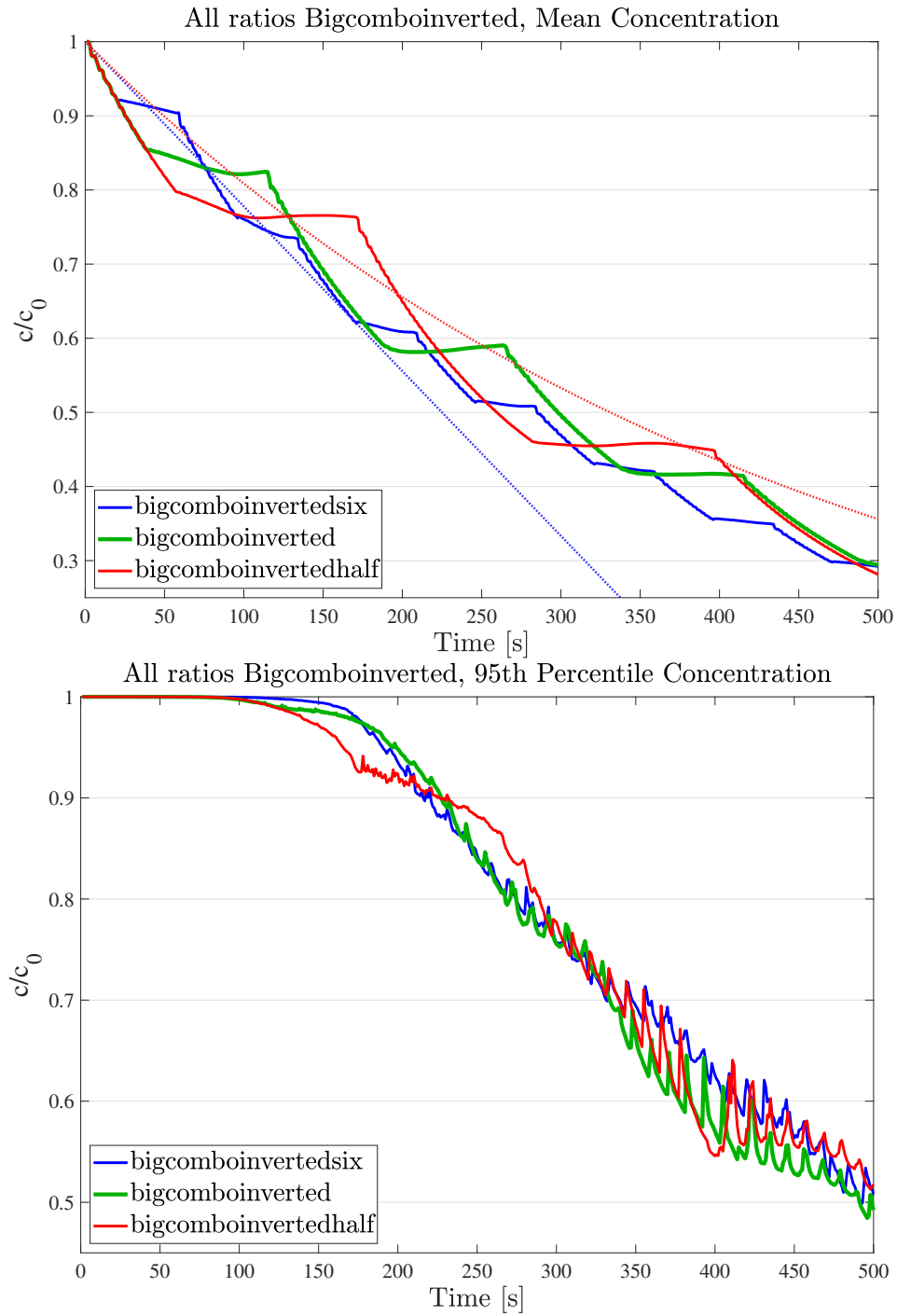
95 th percentile	1/6	1/3	1/2
allopen		0.857	0.849
combo	0.893	0.981	0.978
bigcomboinverted	0.818	0.806	0.812
twoopen	0.789	0.794	0.808

Mean Concentration	1/6	1/3	1/2
allopen		0.621	0.618
combo	0.577	0.598	0.611
bigcomboinverted	0.565	0.584	0.583
twoopen	0.598	0.594	0.580









Experiments comparison

It is possible to compare simulations to corresponding experiments and see whether averaged quantities match each other or differ significantly. Besides the agreement in itself, *reliability coefficients* can be tested in the assumption that simulations tend to be more accurate than experiments, and, therefore, validate all experiments results which are deemed reliable according to coefficients (defined in chapter 3). The last column shows the relative difference of experiments values with respect to simulations values, interpreting this difference as experimental errors. For a comparison the overall data set variation (difference of maximum and minimum value relative to average) is 36.2 % for experiments and 12.1 % for simulations. Please note that *strangecombo* belongs to the one sixth series in experiments while the simulation to the one third ratio series.

series	combination	r_1	r_2	95^{th}_{exp}	95^{th}_{sim}	\bar{c}_{exp}	\bar{c}_{sim}	$\delta_{\bar{c},exp}$
old0.33	twoclose	0.92	0.37	1.080	0.995	0.659	0.651	+1.3 %
new0.33	twoopen	0.45	0.26	0.807	0.794	0.545	0.594	-8.3 %
new0.33	allopen	0.31	0.23	0.936	0.857	0.615	0.621	-0.8 %
new0.33	combo	0.45	0.26	0.946	0.981	0.564	0.598	-5.8 %
new0.33	oneopen	0.34	0.22	0.876	0.966	0.568	0.648	-12.4 %
new0.33	supercombo	0.31	0.26	0.815	0.808	0.589	0.630	-6.5 %
0.166	bigcomboinv.	0.14	0.15	0.767	0.818	0.548	0.565	-6.0 %
0.166	combo	0.22	0.15	0.911	0.893	0.533	0.577	-7.5 %
0.166	strangecombo	0.12	0.14	0.781	0.804	0.567	0.583	-2.8 %
0.166	twoopen	0.16	0.24	0.836	0.789	0.601	0.598	+0.6 %
0.5	allopen	0.64	0.34	0.796	0.849	0.557	0.618	-9.8 %
0.5	combo	-0.01	0.40	1.064	0.978	0.714	0.611	+16.8 %
0.5	supercombo	0.03	0.35	0.871	0.835	0.671	0.633	+5.9 %
0.5	twoclose	0.16	0.47	1.063	0.977	0.753	0.645	+16.7 %

Examining the table it seems that experiments and simulations mostly agree and when they don't the explanation can be partially found in the reliability coefficients: coefficients much lower than the exchange ratio of the series denote a decay biased towards higher values, while coefficients much higher denote a decay biased towards lower values. It is also true that experimental 95th percentiles (data set mean of 0.896) tend to be slightly higher than simulations ones (data set mean of 0.881), because of experimental disturbances as nonuniform initial distribution. Experimental averaged values, on the other hand, tend to be lower in experiments (0.606 for experiments and 0.614 for simulations), possibly because of the leaking error and/or an enhanced mixing.

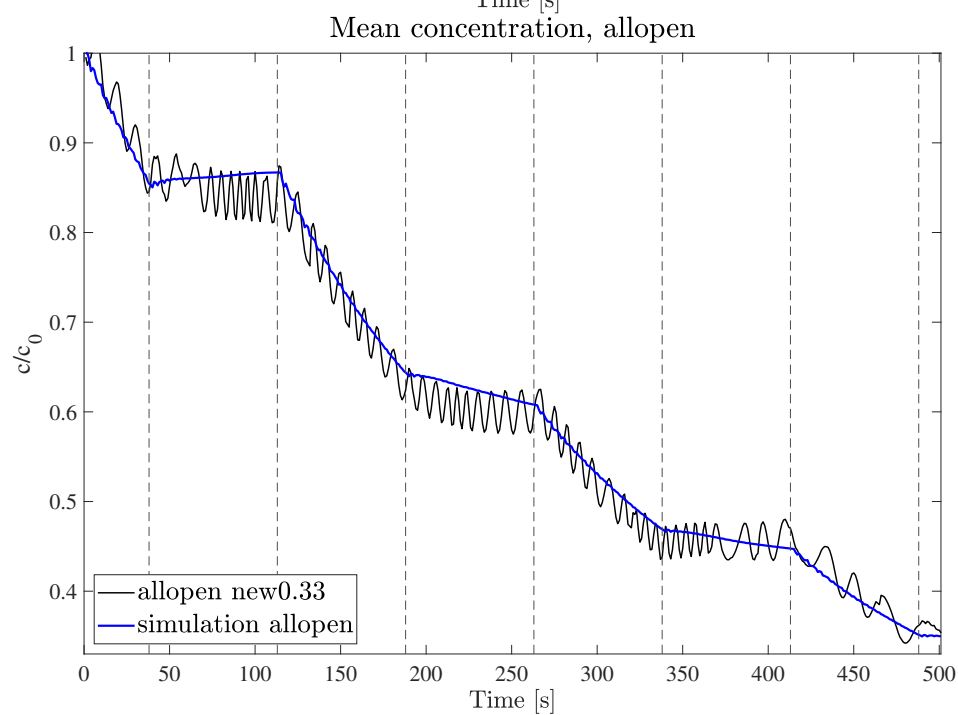
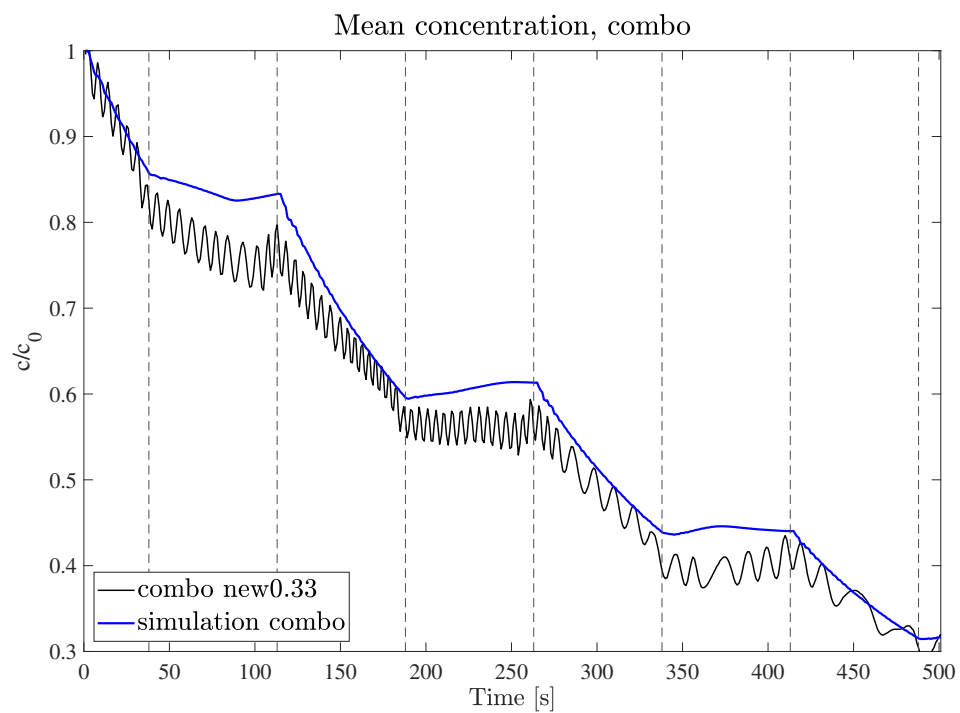
Several experiments show values deviations which can not be explained in terms of reliability coefficients; the match percentage between *reliability coefficients* prediction and difference with experiments varies both for 95th percentile and mean concentration:

series	95 th	\bar{c}
1/6	0 %	25 %
1/3	50 %	33 %
1/2	100 %	100 %

Overall, coefficients criterion and deviation from simulation values match 50 % of the cases, which, in itself, suggests no correlation. However, it is possible to see a strong correlation between the coefficients match and the exchange ratio: for high exchange ratios the match is solid while for low exchange ratios an inverse relation could be valid. An inverse relation would mean that positive exchange ratio variations cause a decrease in the decay (higher values of maximum and mean concentration), by hindering the mechanism of the combinations.

However, other factors may influence the difference between experiments and simulations at lower ratios: in *combo* from 1/6 series, for example, the initial opening is delayed by ten seconds, and the outflow phase is delayed by around two seconds (*strangecombo* behaviour); this, which can not be represented by the exchange ratio, seems to favour a localisation of entrained water and, thus, the circulation mechanism. This favourable effect can be seen also as a desirable feature and could be implemented in real-case scenarios. *Oneopen* from the 1/3 series could be favoured by an initial flow pattern from mixing and slight asymmetry in lagoon structure (angled orientation).

In any case, as experiments and simulations look very similar in their patterns and timing, therefore both seeming to represent correctly their combination, this analysis main conclusion is that initial conditions and deviations from boundary conditions have an effect similar to the variance of opening combinations; nevertheless, once these conditions are fixed, circulation patterns can decrease significantly concentration decay.



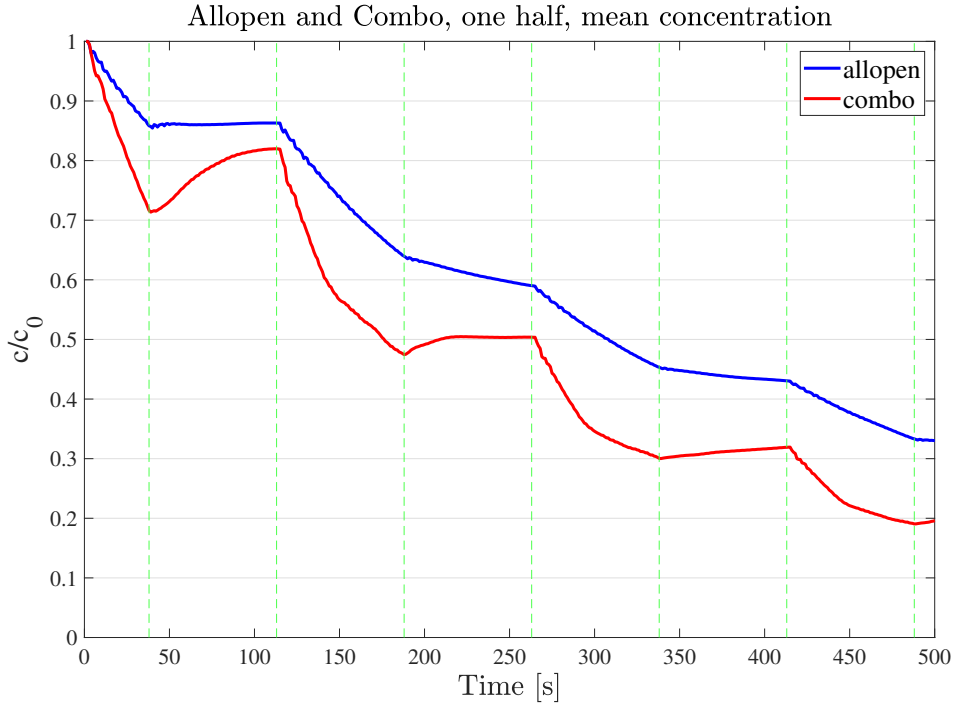
Half lagoon concentration

In order to evaluate the *combo* potential of flushing efficiency in a localised area of the lagoon, a comparison between *allopen* and *combo* for the half of the lagoon at lower concentration in the *combo* combination (the one where the inflow inlets is open) is presented.

	\bar{c}	95 th	50 th	σ_n
allopen	0.61	0.86	0.67	0.28
combo	0.49	0.74	0.67	0.44
difference	20%	14%	-1%	-54%

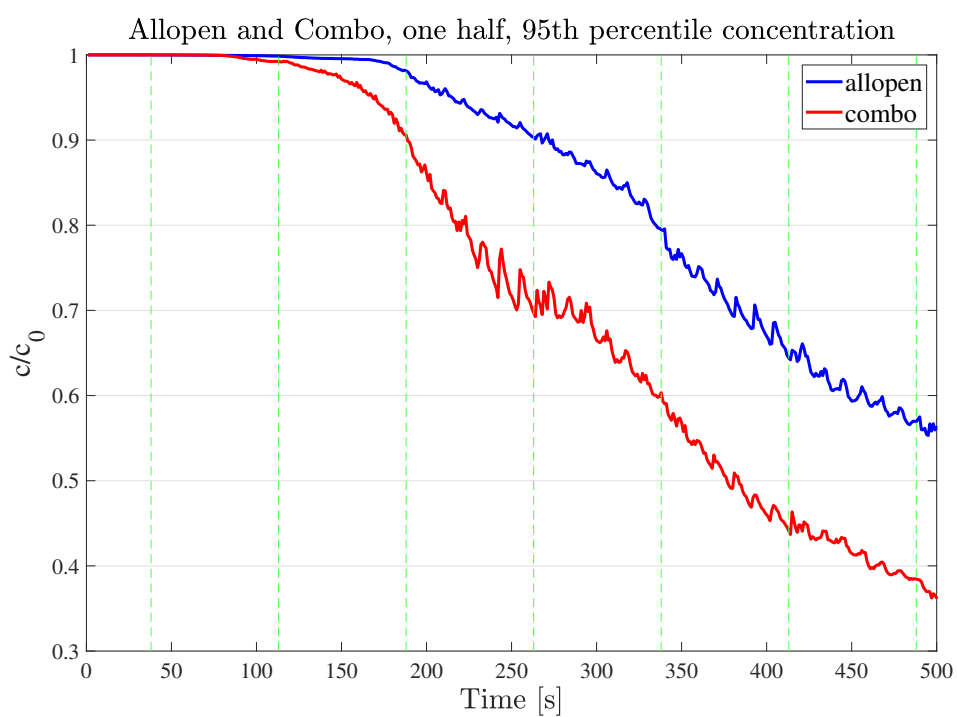
A great difference appears clear, both in terms of mean and 95th percentile concentration. Median concentration and standard deviation show an inverted scenario which is mainly owing to the choice of the region: the *combo* values would be lower if a restricted portion were considered.

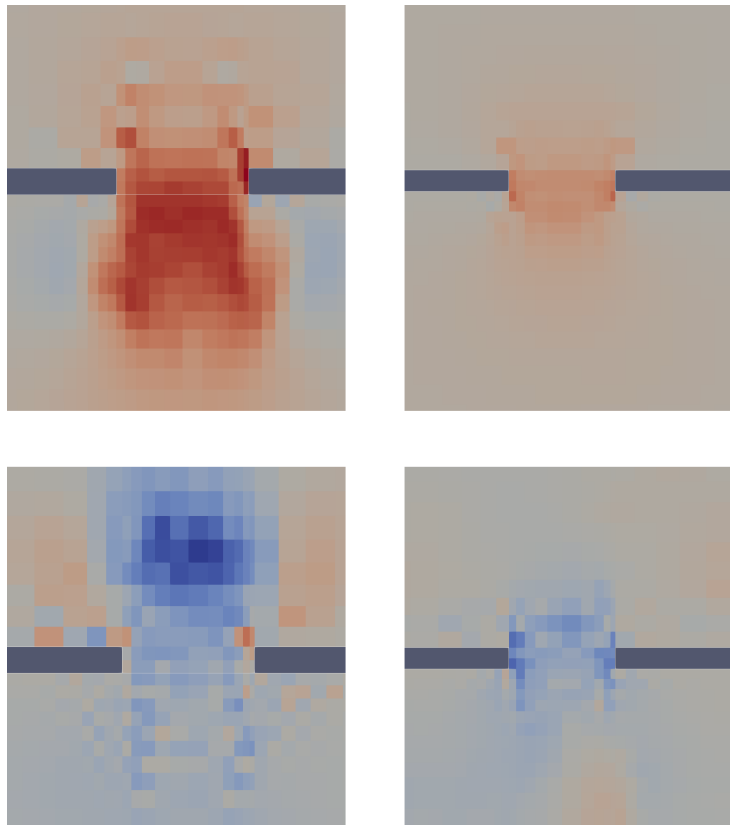
In *combo*, the decay in mean concentration reflects what happens at the inlet: low concentration water enters and lowers mean concentration in inflow phase, mixing raises concentration in outflow phase.



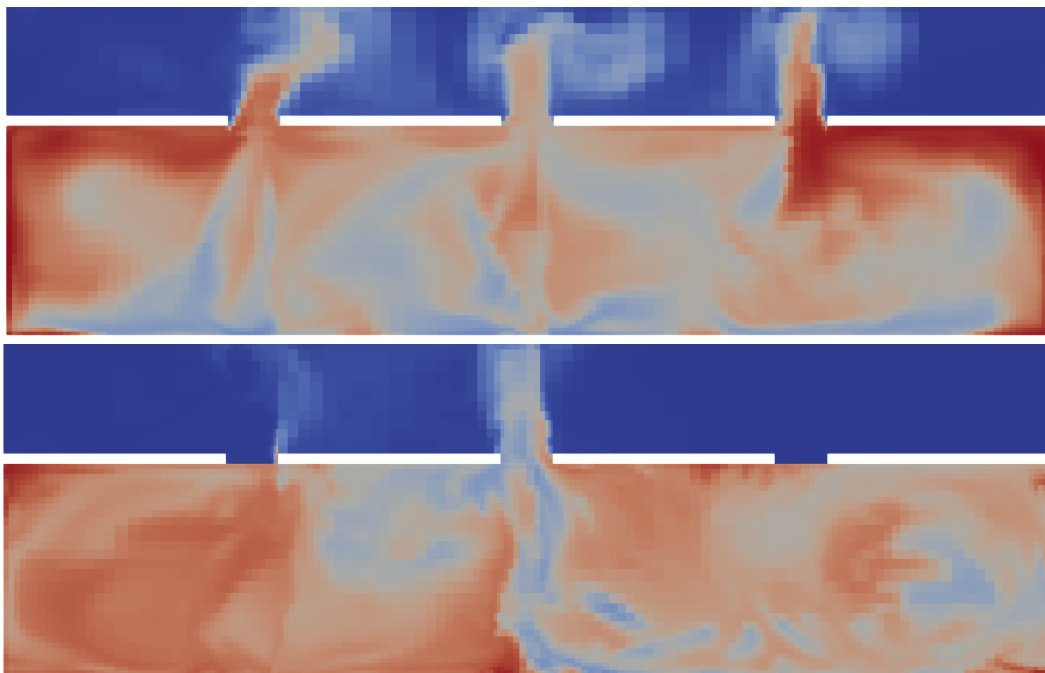
Flow features

In this paragraph more imagery is provided with regard to flow features, comparison between experiments and simulations, and comparisons between simulation and simulation.

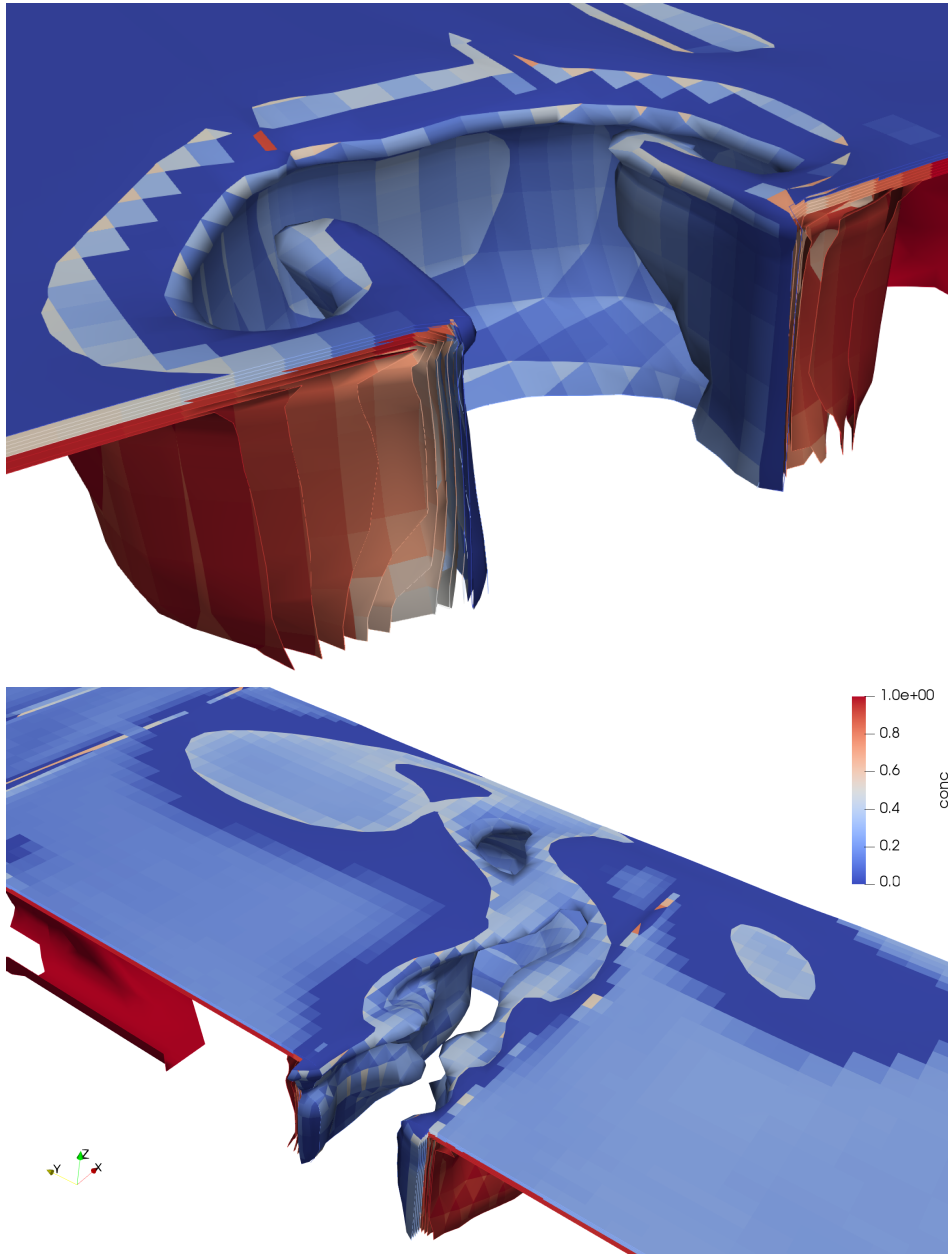




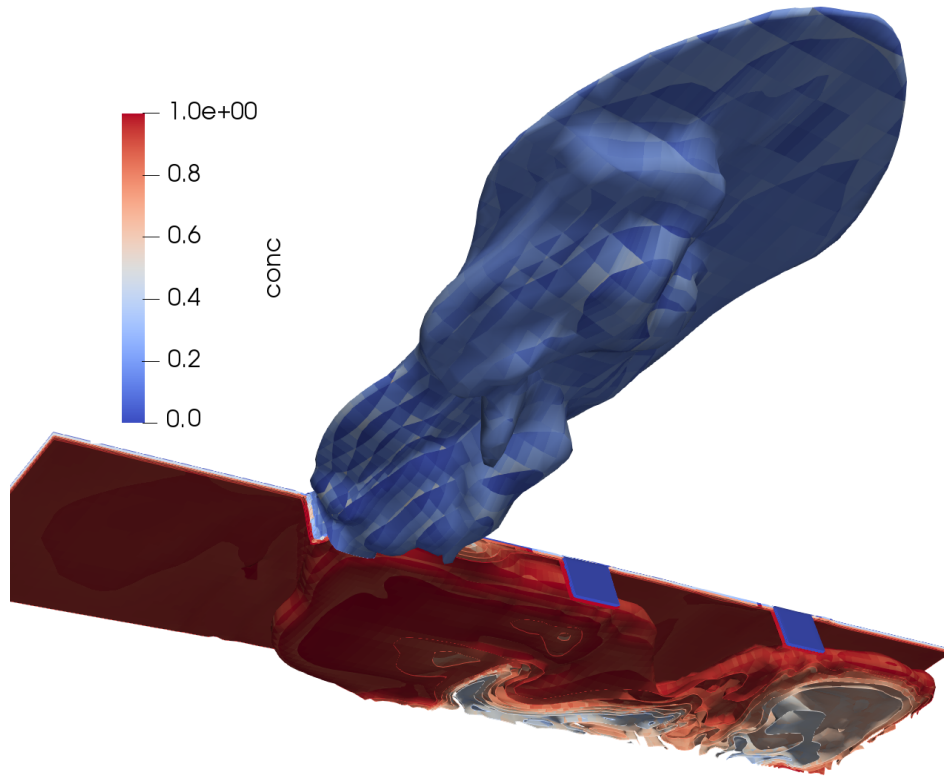
Parallel-to-inlets velocity in *supercombo* (on the left, only one inlet open) and *allopen* (on the right three inlets open) at $t = 5$ (inflow) and $t = 42$ (outflow). Scalewise red denotes a velocity of 6 cm/s, blue -6 cm/s



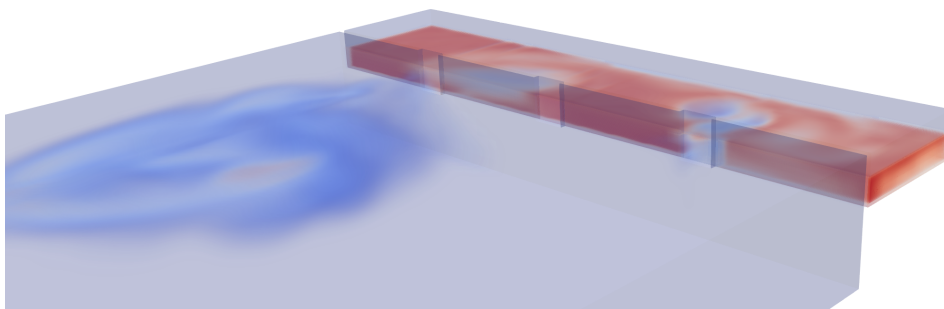
Visual difference between *allopen* and *supercombo* at $t = 225$, 95th percentile differs by 16 % while mean is very close



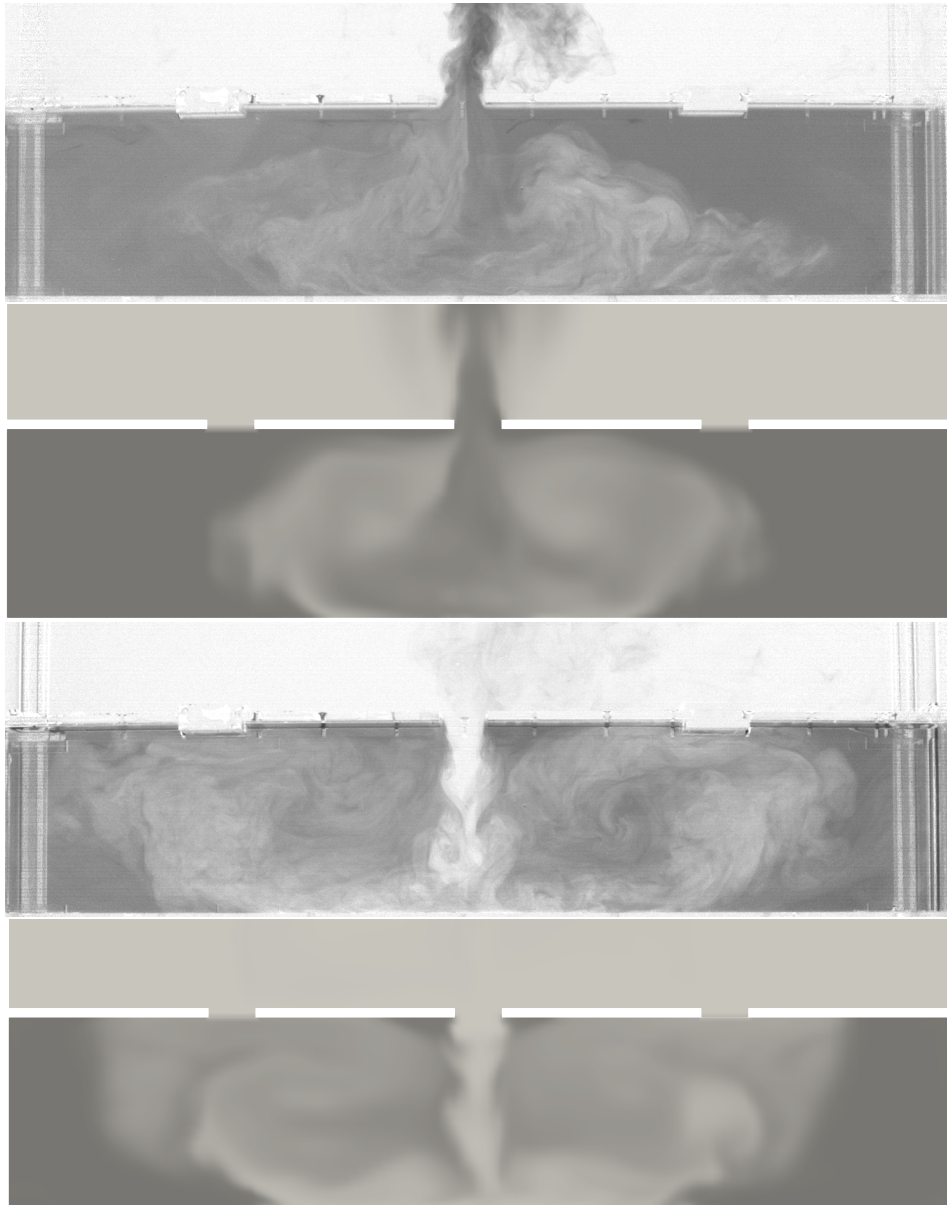
Contour visualisation with lower limit $c = 0.2$, *combo* at $t = 5$, $t = 35$ (inflow phase, top view)



Contour visualisation with lower limit $c = 0.2$, *combo* in outflow phase (down view)



Volume visualisation with lower limit $c = 0.2$, *combo* at start of second inflow phase



Comparison between experimental and simulated *oneopen* ($r = 1/3$), at $t = 70$ and at $t = 182$

Bibliography and sitography

For OpenFOAM a useful general guide (free and open-source) is the OpenFOAM® Introductory Course material by WolfDynamics, a spinoff of the University of Genoa. The author is Joel Guerrero.

<http://www.wolfdynamics.com/tutorials.html?layout=edit&id=163>

http://www.dicat.unige.it/guerrero/openfoam_course/teaching_openfoam_intro.html

Another useful resource, especially for the Volume of Fluid (VoF) method, has been the phd thesis of Santiago Márquez Damián, which can be found in

<http://openfoamwiki.net/index.php/User:Santiagomarquezd>

For the same subject a strong reference, quoted often in the thesis above, is Henrik Rusche's phd thesis

<https://spiral.imperial.ac.uk/handle/10044/1/8110>

Another resource for *interFoam* and the VoF method is this 2008 tutorial by Hassan Hemida:

http://www.tfd.chalmers.se/~hani/kurser/OS_CFD_2007/HassanHemida/Hassan_Hemida_VOF.pdf

A very detailed and comprehensive guide for the Finite Volume Method (FVM) and Large Eddy Simulations (LES) (turbulence modelling in general) is the book:

An Introduction to Computational Fluid Dynamics - The Finite Volume Method, H K Versteeg and W Malalasekera, 2nd edition, Paerson, 2007

But probably the most important guide has been the *cfD-online* OpenFOAM forum:

<https://www.cfd-online.com/Forums/openfoam>

There are a lot of useful discussions, which are fundamental, given the lack of documentation in OpenFOAM.

Commonly used resources for OpenFOAM are listed in this *openfoam.com* page:

<https://www.openfoam.com/documentation/overview>

But the unofficial OpenFOAM wiki is even more helpful:

http://openfoamwiki.net/index.php/Main_Page

The code is commented in the API guide:

<https://www.openfoam.com/documentation/guides/latest/api/index.html>

And the source code of the various versions of OpenFOAM can be found here:

<https://github.com/OpenFOAM>

As for *MATLAB*, it is very well documented by its developers: <https://www.mathworks.com/help/matlab/index.html>

More information on CINECA and their HPC (High Performance Computing) services can be found here:

<https://www.cineca.it/en>

and for the ISCRA projects here:

<https://www.hpc.cineca.it/services/iscra/iscra-general-information>

All links are working at the time of writing, april 2021.

Conclusions

Brief summary of the studied problem

The thesis work consisted in analysing the general problem of a tide-forced lagoon-sea water exchange in the subsequent conditions:

- three inlets are present, as in the case of the *Lagoon of Venice*,
- opening and closing combinations act at the inlets and influence the flow patterns,
- combinations are mostly in phase with the tidal cycle and two of them are half phase shifted,
- an initial tracer concentration is spread uniformly across the lagoon domain,
- the concentration decay in the lagoon is studied both in terms of mean and 95th percentile concentration;
- about half of the combinations consist in varying configurations of opened and closed inlets at different tide phases (*forced* or *artificial* combinations) ,
- the other half consist in fixed opening configurations during both inflow and outflow phases (*natural* combinations).

Three series of experiments have been conducted (chapter 3), varying the *exchange ratio* r (the ratio between exchange volume over a half period time and mean volume of the lagoon) and keeping the total volume exchanged (sum of all exchanged volumes) fixed. Results were unclear and overlapping at first and more theoretical study have been made (chapter 2). Important theoretical properties and ideal models have been developed and thus a deeper understanding of the phenomena at play, in general, and of experimental results, consequently. A further analysis in terms of computational simulations (chapter 4) have shed more light on opening combination patterns and on differences in concentration decay.

Main results

The most important theoretical results are:

- three models (*Perfect Mechanism* with steep linear decay, *Perfect Mixing* with exponential decay, and *Reversed Mechanism* with no decay) encompass all combinations at initial, intermediate and late stage, and establish decay rate theoretical limits
- the slope of mean concentration decay graph during outflow phase is a good indicator of efficiency: a negative slope denotes the presence of a favourable mechanism (flushed water has higher concentration than average in the lagoon basin, decay closer to *Perfect Mechanism* model), a positive slope denotes an adverse mechanism (decay closer to *Reversed Mechanism* model), a neutral slope denotes similarity to the *Perfect Mixing* model
- the slope of the mean concentration decay during inflow phase is independent of the combination (while flushed water concentration depends on the flow pattern in the lagoon, entrained water from the sea has a very similar concentration in all cases)
- exchanges with the same exchange rate r/T have the same decay interpolation curve in the models; fixing r/T (as in the experiments) is equivalent to fixing the total exchanged volume
- when mixing and mechanism models are combined, lower exchange ratios r (or shorter periods T) exchanges have a steeper decay than higher exchange ratios (longer periods) ones

Both experiments and simulations confirm the validity of the listed properties.

Experiments and simulations provide clear results:

- Given a criterion of flushing efficiency (mean, median or maximum concentration) there is always a combination more efficient than the natural configuration *allopen* (all three inlets open during both inflow and outflow phase). The relative increase of decay is about 9% in terms of mean concentration and 8% in terms of 95th percentile concentration.
- The lower the exchange ratio r , the more efficient are externally forced combinations; *natural* combinations have a similar (i.e. *twoopen*) or less efficient (i.e. *allopen*) decay. This is important because lower ratios correspond to the sea level rise scenario, and, therefore, it means that forced combinations can help mitigating climate change effects.
- Opening lateral inlets during inflow phase (both of them as in *twoopen* and *bigcomboinverted*; or alternately, as in *supercombo*), while closing the central inlet, is clearly more advantageous than opening the central inlet while closing the lateral ones. Outflow phase configuration is less important and as a

consequence of this the natural configuration *twoopen*, thanks to its simplicity, represents a very good alternative to *allopen*.

- Half period shifted combinations (*strangecombo*, *strangebigcombo*) provide the earliest decay of maximum concentration and represent a very good alternative as well.

Further developments

More indepth studies can be made:

- considering an object of significant size (such as the city of Venice in its lagoon) in central and lateral position,
- considering different concentration sources,
- considering the effect of the wind,
- varying the phase shifting and timing (also delaying gates opening) in order to optimise jets entrainment in the lagoon basin and thus the flushing mechanism.

These further studies would provide a new interesting perspective on the other main factors in the lagoon dynamics and on combination optimisation. The relative increase in decay could potentially double.

Final words

Even in its drastic simplifications, the work has shown a variety of properties and solutions which can be applied to real-case scenarios. Some of them may be very basic, but they all contribute to providing a deeper understanding of the possibilities given by a mobile barriers system, such as the MOSE one. Just as the conceptual models of chapter 2 guided the interpretation of experimental results, the whole framework of combinations provides a new level of theoretical comprehension and can be seen as a reference for engineering applications. Ultimately, a continuous refining of combinations design in terms of timing, inflow jets penetration, pollutants sources location, weather conditions, and even gates opening fraction, can lead to the primary tool for the environmental management of the Lagoon of Venice.

**Studio della circolazione marina
indotta da schemi di apertura-chiusura
del sistema MOSE
in un modello semplificato
della Laguna di Venezia**

SINTESI IN ITALIANO

Breve introduzione

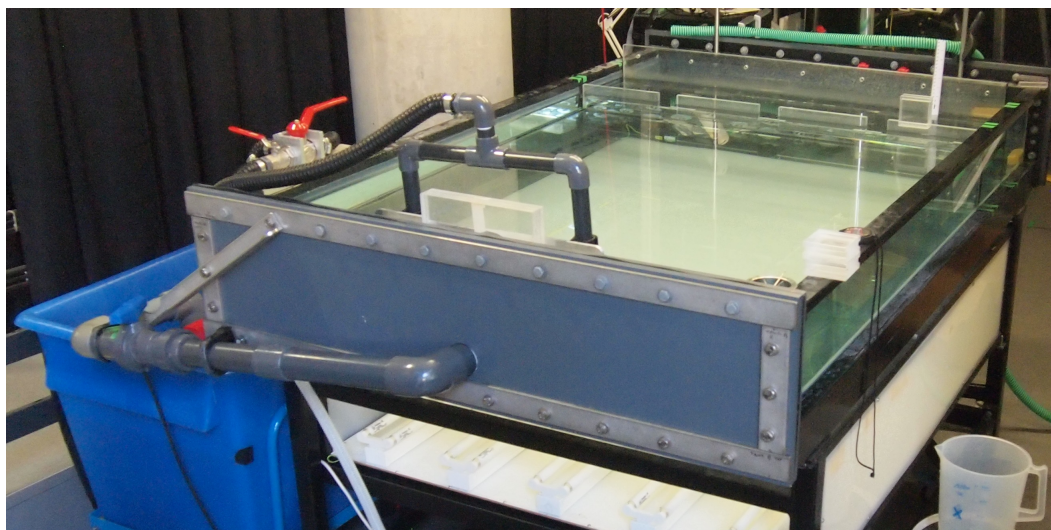
La laguna di Venezia è la laguna più estesa del Mar Mediterraneo, nonché la più celebre al mondo: la sua fama nasce dell'elevatissimo patrimonio artistico e culturale della città di Venezia, che sorge nel suo cuore, e l'intera laguna è tutelata come sito UNESCO dal 1987. In Italia è ben noto che, a causa dell'intervento antropico in laguna (sfruttamento di fluidi e deviazione dei corsi d'acqua dolce con conseguente subsidenza) e a livello globale (aumento concentrazione di gas climalteranti con conseguente surriscaldamento globale e innalzamento dei livelli dei mari), gli abitati urbani e insulari sono interessati sempre più frequentemente da allagamenti per picchi di alta marea (l'"acqua alta"). Per far fronte a tale problema è stato costruito, fra numorese controversie, un sistema di barriere mobili alle tre bocche di porto della laguna, il *MOSE* (MOdulo Sperimentale Elettromeccanico). Il sistema è formato da 78 paratoie a ventola, che, tramite iniezione di aria compressa, si sollevano temporaneamente dagli alloggiamenti a fondo mare, e permettono di isolare idraulicamente la laguna dal Mar Adriatico. La soluzione, pur molto discussa, rispetta i vincoli di tutela del paesaggio, del trasporto marittimo e delle attività economiche.

Il progetto in questione mira a fornire una comprensione di base del possibile utilizzo del MOSE come strumento di gestione ecologica della laguna di Venezia, in uno scenario prossimo in cui la prolungata chiusura della laguna richieda un'opportuna ricircolazione delle acque: la comunicazione laguna-mare è fondamentale per l'apporto di ossigeno e nutrienti del mare, da un lato, e per lo smaltimento delle sostanze inquinanti dovute all'attività antropica, dall'altro.

In particolare, è studiata la possibilità di creare *combinazioni di circolazione*, aprendo e chiudendo le bocche al variare della marea. Il modello idraulico è estremamente semplificato in un parallelepipedo rettangolo di $1,20 \times 0,24 \times 0,05 \text{ m}^3$; pertanto ne consegue un limite di applicabilità ma, nel contempo, una maggiore afferenza teorica: qualsiasi bacino idrico semichiuso sottoposto a forzante di marea e su cui sia possibile un controllo sulla chiusura delle bocche è ascrivibile allo studio in oggetto.

Lo scopo principale, dunque, non è quello di modellare la laguna di Venezia in tutti i suoi fenomeni (batimetria, trasporto di sedimenti, immissioni fluviali, salinità etc.) ma di estrarne una caratteristica particolare e di studiarla variandone i parametri che la costituiscono. Anche in ragione di ciò, sono sviluppate le basi teoriche dello scambio fra due bacini sottoposti a forzante di marea, che rappresentano lavoro originale di tesi.

Il bacino della laguna è ricreato fisicamente da una struttura in acrilico posta in una vasca; un sistema di tubazioni collega la vasca a una cisterna, e, attraverso una pompa sommergibile ad accensione e spegnimento periodici, è simulata la marea. Del colorante alimentare, uniformemente distribuito all'inizio degli esperimenti, è utilizzato per studiare il decadimento della concentrazione nel bacino.



Modelli Concettuali

Sono stati elaborati tre modelli con ipotesi molto semplificative al fine di caratterizzare le curve di decadimento della concentrazione in alcuni comportamenti fondamentali. Lo scambio avviene tra un corpo idrico con volume vol_{lag} (la "laguna") e un corpo idrico a volume $R vol_{lag}$ (il "mare"); periodicamente (ogni $T/2$, periodo T di marea) una quantità $r vol_{lag}$ (con r detto *rapporto di scambio*) viene scambiata dal "mare" alla "laguna" (flusso in ingresso, marea crescente) o dalla "laguna" al "mare" (flusso in uscita, marea calante). Gli scambi, nei modelli come negli esperimenti, cominciano a metà di una fase di marea crescente, quando il livello dell'acqua nei due bacini è il medesimo; dopo un tempo $T/4$ (con T periodo di marea) segue la fase di marea calante, di durata $T/2$, quindi la fase di entrata della medesima durata e così via.

MESCOLAMENTO PERFETTO: la concentrazione è istantaneamente uniforme; in fase di marea crescente il suo valore pari al valor medio ponderato fra concentrazione presente in laguna e concentrazione nel volume di scambio, dunque è costante in fase di marea calante. L'ipotesi è valida in entrambi i bacini.

Si dimostra nell'elaborato che il decadimento corrispondente ha limite per $r/T \rightarrow 0$:

$$c(t)/c_0 = e^{-\frac{r}{T} t}$$

MECCANISMO PERFETTO: il volume di scambio in ingresso nella laguna, a concentrazione minore, viene trattenuto, mentre il volume d'uscita è selezionato in modo da avere la massima concentrazione presente nella laguna. Nel bacino del mare rimane l'ipotesi di mescolamento perfetto.

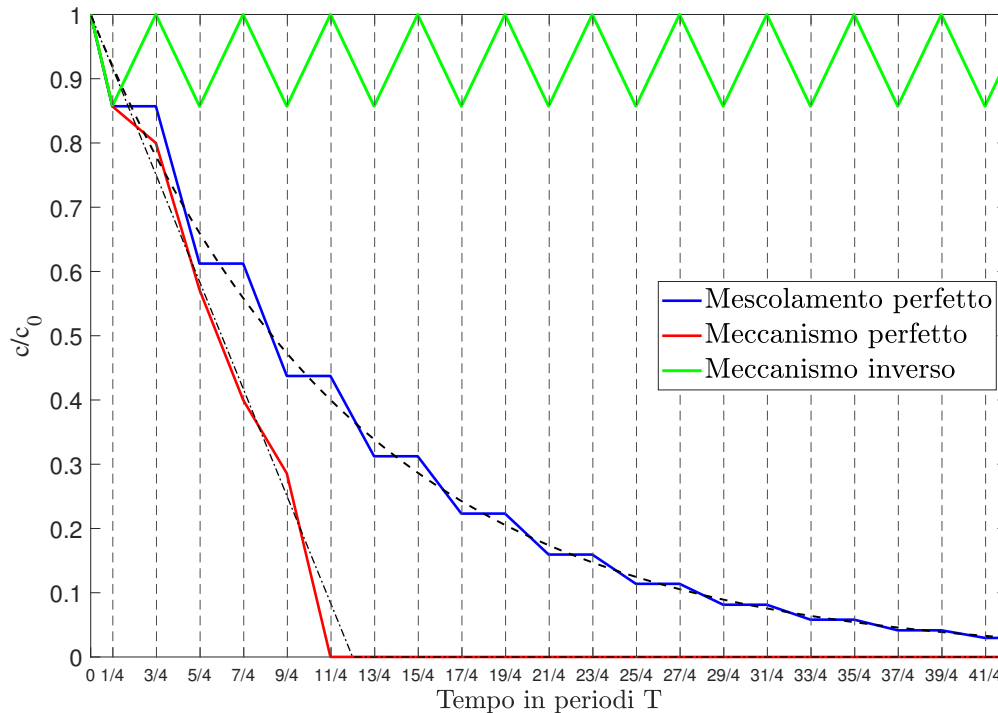
Si dimostra nell'elaborato che il decadimento corrispondente ha limite per $r/T \rightarrow 0$:

$$\bar{c}(t)/c_0 = 1 - \frac{r}{T} t$$

MECCANISMO INVERSO: il volume di scambio in ingresso nella laguna, a concentrazione minore, viene selezionato in modo da essere anche il volume d'uscita. Nel bacino del mare rimane l'ipotesi di mescolamento perfetto.

Si dimostra nell'elaborato che il decadimento corrispondente ha limite per $r/T \rightarrow 0$:

$$\bar{c}(t)/c_0 = 1$$



Sussistono inoltre delle proprietà molto semplici ma importanti per l'interpretazione delle curve di decadimento, in particolare in termini di concentrazione media:

INDIPENDENZA DELLA PENDENZA IN FASE DI MAREA CRESCENTE: per definizione di concentrazione e di media, il decadimento di concentrazione media in fase di flusso entrante è indipendente da come venga introdotto il volume di scambio, e dunque dagli schemi di apertura-chiusura delle bocche

PENDENZA NELLA FASE DI MAREA CALANTE ED EFFICIENZA: una pendenza positiva indica che il volume sottratto alla laguna ha concentrazione minore del valor medio nella laguna, e dunque una situazione che si avvicina a quella del modello a meccanismo inverso; viceversa, una pendenza negativa denota la presenza concentrazioni maggiori della media in uscita e quindi meccanismo di circolazione favorevole (in sintonia col modello a meccanismo perfetto). Una pendenza nulla è coincidente con quella del modello a mescolamento perfetto.

EQUIVALENZA RISPETTO AI TASSI DI SCAMBIO r/T : si dimostra agevolmente che per i modelli ideali sussiste un'equivalenza fra rapporti di scambio e periodi diversi

a condizione di eguaglianza del tasso di scambio r/T . Tale equivalenza è evidente nelle formulazioni analitiche dei modelli.

MAGGIORE EFFICIENZA PER RAPPORTI DI SCAMBIO RIDOTTI: fissato r/T , in un modello ibrido fra mescolamento e meccanismo, si ha maggior decadimento per rapporti di scambi minori

Inoltre, si è provato a raffinare la modellazione introducendo la geometria a tre ingressi e ipotesi aggiuntive: l'intento è di rappresentare efficacemente la variabilità data da diverse combinazioni di apertura e chiusura delle bocche. Tale modellazione ha avuto un successo solamente parziale ed è stata possibile solo abbandonando il significato fisico degli scambi: attraverso due coefficienti (uno di meccanismo e uno di mescolamento) è stata realizzata una gradazione fra i tre modelli sopraindicati basata sul concetto di *efficienza di ventilazione*. Ciò rappresenta un risultato teorico non del tutto privo di significato: il modello unifica i tre modelli precedenti, tiene conto della variabilità delle combinazioni e un offre un'idea su quanto una certa configurazione si presti ad essere efficiente rispetto a un'altra. Ma tale significato è artificiale e lontano dalla realtà fisica del problema alla base: in particolare, il modello non tiene conto della dinamica interna dovuta al flusso dei jet d'ingresso, i quali possono concentrare il mescolamento in alcune zone ed escluderne altre.

Risultati sperimentali

Gli esperimenti sono divisi in tre serie, corrispondenti a tre diversi rapporti di scambio r : 1/6, 1/3 (vicino a quello reale della laguna) e 1/2. La quantità r/T è fissata in modo che il volume totale scambiato sia il medesimo; un valore di r più ridotto, inoltre, implica valori minori di ampiezza della marea e simula uno scenario di innalzamento del livello del mare.

Q_{pump} cm ³ /s	Period s	cycles	Ex. vol. cm ³	Tot ex. vol cm ³	Amplitude cm	Ex. ratio	Q_{lagoon} cm ³ /s
545,3	75	30	20450	144000	0,833	0,166	64
545,3	150	15	40900	144000	1,666	0,33	64
545,3	225	10	61350	144000	2,5	0,5	64

I dati sperimentali sono costituiti da *frame* fotografici in gradazioni di grigio; tramite opportuna calibrazione è stata definita una relazione fra luminosità dei *pixel* e concentrazione. I frame sono dunque convertiti in distribuzioni di concentrazione secondo per secondo e manipolati con *Matlab*, un noto ambiente di calcolo numerico.

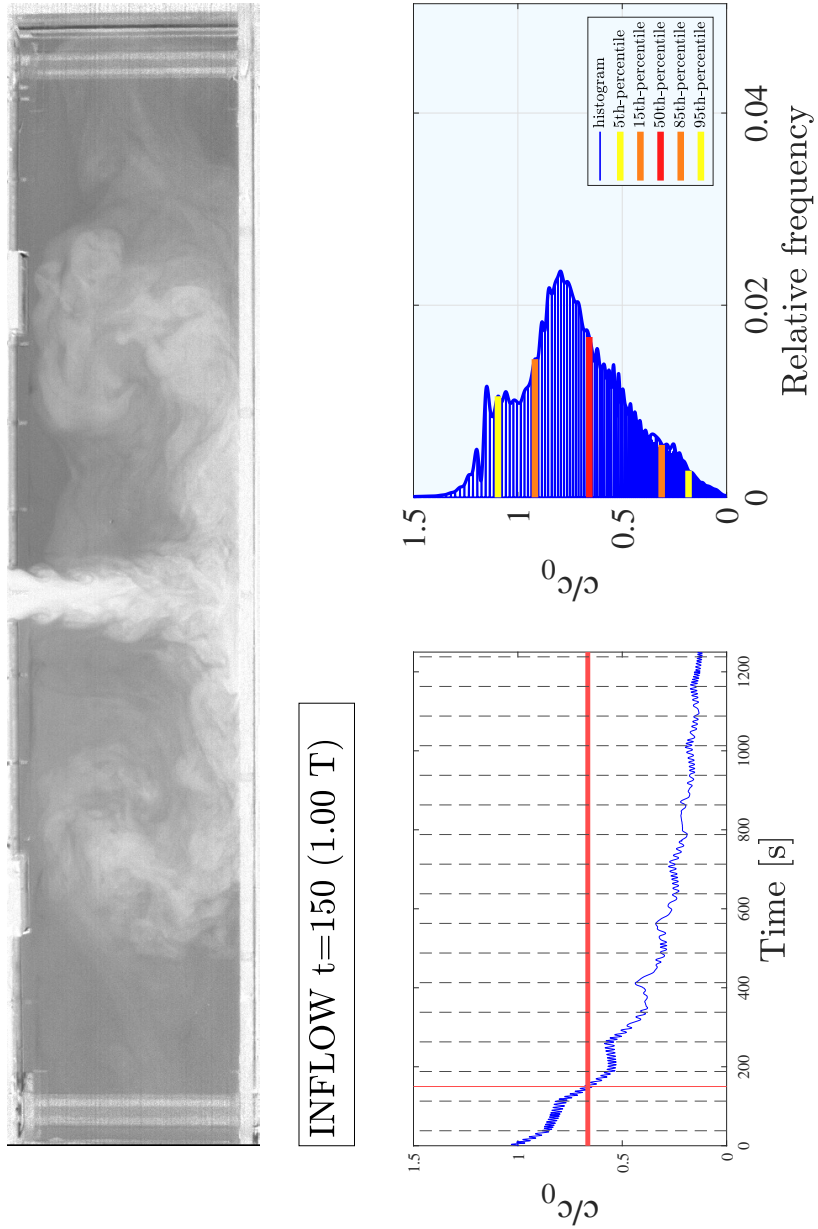
Queste sono le principali combinazioni studiate, \uparrow per ingresso aperto sia in fase di entrata che di emissione, $-$ per ingresso chiuso; \downarrow per fase di ingresso, \uparrow per fase d'uscita:

Allopen	↑	↑	↑	
Oneopen	-	↑	-	
Twoopen	↑	-	↑	
Twoopen lateral	↑	↑	-	
Twoclose	↑	-	-	
Combo	↓	-	-	in
	-	-	↑	out
Badcombo	↓	-	-	in
	-	↑	-	out
Goodcombo	↓	-	↓	in
	-	↑	↑	out
Easycombo	↓	↓	-	in
	-	↑	↑	out
Bigcombo	-	↓	-	in
	↑	-	↑	out
Bigcombo inverted	↓	-	↓	in
	-	↑	-	out
Supercombo	↓	-	-	in
	-	↑	-	out
	-	-	↓	in
	-	↑	-	out
Supercombo inverted	-	↓	-	in
	↑	-	-	out
	-	↓	-	in
	-	-	↑	out

Sono anche state sperimentate due combinazioni con apertura e chiusura in controfase rispetto alla marea, *strangecombo* e *strangebigcombo*. *Allopen* è la configurazione corrispondente ad assenza di barriere, ed è detta *combinazione naturale*.

In generale le combinazioni si possono dividere in

- "artificiali" o "esternamente forzate" quando la configurazione di chiusura varia nel tentativo di imprimere un meccanismo di circolazione all'interno della laguna (tutte le combinazioni con la parola "combo" al loro interno)
- "naturali" o "a meccanismo naturale" quando la configurazione è fissa e il flusso interno ne è diretta conseguenza (*Allopen*, *twoclose* etc.)



Esempio di *frame* con grafico di concentrazione media e distribuzione in frequenza, combinazione *oneopen*

Stima degli errori

Purtroppo gli esperimenti hanno presentato diversi tipi di errore (fuoriuscite non controllate, asimmetrie, circolazioni aggiuntive ed altri), per poterne stimare l'entità sulle curve di decadimento finali è stata sfruttata una proprietà teorica, evidente nei modelli: la concentrazione media al termine di una fase di ingresso deve avere necessariamente un valore

$$c_2 = \frac{c_1 (1 - r/2) + c_{sea} r/2}{1 + r/2} \approx c_1 \frac{1 - r/2}{1 + r/2}$$

dove c_1 è la concentrazione media della laguna all'inizio della fase di ingresso, c_2 la concentrazione media nella laguna al termine della stessa e c_{sea} la concentrazione dell'acqua di scambio proveniente dal bacino del mare.

Tale relazione è facilmente invertibile in:

$$r^* = 2 \frac{c_1 - c_2}{c_1 + c_2 - c_{sea}} \approx 2 \frac{c_1 - c_2}{c_1 + c_2}$$

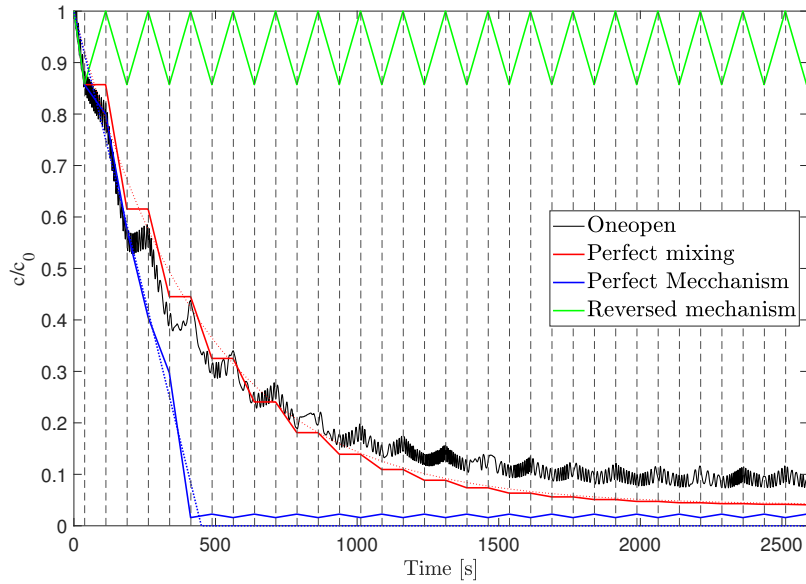
la quale offre una stima del rapporto di scambio r a partire dai dati rilevati di concentrazione media. Noto il valore teorico di r , la stima è confrontata con tale valore e costituisce un indicatore di affidabilità dei dati. Tale strumento fornisce informazioni circa il buon esito degli esperimenti e permette di giudicare criticamente i risultati finali e le conclusioni che se ne possono trarre. Nel seguito r_1 è il rapporto stimato sulla prima fase iniziale di durata $T/4$, quando le condizioni sperimentali sono più sensibili agli errori; r_2 invece è una media delle prime fasi successive alla prima. Per convenzione, quando non riportati r_1 ed r_2 , i valori poco affidabili saranno evidenziati in *italico*.

Occorre precisare che errori non dovuti allo scambio idraulico possono avere un'influenza non trattabile in modo sistematico, come riscontrato successivamente nel confronto con le simulazioni numeriche.

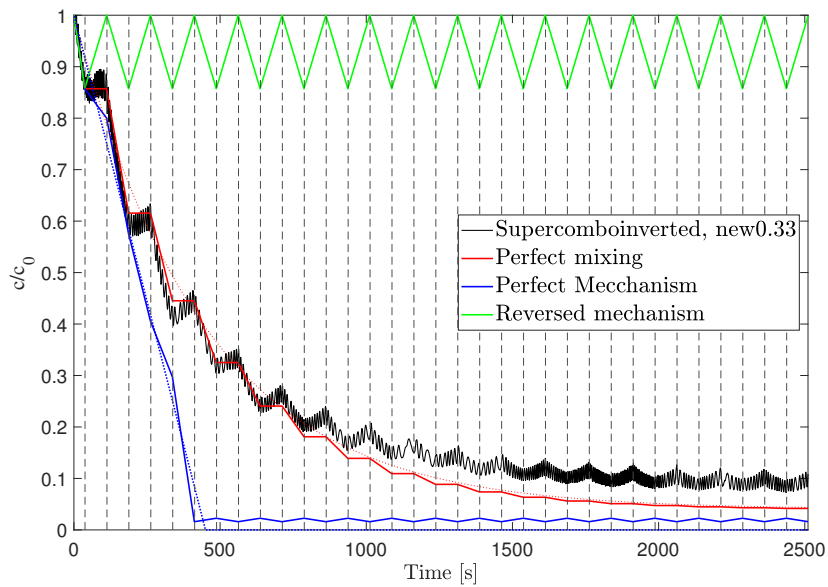
Risultati sperimentali, modelli e schemi di circolazione

Dall'andamento delle curve di decadimento si nota che alcune combinazioni si predispongono meglio di altre a rappresentare i modelli ideali definiti in precedenza. In generale, la presenza di un meccanismo si nota nella pendenza negativa delle curve di decadimento in fase di fuoriuscita, una pendenza nulla indica un buon mescolamento e una pendenza positiva indica la presenza di un meccanismo inverso. Quest'ultimo caso si verifica sempre nelle fasi inoltrate del decadimento, quando alcune parti stagnanti nel bacino mantengono una concentrazione più elevata.

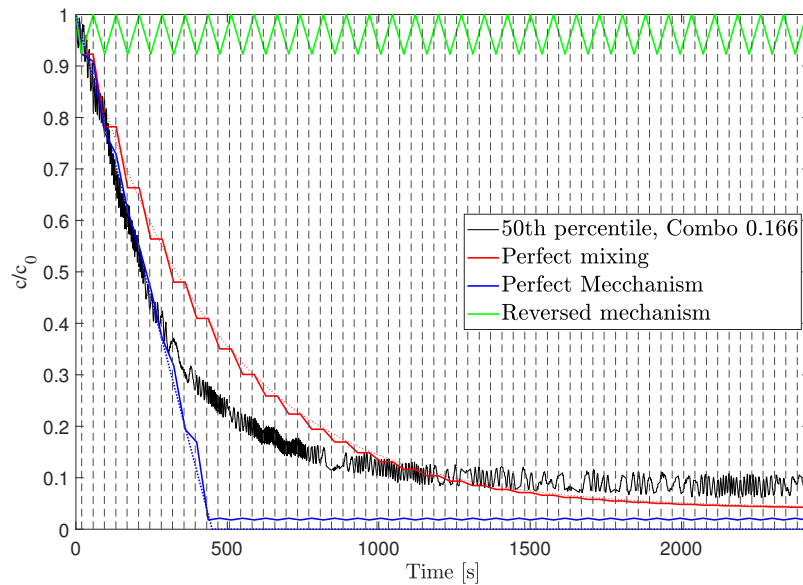
Per indagare oltre è necessario considerare lo schema di circolazione che si crea all'interno della laguna, nel seguito sono forniti alcuni esempi.



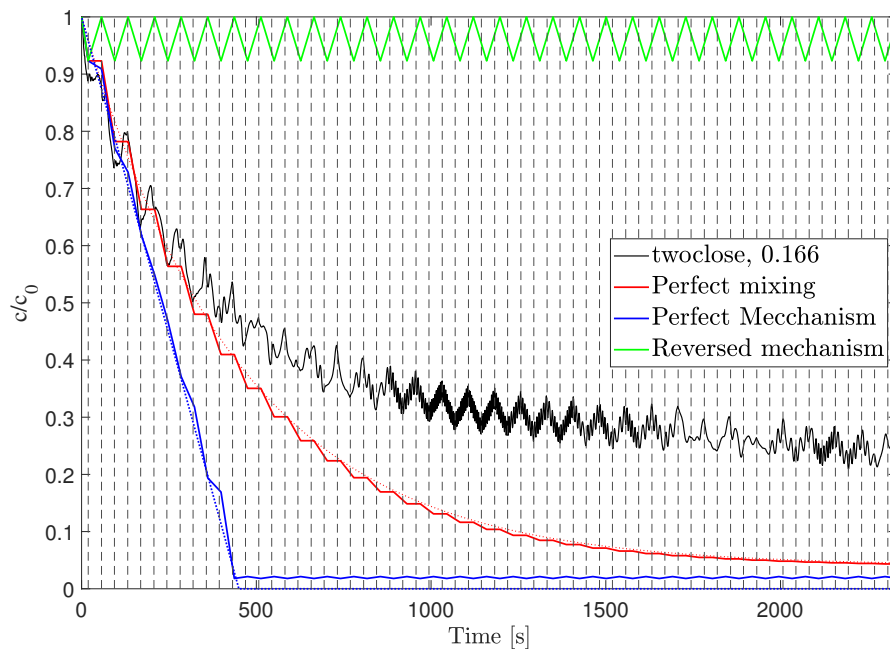
Oneopen (c a c), serie *new0.33*. La concentrazione media segue l'andamento lineare nelle prime fasi, poi il meccanismo diventa contro-efficiente



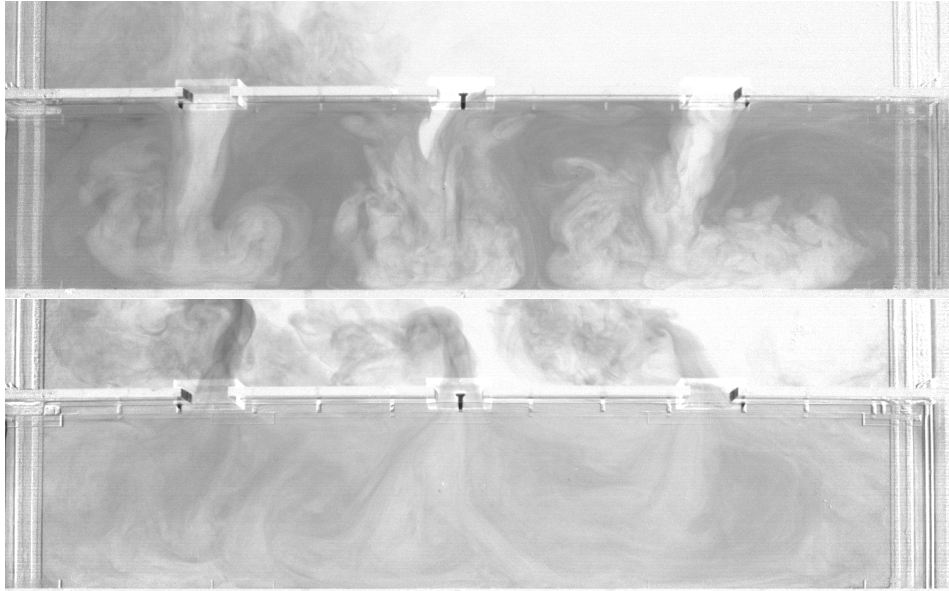
Supercomboinverted serie *new0.33*. La concentrazione media segue il modello di *Mescolamento Perfetto* durante le prime fasi



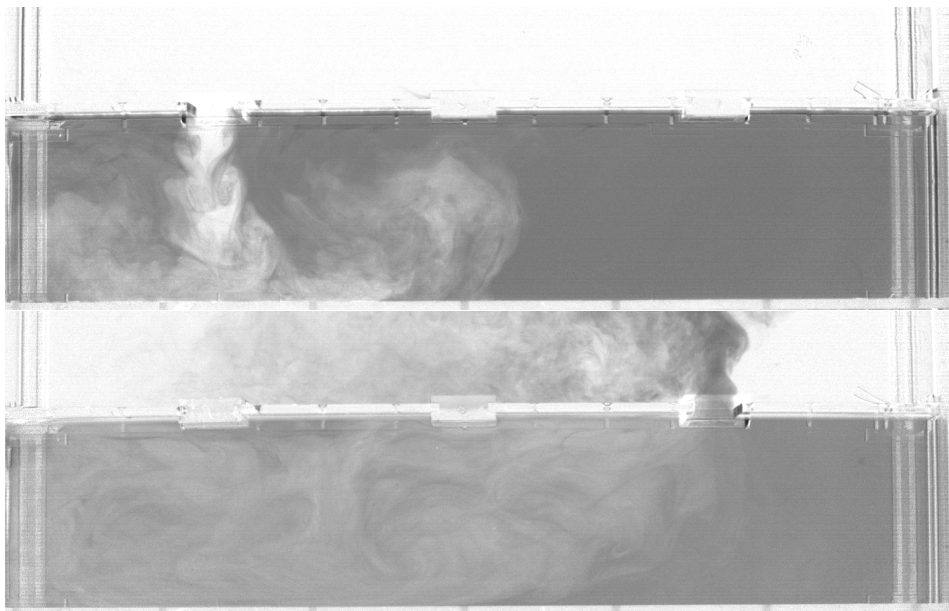
Combo (c c a - in, a c c - out) serie *0.166*. La concentrazione mediana segue l'andamento lineare del *Meccanismo Perfetto* per diversi cicli, dopodiché la combinazione perde di efficienza non agendo uniformemente



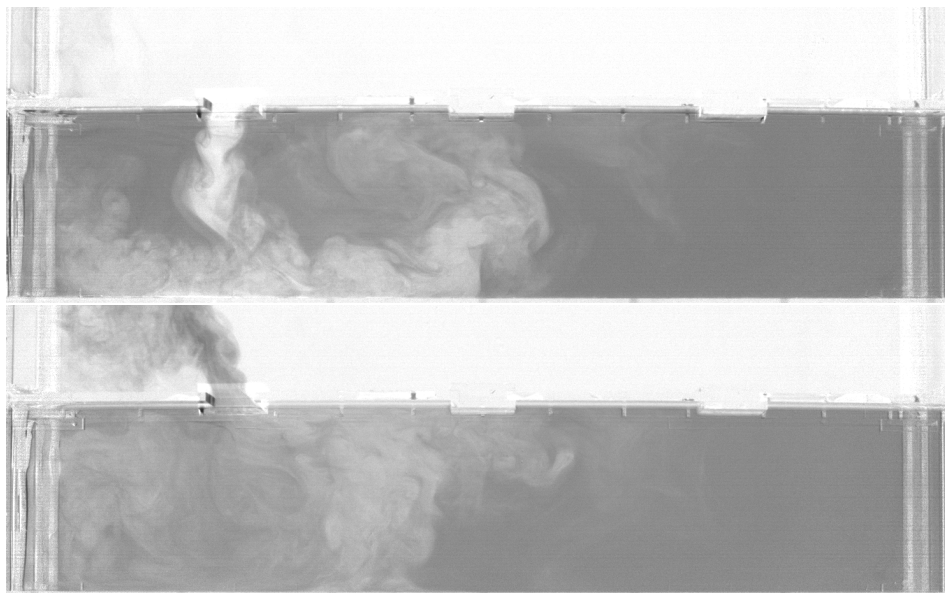
Twoclose serie *0.166*. La concentrazione media mostra un comportamento a *Meccanismo Inverso*



Schema di circolazione per fase di ingresso e uscita, *allopen*



Schema di circolazione per fase di ingresso e uscita, *combo*



Schema di circolazione per fase di ingresso e uscita, *twoclose*

Risultati

Al fine di evitare una grande mole di confronti grafici (sono stati condotti oltre cinquantacinque esperimenti) sono state definite della quantità chiave mediate sui primi 956 s: la concentrazione (normalizzata rispetto alla concentrazione iniziale) media \bar{c} , la deviazione standard normalizzata σ_N , il valore mediano della distribuzione e il 95^{mo} percentile. La durata scelta corrisponde a un intervallo abbastanza corto da cogliere le differenze delle combinazioni nei primi cicli ma abbastanza lungo da non risentire di eventuali errori iniziali. Si nota che i valori mediani sono piuttosto correlati ai valori medi e definiscono il comportamento di massima sulla laguna; deviazione standard e 95^{mo} percentile, invece, mostrano quanto il decadimento sia uniforme.

Si riportano quindi alcuni risultati salienti sul 50^{mo} e il 95^{mo} percentile. In questa sintesi per semplificare sono stati rimossi alcuni risultati ritenuti non affidabili ed altri meno rilevanti.

<i>Tutte le serie</i>		r_1	r_2	50^{th}	95^{th}
0.166	combo	0.22	0.15	0.34	0.75
new0.33	combo	0.45	0.26	0.37	0.80
0.166	twoopen lateral	0.17	0.22	0.37	0.85
0.166	bigcomboinverted	0.14	0.15	0.39	0.55
new0.33	oneopen	0.34	0.22	0.40	0.64
0.166	strangecombo	0.12	0.14	0.41	0.57
0.5	bigcombo	0.50	0.40	0.41	0.71
old0.33	all open	0.34	0.29	0.41	0.71
0.166	supercomboinverted	0.19	0.15	0.43	0.62
new0.33	supercombo	0.31	0.26	0.44	0.61
0.5	oneopen	0.48	0.36	0.44	0.76
0.166	twoopen	0.16	0.24	0.44	0.62
new0.33	allopen	0.31	0.23	0.44	0.73
new0.33	easycombo	0.30	0.26	0.46	0.85
0.5	twoclose	0.16	0.47	0.60	0.96

Ordinamento per 50^{mo} percentile

I risultati dimostrano che diverse combinazioni portano a decadimenti più rapidi della configurazione naturale *allopen* sia in termini di 50^{mo} percentile che di 95^{mo} percentile. In particolare, *combo* e *bigcomboinverted* hanno concentrazione mediana inferiore a quella della configurazione naturale *allopen*. Considerando valori vicini a quelli massimi (95^{mo} percentile), *bigcomboinverted*, con i suoi jet laterali e deflusso centrale (*twoopen+oneopen*), e *strangecombo*, con le chiusure in controfase di marea,

<i>Tutte le serie</i>		r_1	r_2	50^{mo}	95^{mo}
0.166	bigcomboinverted	0.14	0.15	0.39	0.55
0.166	strangecombo	0.12	0.14	0.41	0.57
new0.33	supercombo	0.31	0.26	0.44	0.61
0.166	supercomboinverted	0.19	0.15	0.43	0.62
0.5	goodcombo	0.68	0.37	0.41	0.62
0.166	twoopen	0.16	0.24	0.44	0.62
0.166	strangebigcombo	0.11	0.14	0.42	0.63
new0.33	oneopen	0.34	0.22	0.40	0.64
old0.33	all open	0.34	0.29	0.41	0.71
0.5	bigcombo	0.50	0.40	0.41	0.71
0.166	allopenagain	0.18	0.14	0.45	0.73
0.5	oneopen	0.48	0.36	0.44	0.76
new0.33	combo	0.45	0.26	0.37	0.80
new0.33	easycombo	0.30	0.26	0.46	0.85
new0.33	twoopen lateral	0.42	0.26	0.42	0.87
0.5	twoclose	0.16	0.47	0.60	0.96
old0.33	badcombo	0.22	0.32	0.46	1.15

Ordinamento per 95^{mo} percentile

assicurano un efficace mescolamento, sensibilmente migliore di quello di *allopen*. È dunque possibile concludere che, fissato un obiettivo di decadimento, esiste una combinazione migliore di *allopen*.

Confrontando *allopen* ad $r = 1/3$ con *combo* si ha una riduzione del decadimento in termini mediani del 16%; considerando *supercombo* la differenza da *allopen* è del 14 % in termini di 95^{mo} percentile. Si illustra quindi quanto effettive siano tali differenze con *frame* catturati al tempo $t = 956$ s.

Tuttavia, sussiste incertezza riguardo alla reale efficienza di combinazioni vicine fra loro nei vari ordinamenti; ciò è particolarmente vero per la serie 0.5 ad $r = 1/2$ nella quale la maggiore ampiezza di marea accentua le fuoriuscite e porta a risultati di difficile interpretazione. L'intuito può aiutare molto, entrando nella logica dello schema di circolazione, ma può fuorviare e condurre a conclusioni non sostenute dai dati sperimentali. Donde la necessità di simulazioni di fluidodinamica computazionale: un ambiente numerico omogeneo, pur non eliminando del tutto eventuali errori, facilita un confronto diretto delle varie combinazioni.



Allopen, bigcomboinverted, strangecombo, combo e twoclose dalla serie 0.166 a $t = 956$

Influenza del rapporto di scambio

In generale, all'incremento di T (dovuto all'incremento di r) è possibile congetturare che:

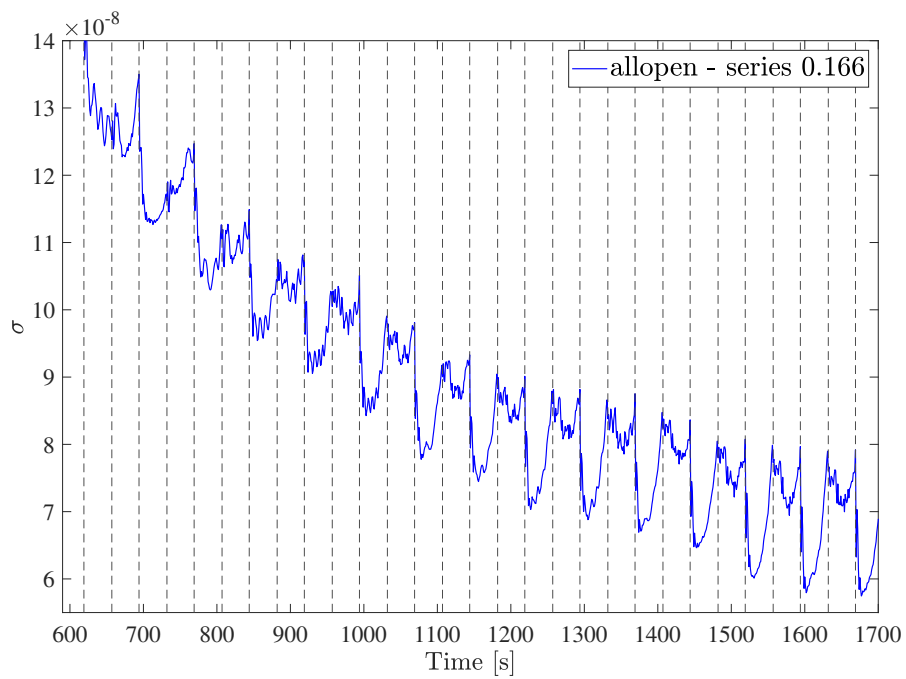
- I meccanismi naturali sono sfavoriti se i jet entranti si chiudono in sé stessi formando celle rotazionali chiuse (ad esempio *oneopen*), mentre se i jet continuano a spingere acqua a concentrazione maggiore verso le bocche di uscita l'effetto è favorevole (ad esempio *allopen*)
- I meccanismi forzati possono essere ostacolati in quanto l'acqua di immissione si avvicina troppo alle bocche di uscita, vanificando il meccanismo (ad esempio *combo*)
- Le combinazioni a meccanismo inverso hanno lo stesso schema di circolazione e non ne subiscono l'influenza (ad esempio *twoclose*)
- Anche le combinazioni pensate per il mescolamento non ne risentono per lo stesso motivo (ad esempio *supercombo*)

50 ^{mo} percentile	0.166	0.33	0.5
allopen	0.60	0.60	0.55
combo	0.51	0.54	0.69
twoclose	0.59	0.61	0.77
supercombo	0.56	0.60	0.69
twoopen	0.61	0.55	
oneopen	0.56	0.55	0.59
bigcombo	0.56		0.57
easycombo	0.58	0.61	0.60
goodcombo	0.60	0.63	0.57
badcombo	0.57	0.51	0.86
twoopen lateral	0.53	0.57	0.69
supercomboinverted	0.59	0.59	0.61

95 ^{mo} percentile	0.166	0.33	0.5
allopen	0.93	0.96	0.80
combo	0.91	0.95	1.06
twoclose	1.07	1.08	1.06
supercombo	0.92	0.82	0.87
twoopen	0.84	0.81	
oneopen	0.85	0.88	1.01
bigcombo	0.82		0.92
easycombo	0.92	0.99	0.97
goodcombo	0.84	0.85	0.86
badcombo	1.11	1.26	1.18
twoopen lateral	0.98	0.99	1.03
supercomboinverted	0.85	0.90	0.95

Impronte di combinazione nella deviazione standard

È stata notata la formazione di uno schema ricorrente nei grafici della deviazione standard in fase attardata degli esperimenti, quando lo scambio assume dei caratteri semi-stazionari. Tale schema è caratteristico delle combinazioni, seppure sia più evidente nel rapporto 1/6. È ancora da valutare l'importanza della forma di tali curve nell'ottica dell'efficienza di circolazione.

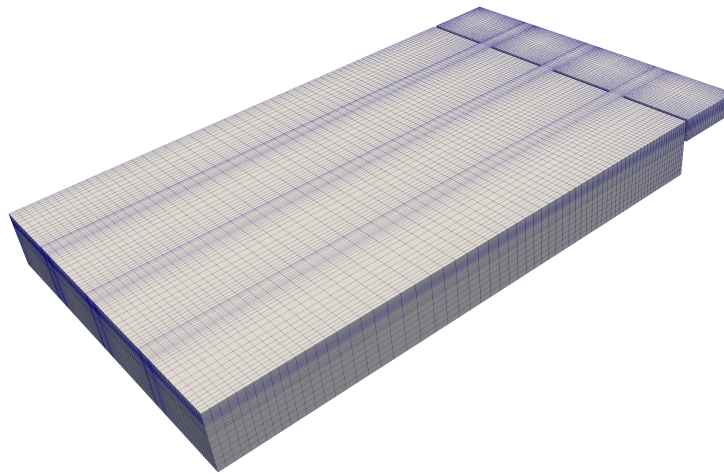


Progressiva formazione di uno schema in $\sigma(t)$, *allopen* da 0.166

Simulazioni

Sono state realizzate delle simulazioni in *OpenFOAM*, una *suite* C++ per la fluidodinamica computazionale (CFD) molto usata in ambito accademico per la sua versatilità e le sue capacità di parallelizzazione. Infatti, essendo OpenFOAM un insieme di librerie *open source*, è modificabile e diverse funzionalità fondamentali come le condizioni al contorno per gli schemi di apertura-chiusura o la correzione della diffusione numerica sono state implementate ad hoc per il computo. Inoltre, data la mole di computo richiesta (67448 *core hours* in retrospettiva), si è usufruito di CINECA, il più potente centro di calcolo in Italia per la ricerca, nonché uno dei più potenti al mondo.

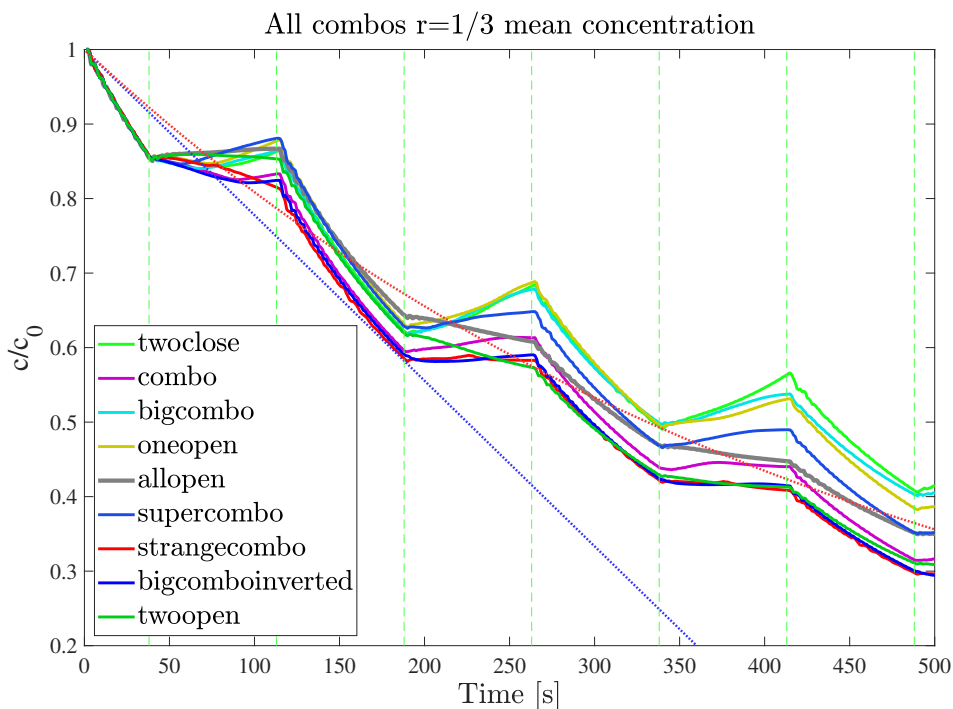
Il modello numerico è calibrato sul modello sperimentale ed è del tutto comparabile con esso. In generale le simulazioni hanno avuto esito positivo e fanno luce sui risultati degli esperimenti. Per economia di calcolo, il tempo di simulazione è di 500 s, più che sufficiente a rilevare i caratteri principali delle combinazioni e vicino ai cambi di marea di ciascuna serie.



Caratteristiche geometriche e di risoluzione spaziale del modello numerico

Nella serie a rapporto $1/3$ è stato predisposto il maggior numero di combinazioni, nove, al fine di studiare le differenze fra le combinazioni; sette sono quelle della serie a $r = 1/2$, dove sono state riscontrate più incertezze sperimentali, e quattro nella serie $1/6$, per un confronto a diversi rapporti.

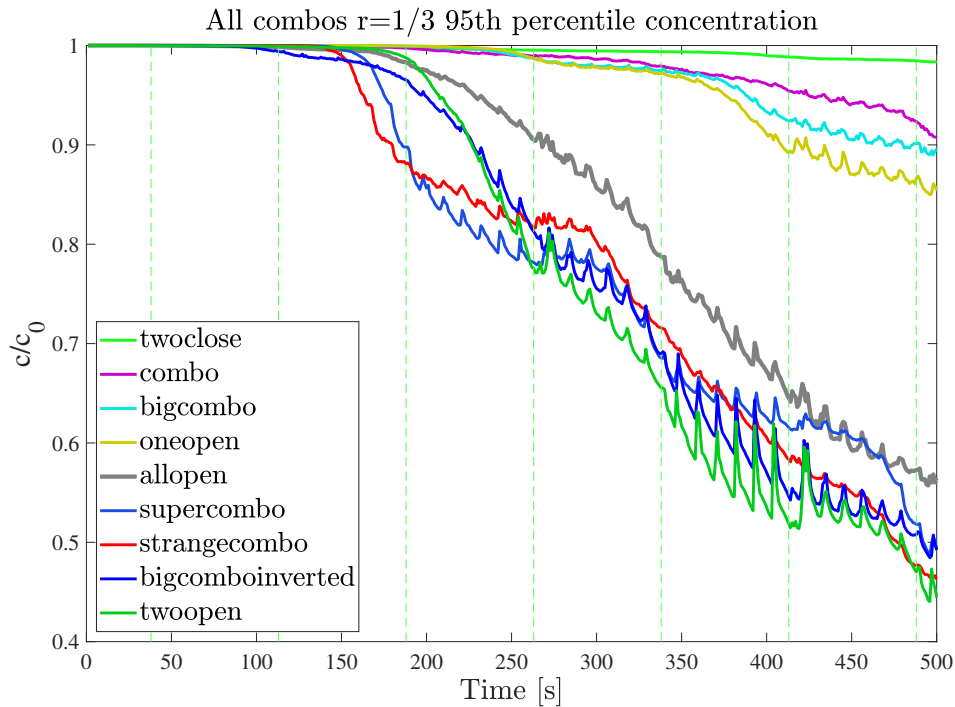
Si riportano, quindi, i dati salienti per la serie $1/3$, con dati quantitativamente significativi per le varie combinazioni. I coefficienti sono mediati rispetto ai 500 s di simulazioni allo stesso modo di quanto fatto per gli esperimenti.



Concentrazione media nella serie 1/3

Concentrazione Media	
strangecombo	0,583
bigcomboinverted	0,584
twopen	0,594
combo	0,598
allopen	0,621
supercombo	0,630
bigcombo	0,646
oneopen	0,648
twoclose	0,651

95 ^{mo} percentile	
twopen	0,794
strangecombo	0,804
bigcomboinverted	0,806
supercombo	0,808
allopen	0,857
oneopen	0,966
bigcombo	0,973
combo	0,981



95^{mo} percentile della concentrazione nella serie 1/3

È inoltre possibile un confronto con gli esperimenti, dove si evidenzia la corretta indicazione dell'errore dei coefficienti r_1 ed r_2 , ma valida per elevati rapporti di scambio.

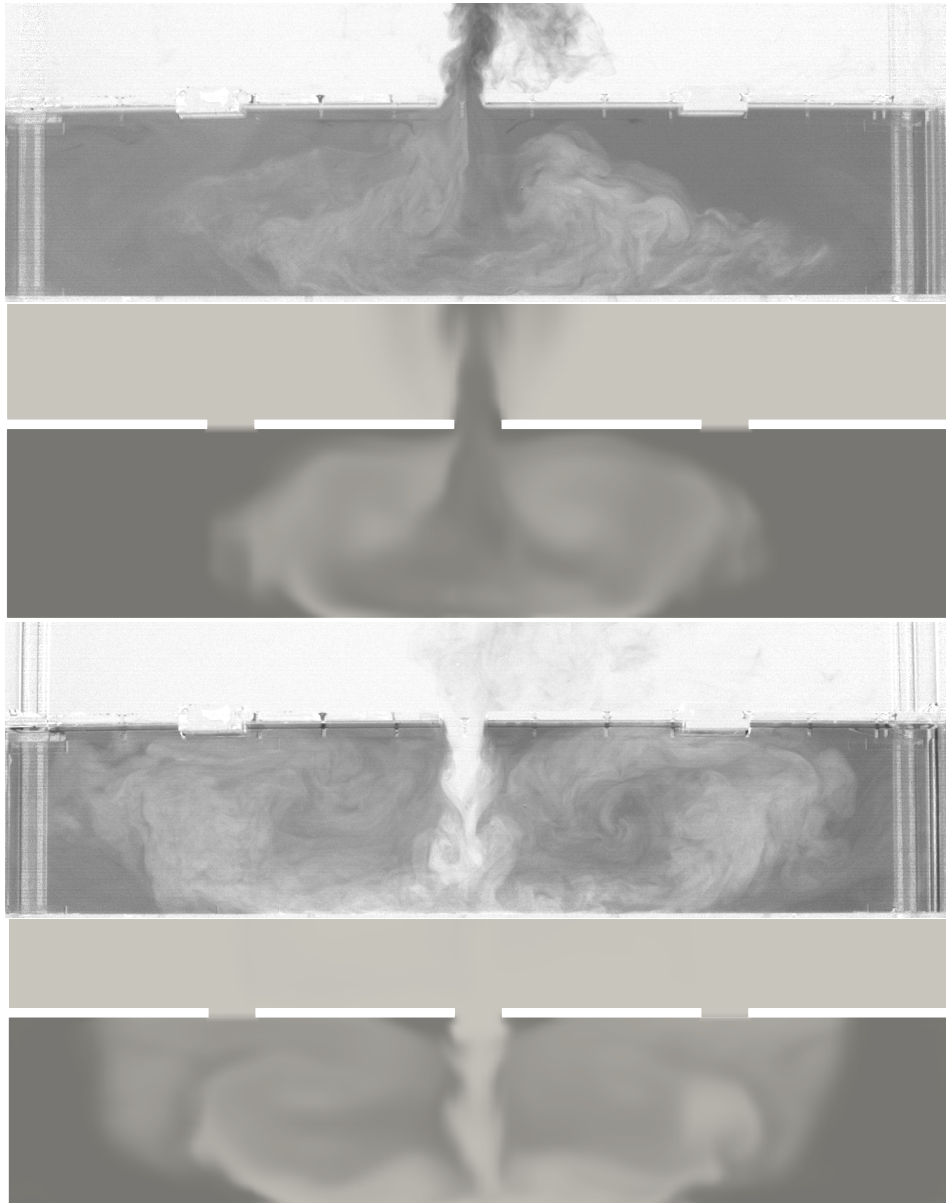
series	combination	r_1	r_2	95_{exp}^{mo}	95_{sim}^{mo}	\bar{c}_{exp}	\bar{c}_{sim}
old0,33	twoclose	0,92	0,37	1,080	0,995	0,659	0,651
new0,33	twopen	0,45	0,26	0,807	0,794	0,545	0,594
new0,33	allopen	0,31	0,23	0,936	0,857	0,615	0,621
new0,33	combo	0,45	0,26	0,946	0,981	0,564	0,598
new0,33	oneopen	0,34	0,22	0,876	0,966	0,568	0,648
new0,33	supercombo	0,31	0,26	0,815	0,808	0,589	0,630
0,166	bigcomboinverted	0,14	0,15	0,767	0,806	0,548	0,584
0,166	combo	0,22	0,15	0,911	0,893	0,533	0,577
0,166	strangecombo	0,12	0,14	0,781	0,804	0,567	0,583
0,166	twopen	0,16	0,24	0,836	0,789	0,601	0,598
0,5	allopen	0,64	0,34	0,796	0,849	0,557	0,618
0,5	combo	-0,01	0,40	1,064	0,978	0,714	0,611
0,5	supercombo	0,03	0,35	0,871	0,835	0,671	0,633
0,5	twoclose	0,16	0,47	1,063	0,977	0,753	0,645

In generale sono confermati i risultati degli esperimenti, con maggiore accuratezza per quanto riguarda le differenze quantitative:

- Dato un criterio di efficienza di circolazione (decadimento della concentrazione media, mediana o massima) esiste sempre una combinazione più efficiente della combinazione naturale *allopen*. L'incremento relativo di decadimento è del 6,1% in termini medi (confrontando *allopen* con *strangecombo*) e del 7,4% in termini di 95^{mo} percentile (confrontando *allopen* con *twoopen*). Questi valori salgono al 20 e 14% considerando solo la metà vicina alla bocca d'entrata in *combo*.
- Al decrescere del rapporto di scambio (da 1/2 a 1/3 e 1/6) si ha un miglioramento delle combinazioni *esternamente forzate*, per localizzazione degli scambi interni; le combinazioni *naturali* hanno un decadimento simile (i.e. *twoopen*) o meno efficienti (i.e. *allopen*). Ciò è importante considerando le implicazioni dei cambiamenti climatici, ovvero il diminuire del rapporto di scambio a causa dell'innalzamento del medio mare.
- L'apertura delle bocche laterali nella fase di flusso entrante (entrambe in *twoopen* e *bigcomboinverted*, alternativamente una e l'altra in *supercombo*), con la contemporanea chiusura della bocca centrale, è associata al meccanismo più efficiente, sia in termini medi che massimi. La configurazione in deflusso è meno importante e *twoopen*, grazie alla sua semplicità, rappresenta un'alternativa sicuramente migliore di *allopen*. Anche *Combo* potrebbe rilevarsi un'ottima alternativa una volta implementata in scala reale, con tutte le variabili del caso.
- Le combinazioni *strange*, ovvero quelle per cui lo schema di apertura e chiusura sia sfasato di mezzo periodo rispetto alla marea, rappresentano ottime opzioni, specie in termini di concentrazione massima a breve termine.

Conclusioni

Anche nelle sue drastiche semplificazioni, il lavoro di tesi ha mostrato una varietà di proprietà e soluzioni che possono essere applicate a casi studio reali. Alcune di queste sono molto semplici, ma tutte contribuiscono a fornire una comprensione più approfondita delle possibilità date da un sistema a barriere mobili, quale quello del MOSE. Allo stesso modo in cui i modelli concettuali hanno guidato l'interpretazione dei risultati sperimentali, l'intero insieme di combinazioni getta le basi per un nuovo livello di comprensione teorica, un grado intermedio di astrazione rispetto alle applicazioni ingegneristiche. In ultima istanza, un continuo raffinamento nella calibrazione delle combinazioni in termini di tempistica e penetrazione dei getti di entrata, posizione delle sorgenti inquinanti, condizioni meteorologiche, sino a frazione di apertura delle bocche, può dare vita allo strumento principe nella gestione ecologica della Laguna di Venezia.



Confronto fra esperimento e simulazione di *oneopen* ($r = 1/3$), a $t = 70$ e $t = 182$